Durham E-Theses

Validation of a model for thermal emission

Hughes, P.A

Validation of a Model for Thermal Emission.

by

P. A. Hughes, B.Sc., M.Sc.

A Thesis submitted to the University of Durham

in accordance with the Regulations for

admittance to the Degree of Doctor of Philosophy.

Department of Physics,

University of Durham.
April, 1986.

13 FEB 1987

Abstract

An introduction to the more general aspects of thermal models is followed by a brief outline of the construction and range of possible applications of the computer models developed at the University of Durham. The physical basis behind one of these models, which predicts temperatures both at the surface and within a one-dimensional non-vegetated object, is considered in some detail, and the construction of the model is outlined. The sensitivity of the temperature predictions to changes in the values of the input parameters required by the model are also discussed.

Equipment was designed specifically to collect sufficient ground truth data to enable the validation of the model, and there is a complete description of the construction and operation of the apparatus. The subsequent interpretation of the data using the computer is also described.

The validation of the model was carried out for two roads with concrete and asphalt surfaces, and consisted of a comparison between surface temperatures predicted by the model and those measured by a radiometer. The results of the comparison are discussed in some detail. The suitability of the model to predict temperature contrasts between two different surfaces was also investigated using the validation data. The model was next applied to the more complex problem of simulating the thermal behaviour of a south facing vertical sandstone wall. A comparison between the predictions of the model and data measured by a radiometer is given, and the problems that this type of simulation entails are discussed.

A summary is given of the work carried out with the model, and suggestions are made for improvements to the model. Finally, the development of future types of model is considered.

Preface

This thesis describes the work carried out by the author at Durham, between October 1982 and October 1985. The work falls into two main areas; the first involving the thermal data acquisition equipment described in Chapter 4, and the second involving the use of a computer model for the simulation of the thermal behaviour of one-dimensional, non-vegatated objects.

The equipment was commisioned at Durham Observatory by the author, who was also responsible for the collection of thermal and meteorological data while the equipment was operating over the period from February 1983 to May 1984. The computer programs described in the Appendix for the interpretation of the data recorded by the equipment were written by the author.

The computer model that was used by the author had been developed by Dr. A. B. Rimmer at the University of Durham, and the three main areas of work involving the model are described in Chapters 3, 5, and 6. Firstly, the author investigated the sensitivity of the surface temperature predictions of the model to changes in the values of certain parameters required as input by the model. This was in order to obtain an understanding of the relative importance of each of the parameters, and hence to determine which would need to be measured with the greatest care. Secondly, the author carried out a validation exercise on the model, and examined its ability to predict temperature contrasts between different surfaces. Thirdly, the author used the data collected at Durham Observatory in an attempt to simulate the thermal behaviour at the surface of a south facing vertical sandstone wall.

Contents

Chapter 1 Introduction.

1.1 General aspects of the thermal behaviour of terrestrial objects.

All man-made and natural terrestrial objects are sources of long-wave infra-red radiation. This results from interactions with their surroundings and the re-radiation of energy gained by absorbing short-wave radiation from the Sun. The long-wave radiation is mainly emitted in the range from 4 to 50 μm, with a maximum at about 10 μm. Terrestrial objects are usually assumed to behave as grey body emitters and receivers of long-wave radiation, and their behaviour is characterized by the Stefan-Boltzmann law. This law gives the radiative flux emitted or received by a surface, and is expressed as,

$$\text{Radiative Flux} = e\,\sigma\,T^4 \qquad (1.1)$$

where e is the infra-red emissivity of the surface,

σ is the Stefan-Boltzmann constant,

and T is the temperature of the object.

The value of the emissivity of a surface will be in the range from 0 to 1, with the upper limit corresponding to a black body. Typically, the emissivities of most natural surfaces are in the range from 0.90 to 0.95.

Most of the long-wave radiation that is emitted from a surface is absorbed by atmospheric constituents, which include water vapour, carbon dioxide and ozone. These molecules have strong absorption bands in the infra-red region, and absorb about 90% of the long-wave flux. This energy is subsequently emitted by the atmosphere as long-wave counter radiation, and a proportion of this is radiated back to the Earth's surface. However, there is a region in the infra-red spectrum between the wavelength limits of 8 and 14 μm where little absorption takes place. This is known as the atmospheric window and is generally chosen as being the most suitable for the operation of remote sensing infra-red detectors. The two main factors which influence this

choice are the low attenuation of the emitted radiation flux from terrestrial surfaces, and the fact that the short-wave flux received from the Sun does not extend into this region. Most work concerned with the measurement and simulation of the thermal behaviour of terrestrial objects has therefore been concentrated on the 8 to 14 μm band. The measurement of the flux emitted by a surface within this range is most conveniently expressed in the form of a radiation temperature. This is defined as the effective temperature of a black body, with an emissivity of unity, that would emit the same flux of radiation in the 8 to 14 μm band. The actual temperature of the surface can be obtained by using the Stefan-Boltzmann law, provided the emissivity is known.

1.2 Construction and application of thermal models.

The aim of thermal models is to predict the thermal behaviour at the surface and within a particular object of interest over a specified period of time. Most models are based on the solution of a differential equation which describes the transfer of heat within the medium of interest. The construction of a typical model can be conveniently split into four main sections;

1. The boundary conditions required to produce a unique solution of the differential equation are defined.

2. The initial distribution of heat within the medium is specified.

3. The differential equation is solved using an approximate analytic or numerical method.

4. The solution is used to generate the particular temperature predictions specified by the application of the model.

The main difference between models is usually in the method chosen to solve the differential equation representing heat conduction, and these have included the use of Fourier series, finite difference, and finite element methods. The latter two methods have been included in the computer models developed at Durham, which are described in Section 1.3.

The temperature predictions generated by computer models are frequently

used to interpret remotely sensed thermal data, which may be obtained for a wide variety of reasons. One of the largest areas of application is in geological research, where the predictions of the model may be compared with recorded thermal data in order to deduce the types of materials comprising the area under investigation. Typical examples of this type of work are described by Watson, 1975, for the analysis of satellite recorded thermal images of the Earth's surface, and Khale, 1977, for an investigation of the surface thermal inertia values of a region of the Mojave Desert. Alternative applications include the use of ground based imaging systems for the detection of personnel and equipment in military operations. In this case, the model may be used to investigate the contrasts between different surfaces and hence to evaluate the effectiveness of camouflage techniques under different meteorological conditions.

The initial work carried out with the general purpose model developed at Durham consisted of a validation exercise, which compared the predicted and measured temperatures for two flat roadways with concrete and asphalt surfaces over a period of six consecutive days. Previous work of a similar nature has been done by Jacobs, 1976, and Link et al., 1981, although neither study was is in as much detail or covered as wide a range of weather conditions as the work carried out at Durham. Jacobs attempted to simulate the thermal behaviour of a layer of asphalt on soil, while Link et al. investigated concrete and soil surfaces. However, in both cases only single modelling periods of 24 hours were considered, and the weather conditions were either ideal or approximated by analytical functions. A more detailed comparison of the results obtained using the model at Durham and those of other authors is given in Chapter 7. The data used for the validation of the Durham model were also used to examine the ability of the model to predict temperature contrasts between concrete and asphalt surfaces. Link et al., 1981, conducted a similar investigation for temperature contrasts between soil and concrete surfaces, and these results are also discussed in Chapter 7.

The second application of the general purpose model was in the more difficult problem of simulating the thermal behaviour of a vertical sandstone wall, which comprised part of the Observatory at Durham.

1.3 The computer models developed at Durham.

The models developed at Durham were designed for three different types of application, although their construction and method of use are generally similar. All of the models have been designed to predict the variation of temperatures at the surface and within one-dimensional structures, where it can be assumed that heat transfer is restricted to one direction. These structures may consist of several planar layers of materials with different thermal properties, provided their extent in the plane perpendicular to the direction of heat transfer is large compared to that in the plane parallel to the heat transfer. The models generate the required temperature predictions by solving a differential equation describing heat conduction within the structure, subject to the appropriate boundary conditions.

The general purpose model for objects with non-vegetated surfaces was the first to be developed. The earliest versions were written in the BASIC programming language and run using a Tektronix 4052 computer, but the limitations of the available memory space and processing speed of the computer meant that it was only possible to simulate the thermal behaviour of very simple structures. This problem was overcome when the model was later rewritten in FORTRAN IV and transferred to a mainframe IBM 4341 computer. The investigation of the simulations produced by this version of the model is described in Chapters 3, 5 and 6, which includes the validation of the model for two different surfaces over a period of fine weather in April 1982.

The second model was developed with the aim of simulating the temperature profile in a layer of snow. This is a very complex problem due to the changes in structure and other physical properties of the snow which occur with time and if melting takes place. It was therefore necessary to restrict the use of

the model to the simpler case of a dry, homogenous snow layer of uniform density. It is assumed that the dominant mechanism for heat transfer consists of conduction between snow grains, but the smaller contribution from vapour diffusion is also included. Unfortunately, the restrictions on the use of the model meant that the only suitable data available for validation of the model were recorded at Durham Observatory over a very short period in February 1983. The predictions of the model did not follow the rapid variations of the measured surface temperature particularly well, and it would therefore be worthwhile to repeat the validation exercise if data recorded under more suitable conditions were available.

The third model simulates the thermal behaviour of a layer of vertically growing vegetation, such as grass. It is assumed that the vegetation acts as a single, one-dimensional layer parallel to a soil surface, and that all heat fluxes act perpendicularly to the vegetated layer. The model was validated for a grass lawn at Durham Observatory using data recorded under conditions of fine weather in August 1983. In the future, a further model could be developed to cover the more complex problem of simulating the thermal behaviour of trees and bushes.

1.4 Measurements of data required as input for the model.

At the same time as the models were being developed at Durham, a comprehensive program of data acquisition was commenced with the intention of obtaining sufficient data to enable the validation of the three models. The effective radiation temperatures of a wide variety of both natural and man-made surfaces were measured under different weather conditions, with values for the important meteorological parameters being recorded at 15 minute intervals. The equipment that was used consisted of an automatic weather station and a system designed and constructed at Durham specifically to measure and record surface radiation temperatures. The latter operated by pointing a radiometer at the surfaces of interest and recording the thermal

emission in the 8 to 14 μm band. The movement of the radiometer was under the control of a computer, and the frequency with which measurements were made could be specified by the operator. There was also a set of 32 temperature sensors available for static measurements of contact temperatures. This set of equipment and the automatic weather station are described in more detail in Chapter 4.

Measurements of meteorological and surface temperature data were initially made for a short period at Ouston, Northumberland during April 1982, and then almost continuously between February 1983 and May 1984 at Durham Observatory. This resulted in a the production of a large database, containing measurements made on a variety of both vegetated and non-vegetated surfaces under a wide range of weather conditions, including a period of snow in February 1983. The database is now stored on a standard 9-track tape, in a format suitable to be read by most mainframe computers.

1.5 Method of use of the computer models developed at Durham.

Although the models described in the previous section are suitable for application to widely different types of objects, the method of operation for all three models is very similar. The first stage in the process is to set up a data file containing the values for the parameters required by the model. The exact nature of these parameters and their significance is described in Chapter 3, but they can be roughly split into five main groups. Site characteristic parameters give the geographical location of the object and the angles of azimuth and inclination of its surface, and the surface parameters consist of the long-wave emissivity and short-wave albedo. The material parameters contain information about the composition of the object, and the initial temperature profile specifies the distribution of heat through the object at the start of the modelling period. Lastly, the meteorological parameters represent the variation of the weather conditions at the surface of the object during the modelling period. The values for these parameters may

either be measured at the location of the object of interest or derived from measurements given in reference tables. Alternatively, if a hypothetical case is being considered then any suitable values may be used. This may occur if a sensitivity analysis is being carried out to investigate how sensitive the predictions of the model are to changes in the value of the input parameters.

The next stage in the process is to select the length of the modelling period and the time interval between updating the predicted temperature profile within the structure. A 24 hour modelling period was used for most applications at Durham, and the interval between updating the temperature profile was normally 15 minutes. These values are also entered in the input data file, and the model may then be run to generate the required temperature predictions.

The general purpose model has been used in this manner to produce the results described in later chapters. In most of these applications, the surface temperature predictions are compared either with measurements made by a radiometer, or with other sets of temperature predictions. However, the model may also be used to predict the diurnal variation of the surface temperature contrast between two different surfaces, provided they both satisfy the relevant conditions governing the use of the model. The method used is firstly to obtain the surface temperature predictions for the object of interest over the modelling period, and then run the model again with the input data file for the model suitably modified to describe the characteristics of the background material surrounding the object. The ability to predict the temperatures of the object and its surroundings is particularly important if the model is to be used for purposes such as the evaluation of camouflage, where effectiveness may be measured by the magnitude of the temperature contrast.

1.6 Scope of the work.

The following chapters describe the work carried out with the general purpose computer model for objects with non-vegetated surfaces, and the methods used to obtain the data required as input for the model. The theoretical basis for the model is outlined in Chapter 2, which begins by considering the one-dimensional equation of heat conduction and how it may be solved to provide the required temperature predictions. The formation of the boundary conditions for the solution of the equation is then described, followed by a discussion of how the model is used and the input data that are required. Chapter 3 contains the results of a sensitivity analysis which shows how uncertainties in the values of the input parameters for the model might affect the temperature predictions.

The equipment used to acquire the data required as input for the model is described in Chapter 4, along with the methods of storage used for the data. The programs which were developed to operate the equipment under the control of a computer, and those for the subsequent off-line analysis of the data, are outlined in the Appendix.

Chapter 5 contains the results of the validation of the general purpose computer model, which verified that the model could produce accurate simulations of the known thermal behaviour of a real object under specified weather conditions. The validation exercise was carried out for two simple structures comprising concrete and asphalt surfaces, and the method used consisted of comparing the diurnal variation of the surface temperatures predicted by the model with those measured by a radiometer. The results of this chapter are also used to evaluate the ability of the model to predict temperature contrasts between the two surfaces.

Chapter 6 contains the results of an attempt to simulate the behaviour of the surface temperature of a vertical south facing sandstone wall, which was a much more difficult modelling problem than was encountered in the validation exercise. It was found that the agreement between the predictions of the model

and measurements made by a radiometer was not so good as for the concrete and asphalt surfaces, and the possible reasons for this are discussed.

In the conclusion, the significance of the results from the previous chapters is discussed, and the current improved design of the equipment used to measure surface temperatures is described. This is followed by suggestions for improvements to the present version of the general purpose model, and finally there is an analysis of the likely directions for the development of future models, taking into account the experience gained in the use of the current model.

Chapter 2   Theory and construction of the general purpose model to simulate

the thermal behaviour of non-vegetated objects.

2.1 Introduction.

The temperatures both at and below the surface of a simple structure will

vary throughout the day due to the magnitude of the net heat flux and whether

it is directed into or out of the structure. This is known as the diurnal

temperature wave, and typically extends to a depth of around 1 m for soil. It

is caused by variations in the heat fluxes incident on the surface of the

structure, which in turn leads to heat being conducted through the structure

from warmer to cooler regions. The type of fluxes which are acting on most

non-vegetated surfaces are shown in Fig. 2.1, and the typical diurnal

variation in these fluxes for a soil surface is shown in Fig. 2.2. The

resulting change in the temperature profile with time of day for a homogenous

soil column is shown in Fig. 2.3.

The general purpose model was developed with the aim of simulating the

temperature variations both at the surface and within a one dimensional

non-vegetated medium under a wide variety of weather conditions. The

temperature profile within the medium is derived from the solution of the

differential equation of heat conduction, subject to boundary conditions at

the surface and a specified depth representing the lower boundary. The

restriction on the use of the model is that it must be possible to assume that

heat transfer only occurs in one direction within the medium, which restricts

the application of the model to certain types of simple one-dimensional

targets. Objects suitable for simulation are basically composed of materials

which are homogenous and have a thermal conductivity which is independent of

position. The model can also be applied to composite structures consisting of

several uniform layers of materials with different thermal properties.

Considering the most common case where the heat flux is vertical, the layers

must have horizontal upper and lower boundaries, with the width in the

horizontal plane being large compared with the depth in the material which is influenced by the diurnal temperature wave. In addition, it must also be possible to assume that there are no internal heat sources in the structure, and that heat transfer does not occur due to water.

In the next section of this Chapter, the heat conduction equation is explained along with a brief description of the types of numerical methods which have been used to solve it. The upper boundary condition for the solution of the equation is obtained from the equation of balance of the heat fluxes acting at the surface, and Section 2.3 contains a description of the parameterisations used to estimate the magnitudes of these fluxes. This is followed by a brief description of the definition of the lower boundary condition. Finally, in Section 2.5, a flowchart for the model is given and the use of the model on a mainframe computer is outlined.

2.2 The heat conduction equation.

Let us consider the structure illustrated in Fig 2.4, which satisfies the conditions for the use of the one-dimensional model outlined in Section 2.1. The one-dimensional equation of heat conduction may be used to represent the heat transfer within the structure, and can be written as follows;

$$\alpha \frac{\partial^2 T}{\partial z^2} = \frac{\partial T}{\partial t} \tag{2.1}$$

Where α is the thermal diffusivity of the material, and is defined by;

$$\alpha = \frac{k}{\varsigma c} \tag{2.2}$$

where; k = Thermal conductivity of the material,

ς = Density,

and c = Specific heat.

Equation 2.1 is a linear homogenous second order partial differential equation, and consists of a first order derivative in time and a second order derivative in distance. The unique solution of the equation for $0 \leqslant z \leqslant h$ in the one-dimensional structure and for $t > 0$ is obtained by specifying the initial temperature profile in the structure at time $t=0$, along with the boundary conditions at the two outer surfaces of the structure with $z=0$ and $z=h$. The boundary condition at the lowest point, $z=0$, is specified by a constant temperature, and can be written as;

$$T(z=0,t) = T_o \qquad (2.3)$$

where T_o is a constant temperature.

The second boundary condition is obtained by specifying the net heat flux at the surface, and is written as,

$$k \frac{\partial T}{\partial z}\bigg|_{z=h} = G \qquad (2.4)$$

where G is the net heat flux,

and $\frac{\partial T}{\partial z}\bigg|_{z=h}$ is the temperature gradient at the surface.

The value of the net flux is calculated from the equation of energy balance, which equates the fluxes acting at the surface. This equation can be written as;

$$S + R + H + L + G = 0 \qquad (2.5)$$

where; S = Total absorbed short-wave solar flux,

R = Net absorbed long-wave flux,

H = Sensible heat flux,

and L = Latent heat flux.

The fluxes are considered to be positive if they are directed towards the boundary between the surface and the atmosphere. Substituting for G in Equation 2.4 leads to the boundary condition taking the form;

$$k \frac{\partial T}{\partial z}\bigg|_{z=h} = S + R + H + L$$

(2.6)

These fluxes are represented in the model by the mathematical parameterisations which are functions of the surface temperature, with the exception of the equations used to calculate the incident short-wave solar flux. When these parameterisations are substituted into Equation 2.6, the result is that the boundary condition becomes a non-linear function of the surface temperature. It is then not possible to solve the heat conduction equation by analytic methods, and it is therefore necessary to use a suitable approximate numerical method to solve it.

The first version of the general purpose model was developed for use on a Tektronix 4052 computer, and used an explicit finite difference method to solve the equation. This had the advantage of simplicity, but the disadvantage that a stability criterion had to be met. This is a function of the vertical step size in the structure between points at which predicted temperatures are required, and the time steps between updating the temperature profile within the structure. It is also a function of the diffusivity of the material from which the structure is composed. For a typical example, assuming a diffusivity between 0.001 and 0.05 cm^2s^{-1}, and a vertical step size of 1 cm, then this imposes the condition that the time step must be less than 60 seconds. As a result of this, a large amount of processing time is required, and combined with the small memory space available in the micro-computer meant that the applications of the model were rather limited. Two other versions of the model were developed in an attempt to overcome this problem, and these used implicit finite difference and finite element methods to solve the heat conduction

equation. These were not restricted in the choice of time step through a stability criterion, but the limitations of the computer still meant that only simple targets could be modelled. This lead to the development of the currently used version of the model, which is designed for use on larger mainframe computers and is written in standard FORTRAN IV. This model was developed from the micro-computer model which used the finite element solution method, and also has improved parameterisations for some of the heat fluxes at the upper boundary.

In terms of the accuracy of the predicted temperatures, there is little to distinguish between any of the solution methods mentioned. A comparison of the temperature predictions of these models for the same surface and under identical weather conditions showed that the predicted temperatures were in agreement to within about 0.1 °C.

2.3 The Upper Boundary Condition.

As mentioned in the previous section, the upper boundary condition is obtained from the energy balance equation at the surface, Equation 2.5. In the following sections, brief descriptions are given of the methods by which the values for these fluxes are obtained in the general purpose model.

2.3.1 The solar flux.

2.3.1.1 The solar flux incident on the surface of the Earth.

The solar flux is the only term in the equation of energy balance which is generated by a source independent of the surface on which it is incident, and while it is acting during the daylight hours has a great amount of influence on the temperatures both at the surface and within the material.

The magnitude of the solar flux incident at the top of the atmosphere varies slightly through the year with changes in the Earth's orbit. Virtually all of the radiation is composed of wavlengths in the range from 1500 nm to

4 μm, and 9% of this is in the U.V. region, 45% is visible light, and 46% is infra-red radiation. The magnitude of the flux reaching the surface is determined by absorption and scattering interactions with the gases and particles present in the atmosphere. The scattered radiation is generally known as the diffuse flux, while the radiation which passes through the atmosphere without interacting is referred to as the direct flux.

Scattering of the solar flux is caused mainly by dust particles and air molecules. If the diameter of the scattering centre is less than one tenth of the wavelength of the incident radiation, then wavelength dependent Rayleigh scattering will occur. However, if the particles are larger, then the scattering becomes independent of wavelength. About 6% of the flux incident at the top of the atmosphere is scattered back into space, while about 20% reaches the surface as diffuse solar flux.

The absorption of solar flux by atmospheric constituents occurs in two main wavelength bands. Almost all of the incident radiation with wavelengths below 3000 nm is absorbed by ozone and oxygen (O_2) molecules, while the primary causes of absorption of wavelengths above 7000 nm are water vapour and carbon dioxide molecules. The energy absorbed in this way is re-emitted as longer wavelength infra-red radiation, and the resulting flux reaching the surface of the earth is dealt with in Section 2.3.2.

So far, it has been assumed that the atmosphere is free from clouds. However, clouds are usually present to some degree and affect the solar flux in three ways. They refect a proportion of the flux back into space, and increase the diffuse flux component through scattering within the cloud. The water vapour in the clouds also absorbs solar energy. The amount of influence that they have on the magnitude of the solar flux reaching the surface depends on the type of cloud and such factors as their height and thickness. A wide range of types of cloud are commonly observed, and range from thin, high altitude clouds to thick, low level stratus types. The former has the least effect on the solar flux, while the latter interacts very strongly, and does

not allow any direct solar radiation to reach the surface.

It is clear that the interaction between the solar flux and the atmosphere is very complex, and it is therefore difficult to simulate this behaviour accurately. The general purpose model includes a separate mathematical model as a basis for the calculation of the solar flux. This was created by Lacis and Hansen in 1974, and uses empirical relationships to take into account the effects of scattering and absorption by water vapour and ozone. Absorption due to carbon dioxide and molecular oxygen is not included as their combined effect is assumed to be negligible. There are two main advantages to recommend the use of this model. Firstly, because it is relatively simple, it does not require a large amount of computer memory space or a long processing time. Secondly, the empirical relationships are in terms of meteorological parameters which are commonly recorded at most weather stations, such as the wet and dry bulb depression and the air pressure.

The end result of the model is a prediction of the solar flux which would arrive at the specified plane under a cloudless sky. As discussed previously, the effects of clouds can not be ignored, so the predicted flux therefore needs to be modified to take their effects into account. This is not a simple task, as cloud formations may change rapidly and accurate observations are difficult and generally infrequent. A simple approach was chosen in the general purpose model, where the predicted flux was multiplied by a short-wave cloud cover factor. The value of this factor can be obtained from data provided by Kondratyev, 1969, and depends on the solar elevation and the type of cloud obscuring the sun. A more detailed description of the significance and effects of this parameter on the temperature predictions of the model is given in Section 3.3.6.3 of Chapter 3, which is concerned with the sensitivity analysis carried out on the general purpose model.

The simple model described in the previous paragraphs will give a reasonable estimate of the solar flux, but if greater accuracy is required, it is necessary to make direct measurements of the flux with a solarimeter.

However, the latter is only possible for certain applications of the model, which include, for example, the validation of the model described in Chapter 5.

2.3.1.2 Absorption of the solar flux.

The solar flux incident on a surface consists of the direct and diffuse components described in the previous section, and has to be split into these components in order to calculate the net absorbed flux. This is necessary for two main reasons. Firstly, the effective albedo of the surface is different for the two components, and secondly, if the surface of interest is not horizontal, the incident direct flux component will depend on the angle of inclination of the surface.

In general, the albedo is a function of the angle that the sun makes with the normal to the surface, z, and typical examples of this variation for different surfaces are shown in Fig. 2.5. This behaviour is represented in the model by the Fresnel reflection characteristic,

$$\alpha (z) = \alpha_o + (1 - \alpha_o) \times \exp (-0.1 \times (90-z)) \qquad (2.7)$$

where α_o is the albedo of the surface as z approaches $0°$.
The value of the solar zenith angle is calculated through an equation which depends on such factors as the inclination and azimuth angles of the surface which may be easily measured. The derivation of the relevant equation by a geometerical method is explained in some detail by Sellers, 1965.

The diffuse flux is considered to be isotropic, and is calculated from the equation given by Kahle, 1977,

$$S_D = (0.15 - 0.1 \cos(z)) \times S_T \qquad (2.8)$$

where S_T is the total short-wave flux incident on a horizontal surface.

The albedo of the surface for the incident diffuse flux is given by
özisik, 1973, and is obtained from summing the ratio of the incident to the
reflected fluxes over the 180° possible range of angles of incidence.

$$\alpha_D = 0.5 \times (1 + \alpha_o) \qquad (2.9)$$

Hence the diffuse flux absorbed by the surface is,

$$A_D = S_{D^o} \times (1 - \alpha_D) \times f \qquad (2.10)$$

where f is the fraction of the sky that is unobscured as viewed from the
surface.

In the case of the direct flux, the component absorbed by a surface with
solar zenith angle i is simply,

$$A_I = S_I \times (1 - \alpha(i)) \qquad (2.11)$$

where S_I is the incident direct flux component normal to the surface.
The value of S_I is assumed to be zero if the sun is obscured by clouds, or is
otherwise calculated in the general purpose model by subtracting the value of
the diffuse flux component calculated in Equation (2.8) from the total flux
incident on the surface. If necessary this may then be multiplied by the
appropriate factor to transfer from a horizontal to an inclined surface, i.e.

$$S_I = (S_T - S_D) \times \frac{\cos(i)}{\cos(z)} \qquad (2.12)$$

where i is the solar zenith angle for an inclined surface, and z is the angle
for a horizontal surface.

The third source of short-wave flux incident on a surface consists of
radiation which has been reflected from the surroundings. This can be

considered as diffuse flux, is assumed to be approximately given by,

$$A_R = S_T \times \alpha \times (1 - \alpha_D) \times (1 - f) \qquad (2.13)$$

where α is the average albedo of the material surrounding the surface.

In summary, the total flux absorbed by the surface consists of the three components described above, and is therefore given by,

$$S = A_I + A_D + A_R \qquad (2.14)$$

2.3.2   The long-wave flux.

2.3.2.1 Radiation emitted from the surface.

The surface of the earth has an average temperature of about 285 K due to the heating effect of short-wave radiation, which results in it acting as a source of long-wave radiation. It is assumed to behave as a grey body, and most of the radiation is emitted in the range from 4 to 50 µm, with a maximum at about 10 µm. The magnitude of the emitted flux is given by the Stefan-Boltzmann law,

$$\text{Radiative Flux} = e \, \sigma \, T^4 \qquad (2.15)$$

where T is the temperature of the surface,

   σ is the Stefan-Boltzmann constant,

  and e is the infra-red emissivity.

The value of the infra-red emissivity depends on the type of surface from which the radiation is being emitted. It is in the range from 0 to 1, with the upper limit corresponding to a black body emitter. The value of the emissivity also varies with angle in a similar manner to that shown by the short-wave albedo, and this is expressed by Paltridge and Platt, 1974, as,

$$e(z) = e_0 \times (1 - \exp(-0.1 \times (90-z))) \qquad (2.16)$$

where e_0 is the emissivity when the viewing angle with the normal, z, is $0°$.

The net long-wave flux at the surface of the earth is the result of three components. This can be expressed in the following equation;

$$\text{Net Radiation} = \text{Terrestrial Radiation} - \text{Counter Radiation}$$
$$- \text{Radiation from Surroundings} \qquad (2.17)$$

The first component is simply given by the Stefan-Boltzmann law (Equation 2.15), while the other two are more difficult to calculate, and are explained in more detail in Sections 2.3.2.2 and 2.3.2.3.

2.3.2.2 Counter radiation.

The counter radiation is the downward flux of long-wave radiation which is emitted by atmospheric constituents and clouds. The atmosphere absorbs about 91% of the terrestrial radiation emitted by the surface of the earth, while the remainder is lost to space through the atmospheric window between 8.5 and 11 μm. The main absorbers of the radiation are water vapour, and to a lesser extent ozone and carbon dioxide. They re-radiate a proportion of the absorbed energy back towards the surface of the earth also as infra-red radiation, 90% of which originates in the lowest 800 to 1600 m of the atmosphere. This flux is usually expressed as a function of the air temperature at screen height, i.e.,

$$\text{Radiative Flux} = e_1 \, \sigma \, T_1^4 \qquad (2.18)$$

where T_1 is the air temperature,

and e_1 is the effective emissivity of the atmosphere.

As the atmospheric constituents are selective absorbers and emitters of

radiation, their emissivity is dependent on the wavelength of the radiation. The effective emissivity of the atmosphere is therefore used to represent the average emissivity over the entire range of wavlengths in the long-wave spectrum considered, and will depend on the relative concentrations of the absorbing gases. The value of this parameter is evaluated from an empirical expression in terms of more readily measureable quantities. Many such expressions have been proposed, and in the general purpose model an equation suggested by Idso, 1981, is used. This is written as,

$$e_1 = 0.70 + 5.95 \times 10^{-5} \times p \times \exp(1500/T_1) \qquad (2.19)$$

where T_1 is the air temperature at screen height,

and p is the vapour pressure in millibars.

When there are clouds in the sky, there will be a further contribution to the downward flux. This flux is calculated using the method suggested by Kimbal et al., 1982, where the cloud radiation is assumed to be transmitted only through the 8 to 14 µm atmospheric window. The atmospheric component of the flux is assumed to be unaffected by the presence of clouds, as most of the flux emitted by the atmosphere originates at levels below normal cloud base heights. The flux calculated by using empirical equations in terms of parameters such as the cloud base height and degree of cloud cover. The latter parameter is represented in the general purpose model by the long-wave cloud cover factor, the value of which ranges from zero for a clear sky to one for complete, dense cloud cover. The value of this factor is derived from radiometer measurements of the sky as described in Section A.3.1.2. The value of the flux is finally multiplied by the fraction of the sky which is visible from the surface of interest.

2.3.2.3 Radiation from surrounding objects.

The sources of this radiation flux are the objects which may obscure the field of view of the sky from the surface of interest, and typically include trees, bushes, and buildings. Two main assumptions are made in order to

simplify the calculation of the value of this flux. Firstly, it is assumed that the radiation is contained entirely within the 8 to 14 µm band. Secondly, that the radiation behaves as if it was generated by a single black body, with the surface temperature equal to the average of the surface radiation temperatures of the surrounding objects. The equation used to determine the flux is written;

$$\text{Radiation from Surroundings} = 0.5 \times \sigma \times T_2^4 \times f_8 \times (1-f) \qquad (2.20)$$

where T_2 is the average surface temperature,

f_8 is the fraction of radiation emitted in the 8 to 14 µm band,

and $(1-f)$ is the fraction of sky obscured.

The factor of 0.5 arises from integrating the fluxes arriving from elements over the surface of a hemisphere, and the value of f_8 is obtained from an equation used by Kimbal et al., 1982, in their analysis of the flux arriving from clouds.

2.3.3 The sensible heat flux.

The sensible heat flux consists of the flow of heat between the ground or the surface of interest and the atmosphere. The diurnal variation of this flux is shown in Fig. 2.2. It is usually directed away from the surface during the day, and in the opposite direction at night when the air temperature is warmer than the surface temperature.

There are two mechanisms by which heat is transferred between the atmosphere and the surface. A thin laminar boundary layer extends for a few millimetres from the surface, and within this region, energy transfer takes place by molecular conduction under the influence of high temperature gradients. As the distance from the layer is increased, energy transfer by turbulent eddies rapidly becomes the dominant process for energy transfer. The magnitude of the flux is calculated from an equation used by Khale, 1977,

$$H = \rho \times c_p \times C_D \times W \times (T_1 - T_2) \qquad (2.21)$$

where T_1 is the air temperature at a height of 1.5 m,

T_2 is the surface temperature,

W is the windspeed corrected for gustiness, equal to the measured windspeed with 2 m/sec added,

C_D is the drag coefficient,

c_p is the specific heat capacity of dry air at constant pressure,

and ρ is the density of air at the surface.

The drag coefficient, C_D is evaluated from;

$$C_D = 0.002 + 0.006 \times (Z/5000) \qquad (2.22)$$

where Z is the altitude of the surface above sea level.

2.3.4 The latent heat flux.

The latent heat flux is normally directed towards the atmosphere, and is due to water evaporating from a wet surface. Alternatively, when water vapour condenses from the atmosphere onto the surface to form dew, the flux will then act in the opposite direction.

The mechanisms by which water vapour is transferred between the atmosphere and the surface are similar to that described for the sensible heat flux. In this case, the water vapour molecules move across the boundary layer under the influence of a vertical humidity gradient. As the distance from the layer is increased, the dominant process then becomes turbulent transfer.

The parameterisation used for this flux was obtained from Khale, 1977, and is expressed as,

$$L = \rho \times C_D \times W \times 1 \times (q_2 - q_1) \qquad (2.23)$$

where l is the latent heat of evaporation,

q_1 is the mixing ratio of the air at a height of 1.5 m,

q_2 is the mixing ratio of the air at the ground,

and W, ϱ and C_D are as defined in Section 2.3.3.

The mixing ratio of the air at the ground is evaluated from;

$$q_2 = M \times q'$$
(2.24)

where M is the moisture factor,

and q' is the saturation mixing ratio of the air at the temperature of

the surface.

The moisture factor, M, represents the state of saturation of the surface with values ranging from zero for a dry surface to one if the surface is totally saturated. The value of the mixing ratio is obtained from;

$$q = \frac{0.622 \times v}{(p-v)}$$
(2.25)

where v is the vapour pressure at 1.5 m,

and p is the atmospheric pressure.

2.3.5 The net heat flux into the structure.

Heat is tranferred by conduction through the material of the structure under investigation, and assuming the effects of heat transport due to moisture can be ignored, then Equation 2.4 may be used to describe this flux in terms of the conductivity of the material and the temperature gradient at the surface. In the general purpose model, the magnitude of the flux is calculated by solving the heat balance equation, Equation 2.5, with the net flux as the unknown quantity. The values for the other fluxes in this equation are obtained by using the parameterisations described previously.

2.4 The lower boundary condition.

As stated in Section 2.2, the lower boundary condition is specified by a constant temperature at a fixed depth beneath the surface of the structure, and it is assumed that there are no heat fluxes passing through this level in either direction. If sources of heat within the structure can be ignored, then the lower boundary will be located at a depth greater than or equal to the lowest point influenced by the diurnal temperature wave. The minimum depth for the lower boundary depends on the materials of construction involved, but it is typically about 1 m for soil. This is illustrated in Fig. 2.3, which shows the typical behaviour of the diurnal temperature wave in a soil column.

2.5 Construction and application of the model.

Apart from the choice of the numerical method used to solve the differential equation of heat conduction, all of the versions of the model mentioned in Section 2.2 are basically constructed in the same way. A flowchart showing the general method by which the model predicts temperatures at the surface and within the material is given in Fig. 2.6.

The use of the mainframe general purpose computer model is extremely simple, and only requires the creation of a data file containing the values for parameters used by the model. The nature of these parameters are briefly outlined in Table 2.1, and consist of either time independent or time dependent values. The latter are specified in the data file along with the time at which they were recorded. The first part of the program reads in the parameter values from the data file, and assigns these values to the appropriate variables. The next section of the program is only important if an explicit finite difference method is being used to solve the equation of heat conduction, and checks that the stability criterion is satisfied. The following section uses linear interpolation between the time dependent data points to estimate the values of the parameters at the specified time intervals from the beginning to end of the modelling period. For all of the

applications of the model described in later chapters, the 24 hour modelling period ran from noon to noon, and the time interval was 15 minutes. This was chosen to coincide with the frequency at which weather measurements were recorded, and it was also roughly the same as the frequency with which measurements of the cloud cover factor and representative temperature of the surroundings were made. If the incident solar flux is not input as data, then this is calculated at the required time intervals using the method described in Section 2.3.1.

The next part of the program is concerned with the prediction of the surface temperatures and the temperature profile within the structure, which is obtained by solving the heat conduction equation as described in Section 2.2. The procedure is illustrated in Fig. 2.6, and is repeated to calculate the updated values at the specified time interval. Finally, a summary of the predicted temperatures is printed, and if applicable these can be compared with temperatures measured by a radiometer.

Table 2.1   Data required as input for the model.

Time independent parameters.

1. Physical properties of the target.

Material and surface properties.

Geographical location and inclination of the surface.

Initial temperature profile within the structure.

Temperature at the lower boundary point.

2. Parameters determining the output of the model.

Starting time and duration of the modelling period.

Time interval between predicting updated temperatures.

Time dependent parameters.

1. Recorded at fixed intervals by weather station.

Weather conditions at the site.

Short-wave cloud cover factor;

(estimated from solarimeter measurements.)

2. Derived from measurements made by the radiometer.

Representative temperature of the surroundings.

Long-wave cloud cover factor.

Measured surface temperature;

(for comparison with the predictions of the model.)
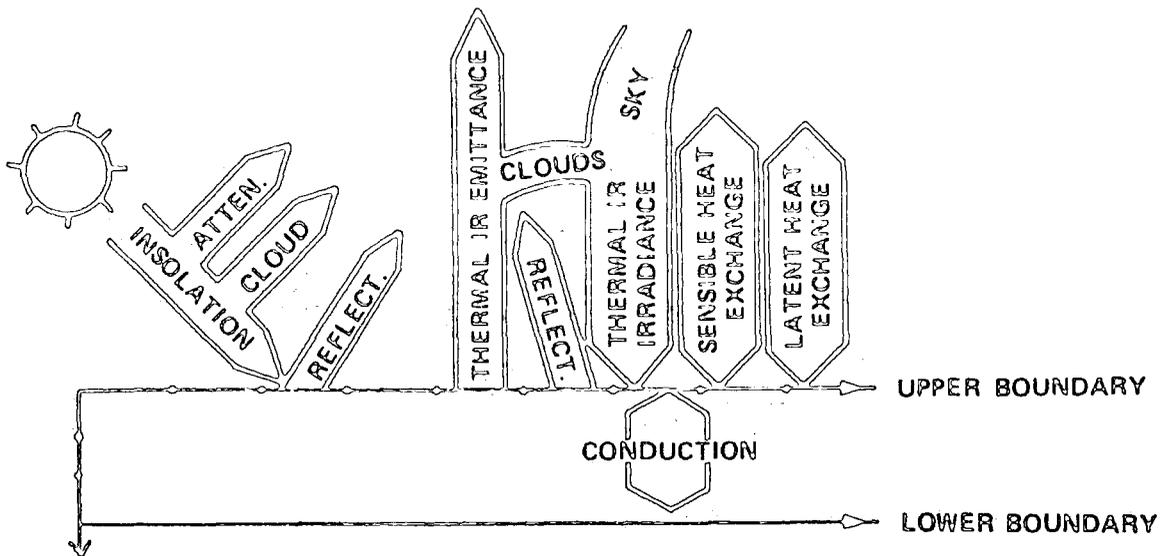
Fig. 2.1   Fluxes incident on a non-vegetated surface.

(Adapted from Balick et al., 1981.)
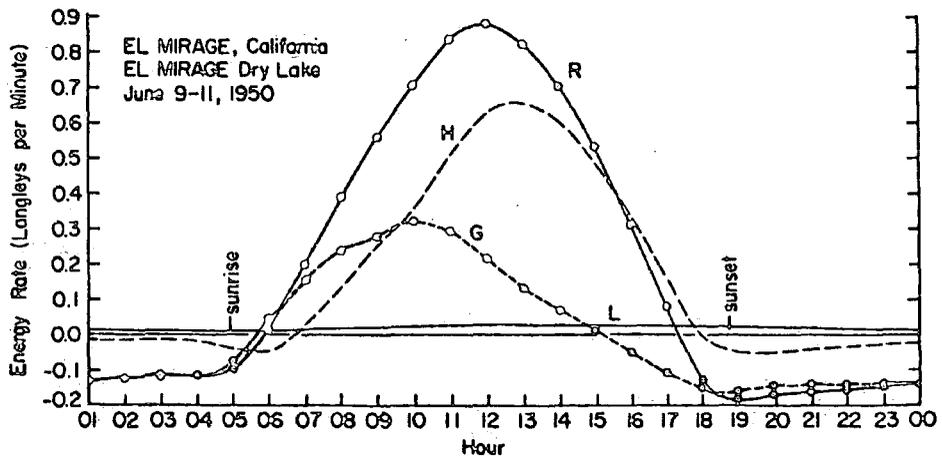
KEY

R = Net difference between the absorbed short and
    long-wave fluxes and the emitted long-wave flux.
G = Net flux into the ground.
L = Latent heat flux.
H = Sensible heat flux.

(1 Langley.min^{-1} = 697.6 Wm^{-2})

Fig. 2.2   Typical diurnal variation of fluxes acting on a

soil surface.

(From Sellers, 1965.)
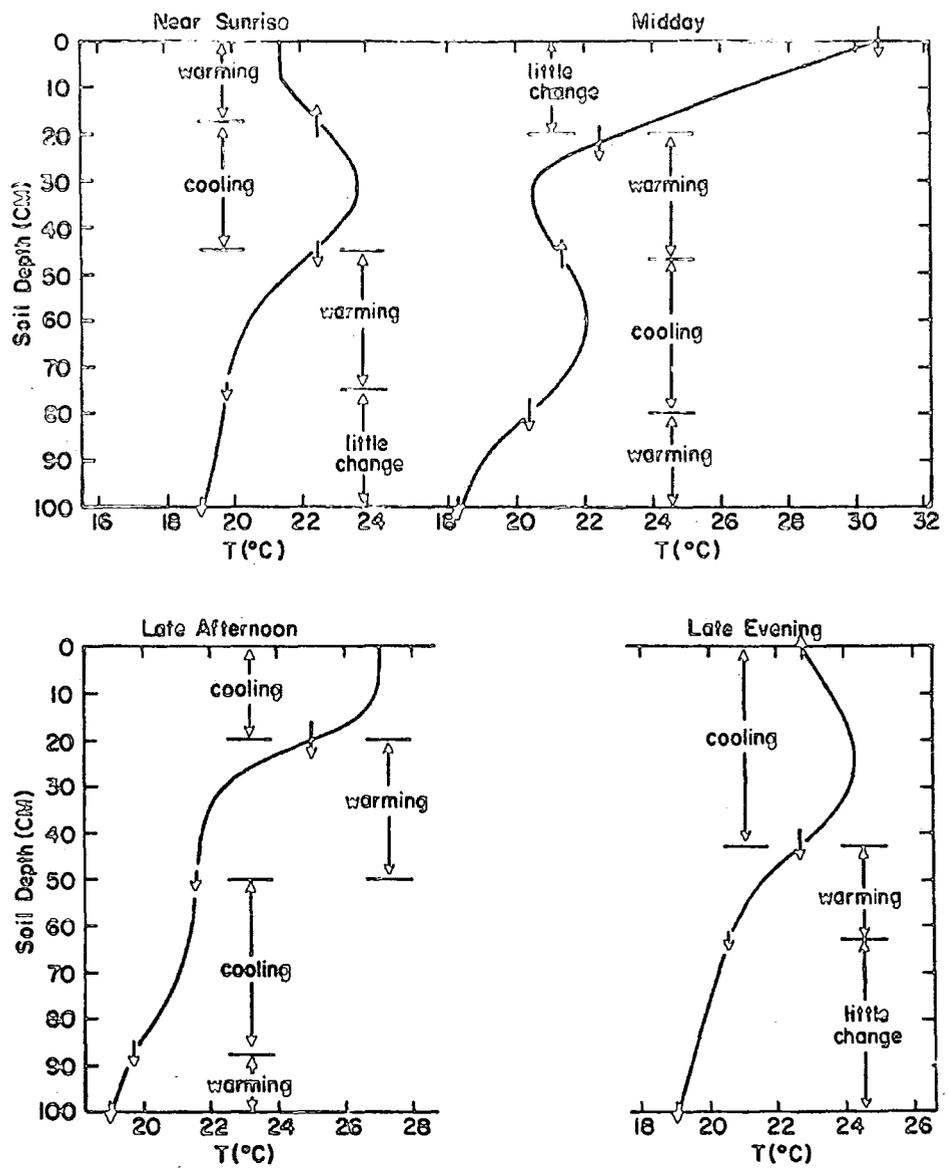
Fig. 2.3 Typical diurnal variation of the temperature profile within a column of soil.

(From Sellers, 1965.)
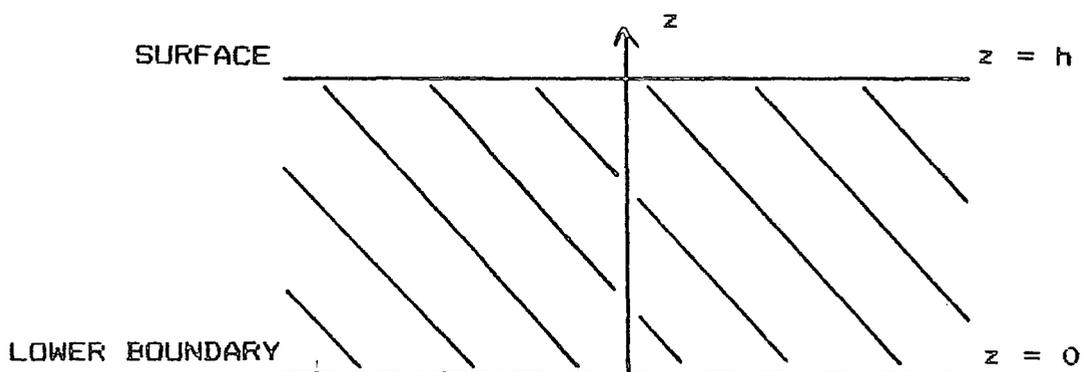
Fig. 2.4 The one-dimensional structure for which the temperature profile is to be determined.
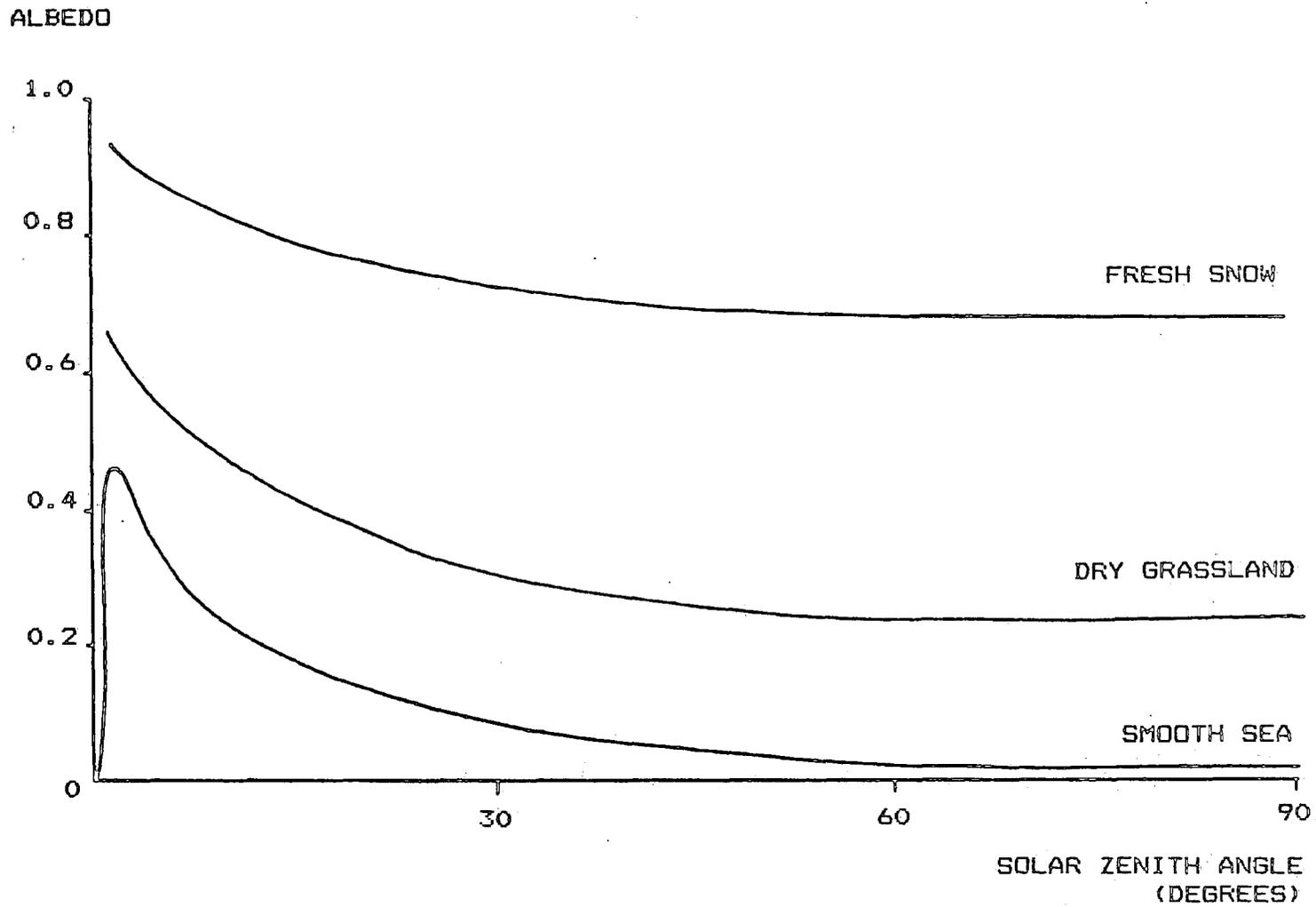
Fig. 2.5 Examples of the variation of albedo with solar zenith angle for different surfaces.
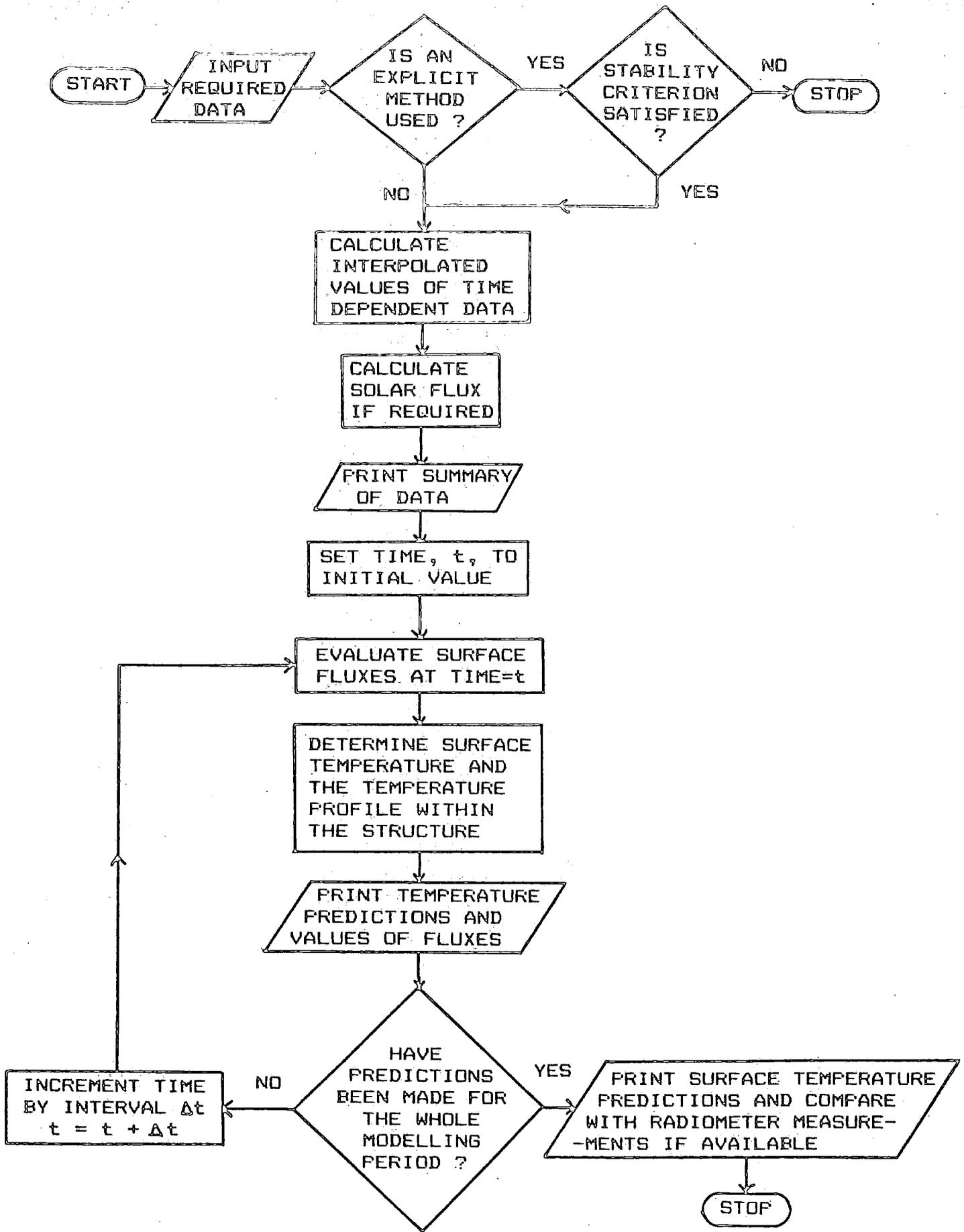
Fig. 2.6   Flowchart for the general purpose model.

Chapter 3 Sensitivity analysis of the general purpose model.

3.1 Introduction.

A sensitivity analysis was carried out on the general purpose model which is used on a mainframe IBM 4341 computer. The reason for this exercise was to evaluate the effects produced in the temperature predictions of the model by changes in both the surface and material properties of the target of interest, and changes in the local weather conditions. The results can then be used to determine which of the parameters need to be measured most accurately. In cases where the parameter can only be estimated with a low degree of accuracy, for example the cloud cover factors or the amount of surface moisture on the target, the results of the analysis will show the uncertainty in the temperature predictions of the model introduced by errors in the estimation of these parameters.

The first stage in the sensitivity analysis was to set up a file containing data for a suitable target over a 24 hour period. The parameters used for this standard day are described in more detail in the next section, but generally fall into two main categories. Firstly those which are basically constant, such as the parameters which describe the characteristics of the site and the materials of composition of the target, and secondly parameters which exhibit a variation in magnitude over the 24 hour period, such as the incident short-wave solar flux.

The sensitivity analysis was carried out by varying one of the parameters in the data file at a time through the range of values likely to be normally encountered, while keeping the other parameters fixed at the values used to obtain the standard prediction. The restriction of altering only one parameter at a time was chosen to simplify the analysis. This was necessary as the number of possible combinations of different parameter values would be very large. There is also the added advantage that the variation of only one of the parameters means that its influence on the model temperature prediction can be

seen very easily. The results of the analysis are discussed in Section 3.3, and graphs are included to show the variation of the predicted diurnal surface temperature wave with changes in certain parameter values.

3.2 Values of parameters used in the standard prediction.

In this section, the values of the parameters used as input for the model will be given. These values were used to set up the standard prediction of the diurnal surface temperature wave for the target.

3.2.1 Properties of the concrete target and its surroundings.

The target used for this analysis was constructed as shown in Fig. 3.1, and consisted of a concrete surface with layers of gravel and soil beneath. Each of the layers was assumed to be homogenous and to be of uniform thickness. The thermal properties of these materials were obtained from the results of measurements made by Balick et al., 1981, and are listed in Table 3.1. Table 3.2 gives the relevant surface properties for concrete. The albedo and emissivity are typical values for concrete, and as the surface was assumed to be dry, the moisture factor was set to zero.

The concrete target was assumed to be located in an exposed site, at an altitude of 133 m above sea level. The surface of the target was horizontal with azimuth and inclination angles of 0°, and not shaded from the sun by obstructions. The geographic location was taken to be Ouston, Northumberland, which is at a latitude of 55° N. The 24 hour period for the standard temperature prediction was taken to be from 12:00 21st April to 12:00 22nd April 1982.

The initial temperature profile was obtained by the following procedure. Firstly the temperature profile throughout the composite structure was set to a uniform value. This was arbitrarily chosen to be the same as the temperature at the lower boundary, which was derived from the soil temperature measured at

a depth of 1 m at Durham Observatory over the 24 hour period. The other parameters in the input data file for the model were set to the values chosen for the standard prediction, which are given in this section and in Section 3.2.2. After running the model with this initial profile, the final predicted profile at the end of the 24 hour period was used to replace the original and the model run again with the same meteorolgical conditions and values for the other parameters. This was repeated until a stable predicted temperature profile in the material was obtained, such that running the model with these values generated a final profile at the end of the 24 hour period which agreed with the initial case to within around 0.1 °C. The resulting predicted diurnal surface temperature wave for the target was then taken as a standard for comparison with the results obtained when parameters in the data file were varied. However, if there was a change in the construction of the target, for example when the thickness of the layers of material were varied, then a new profile was formed by the method described above. The initial temperature profile which was used for the standard prediction is shown in Fig. 3.2.

Table 3.1   Material properties of the constituents of the target.

Material	Conductivity	Diffusivity
Concrete	1.54 W m^{-1} K^{-1}	7.2 x 10^{-7} m^2 s^{-1}
Gravel	3.00 W m^{-1} K^{-1}	8.0 x 10^{-7} m^2 s^{-1}
Soil	0.70 W m^{-1} K^{-1}	4.7 x 10^{-7} m^2 s^{-1}

Table 3.2   Surface properties of concrete.

Parameter	Value
Vertical albedo	0.30
Vertical emissivity	0.97
Moisture factor	0.00

3.2.2 Meteorological conditions.

The weather conditions were specified every 15 minutes in the data file, and, apart from the incident solar flux, were assumed to have constant values during the 24 hour period of interest. These values are given in Table 3.3, along with the other meteorological data required by the model. The sky was assumed to be clear, so both the long-wave and short-wave cloud cover factors are zero. The incident solar flux on the concrete was predicted by the model using the parameterisation of Lacis and Hansen, 1974, as described in Section 2.3.1.

Table 3.3   Meteorological conditions used for the standard prediction.

Parameter	Value
Air temperature	10 °C.
Wet and dry bulb depression	2 °C.
Wind speed	5 m s^{-1}.
Long-wave cloud cover factor	0
Short-wave cloud cover factor	0
Cloud base height	500 m.
Density of air	1.25 kg m^{-3}.
Atmospheric pressure	1000 mb.

3.3 Results of the sensitivity analysis.

The results of the analysis are summarised in Table 3.4, and discussed in the following sections.

Table 3.4 Relative sensitivities of surface temperature predictions
to changes in parameter values.

Most sensitive.

Air temperature   Windspeed

Vertical emissivity   Vertical   albedo

Moderately sensitive.

Conductivity of the top layer   Density of air

Thickness of the top layer   Surface altitude

Slightly sensitive to insensitive.

Wet and dry bulb depression   Surface atmospheric pressure

Conductivity of second layer   Thickness of second layer

Conductivity of third layer   Diffusivity of all layers

Initial temperature profile   Lower boundary condition

3.3.1   Site characteristic parameter.

3.3.1.1 Surface altitude.

The results of the sensitivity analysis for altitudes   ranging   from   sea
level to 1500 m are plotted in Figure 3.3, and it can be seen that the
differences between the predicted temperatures   for   different   altitudes   are
larger during the day than at night. This behaviour occurs as a result of the
dependence of the sensible and latent heat fluxes on the surface altitude, via
the empirical drag coefficient, C_D. The surface altitude is used to   evaluate
the   drag   coefficient   as   shown   in Equation 2.22, which is then used in the
sections of the model concerned with the calculation of the sensible and
latent heat fluxes. An explanation of how these fluxes influence the predicted
temperatures is given in Section 3.3.5.2, with reference to the sensitivity
analysis carried out on the value of the windspeed.

3.3.2   Surface parameters.

3.3.2.1 Vertical emissivity.

The model predictions were found to be very sensitive to this parameter, and the results of the sensitivity analysis are plotted in Fig. 3.4. The graph shows that a change in the emissivity of the surface produces a uniform change in the predicted temperature over the 24 hour period. It can also be seen that as the emissivity is increased or decreased from the value used in the standard prediction, then the predicted temperature will show a corresponding increase or decrease.

3.3.2.2 Vertical albedo.

The model predictions are also very sensitive to this parameter, and the results of the sensitivity analysis are plotted in Fig. 3.5. It can be seen from the graph that the variation of this parameter has greatest effect during daylight hours, when decreasing the albedo causes the predicted temperatures to rise as additional short-wave radiation is absorbed. At night, the incident short-wave solar flux is zero, so the predictions are independent of the albedo.

3.3.3   Material parameters.

3.3.3.1 Conductivity of the top layer.

The effects of altering the conductivity of the top layer of the three layer composite structure are shown in Fig. 3.6. It can be seen that a variation of 30% from the value used for the standard prediction is required to produce a maximum change in predicted temperatures of 1 °C. Other predictions plotted on this graph show the effects of larger changes in the conductivity, and correspond to the results which would be obtained if a material other than concrete was used for the top layer of the structure.

3.3.3.2 Conductivity of the second layer.

The model was found to be much less sensitive to changes in this parameter. It was found that an increase of 100% or decrease of 50% in the value used for the standard prediction was required to produce a maximum change in predicted temperatures of 1 °C. Both of these extreme cases correspond to a change in the material of construction of the layer, and therefore it can be assumed that the model is insensitive to changes in the value of this parameter within the range of likely values for the given material of construction.

3.3.3.3 Conductivity of the third layer.

The model was found to be insensitive to even large variations of this parameter.

3.3.3.4 Diffusivity of the top layer.

The predictions from the model were found to be relatively insensitive to increases of up to 100% in this parameter. However, when a lower value was used, the predictions started to show a distinct difference from the standard case after the parameter was decreased by over 50%. However, as mentioned previously in Section 3.3.3.2, variations of this magnitude would correspond to a change in the material of construction.

3.3.3.5 Diffusivity of the second and third layers.

The model predictions were found to be insensitive to variations in the values of both of these parameters.

3.3.3.6 Thickness of the top layer.

Variation of this parameter requires a change in the structure of the target. When the thickness of the top layer is changed, the thickness of the third layer is adjusted to keep the total depth of the structure being

modelled to the original figure of 1 m. The thickness of the middle layer is not changed.

The method used to carry out the sensitivity analysis was to first define the new structure, and set the initial temperature profile to a constant value of 10 °C throughout. The method described in Section 3.2.1 was used to obtain a stable profile in the structure, and the temperature predictions for the 24 hour period could then be compared with those of the standard prediction.

The results obtained are shown in Fig. 3.7. It can be seen that the model is not very sensitive to increases in the thickness of the layer; a 100% increase produces a maximum change in the prediction of 1 °C. However, the model is more sensitive to decreases in the layer thickness, with the same change in the temperature predictions being produced by a decrease in thickness of 60%. This is not surprising as the material properties of the second layer are significantly different from those of the top.

3.3.3.7 Thickness of the second layer.

The sensitivity analysis for this parameter was carried out in the same way as described in the previous section. In this case however, the thickness of the middle layer of the composite medium was varied, while the thickness of the top layer was kept constant, and the thickness of the third layer adjusted to keep the total thickness of the structure being considered to a value of 1 m.

The results of the analysis showed that the temperatures predicted by the model were insensitive to variations of this parameter, provided that the thickness of the layer was not reduced by much more than 50% of the value used in the standard prediction.

3.3.4 Initial temperature profile and lower boundary condition.

3.3.4.1 Initial temperature profile.

This consists of a series of temperatures at given depths in the

structure, at the time corresponding to the start of the modelling period. The lowest point for which a temperature is specified is chosen to coincide with the lower boundary, and therefore is represented by a constant temperature. The profile is updated by the model at a specified time interval during the modelling period. The time interval was chosen to be 15 minutes for most applications of the model, as this produced a good idea of the thermal behaviour of the structure without requiring a large amount of computer time.

The depth of the points for which the temperature data are given in the initial profile are determined by firstly splitting the structure into a series of planar layers, or elements, of a given thickness. The number of points in the element for which temperatures are to be given initially, and later updated by the model, is then specified. These points, or nodes, are spaced with equal separations through the element, and include the top and bottom surfaces. The restriction on the choice of the thickness of the elements is that they must contain homogenous material, and they are generally chosen to coincide with layers of particular interest in a multilayered structure. Most materials with low heat conductivities exhibit the greatest variation of temperature close to the surface, so small element lengths of about 0.5 cm are chosen. As the depth increases, so the influence of the energy balance at the surface decreases, and larger element lengths are chosen. Typically this may be up to 40 cm for the element with the lower boundary at its lower surface.

The temperature profile at the start of the modelling period was calculated by using the method described in Section 3.2.1. In the case of the standard prediction, it was assumed that there was initially a constant temperature of 7.7 °C throughout the structure, and six repetitions of the method were required to produce the stable profile which was subsequently used. For the purposes of the sensitivity analysis, it was decided to repeat the process described above using two different values for the initial constant temperature throughout the structure. When a value of 0 °C was

assumed, a stable temperature profile was obtained after nine repetitions of the method, while only three repetitions were required when the initial temperature was changed to 15 °C. The resulting three stable profiles had surface temperatures which agreed to within about 0.3 °C, and the surface diurnal temperature waves predicted by the model over the 24 hour period were found to be very similar, with a maximum difference of about 0.5 °C. However, the differences became larger as the depth below the surface increased, until at the lower boundary the temperatures were fixed at the values of 0 °C, 7.7 °C, and 15 °C as specified originally.

These results suggest that as long as a reasonable idea of the temperature is known at some point in the structure under investigation, and provided there are no restrictions on the number of times that the model may be run in order to obtain a stable initial temperature profile, then the surface diurnal temperature wave predicted by the model is reasonably independent of the initial temperature profile. However, if it is required to predict the temperature at a particular depth in the structure, then clearly the initial temperature profile will have proportionately more influence on the resulting temperature predictions as the depth increases.

3.3.4.2 Lower boundary condition.

The solution of the one dimensional equation of heat conduction requires two boundary conditions to be specified. The lower boundary condition is defined by a constant temperature at the lower boundary point, which is located at the greatest subsurface depth in the structure to which predicted temperatures are required. This is usually chosen to be 1 m, which is the typical limit of the depth to which the diurnal temperature wave penetrates natural materials such as soil. It is therefore possible to assume a constant temperature at this depth over the 24 hour period to be modelled.

The lower boundary temperature is specified as the last value in the initial temperature profile for the structure to be modelled. The sensitivity

analysis was carried out by changing this temperature, and then running the model using the modified profile. Values of 1 °C and 10 °C were chosen for comparison with the standard prediction, which used a temperature of 7.7 °C obtained from measurements at a depth of 1 m made at Durham Observatory over the 24 hour period of interest.

The results of the analysis showed that the surface temperature predictions of the model were insensitive to variations of this parameter, and that the final temperature profile in the structure was only affected at depths greater than 60 cm.

3.3.5 Meteorological parameters.

3.3.5.1 Air temperature.

As shown in Fig. 3.8, the model predictions are very sensitive to air temperature. The sensitivity is such that a change in the air temperature of 5 °C gives rise to a change in the same direction of about 4 °C in the predicted temperatures. This high sensitivity arises because the air temperature is used in many calculations in the program. For example, it affects the calculated value of the incident solar flux through the dependence of the amount of water vapour in the air on the air temperature. Other fluxes which are calculated using the air temperature are the sensible heat flux, the latent heat flux, and the net long-wave flux.

3.3.5.2 Windspeed.

This parameter is used in the calculations to determine the sensible heat flux and the latent heat flux, although the latter can be ignored as it is zero over the 24 hour period considered. The results of the sensitivity analysis are shown in Fig. 3.9. It can be seen from the graph that the model is very sensitive to changes at low windspeeds, but becomes less sensitive as the windspeed is increased. The reduction in sensitivity arises because of the dependence of the sensible heat flux on the windspeed and the difference in

temperature between that of the surface and free air, as shown in Equation 2.21. As the windspeed increases, the temperature difference between the surface and free air will decrease as the surface contact temperature approaches the constant air temperature of 10 °C. This results in a reduction in the variation between the maximum and minimum predicted temperatures as the windspeed is increased, as shown on the graph.

The other feature shown by the graph is that changes in windspeed have the greatest effect on the predicted temperatures during the day. This is when the sensible heat flux has a maximum value due to the surface temperature being much higher than the air temperature. The heat flux is directed upwards, and heat is transferred by warm air rising from the hot surface to the cooler surrounding air. After sunset, the surface starts to cool, and the sensible heat flux decreases until the temperature of the surface falls below the air temperature. The heat flux then acts in the opposite direction, although with a magnitude much smaller than the daytime values. This is because of the reduced temperature difference between the surface and air at night, and the fact that heat transfer from the air to the surface is reduced because warm air tends to rise rather than fall. It is therfore apparent that as the magnitude of the sensible heat flux is lower at night, then the importance of the windspeed in determining the predicted surface temperature will be correspondingly reduced.

3.3.5.3 Wet and dry bulb depression.

This parameter is used in the model to determine the vapour pressure of the air and the saturated vapour pressure at the given air temperature. These two quantities can be used to calculate the relative humidity of the air. This is obtained from Equation 3.1, and is usually expressed as a percentage.

$$\text{Relative Humidity} = \frac{\text{Actual water vapour pressure}}{\text{Sat. vap. press. at given temp.}} \qquad (3.1)$$

The sensitivity analysis for this parameter was carried out over a range of relative humidity values from 25% to 100%, and the maximum difference between the predictions corresponding to these values was of the order of 0.5 °C. It was therefore decided that the model was insensitive to variations in the wet and dry bulb depression.

3.3.5.4 Density of air.

The predictions of the model were found to be moderately sensitive to the density of air, and the results of the analysis are plotted in Fig. 3.10. The maximum difference between the standard prediction and the predictions at either the upper or lower limit to the density occurs during the day, and is equal to about 1 °C. However, the upper and lower limits plotted on the graph represent rather extreme values, and under normal weather conditions it would be reasonable to expect that the density would stay fairly constant between limits of 1.1 and 1.3 gm/cc.

In the evening, the difference between the predictions decreases, becoming zero at night. This behaviour occurs because the density of air is used in the calculation to evaluate the sensible heat flux, and as explained in Section 3.3.5.2, the magnitude of this flux is lower at night than during the day, so the effects of varying the density of air on the predicted surface temperature are reduced.

3.3.5.5 Surface atmospheric pressure.

This parameter is used in the calculations to determine the water vapour pressure and the saturation mixing ratio. The results obtained with atmospheric pressures varying from 950 millibars to 1050 millibars showed that the model predictions were insensitive to this parameter.

3.3.6 Parameters which influence the temperature predictions of the model under cloudy conditions.

The sensitivity analysis for the effects of clouds on the temperature predictions of the model was restricted to a few very simple cases, where it was assumed that one of the three parameters, consisting of the short-wave and long-wave cloud cover factors, and the cloud base height, may be varied while the other two remained at constant values. This was mainly because a thorough investigation would require the production of many sets of results due to the large number of possible combinations of values for the three parameters. Also, under normal weather conditions the type and number of clouds present can change very rapidly, and consequently it would be difficult to apply the results generated by a sensitivity analysis to real modelling problems.

3.3.6.1 Long-wave cloud cover factor.

The long-wave cloud cover factor has a range of values from 0 to 1, with the lower limit representing a clear sky. It is derived from measurements made by the radiometer, and because of this it is not possible to estimate the value of this parameter by direct observation of the type of cloud or the cloud base height. The factor is used to obtain a value for the downward long-wave radiation flux due to the clouds, as described in Section 2.3.2.2.

The results of the sensitivity analysis on the long-wave cloud cover factor are shown in Fig. 3.11, which were produced with the cloud base height fixed at 500m and the short-wave cloud cover factor set to zero. It can be seen from the graph that the change in the surface temperature prediction is proportional to the change in the long-wave cloud cover factor. This can be explained by the fact that as the cloud cover factor increases, so does the downward long-wave radiation flux from the clouds, and hence the surface temperatures rise.

3.3.6.2 Cloud base height.

This parameter is used to calculate the temperature of clouds at the specified base height. The cloud temperature is then used in the calculation to determine the downward long-wave radiation flux due to the clouds.

A different standard prediction had to be defined for comparison purposes in the sensitivity analysis on the cloud base height. This was because the previous standard prediction was based on an artificial day with the long-wave cloud cover factor set to zero, which resulted in the model predictions being independent of the value of the cloud base height. The new standard day was defined with the long-wave cloud cover factor (CLFAC) set to a constant value of 1.0, so that the variations of the cloud base height would have the maximum influence on the resulting temperature predictions of the model. The cloud base height for the standard day was set to a typical value for low altitude cloud of 500m.

The predictions of the model for cloud base heights ranging from 500m to 10km are shown in Fig. 3.12, and the types of cloud typically found at these altitudes are given in Table 3.5. It can be seen from the graph that the model predictions are not very sensitive to variations in this parameter.

Table 3.5   Typical base heights of various types of cloud.

Low level	Base height (m)	High level	Base height (m)
Stratus	Surface to 600	Cirrus	
Stratocumulus	300 to 1350	Cirrostratus	6000 to 12,000
Cumulus	300 to 1500	Cirrocumulus	
Cumulonimbus	600 to 1500		

Medium level	Base height (m)
Nimbostratus	Surface to 3000
Altostratus	2000 to 6000
Altocumulus	2000 to 6000

3.3.6.3 Short-wave cloud cover factor.

The short-wave cloud cover factor is used in the calculation to determine the solar flux in the 250 to 3000 nm band incident on the surface of the earth. The factor may have a value in the range from 0 to 1, the lower limit being applicable when the sky is completely free from cloud. If cloud is present, the non-zero value of the cloud cover factor causes the calculated direct component of the short-wave solar flux to be set to zero, and the diffuse component to be multiplied by (1.0 - cloud cover factor). The value of the factor may be obtained from data provided by Kondratyev, 1969, which gives the ratio of the magnitude of the incident short-wave solar flux on the surface of the earth when the sun is obscured by a cloud to that which would be received if there were no clouds present. The values for the ratios depend on the type of cloud present and the solar elevation. For example, a medium level cloud such as one of the altocumulus type was obscuring the sun, then the short-wave cloud cover factor would be between 0.90 and 0.65, corresponding to solar elevations ranging from 5° to 45°. If the cloud was of the low level stratus type, the cloud cover factor may reach the maximum value of 1.0, as this type of cloud causes a great deal of attenuation in the incident solar flux.

The standard day for comparison purposes was chosen to be the same as that described in Section 3.3.6.2. The sensitivity analysis was carried out by running the model with different values of the cloud cover factor, which were assumed to correspond to the presence of different types of cloud. In order to simplify the analysis as much as possible, the changes in the cloud cover factor which would arise due to the variation of the solar elevation were ignored, and it was kept constant at the selected value over the 24 hour period.

The results of the analysis are plotted in Fig. 3.13, and it can clearly be seen that as soon as the short-wave cloud cover factor is greater than zero, the loss of the direct solar flux causes a rapid and significant drop in

the predicted surface temperature. As the cloud cover increases, then the predicted temperatures fall as the incident diffuse solar flux is correspondingly reduced. When the cloud cover factor is set to the maximum value of 1.0, the incident solar flux is reduced to zero, and the predicted temperatures exhibit slow cooling over the 24 hour period.

The sensitivity analysis on the short-wave cloud cover factor was carried out mainly for interest, as in the majority of applications of the model, the solar flux would be obtained from direct measurements made by the weather station rather than by calculation. There are two main reasons for measuring the flux rather than calculating it. Firstly, the data given by Kondratyev for the short-wave cloud cover factor are based on a limited number of measurements, and are therefore not likely to be very accurate. Secondly, the values of several parameters required for the calculation of the flux, including the variation with time of the cloud type and proportion of sky covered by cloud, have to be estimated by an observer. This will also contribute to errors in the calculation of the flux, as it is impractical both to estimate values for these parameters with a high degree of accuracy and to repeat the measurements more than a few times a day.

3.3.7 Parameters not included in the sensitivity analysis.

3.3.7.1 Moisture factor.

This parameter indicates the moisture content of the surface being modelled, with allowed values from 0.0 to 1.0 corresponding to surface conditions ranging from completely dry to totally saturated. The moisture factor is used in the calculation to determine the latent heat flux, as described in Section 2.3.4 of Chapter 2. The value of the moisture factor used as input for the model is normally restricted to zero for two reasons. Firstly due to the difficulty in measuring the moisture content of the surface, and secondly because changes in the state of saturation will affect the values of other parameters, such as the thermal conductivity and diffusivity of the

material, and the emissivity and albedo of the surface. The concrete surface used in the sensitivity analysis was considered to be dry for the standard prediction, and as there is no facility in the program to compensate for the effects of moisture on the values of the quantities listed above, it was not possible to carry out a sensitivity analysis for the moisture factor.

3.3.7.2 The average temperature of objects surrounding the surface.

This is used in the calculation of the net long-wave radiative flux. However, as the concrete surface used in the sensitivity analysis was horizontal and had a completely unobscured view of the sky, the value of this parameter had no effect on the value of the flux.

3.3.7.3 Average ground albedo.

This parameter determines the magnitude of the reflected short-wave solar flux from objects which surround the surface being modelled and obscure its field of view of the sky. However, as mentioned in Section 3.3.7.2, the concrete surface used for this sensitivity analysis is assumed to have a completely unobscured 180° field of view of the sky, and will therefore not receive any reflected short-wave solar flux.

3.3.7.4 Other parameters used to calculate the incident solar flux.

These include parameters such as the geographical location of the site and the time of year. It was felt that they was likely to be little uncertainty involved in specifying the values of these parameters when the model was in use.

5 cm   Concrete

20 cm Gravel

75 cm Soil
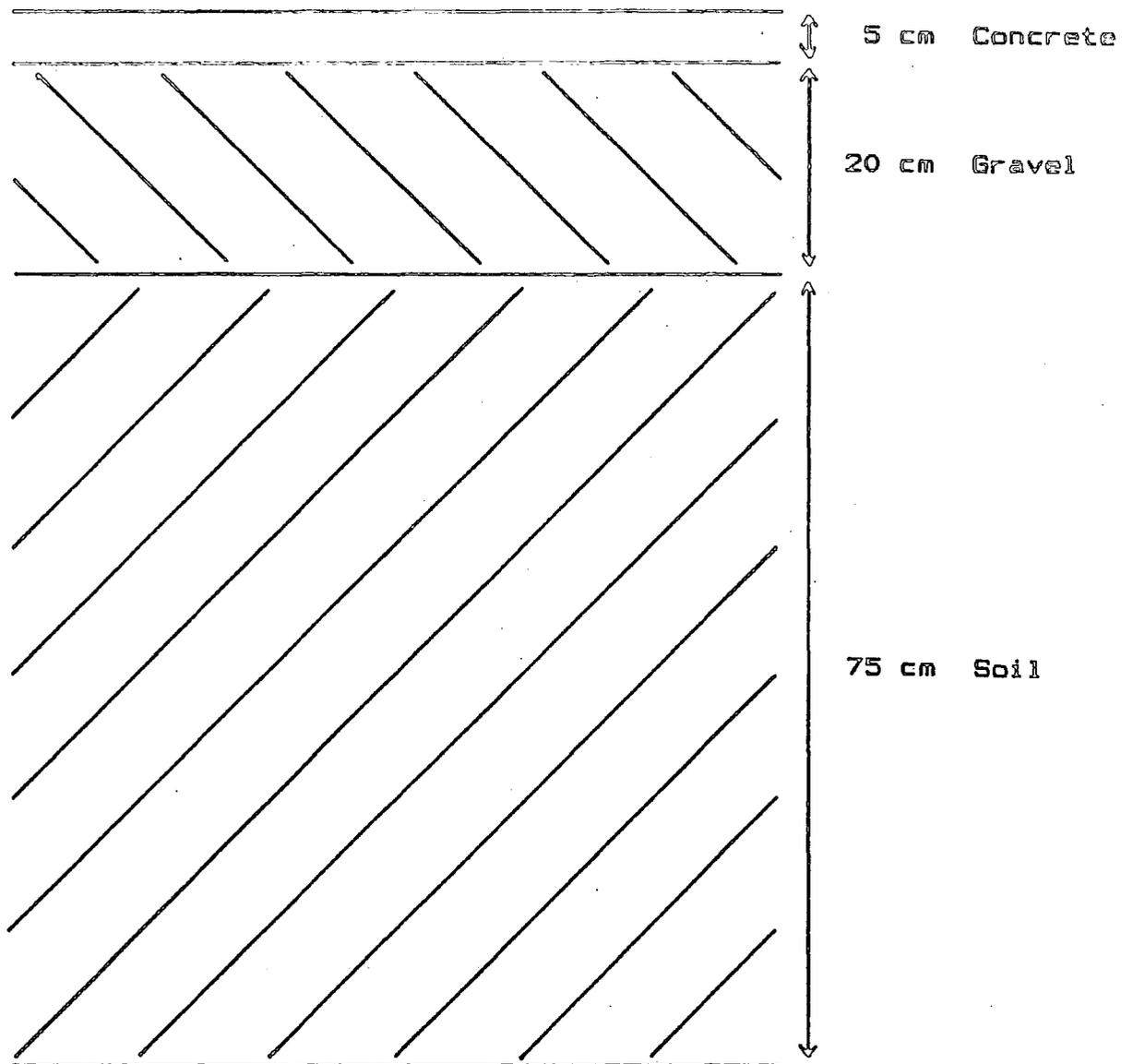
Fig. 3.1 Diagram of the concrete surface and the underlying layers comprising the structure used in the sensitivity analysis.

Fig. 3.2
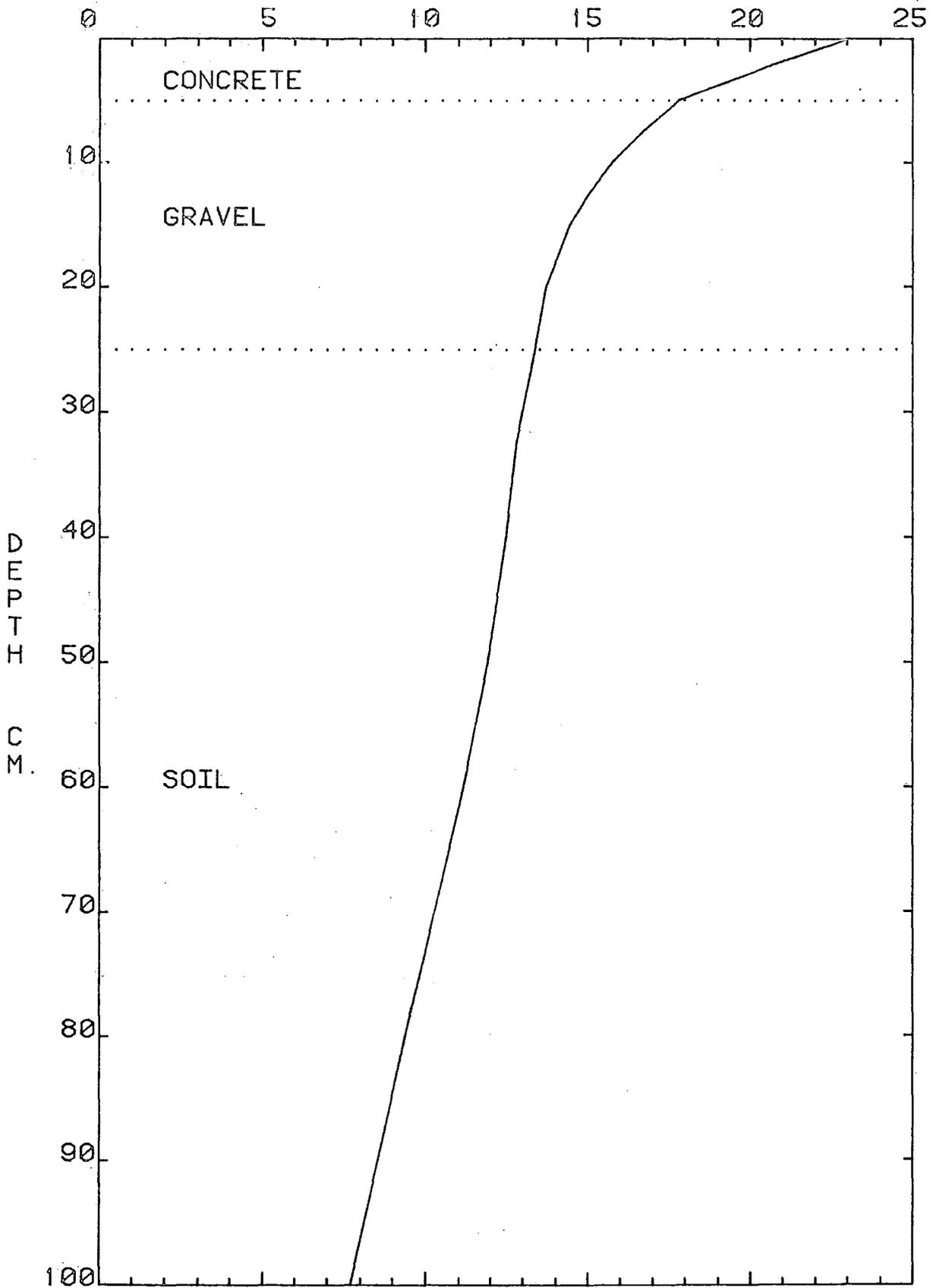
INITIAL TEMPERATURE PROFILE IN THE COMPOSITE
MATERIAL AS USED IN THE SENSITIVITY ANALYSIS.

SENSITIVITY OF EFFECTIVE RADIATIVE TEMPERATURE
PREDICTIONS TO CHANGES IN SURFACE ALTITUDE.

Fig. 3.3
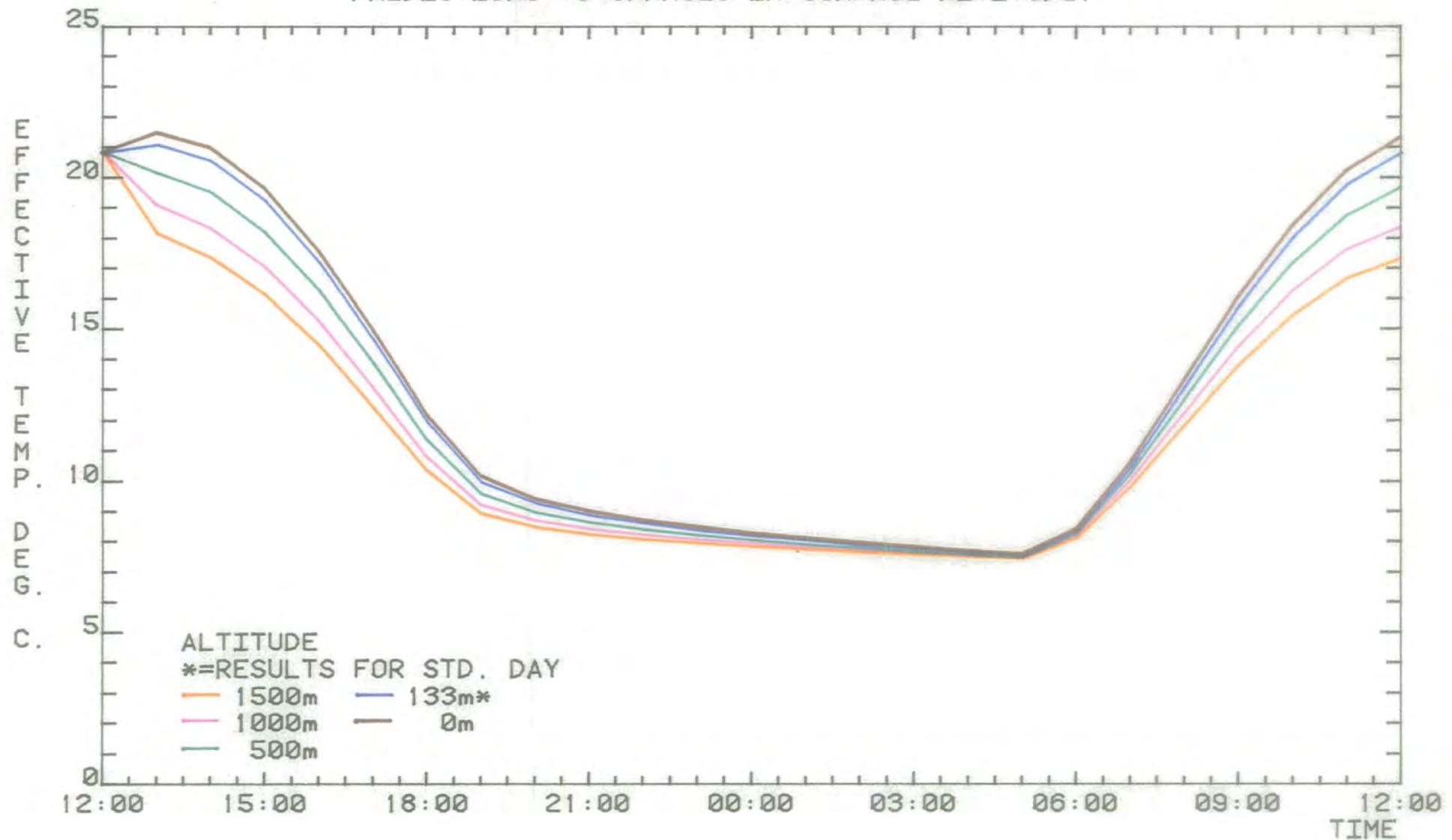
SENSITIVITY OF EFFECTIVE RADIATIVE TEMPERATURE PREDICTIONS TO CHANGES IN VERTICAL EMISSIVITY.

Fig. 3.4
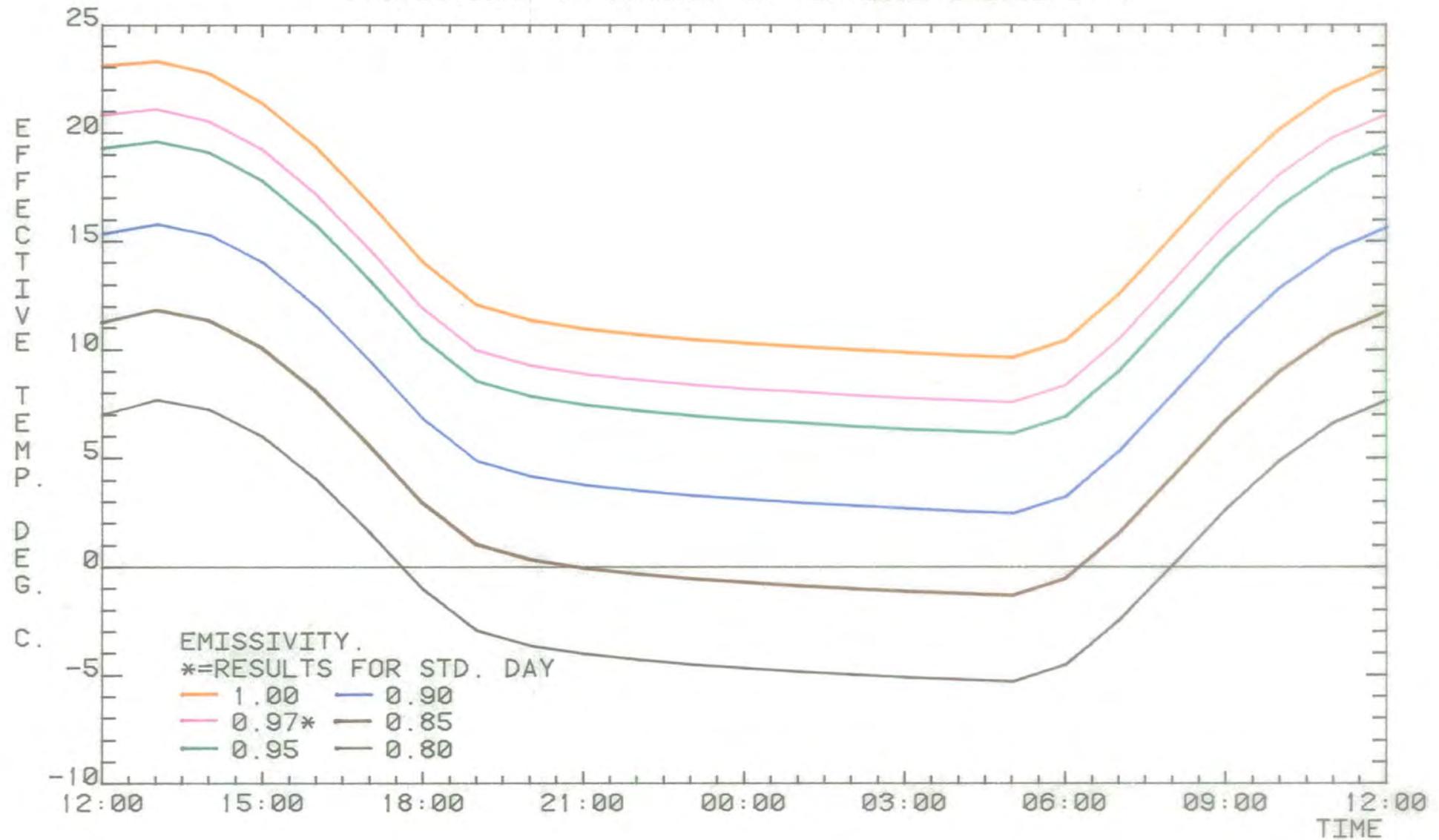
SENSITIVITY OF EFFECTIVE RADIATIVE TEMPERATURE PREDICTIONS TO CHANGES IN SURFACE (VERTICAL) ALBEDO.

ALBEDO.
*=RESULTS FOR STD. DAY
— 0.6   — 0.2
— 0.4   — 0.0
— 0.3*

Fig. 3.5
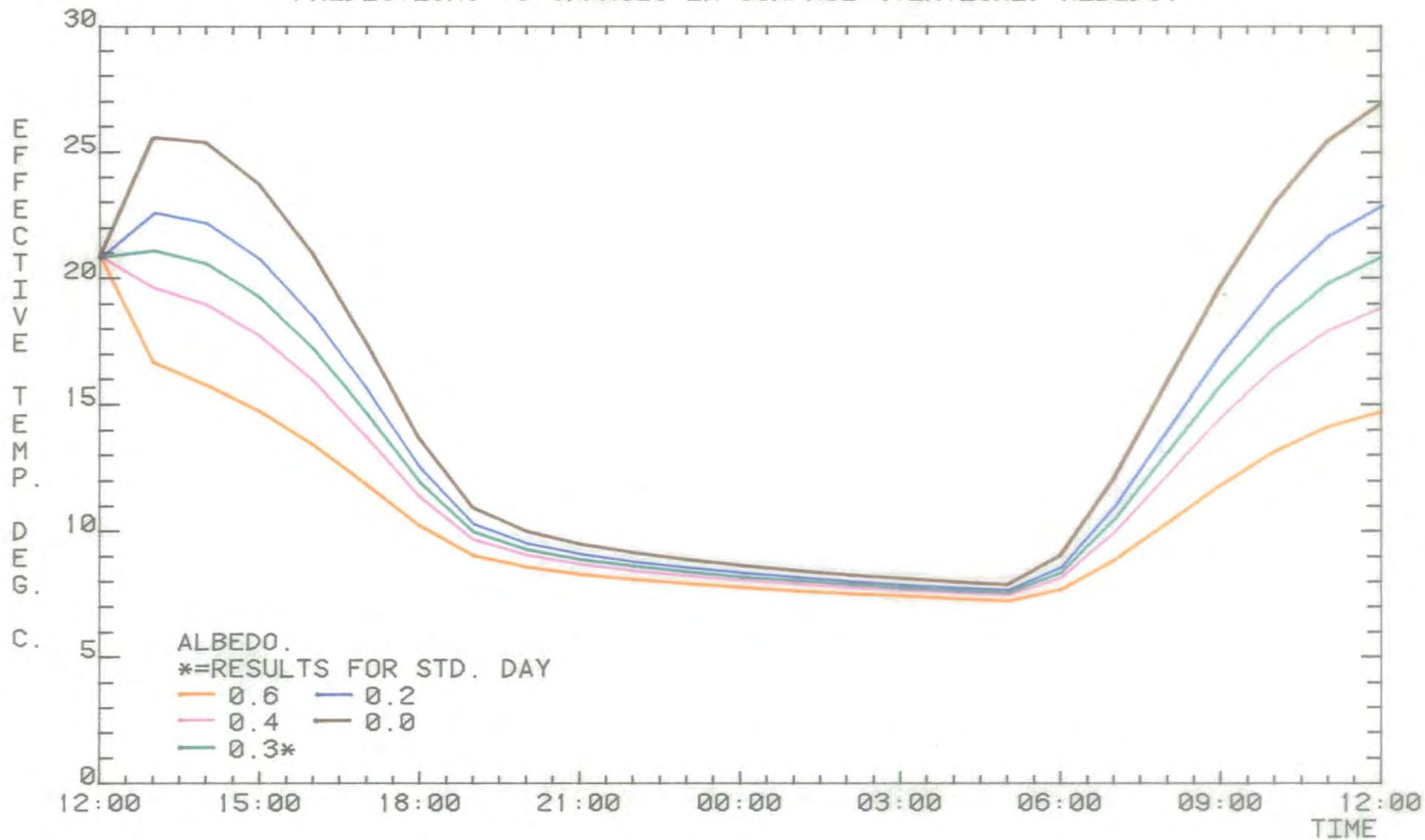
SENSITIVITY OF EFFECTIVE RADIATIVE TEMPERATURE
PREDICTIONS TO CHANGES IN CONDUCTIVITY OF TOP LAYER.

CONDUCTIVITY (W/m.K)
*=RESULTS FOR STD. DAY
5.00   1.54*
3.00   1.00
2.00   0.50
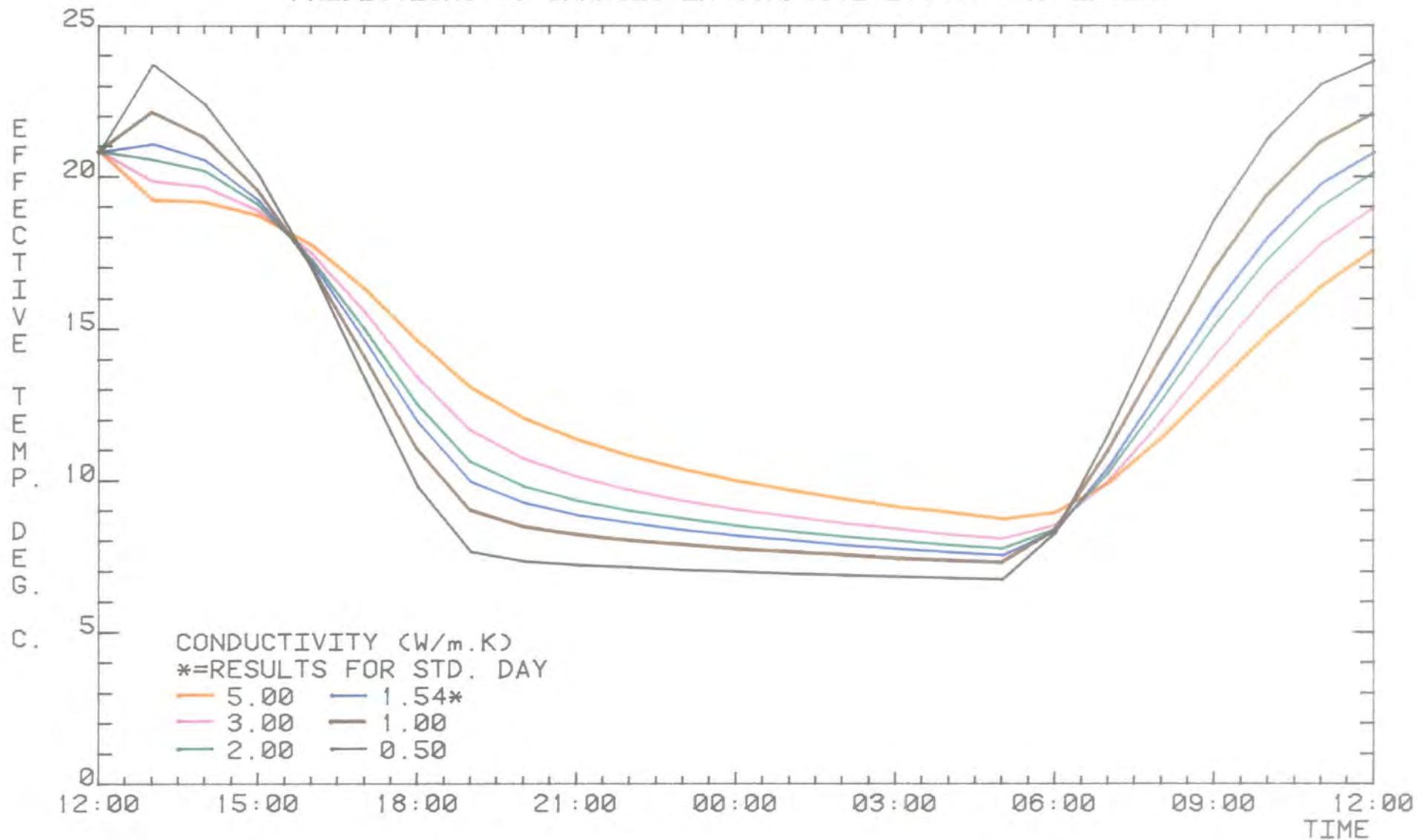
Fig. 3.6

SENSITIVITY OF EFFECTIVE RADIATIVE TEMPERATURE
PREDICTIONS TO CHANGES IN THICKNESS OF TOP LAYER.

Fig. 3.7
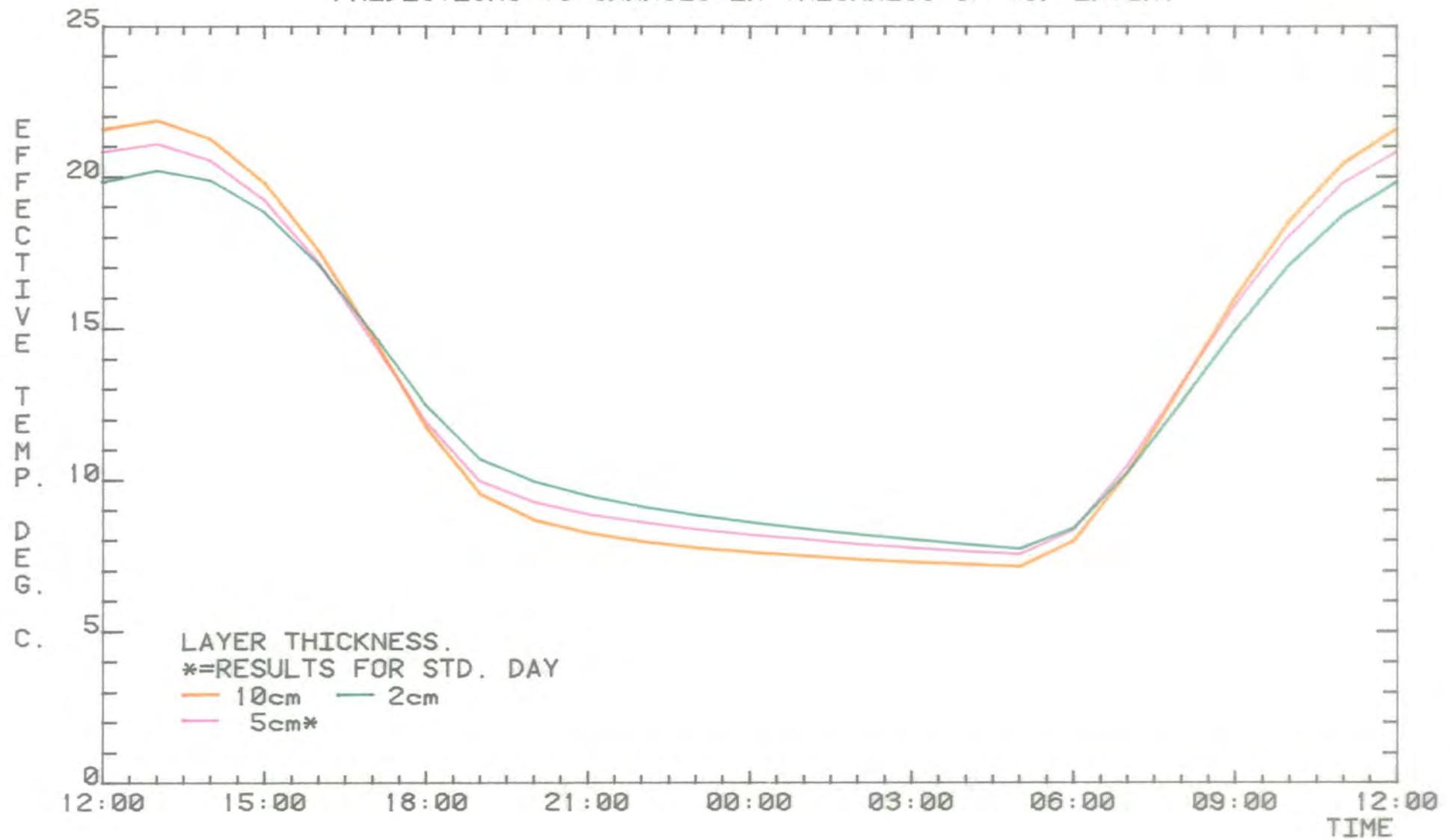
SENSITIVITY OF EFFECTIVE RADIATIVE TEMPERATURE
PREDICTIONS TO CHANGES IN AIR TEMPERATURE.
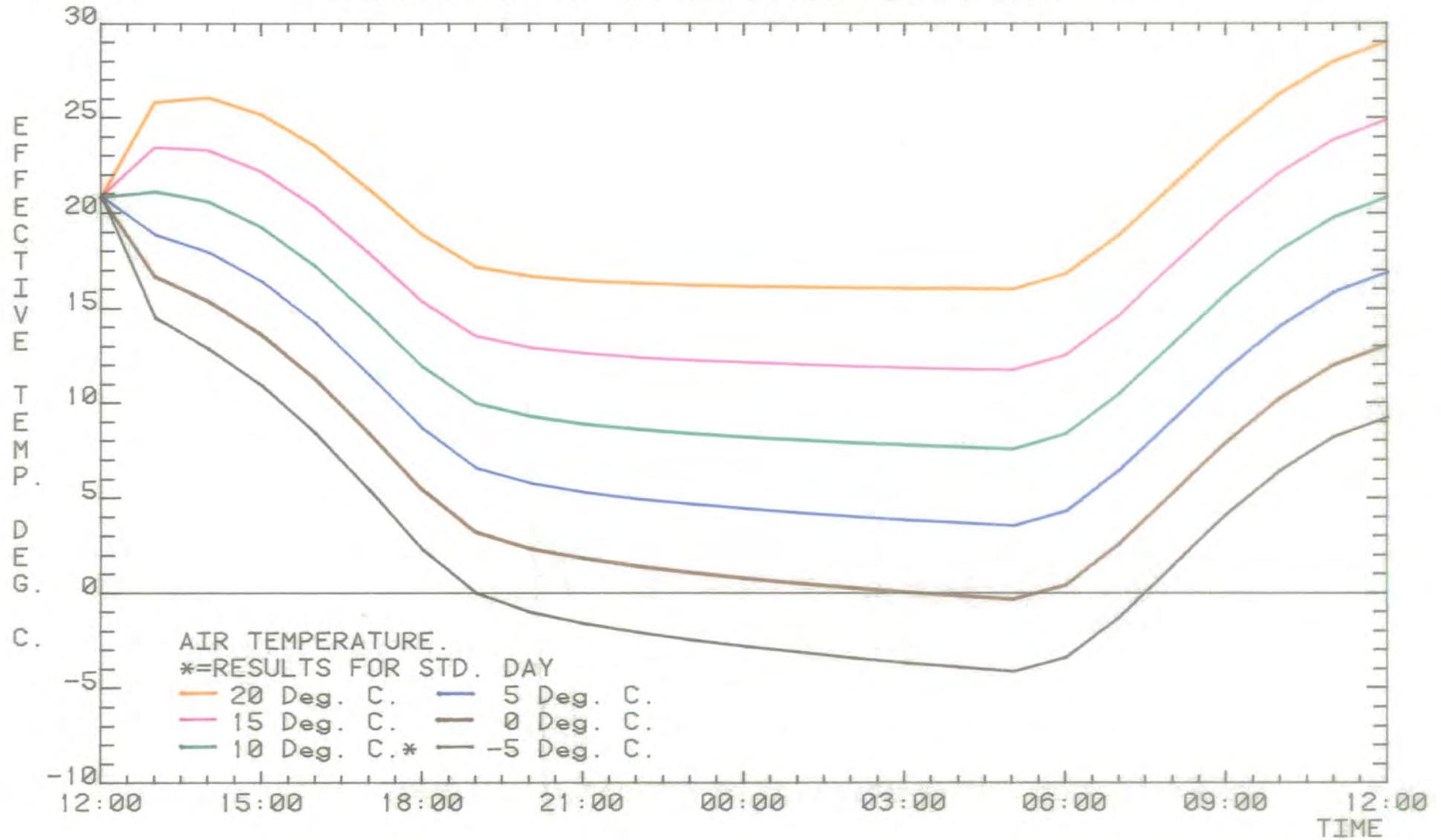
Fig. 3.8

SENSITIVITY OF EFFECTIVE RADIATIVE TEMPERATURE
PREDICTIONS TO CHANGES IN WIND SPEED.
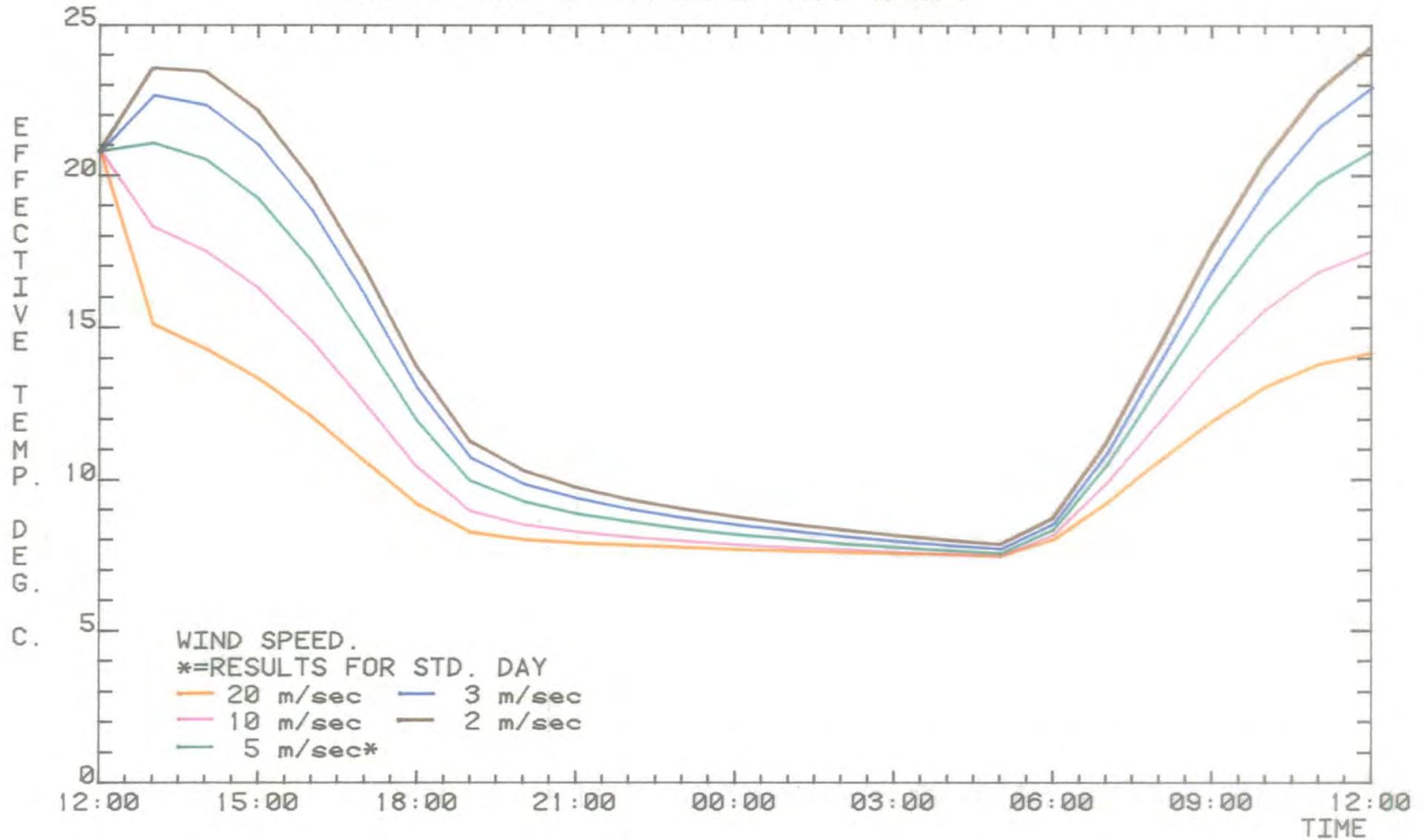
Fig. 3.9

SENSITIVITY OF EFFECTIVE RADIATIVE TEMPERATURE
PREDICTIONS TO CHANGES IN THE DENSITY OF AIR.
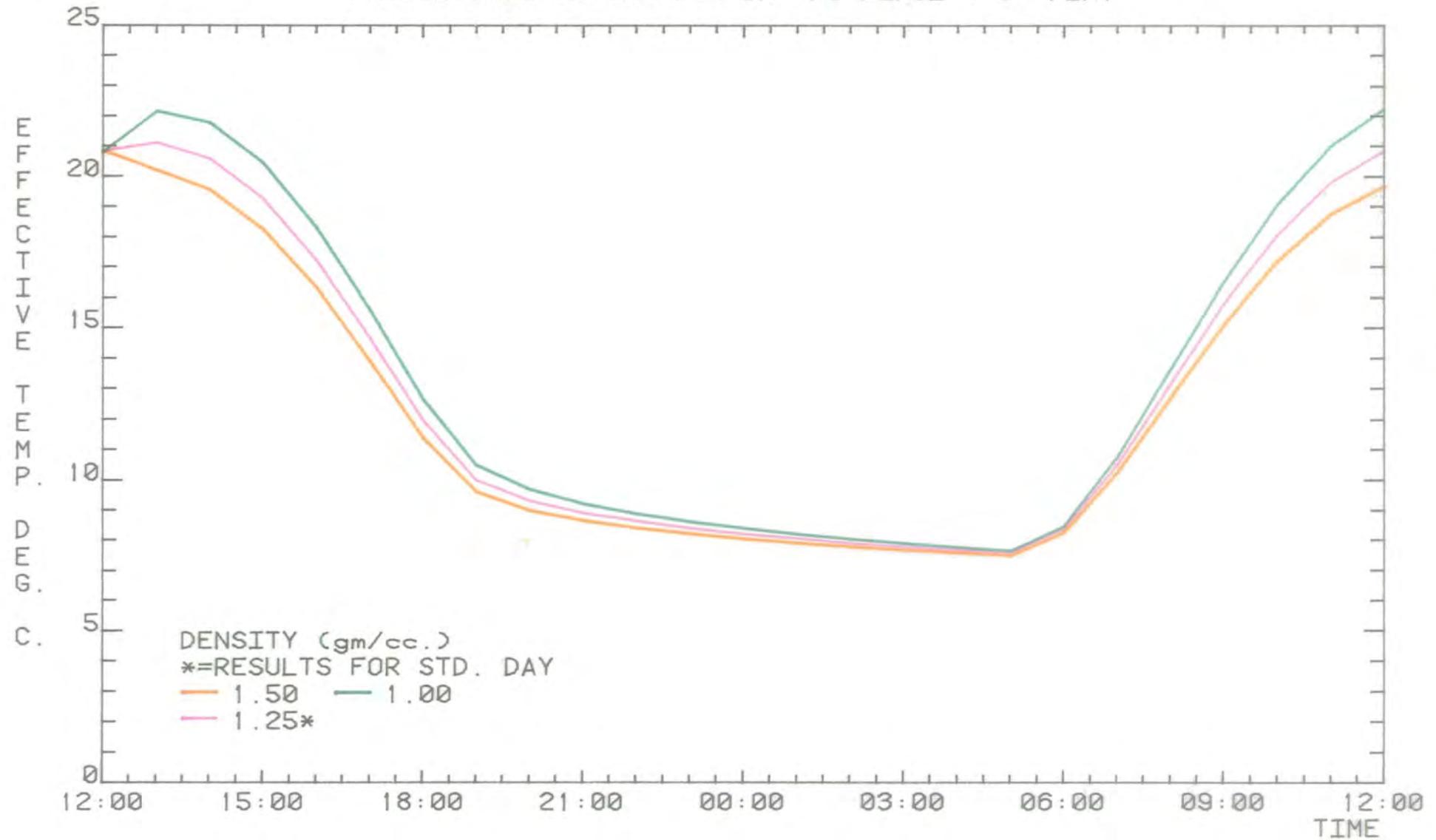
Fig. 3.10

SENSITIVITY OF EFFECTIVE RADIATIVE TEMPERATURE
PREDICTIONS TO CHANGES IN LONG WAVE CLOUD COVER FACTOR.

CLOUD COVER FACTOR.
*=RESULTS FOR STD. DAY
—— 1.0 —— 0.0*
—— 0.5
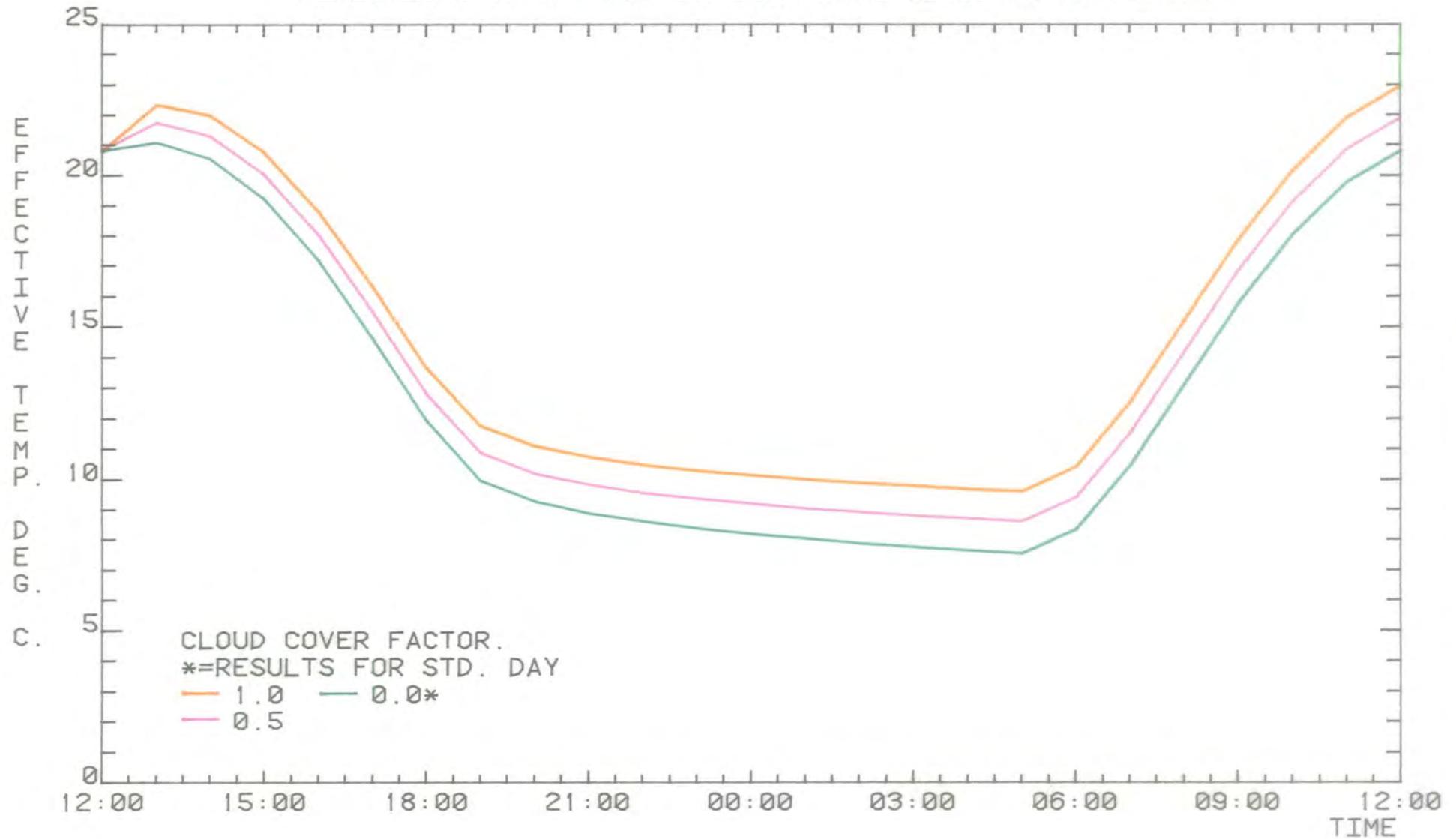
Fig. 3.11

SENSITIVITY OF EFFECTIVE RADIATIVE TEMPERATURE
PREDICTIONS TO CHANGES IN CLOUD BASE HEIGHT, (CLFAC=1.0).

Fig. 3.12
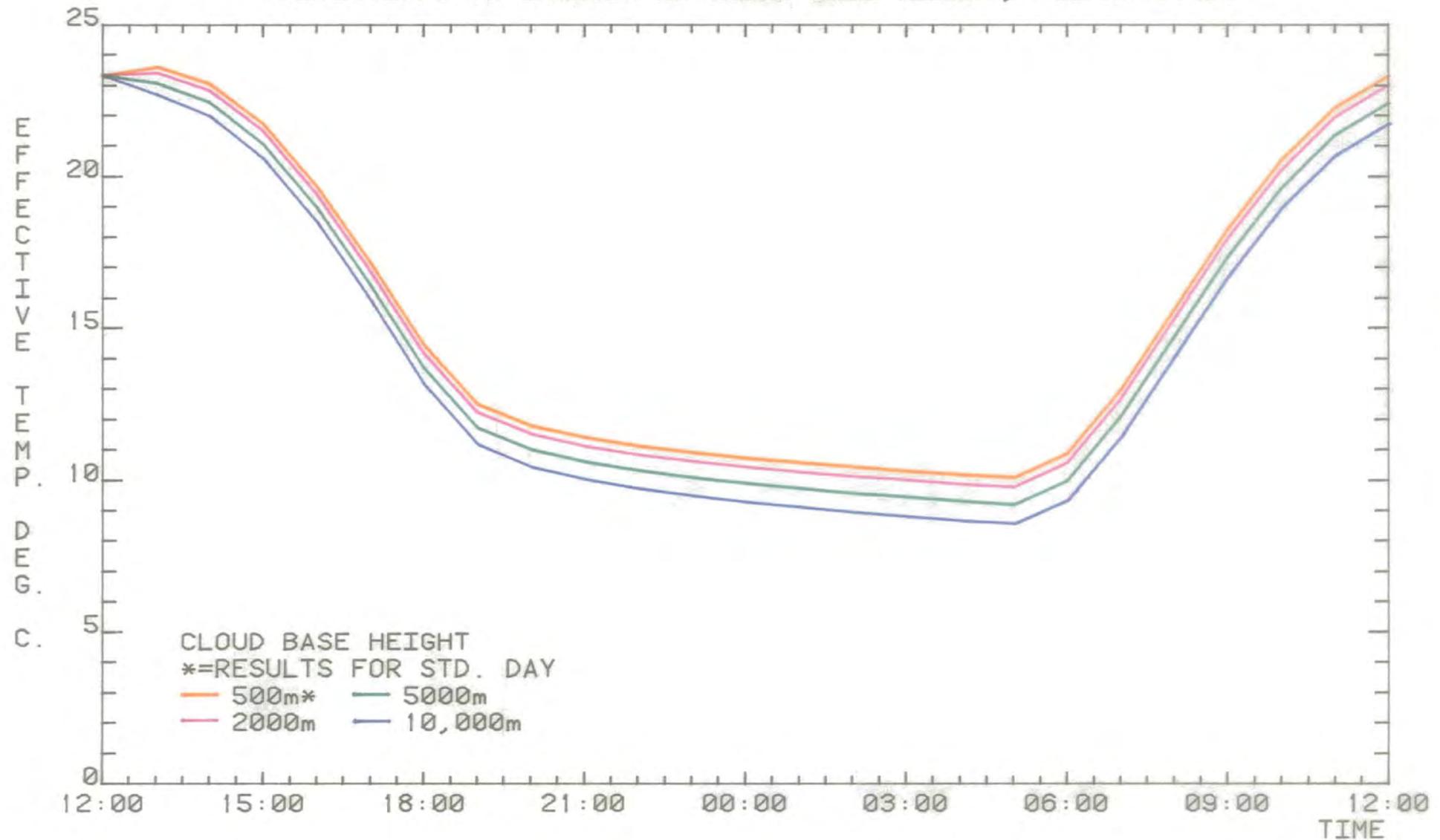
SENSITIVITY OF EFFECTIVE RADIATIVE TEMPERATURE
PREDICTIONS TO CHANGES IN SHORT WAVE CLOUD COVER FACTOR.

CLOUD COVER FACTOR
*=RESULTS FOR STD. DAY
— 1.00   — 0.10
— 0.50   — 0.01
— 0.25   — 0.00*

Fig. 3.13
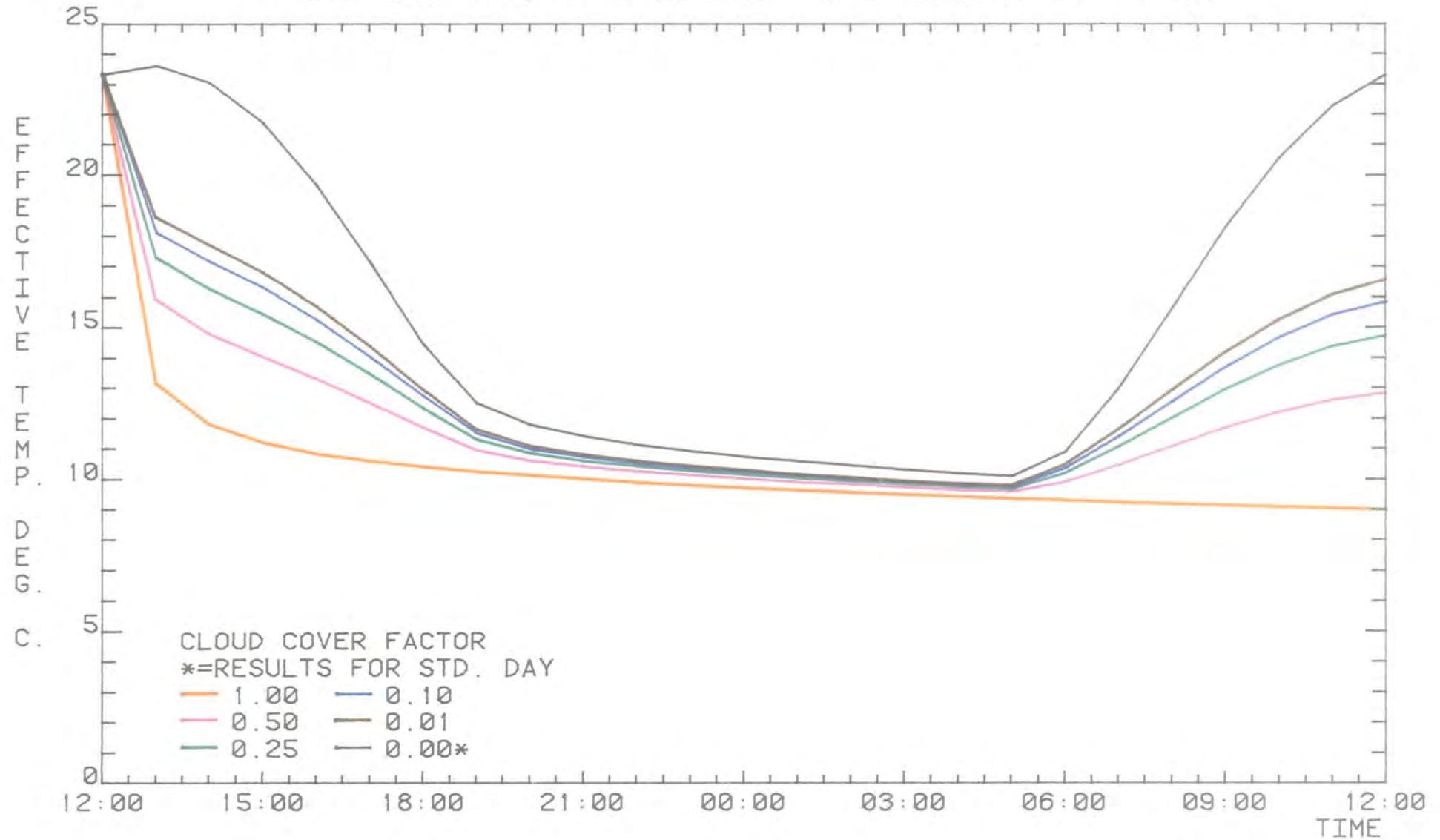
Chapter 4.   Equipment used for the collection of ground truth data for

            validation of the model.

4.1 Introduction

       The aim of this chapter is to give a detailed account of the equipment

developed at the University of Durham for automated radiant and contact

temperature measurements. The equipment was constructed to provide temperature

data for a wide range of natural and man-made targets, which, when combined

with data from an automatic weather station, could be compared with

mathematical model predictions. The results of these comparisons may then be

used to validate the model. With these objectives in mind, a system capable of

continuously measuring and recording radiation temperatures of a set sequence

of targets was constructed.

       A block diagram of the equipment is shown in Fig. 4.1. The system uses a

Tektronix 4052 computer to control a pan and tilt unit carrying a Barnes PRT5

precision radiometer and a CCTV camera. These instruments are mounted on the

moveable platform such that their viewing axes are parallel. The radiometer

operates in the 8 to 14 micron band, and is normally used on a scale which

covers from -20 to +35 °C. The CCTV camera allows the accurate pointing of the

radiometer when the system is operating under manual control to specify a

sequence of targets; it also provides a check on whether or not the target is

still in the field of view of the radiometer when the system is under

automatic computer control. A further feature of the equipment is a set of 32

contact temperature sensors. The weather station runs independently of the

main apparatus, and uses a logger to record data on magnetic tape. The data

are then periodically transferred from the weather data logger to the

Tektronix 4052 system, via its RS232C interface.

       The equipment was in almost continuous operation at Durham Observatory

from February 1983 to May 1984, and data have been recorded for a wide range

of targets. These include trees, bushes, various parts of a large lawn, the

dirt road leading up to the Observatory, and the sandstone walls of the building itself. Measurements have also been made of the sky temperature at several angles of elevation, which are used to estimate the long wavelength radiation flux from the sky. Until April 1984 the data were stored on an extensive library of DC300 magnetic tape cartridges. A database of all the measurements has been set up, and this can be reduced to an easily readable graphic form with the software currently available.

In the next sections of this chapter, the construction, resolution, and accuracy of the equipment will be discussed in more detail. Reference will be made to the main components of the system as outlined in the block diagram. This will include, for example, the autoguidance system used to control the pan and tilt head, and the electronics necessary to convert the radiometer and temperature sensor outputs to a form readable by the computer. The location, operation, and type of information available from the automatic weather station is also described.

4.2   Outline of the data acquisition system.

4.2.1 Introduction.

The main components of the system have been shown in Fig. 4.1 and are discussed in greater detail in the following sections.

4.2.2 Operator's console.

The operator's console is a metal structure designed to house the Tektronix 4052 computer and the electronics needed to interface it to the pan and tilt head, the radiometer, and the contact temperature sensors. The unit is intended for use indoors and can easily be dismantled into 3 pieces for transportation between operating sites. The layout of the console is shown in Fig. 4.2, in which the main components are indicated. These are described in the following paragraphs.

4.2.2.1 Tektronix 4052 computer.

This is a desktop computer which uses the BASIC programming language, and has a memory workspace of 64 k bytes. It has a built-in tape drive, which uses standard DC300 magnetic tape cartridges for storage of data or programs. These tape cartridges are available with two storage capacities; the normal length tape will hold 300 k bytes and the extended version up to 400 k bytes. The computer is also equipped with a real time clock ROM pack.

Communication with external devices can take place through either the General Purpose Interface Bus (GPIB) interface, which conforms to IEEE standard 488 (1975), or the data communications interface, which conforms to RS-232C standards. A block diagram outlining the connections between the computer and the external devices which are used with these interfaces is given in Fig. 4.3. The GPIB interface uses byte serial data transmission and is accessed by BASIC language commands. The GPIB is used during on-line data acquisition for communication with the 11-bit bus controller and the motor controller. The former gives the readings from the 4 ADC units on the 11-bit bus, which provides the current position of the pan and tilt head and the readings from the temperature sensors and radiometer. The motor controller operates a DAC unit, which generates the voltages necessary to move the pan and tilt head when under computer control. When the computer is carrying out off-line data analysis, this interface is commonly used to send data to devices such as a graph plotter, second tape drive, or line printer (via a Centronics printer interface on the IEEE bus).

The data communications interface allows bit serial data transmission with host computers and other RS-232C compatible devices, at rates of up to 9600 baud. The computer can be used simply as a terminal, where data are sent from the keyboard and received on the screen, or in an alternative operating mode, ASCII data can be sent from or received by the internal tape drive. When the computer is in normal BASIC operating mode, the RS-232C interface can be accessed for data transfer by using BASIC input or output commands with a

primary address of 40. The computer is used in this mode for the transfer of weather data from the Microdata logger.

A comprehensive software library has been developed to use with the computer. This covers data acquisition and analysis, with the latter making use of the storage tube screen on the computer for graphical presentation of data. The software library is described in more detail in the Appendix.

4.2.2.2 Servo controller.

The servo controller is a type 485 model manufactured by Dennard Ltd., and its purpose is to control the position of the pan and tilt head. Operation under manual or computer control is selected by two switches located on the panel above the unit. If the system is under manual control, as for example when specifying a new sequence of targets for later measurement, movement of the pan and tilt head is achieved by using a joystick potentiometer to adjust the voltage supplied to the pan and tilt motors. When the system is carrying out routine data logging under computer control, voltages generated by a DAC unit under instructions from the computer are used instead of the joystick. The process of automatic guidance by the computer is discussed in more detail in Section 4.6.

4.2.2.3 CCTV Monitor.

This is used to display the picture from CCTV camera, which is located in the instrument package on the pan and tilt head platform. A circle is drawn on the screen to correspond with the field of view of the radiometer. This allows targets in the sequence to be accurately specified, and when the system is in the routine data logging mode, the TV camera can be used to check that the radiometer is still on target.

4.2.2.4 Printer.

A standard 80 column dot matrix printer is normally used for purposes

such as producing hard copy of data from the computer. It is connected to the computer via a Centronics interface unit on the IEEE bus.

4.2.2.5 Analogue meter.

This is calibrated to display the radiation temperature in °C of the target currently being measured by the radiation thermometer.

4.2.2.6 Switched mains supply to the mother box.

These switches control the mains supply to the radiation thermometer, the CCTV camera, the floodlight attached to the instrument package on the pan and tilt head platform, and the power supply for the communications system between the operation console and the field station.

4.2.2.7 Telephone.

This is connected to a similar handset in the field station, and allows communication between the two units. The power supply for the telephone system is located in the field station.

4.2.2.8 Connectors.

These are used for two purposes. Firstly, to connect with the 50 m cable harness carrying power and signals to and from the field station, pan and tilt head, and instrument package. The other connectors are used simply to link the upper and lower halves of the console, enabling the unit to be easily dismantled for shipping.

4.2.2.9 Electronics crate.

This contains the circuits needed to interface the computer with the pan and tilt head, radiometer, and contact temperature sensors. An electronic block diagram for the system is illustrated in Fig. 4.4, which shows the GPIB connection with the computer. In all, there are 12 modules in the crate, and

it is also equipped with the necessary power supplies (+5 V and ±12 V) for the circuits. The function of each of the circuits is briefly described below, and later in more detail in the relevant section of this chapter.

1. DAC & motor controller.

The motor controller contains a Mostek F8 single chip microprocessor, which is programmed to control a DAC unit under instructions received from the computer via the IEEE bus. The DAC supplies analogue voltages to the servo control unit, so determining the movement of the pan and tilt head. The F8 program is contained in an EPROM, which mounts directly onto the microprocessor chip.

2. 11-bit bus controller.

This unit also contains a Mostek F8 microprocessor. It is programmed to read the contents of the four ADC units on the 11-bit bus on command, and transmit the results to the computer over the GPIB.

3. 11-bit ADC unit.

This two channel unit converts the analogue voltages from the two position sensing potentiometers in the pan and tilt head. The digital results are put on the 11-bit data bus when requested by the 11-bit bus controller. The National Semiconductor ADC1211 i.c. is used, which has a conversion time of 100 microseconds.

4. 8-bit ADC units.

There are three 16 channel units, using an 8-bit National Semiconductor ADC0816. Two are used to digitize the output from the temperature amplifier units. One ADC is dedicated to each of the two pairs of octal temperature amplifiers, which are connected to a set of 16 contact temperature sensors. In the third unit, one channel is used to convert the output voltage from the

radiometer, while the other 15 are currently not in use and have their inputs grounded. The digital readings from each of the 16 channels of the three ADCs can be put on the 11-bit data bus on request from the 11-bit bus controller.

5. Temperature amplifier units.

There are four, 8 channel units, and two are dedicated to each set of 16 temperature sensors. The circuit is based on the 747 dual operational amplifier i.c., and converts the current passed by the sensor to a voltage from 0 to 5 V. This is then suitable for conversion by the 8-bit ADC units.

6. Printer interface unit.

This unit contains an F8 microprocessor programmed to receive data from the computer on the GPIB, and convert it to an output suitable for printers with a Centronics type parallel interface.

4.2.3 Field station.

This is a weatherproof, heated box, on top of which is mounted the pan and tilt head carrying the instrument package. It is used to house the hardware associated with the instrument package, which includes the control unit for the radiometer and a transformer to supply power for the floodlight. There is also a telephone connection to the operation console.

4.2.4 Pan and tilt head.

The pan and tilt head is a type 485 model, manufactured by Dennard Ltd. It is a weatherproof unit, and is capable of carrying loads of up to 9 kg. The power supply for the d.c. pan and tilt motors is derived from the servo controller in the main console. The unit pans through an angle of 360°, and the moveable platform will tilt through an angle of ± 180°, at speeds continuously variable from 0° to 12° per second on pan and 0° to 9° on tilt. Inside the unit, two linear potentiometers are used to obtain the current

azimuth and zenith positions of the moveable platform. The operation of the pan and tilt head under computer control is described in more detail in Section 4.6.

4.2.5 The instrument package.

The instrument package is a weatherproof, aluminium box which is fixed to the moveable platform of the pan and tilt head, and is connected to the field station by a short cable harness. Located inside the package are the optical unit of the PRT5 radiometer and a paraxially mounted CCTV camera, as illustrated in Fig. 4.5. A floodlight is fixed to the side of the box, which can be used to illuminate targets in the field of view of the CCTV camera. The CCTV camera lens is protected from rain by a perspex window, and a thin sheet of polyethylene is used to cover the radiometer aperture. It was necessary to carry out calibration work on the radiometer so that the effects of this window could be taken into account during subsequent data analysis. These results also showed that the output reading of the radiometer was sensitive to changes in the ambient temperature. In order to allow for this, a contact temperature sensor was attached to the optical unit of the radiometer, and for subsequent data acquisition the ambient temperature of the radiometer was recorded along with the radiation temperature of the target. The calibration procedure, and method of interpretation of the data from the radiometer, is described in more detail in Section 4.3

4.3 The radiation thermometer.

4.3.1 General description.

The instrument used for remote temperature measurements is a model PRT5 precision radiation thermometer, manufactured by the Barnes Engineering Company. The radiometer consists of an optical unit and a control unit, which are connected by a single multicore cable. The optical unit contains the detector, which compares the amount of energy received from an object with an

internal reference source. The resulting signal from this unit is then processed by the control unit, which produces an output voltage proportional to the energy difference between the target and the reference. The optical head is located in the instrument package on the pan and tilt head platform, and the control unit is located inside the weatherproof box. Power to operate the radiometer can be obtained either from a 240 V mains supply, or the rechargeable batteries in the control unit.

The radiometer covers the 8 to 14 micron band, and has a field of view of 2° FWHM. The absolute accuracy of the radiometer is $\pm$ 0.5 °C, and the temperature sensitivity is better than 0.1 °C. The response time of the detector is variable between 5 and 500 milliseconds, and is normally set to 50 milliseconds. An analogue scale on the control unit displays the measured temperature, and a corresponding output of 0 to 1 V is carried by a co-axial cable to the main console for digitizing and subsequent recording by the computer.

The radiometer can operate on either of two partially overlapping measurement scales, covering radiation temperatures from -20 to +35 °C and +20 to +75 °C. However, as it was impractical to switch between scales while the data acquisition system was in use, all data recorded at Durham Observatory have been on the lower temperature scale. This scale was chosen for two main reasons. Firstly, it was necessary to measure the temperature of sky in several directions, and it was found that these temperatures typically ranged from 10 °C for thick cloud to less than -20 °C for thin, high altitude cloud or clear sky. Secondly, it was felt reasonable to assume that measured temperatures of most terrestrial objects would normally be somewhere between the limits of the scale, and not exceed the upper limit except possibly under conditions of high incident solar flux on calm, cloudless days. This is shown by the data obtained under such conditions in August 1983, in which only the sandstone wall of the Observatory building was measured to have temperatures exceeding the quoted upper limit to the scale. However, this was at most only

by 5 °C, and a later calibration of the radiometer showed that these off-scale values may be reliably used.

4.3.2 Principles of operation.

A block diagram outlining the operation of the radiometer is given in Fig. 4.6. Radiation from a surface arrives at the optical head and is chopped at a rate of 100 Hz before reaching the objective lens. This is a 10 mm f/2.8 lens made from Irtran-2, which has a spectral pass band from around 0.6 to 14 micron. Behind the lens is an interference filter, which restricts the radiation entering the detector to the 8 to 14 micron band. The normalised spectral characteristic of the radiometer, which takes into account the effects of the lens and the filter, is shown in Fig. 4.7. After passing through the lens and filter, the radiation enters the temperature controlled cavity. This is well insulated, and kept at a stable temperature of 45 °C. A thermistor is used to measure its temperature, and if any deviation from the normal operating temperature is detected, the control unit can compensate by adjusting the current supply to the heater blanket surrounding the cavity. The radiation finally falls on the thermistor bolometer detector located at the rear of the cavity. This consists of a 50 micron square thermistor element, which is mounted on the back of a germanium lens.

The effect of the chopper is to cause the detector to be exposed alternately to the incident radiation from the surface and radiation from inside the cavity, which is reflected from the back face of the chopper blade. The resulting output from the detector is proportional to the difference in radiant power received from the two sources. This a.c. signal is sent to the control unit, where it is amplified and converted to d.c. outputs of 0 to 1 V at a source impedance of 10 K and 0 to 50 mV at 500 R. The signal is also displayed as a radiation temperature in °C on an analogue meter, which has a non-linear scale conforming to the response of the detector.

4.3.3 Conversion of the output voltage to a computer readable form.

The 0 to 1 Volt output from the control unit is transmitted via a 75 Ohm impedance co-axial cable to the operation console, where it is directed to one of the 8-bit ADC units. Inside the ADC unit, the signal enters a circuit based on a 747 i.c., which contains two operational amplifiers. This circuit is shown in Fig. 4.8, and it produces two buffered output voltages from the 0 to 1 Volt input.

One of the operational amplifiers is used as a voltage follower with a gain of unity. This is to provide a signal to be used with the analogue meter on the front panel of the operation console. The meter is used to display the equivalent black body temperature of the target, and has a non-linear scale corresponding with that on the radiometer control unit inside the weatherproof box. Calibration is achieved by adjusting a 0 to 10 K variable resistor, which is in series with the output from the voltage follower and the input to the meter on the operation console.

The other operational amplifier in the 747 i.c. is used to provide a 0 to 5 Volt signal suitable as input for the ADC. This is achieved by a simple amplifying circuit with a gain of 5, and by adjusting the variable resistor, it was possible to obtain a maximum difference between measured and expected output voltages of 1.5% over the full range. After amplification, the signal is fed to channel 1 of the ADC unit with board address 6. On this particular unit the other 15 channels are not used, so they are grounded to avoid stray voltages being set up which may corrupt the channel in use.

The ADC unit is based on the 8-bit National Semiconductor ADC0817 i.c., which can convert a voltage in 100 microseconds with an accuracy of $\pm$ 1 LSB. A block diagram outlining the circuit is given in Fig. 4.9. The unit is designed so that the readout can be transmitted to the computer via the 11-bit bus controller and the GPIB. The sequence of operation is initiated when the computer executes a BASIC statement of the form "READ@7,3:X$". The primary address of 7 selects the 11-bit bus controller, and the secondary address

specifies that the 8-bit ADC boards are to be interrogated. The microprocessor
inside the bus controller then activates the 11-bit address bus to control the
operation of the three ADC boards. As can be seen in Fig. 4.9, lines 4 to 6 of
the address bus are used to select one of the ADC boards for data transfer.
The board address is chosen from one of the 8 outputs from the 3-to-8 line
decoder, and the board is selected when the corresponding line makes a high to
low transition. The three ADC boards in use have addresses 4 to 6, and the
data transfer process proceeds in order from lowest to highest address.
Address lines 0 to 3 are used to control the multiplexer, which selects the
analogue channel for conversion in the order from channel 1 to 16. The
resulting digital reading for the channel appears on the tristate data outputs
of the i.c., which are connected to lines 0 to 7 of the 11-bit data bus, and
is received by the bus controller. After the multiplexer has converted all 16
input channels, the 7th address line is used to reset the tristate data
outputs to the high impedance state, and the data transfer is complete from
that particular board. Address lines 4 to 6 are then used to select the board
with the next highest address, and the process repeated until data have been
read from all three boards.

The 11-bit bus controller transmits the data to the computer over the
GPIB in the form of an ASCII string, which is built up from three sets of 16
characters. The sets correspond to the data from the three ADC boards, taken
in the order from lowest to highest board address, with each character in the
set representing a channel on the board in the order from 1 to 16. This can
converted back to the digital reading for a particular channel by finding the
relevant ASCII character and taking its decimal value. This will be from 0 to
255, corresponding to analogue inputs to the ADC from 0 to 5 V.

The digital equivalent of the temperature measured by the radiometer is
determined by taking the appropriate part of the ASCII data string. As the
radiometer uses channel 1 on the ADC with board address 6, this corresponds to
the 33rd character in the string. On conversion to a decimal, the ADC reading

from 0 to 255 will therefore correspond to radiation temperatures from -20 to +35 °C, and consequently temperatures may be measured with a resolution of about 0.2 °C.

4.3.4 Data interpretation.

Calibration data are supplied with the instrument to relate the output voltage from the radiometer to the equivalent black body temperature of the target. The relationship between these two parameters is non linear, and is illustrated in Fig. 4.10. However, this is unsuitable for analysis of the data recorded at Durham as the calibration data does not take into account the plastic window over the viewing aperture of the radiometer. It was therefore necessary to calibrate the radiometer while in operation at Durham, and a black body source capable of generating radiation temperatures in the range from 16 °C to greater than 40 °C, was obtained for this purpose. The method used was to place the black body as close as possible to the viewing aperture in the instrument package, so that the source completely filled the field of view of the detector. The desired black body temperature was then set on the control unit, and time allowed for the source to reach the correct temperature. When the source had stabilized, the computer was used to obtain the digital reading from the 8-bit ADC corresponding to the output voltage from the radiometer. Several readings were taken both with and without the plastic window in place, and the two averages were calculated. This procedure was then repeated for a different black body temperature. The maximum black body temperatures which could be used was limited to about 40 °C, at which point the reading from the ADC reached the maximum value of 255. The minimum temperature which could be used was limited by the cooling fan on the black body source, as it was not found to be very effective in reducing the source temperature when it was close to the ambient air temperature.

The results from the first calibration both with and without the plastic window over the radiometer viewing aperture are given in Fig. 4.11. This shows

a linear correlation between the digital reading from the ADC and the radiation temperature of the black body source in both cases, although the effect of the window is to significantly change the slope of the line. These results were taken with the instrument package removed from the pan and tilt head and placed indoors. This was to ensure that the temperature of the black body source was kept as stable as possible, by reducing the fluctuations which may arise from the effects of direct solar heating or cooling by wind. The air temperature during the calibration was fairly constant at 24 °C, and it was decided to repeat the calibration procedure at other ambient temperatures to see if this had any effect on the results.

The second calibration was carried out on a much cooler day, when the air temperature was 10 °C. This had the advantage that the black body source could initially be used at its lowest temperature setting of 16 °C. The results with the viewing aperture of the radiometer unobscured by the window were approximately the same as before. However, a significant difference was observed between the results of the two calibrations carried out with the window in place, and on plotting the data it was found that while the two lines had similar slopes, the second set of data were clearly displaced from the first.

These results suggested the output from the radiometer was dependent on two parameters. Firstly, the temperature of the window, and secondly, although to a much lesser extent, the results without the window in place suggested a dependence on the ambient temperature of the radiometer optical unit containing the detector. It was therefore decided to measure and record the temperature of the window and radiometer while the system was in operation, and the simplest way of achieving this was to use a contact temperature sensor. As it was impractical to fix the sensor to the window itself, it was decided to attach it to the optical unit of the radiometer. It was therefore assumed that any variations in the temperature recorded by the sensor would be equally experienced by both the optical unit and the inner surface of the

window. The sensor used was one of a standard set of 16, and it was fixed in place to the outer surface of the optical unit. The calibration procedure with the black body was then repeated several times for different ambient temperatures, and the reading from the temperature sensor kept as stable as possible during the calibration.

A multiple regression analysis was used with the results obtained to determine the calibration function. This function was assumed to take the form;

$$T = a + bT_1 + cT_2 \qquad (4.1)$$

where; T = Radiation temperature of the surface being viewed by the radiometer, in °C.

T_1 = Digital reading from the radiometer when viewing the surface at temperature T.

T_2 = Digital reading from contact temperature sensor attached to the optical head of the radiometer.

a,b,c = Regression coefficients determined from the calibration results, with a = -15.3

b = 0.246

c = -0.042

The results show that the effect of the window is to cause the radiometer to give a higher reading than the actual surface temperature, and that the difference between two will increase with a rise in the ambient temperature, as measured by the contact sensor. To obtain an order of magnitude for this effect, it can be assumed that an increase of about 0.2 °C in the temperature measured by the sensor will produce an increase in the ADC reading of + 1 bit. The calibration equation therefore suggests that the difference between the actual surface temperature and that measured by the radiometer will increase by 1 °C for a rise in the ambient temperature of 5 °C.

The temperature sensor was left in position after the calibration of the radiometer was completed, and for subsequent automated acquisition of radiation temperatures, the digital readings from both the sensor and the radiometer were recorded on tape. Analysis of the data recorded in this way was carried out using the above calibration function.

4.4 Contact temperature sensors.

4.4.1 Hardware.

The equipment includes two sets of 16 temperature sensors, which allow the measurement of contact temperatures at distances of up to 100 m from the central console. The wiring layout for one set of sensors is illustrated in Fig. 4.12, and a block diagram outlining the electronics interface between the sensors and the computer is shown in Fig. 4.13.

The sensor in use is an RS590 type, which is a two terminal integrated circuit temperature transducer. It is housed in a cylindrical TO 52 package, of diameter 5 mm and length 4 mm. The maximum operating temperature range is from -55 to +150 °C, and it produces an output current proportional to the absolute temperature. The device has a nominal linear temperature coefficient of 1 μA/K, and is supplied calibrated to provide 298.2 ± 2.5 μA at 298.2 K The deviation of the output current from a best straight line fit is illustrated in Fig. 4.14, which shows that the nonlinearity of the sensor gives rise to a maximum error of 0.8 °C over the entire operating temperature range. However, as only 25 % of this temperature range is normally used and the sensors are individually calibrated before use in the field, the effect of this source of error is greatly reduced.

The main advantage in using this particular type of sensor is that it acts as a high impedance, constant current regulator when supplied with a suitable voltage. The output can therefore be transmitted over long distances by twisted pair cable without significant losses due to line resistance. The

temperature amplifier circuit is used to supply a voltage to the sensor and to convert the regulated current to an output voltage. The choice of circuit components determine the current, and hence temperature, range corresponding to the 0 to +5 V output from the unit. Fig. 4.15 shows the circuit diagram of a temperature amplifier for a single sensor, which is based on the 747 dual operational amplifier. Eight of these circuits are combined on a pcb in a single module, with 2 modules dedicated to each set of 16 sensors.

The output from each pair of 8 channel temperature amplifier modules is converted by the 16 channel ADC unit to a reading in the range 0 to 255 bits, which corresponds to the input voltage range of 0 to +5 V. The 16 channel ADC unit, and the way in which data are transferred from the ADC to the computer, is similar to that described in Section 4.3 with reference to the output from the radiometer.

Calibration of the sensors was carried out by placing the 32 sensors close together inside a draught free room, and allowing them to stabilize in free air. The readings from all 32 ADC channels were recorded, along with the air temperature measured by a mercury in glass thermometer near to the sensors. Several sets of ADC readings were taken at the same temperature to obtain an average, and to check that the output from the sensors was stable. Once calibration had been completed, the combinations of sensors and temperature amplifiers were not changed, as the response of each pair of sensor and associated amplifier circuit will be slightly different. Calibration graphs of ADC reading against temperature recorded by the thermometer show good straight line fits, with correlation coefficients better than 0.99 for most of the sensors. An example of a typical calibration graph is shown in Fig. 4.16. This shows that the useful operating range for an average sensor is from -9 to 44 °C, and that contact temperatures may be measured with a resolution of about 0.2 °C.

4.4.2 Installation in the field.

The disadvantage in using contact temperature sensors is that they will always disturb the surface to be measured, so the true contact temperature can never be measured to a high degree of accuracy. One of the major problems is in fixing the sensor to the surface so that there is good thermal contact between them. The two usual methods are to tape or glue the sensor in position, although both have the disadvantage of causing an unnecessarily large part of the surface to be disturbed. It is also possible to use a high thermal conductivity paste to improve thermal contact. This was investigated by Hübner and Gladen, 1981, who carried out field trials on an asphalt target under conditions of high incident solar flux. The results showed that when a thermally conducting paste was used, sensor readings were 1 to 2 °C higher due to the improved thermal contact. However, one problem which may arise from the use of paste is that some compounds of this type are hygroscopic. This can cause the surface around the sensor to become moist and affect the temperature recorded.

The effect of shielding the sensors from direct solar radiation under clear skies was also investigated in these trials. In the case of the shaded sensor, the temperature reading was found to be 1 to 2 °C higher at night, as the shield reduced the rate of heat loss. The temperature reading also rose more slowly in the morning and reached a peak later than the unshielded sensor. In general, it was found that unshielded sensors followed the variation of the incident direct solar flux fairly closely, but gave a reasonable idea of the behaviour of the temperature of the object. However, the shielded sensors were more affected by changes in the ambient air temperature than the solar flux, and did not show the more rapid fluctuations in temperature which were detected by the unshielded sensor. Under cloudy conditions, the difference in behaviour between the two types of sensor is much smaller, but even so, it would appear to be better not to use sun shields with the sensors.

These results were considered when it was decided to deploy sensors at the Observatory. However, unless the sensors were to be located in positions that were not affected by moisture or rain, then protection against possible short circuiting between the two terminals was required. This was achieved by covering the sensor with a thin layer of black self-amalgamating tape, which has good insulating and waterproofing properties. However there are two main disadvantages with this method. Firstly, even a thin covering of a single layer of tape will result in poor contact between the sensor and the object. Secondly, the addition of the tape covering will increase the thermal inertia of the sensor, and hence affect the response time to changes in the temperature of the object. The first problem can be reduced by removing the layer of tape from the sensitive area of the sensor, and by using a small amount of high thermal conductivity paste between the sensor and the surface whose temperature was to be measured. The second problem can be overcome to a certain extent by using as thin a layer of tape as possible, and by only choosing objects which are unlikely to undergo rapid changes in temperature; an example of this would be a thick stone wall which was in the shade.

A set of eight sensors was deployed on the balcony of the Observatory from 2nd April 1984 until 5th May 1984. The locations of six sensors were chosen to coincide with objects whose radiation temperature was being measured by the radiometer. These included the sandstone wall of the building and the plastic netting which was fixed to it. A complete description of the location of the sensors is given in Table 4.1.

Table 4.1   Locations of contact temperature sensors at Durham Observatory.

Sensor	Location
1	Taped to the asphalt floor of the balcony.
2	At a depth of about 8 mm in the west facing sandstone wall.
3	At depth of about 3 cm in south facing sandstone wall, with the amalgamating tape removed from the sensor.

Table 4.1   (Continued)

Sensor	Location
4	At depth of about 1.5 cm in south facing sandstone wall.
5	Tied to the green mesh on the side next to the south facing sandstone wall.
6	Tied to the opposite side of the mesh to 5, and in roughly the same place.
7	Tied to a nail holding the mesh in place, in contact with the outer surface of the sandstone wall.
8	Shaded, and in free air.

4.4.3 Comparison of target temperatures measured by the contact temperature sensors and the radiometer.

As several of the sensor locations were chosen to coincide with targets measured by the radiometer, it is useful to see how the results obtained from the two sources differ. Analysis of the data recorded after the sensors had been deployed shows that the most suitable weather conditions for comparison purposes were from the afternoon of April 2nd to the morning of April 7th. This consisted of a period of dry weather, when the sky varied between being clear and completely overcast. For the purposes of this comparison, it is sufficient to consider just the 48 hour period from noon on April 4th to noon on April 6th. The first 24 hours of this period consists of generally fine weather, although with some cloud forming on three main occasions. The sky stays clear from the start of the second 24 hours period until about 21:00 on April 5th, and then changes to being completely overcast. This is reflected in the behaviour of the incident short-wave solar flux, as measured by the weather station, and the long-wave cloud cover factor, which is derived from sky temperatures measured by the radiometer. The variation of these parameters over the 48 hour period is shown in Figures 4.17 to 4.20. In the next three sections, the temperatures measured by the contact sensors and the radiometer

will be compared in detail for three different objects.

4.4.3.1 Comparison of recorded temperatures for a south facing sandstone wall.

This is one of the exterior walls of the Observatory building, and is constructed from massive sandstone blocks about 1 m thick. The part of the wall under investigation was on the first floor, and was contained in a region from about 1.5 m to 2.5 m above the level of the asphalt covered floor of the balcony. The wall is partially shaded by a west facing sandstone wall, which projects out from the south facing wall by about 1 m. This shades the region of interest early in the morning, and so the wall first receives direct solar radiation at a later time than for an unobscured south facing wall.

Two contact sensors were buried at different depths in the wall. The sensor at a depth of 3 cm, (reference number 3), did not have a protective covering of amalgamating tape, while the other, (reference number 4), was at a depth of 1.5 cm and had the normal thin covering of tape in place. The temperature of the wall was also measured by the radiometer in two areas near to the location of the sensors. Due to the massive nature of the wall, an exact correspondence between the radiometer targets and the sensor locations is not too important for the purpose of this comparison. However, the geometry of the site means that if the two were separated by a significant distance, the shading effects of the west facing wall nearby would have to be taken into account.

The temperature measurements made on the wall over the 48 hour period of interest are shown in Fig. 4.21 and Fig. 4.22. These two diagrams show the contact temperature measured by sensor number 3, and the temperature of one of the two areas on the wall measured by the radiometer. The temperature recorded by the radiometer is expressed as a radiation temperature; that is the effective temperature of a black body, (with emissivity = 1), which would radiate the same flux as the surface of the wall. This can be converted to the corresponding surface contact temperature using the following equation, which

assumes that the flux measured by the radiometer is entirely composed of radiation emitted by the wall. The radiation emitted by surrounding objects which is reflected off the surface of the wall is excluded in order to simplify the calculation. The equation is derived from the Stefan-Boltzmann law and the definition of emissivity.

$$T_c = (T_R + 273.15) \times e^{-0.25} - 273.15 \qquad (4.2)$$

where; T_c = Contact temperature in °C,

T_R = Radiation temperature in °C,

e = Emissivity of the surface over the operating range of the radiometer.

The emissivity of the wall was not measured at the Observatory, and it is also uncertain whether the wall behaves as a simple grey body, with the emissivity independent of the wavelength of the emitted radiation, or as selective emitter, where the emissivity is a function of emission wavelength. However, measurements on similar sandstone surfaces, (Balick et al., 1981), suggest that the emissivity is likely to be about 0.94 assuming the simpler case of a grey body emitter.

The first graph, Fig. 4.21, shows that the temperature measured by the radiometer follows small, rapid fluctuations in the temperature of the wall. However, because the contact temperature sensor is located below the surface of the wall, its response is much smoother and only shows when large changes in the temperature of the wall occur. The sensor also shows that the temperature inside the wall reaches a peak value later in the afternoon than the surface radiative temperature, and cools more slowly in the late afternoon and in the evening. Overnight, the surface temperature stays relatively constant, while the interior of the wall looses heat by conduction to the surface and becomes cooler. In the morning, the surface radiative temperature rises sharply when the wall begins to receive direct solar radiation, while

the sensor reading rises more slowly as heat from the surface is conducted into the wall material.

The second graph, Fig. 4.22, covers the period from 12:00 on April 5th to 12:00 on April 6th 1984. This is a particularly interesting period to consider as the first 9 hours are totally cloud free, and are followed by complete cloud cover for the remaining time. This is clearly shown in the plots of incident short-wave solar flux and long-wave cloud cover factor in Fig. 4.19 and Fig. 4.20. The behaviour of the measured temperatures of the wall on the afternoon of April 5th is similar to that under similar weather conditions on the previous afternoon. However, when the cloud begins to form, the radiation temperature of the surface of the wall can be seen to stay fairly constant, but the interior temperature of the wall continues to fall as heat is lost by conduction to the surface. This process continues in the morning of April 6th, when the thick cloud cover does not allow sufficient solar flux to reach the wall and start heating the surface up again.

It is also interesting to compare these results with other radiation and contact temperature data available. Radiometer measurements were made on a part of the wall close to the one previously described, and it was found that the variation of radiation temperatures from the two areas over the 48 hour period of interest were virtually identical. A second contact temperature sensor (reference number 4), was located close to the first, but at a depth of 1.5 cm below the surface of the sandstone wall and covered by a thin layer of amalgamating tape. The responses of the two sensors were virtually identical, suggesting that the presence of amalgamating tape had little effect in this case. This is perhaps not surprising, as the results for the first sensor, which did not have a covering of tape and would be expected to have a higher sensitivity to variations in the temperature of the sandstone, showed a smooth response on both graphs.

4.4.3.2 Comparison of recorded temperatures for a south facing sandstone wall

    covered by plastic netting.

The netting was located on the same south facing sandstone wall as described in the previous section, and directly below the area where the exposed wall temperature was measured. There were three contact temperature sensors used in connection with the netting, all of which were covered by a thin layer of amalgamating tape. Two sensors were tied to the netting; one on the side facing the wall, (reference number 5), and the other, (reference number 6), tied on the opposite side and in roughly the same location. The third sensor, (reference number 7), was fixed to one of the nails holding the netting in place, and in contact with the surface of the sandstone wall.

Fig. 4.23 and Fig. 4.24 show the radiation temperature of the netting which covers the wall, and the contact temperature of the wall surface beneath the netting measured by sensor number 7. In this case, the radiation temperatures are similar to those measured for the exposed wall at night, but are lower during the day. The peak contact and radiation temperatures occur at about the same time, and any time lag between the two peaks which may be expected due to the thermal inertia of the sensor is too small to be apparent on the graph.

It can be seen in Fig. 4.23 that the variations in the contact temperature are larger than those exhibited by the measured radiation temperature. This is probably a result of two factors. Firstly, direct solar heating of the sensor, and secondly because the radiometer is measuring the temperature of the netting covering the wall, rather than the surface temperature of the wall as measured by the contact sensor. Therefore, it is likely that while direct solar heating may cause large fluctuations in the surface temperature of the wall, as shown in the response of the contact sensor, the effect of the netting is to significantly reduce the magnitude of these fluctuations as seen by the radiometer. Evidence for this may be obtained from a comparison of the measured radiation temperatures of the

sandstone wall covered by netting, and those for the exposed wall described in the previous section. Fig. 4.21 and Fig. 4.23 show clearly that the measured radiation temperatures are almost identical at night, and exhibit the same cooling effect as heat is lost from the surface of the wall. However, after sunrise, the radiation temperature of the netting increases more slowly than the temperature of the exposed wall surface, and reaches a lower peak temperature in the early afternoon.

It is interesting to compare the results obtained from sensor 7 with those from the other two sensors fixed to the netting. The sensor fixed to the side of the netting next to the wall shows the same type of response as sensor 7, although the magnitude of the variations in temperature during the day are a few degrees larger, and at night the measured temperature is about 3 °C cooler. Sensor 6, on the opposite side of the netting, behaves similarly, but the measured temperature at night is a couple of degrees cooler than that recorded by sensor 5. However, due to the nature of the netting, these large temperature fluctuations are almost certainly due to the effect on the sensors of direct solar heating, cooling by the wind, and variations in the air temperature.

4.4.3.3 Comparison of recorded temperatures for a west facing sandstone wall.

Temperature measurements on the west facing sandstone wall were made at the same height above the balcony as for the south facing wall. The sensor was located at a depth of about 8 mm beneath the surface of the wall, and covered by a thin layer of amalgamating tape. The radiation temperature was measured for an area of the wall close to the sensor, and Fig. 4.25 and Fig. 4.26 show the results obtained. The graphs show that the contact and radiation temperatures are fairly similar in behaviour, reaching a peak temperature at roughly the same time and exhibiting the same type of cooling behaviour at night.

It is interesting to note that although there is good agreement in the

variation of contact and radiation temperatures, the contact temperatures are consistently about 1 °C lower than the radiation temperatures both at night and during most of the afternoon. However, assuming a more realistic value of 0.94 for the emissivity of the wall, the difference between the measured contact temperature, and that derived from the radiation temperature using Equation 4.2, would increase to about 6 °C. It is not apparent what is responsible for this difference, but it may be due to poor contact between the sensor and the wall.

4.4.3.4 Summary.

The results of the last three sections give a good idea of the differences between surface temperatures measured by the radiometer, and temperatures measured by contact sensors both at and below the surface of an object.

In Section 4.4.3.1, the radiation temperature of the surface of a south facing sandstone wall was compared with a sub-surface temperature sensor reading. The radiation temperature fluctuated rapidly under the influence of the surface weather conditions, while the response of the contact temperature sensor was much smoother.

Sections 4.4.3.2 and 4.4.3.3 compare radiation temperatures with surface contact temperatures. In the first section, the results shown in Fig. 4.23 and Fig. 4.24 for the south facing sandstone wall and netting, suggest that the contact temperature sensors are capable of detecting fairly rapid variations in temperature.

In the second section, the contact temperature sensor and the radiometer were used to measure the surface temperature of the west facing sandstone wall. As before, the behaviour of the contact and radiation temperatures was similar, although after assuming a realistic value for the emissivity of the wall there was a significant disagreement between the two sets of measurements.

In general, the results suggest that contact temperature sensors are most suitable for measuring variations in temperature over a period of time, and that absolute values may be more accurately determined with a radiometer. The reasons for this are outlined in Section 4.4.2, which are that it is very difficult to ensure good contact between the sensor and the surface of interest, and that fixing the sensor to an object will cause a change in its thermal properties.

4.4.4 Comparison of air temperatures measured by a contact temperature sensor in free air and the weather station.

One of the set of eight sensors was used to measure the air temperature on the balcony of the Observatory. The sensor was covered with a thin layer of amalgamating tape, shaded, and suspended in free air. In this section, the results from this sensor are compared with the data from the automatic weather station located on the Observatory lawn. The weather station measures the air temperature with a platinum resistance thermometer, which is located inside a screen as described in Section 4.5.2.5. It was not anticipated that the two measurements would be in exact agreement for several reasons. Firstly, the weather station was located about 20 m away from the sensor, and measured the air temperature at a different height above ground. Secondly, although the sensor was shaded and in a relatively sheltered location, it was still subject to the cooling effects of wind. Finally, the sensor was not protected by a radiation screen, so the temperature recorded would be influenced by convective and radiative heat exchanges with the surroundings. These consisted of the asphalt covered floor of the balcony and the sandstone walls of the Observatory building.

It was decided that it was most suitable to compare the data from the weather station and the contact temperature sensor over a similar period to that considered in the previous section. The period from 12:00 on April 2nd to 12:00 on April 6th was chosen, as this contains a varied selection of weather

conditions. Up to about 21:00 on April 5th there was generally fine weather with some short cloudy periods, but afterwards conditions changed to being completely overcast. The short-wave solar flux and long-wave cloud cover factors for part of the period of interest have already been shown in Figures 4.17 to 4.20. The first two graphs cover from 12:00 April 4th to 12:00 April 5th, but are also representative of the conditions on the two previous days. The other two graphs cover from 12:00 April 5th to 12:00 April 6th, and show clearly when the sky became overcast. The weather stayed dry over the four days, and the wind speed was in the range from 1 to 4 metres/sec. Measurements of the air temperature were made by both sensors at roughly the same time interval of 15 minutes.

The two sets of temperature readings are shown in Figures 4.27 to 4.30. In the first of these, the sensor reading is initially higher than the temperature recorded by the weather station. Agreement is then quite good for the period from midnight on April 2nd until noon on April 4th, with a maximum difference between the two readings of about 1 °C. On the afternoon of April 4th, Fig. 4.29 shows that the contact temperature sensor readings are about 2 °C higher than those from the weather station. The reason for this is unclear, although it may be due to radiation from surrounding objects causing the contact sensor to heat up. This is suggested by the disagreement between the readings being greatest in the early afternoon, when the direct solar flux incident on the surrounding walls and balcony roof is highest. Then, in the later afternoon, the difference between the readings is slowly reduced as the solar flux decreases, and better agreement is restored in the evening.

The fourth graph covers from noon on April 5th to noon the next day. Again, disagreement between the two sets of readings can be observed, presumably due to the reasons outlined in the previous paragraph. This might not be expected for the second half of the graph as this period was completely overcast, resulting in there being little direct solar radiation to heat the surroundings of the sensor. However, the difference between the two sets of

temperature data is only about 1 °C at the most.

In summary, it appears that contact temperature sensors may be useful to obtain an idea of how the temperature of free air varies. However, it is possible that radiative and convective heat exchanges with the surroundings may give rise to errors as the sensor heats up, and therefore the readings from the weather station will be more accurate.

4.5   Weather station.

4.5.1 Introduction.

A Didcot automatic weather station and a Microdata M1600L data logger were used to obtain the weather data necessary as inputs for computer modelling. The weather station is illustrated in Figure 4.31, and is designed to record data for seven different weather parameters. The sensors are also shown on the diagram; six are mounted on the mast structure, which consists of two horizontal crossarms attached to a vertical aluminium mast, with the seventh being a freestanding rain-gauge. The mast has a circular alloy base, which is buried in the ground and additional support for the structure is provided by stainless steel guy wires. The sensors are connected via plugs and sockets to a waterproof junction box fixed to the mast. A single multicore cable connects the junction box to the data logger, which is sealed in a weather resistant case. The outputs from the sensors are recorded on magnetic tape, and most of the data have been recorded with an interval of 15 minutes between successive measurements of weather conditions. Values of the following parameters were recorded; solar radiation, net earth/sky radiation balance, wind speed and direction, air temperature, wet and dry bulb depression, and rainfall. The logger is designed so that different interface cards may be used, which enables the sensor output to be logged either instantaneously at the end of the scan, or alternatively an average value over the interval between scans may be found. In the next seven sections, the weather sensors and the data logging system will be discussed in more detail.

4.5.2   Weather sensors.

4.5.2.1 Pyranometer.

This sensor is used to measure the short-wave solar radiation received by a horizontal surface over a field of view of 180°. The instrument in use is illustrated in Fig. 4.32. It is the CM5 version of the Kipp solarimeter, which measures radiation over a wavelength range from 0.3 to 2.5 microns. It is a Moll-Gorczynski type of instrument, in which a thermopile is used as a sensor. The thermopile consists of alternate thin strips of constantin and manganin, arranged as illustrated in Fig. 4.33 to form two sets of junctions; one set along the centre of the thermopile and the other set along the edges on either side. The ends of the strips rest on posts which are fixed to a copper plate of high thermal capacity, such that the posts are in good thermal contact with the plate but electrically insulated from it. Gaps between adjacent strips are filled with a varnish of low thermal conductivity to form a flat surface. The thermopile is blackened and protected by two optically polished concentric glass hemispheres, which are fixed to a heavy metal case. The outer hemisphere is used to protect the thermopile from the effects of wind and rain. The inner hemisphere is used to reduce the radiative and convective heat exchanges between the thermopile and the outer hemisphere, which is affected by the ambient air temperature. All exposed areas of the instrument case are highly polished to reduce absorption of radiation, and a silica gel drier is used to keep the interior of the detector free from moisture. The case is protected from solar heating by a white, circular radiation screen, which also prevents radiation incident from angles outside the 180° field of view from being reflected onto the thermopile via the glass hemispheres. The instrument is mounted at the top of the vertical mast of the weather station, such that the thermopile and screen lie in the same horizontal plane.

When the thermopile is exposed to solar radiation, heat is conducted from the junctions in contact with the supporting posts to the copper plate. The junctions at the centre are therefore hotter than those at the edges,

resulting in the thermopile producing an output voltage proportional to the temperature difference between the two sets of junctions. The instrument was calibrated by the manufacturer and the sensitivity is quoted as 0.117 mV mW^{-1} cm^2, with an accuracy of $\pm$ 1%.

4.5.2.2 Net radiometer.

This instrument measures the difference between upward and downward short and long-wave radiation in the range from 0.3 to 80 microns. The sensor consists of a multiple element copper-constantan thermopile with opposite sets of junctions in contact with two parallel, circular black radiation receivers. The receivers are protected by polyethylene hemispheres, and kept free from moisture by a silica gel drier. The radiometer is located at the end of the lower crossarm of the weather station, and adjusted so that the two receivers are horizontal, with one facing the ground and the other pointing towards the sky. The lower receiver faced a reasonably flat area of grass on the lawn in front of the Observatory. This was chosen as it is free from any strong reflectors of radiation and is representative of the grass surfaces on the lawn which have been simulated with the vegetation model.

In operation, any difference between the upward and downward fluxes will result in a corresponding temperature difference between the two receivers. The thermopile will therefore produce an output voltage, the polarity of which is determined by whether the direction of the net flux is into or away from the ground. The instrument was calibrated by the manufacturer and its sensitivity to differential radiation fluxes is quoted as 0.082 mV mW^{-1} cm^2.

4.5.2.3 Wind speed.

The anemometer is of a standard design, and is capable of measuring wind speeds in the range 2 to 250 km/hr. It is mounted on one end of the upper crossarm of the weather station, at a height of around 2.3 m above ground level. The instrument uses three cups of approximate diameter 12 cm, and

contains a magnetically operated reed switch designed to produce one contact closure per revolution. A pulse counter interface card is used in the data logger to record the total number of complete revolutions made in the interval between successive measurements. The average wind speed over the interval can be found using calibration data supplied with the instrument.

4.5.2.4 Wind direction.

This instrument is also of a standard design, and is located at the opposite end of the upper crossarm to the anemometer. The direction in which the vane is pointing is represented by a voltage produced by a potentiometer inside the sensor. This consists of a chain of 15 resistors of value 68 ohms, combined with 16 magnetically operated reed switches. The switches are connected at one end between adjacent resistors, and at the other to a common output line. In operation, the reed, or pair of adjacent reeds, nearest the orientation of the vane will close, hence producing an output voltage from the sensor. This can be converted to a wind direction provided the instrument is aligned with a known compass direction when the weather station is set up.

4.5.2.5 Thermal radiation screen.

This is used in place of a conventional Stevenson screen, and is illustrated in Fig. 4.34. It is mounted on the lower crossarm of the weather station at the opposite end to the net radiometer. Located inside the screen are two sensors which are used to measure air temperature and wet and dry bulb depression. Both sensors consist of platinum resistance thermometers housed in a protective, thin walled, stainless steel tube. The air temperature sensor contains one element, and is located in free air. The wet and dry bulb depression sensor consists of two sensitive elements, spaced longitudinally about 10 cm apart. One of the elements is covered by a wick, the opposite end of which dips into a water reservoir, while the other element acts as a dry bulb and is located in free air. The thermometers are mounted on top of the

cylindrical aluminium water reservoir, and are protected from direct sunlight by an aluminium radiation shield.

4.5.2.6 Raingauge.

This was located on an exposed part of the lawn a few metres away from the weather station. It is a standard 8" tipping bucket raingauge, with a bucket capacity correponding to 0.5 mm of rain. A magnetically operated reed switch detects when the bucket tips, and the number of contact closures occuring are counted by the interface card in the data logger.

4.5.3 Data logging system.

A Microdata M1600L data logger was used to record the information provided by the instruments on the weather station. The logger is housed in a weather resistant case, and can either be powered by a 240 Volt mains supply or its own internal rechargeable batteries. A single multicore cable runs from a connector at the rear of the logger to a junction box, attached to the vertical mast of the weather station, from which connections are made to the seven weather sensors previously described.

The logger can record data from up to 20 input channels, and nine of these were in use when the equipment was at Durham Observatory. Each of the channels used a signal conditioning card to either provide data or convert the input signal to the form required by the logger. The first two channels were dedicated to a day counter and a real time clock, and the other seven used for the output from the weather sensors. The third channel contained a signal average card, which was used to obtain a value for the average solar flux received by the solarimeter over the logger scan period. This was achieved by using a voltage to frequency conversion process with the amplified output voltage from the solarimeter, followed by a pulse counting stage. The logged reading allowed the average solar flux to be deduced with a resolution of about 2 W m^{-2}. Out of the remaining six cards, two were four decade pulse

counters dedicated to the anemometer and raingauge. The other four were used to convert analogue information from the sensors to the $\pm$ 1 Volt range compatible with the input range of the analogue to digital converter used in the logger. The way in which this was accomplished depended on the type of signal input to the card.

The cards used for the two channels measuring air temperature and wet and dry bulb depression were both similar in design. The thermometer replaced one arm of a resistance bridge circuit for the former, while for the latter, the temperature difference was measured by replacing two arms of the bridge with the wet and dry thermometers. The output voltage of the bridge was then amplified to the $\pm$ 1 Volt level, and after digitization, a reading in the range of -1000 to +1000 was recorded. This corresponds to a maximum theoretical range of -100 to +100 °C, which allows the temperature to be determined with a resolution of 0.1 °C.

The other two interface cards were used with the wind direction sensor and the net radiometer. The first card provided a supply voltage to the potentiometer in the sensor and measured the output voltage from the wiper. The logger reading was proportional to the ratio of the voltages, and the wind direction could be deduced from a calibration graph supplied with the instrument. In the case of the net radiometer, the card simply consisted of an amplifier to raise the output voltage of the net radiometer to the $\pm$ 1 Volt level used in the logger.

All nine channels were recorded at 15 minute intervals in Durham, although the interval may be set to any value within a range from 20 ms to 99 minutes. When the logger is in operation, the reading from any particular channel can be monitored on a liquid crystal display, and is updated either continuously or every time the channel is scanned. Data are recorded on a standard DC300 magnetic tape cartridge, and the tape is divided into 4 separate tracks. When the logger has filled one track, it will automatically rewind the tape and start recording on the next track.

After the measurement period has been completed, data may be analysed using the replay facility on the logger, in which the LCD is used to monitor the recorded data. However for long term storage of the data recorded at Durham, the data were transferred to the Tektronix 4052 computer via the RS232C interface, and stored on standard computer compatible DC300 data cartridges.

4.6   Operation of the data acquisition system under computer control.
4.6.1 General description of the method of computer control.

The autoguidance of the pan and tilt head and the acquisition of temperature data is controlled by the Tektronix 4052 computer, operating under a BASIC program. The program is described in detail in the Appendix, and this section will only be concerned with a description of the autoguidance and data acquisition process.

Initially, the program allows the operator to specify a sequence of objects for which radiation temperatures are to be measured. This is achieved by using the joystick on the servo control unit to move the pan and tilt head, while observing the CCTV monitor showing the region inside the field of view of the radiometer. When the desired object is in the field of view, the position of the pan and tilt head is recorded by presssing one of the user definable keys on the computer. The position of the pan and tilt head is obtained from two sensors, which provide a digital azimuth and zenith reading by the method described in the next section. These readings can be stored on tape for subsequent use by the computer.

When the system is operating in the automatic data logging mode, the operation of the system can be divided into a sequence of four main functional steps. This data acquisition sequence is explained briefly below and outlined in Fig. 4.35.

(1) The current azimuth and zenith positions of the pan and tilt head are obtained.

(2) This positional information is converted to a digital form suitable for transfer to the computer.

(3) The computer reads in the digital position of the pan and tilt head and compares it with the specified value for the object stored in its memory. It then calculates how the pan and tilt head should move so that the radiometer will be pointing at an area closer to the object, and converts this to the appropriate digital code.

(4) The digital output from the computer is converted to an analogue form. This is sent to the servo controller which drives the motors in the pan and tilt head.

At the end of step 4, the sequence repeats itself. This continues until the current position of the pan and tilt head coincides with the stored value in the computer, at which point the desired object will be in the field of view of the radiometer. The computer can then read out the contents of the 8-bit ADC units to find the current readings from the contact temperature sensors and the radiometer.

In the next section, the main steps in the autoguidance and data acquisition procedure are explained in more detail. Fig. 4.4 is a block diagram showing the relevant electronics.

4.6.2   Detailed description of the autoguidance and data acquisition method.

4.6.2.1 Determining the position of the pan and tilt head.

This is achieved by the use of two potentiometers inside the pan and tilt head. These are 10 turn, 1K linear potentiometers which have a small cogwheel attached to the end of the wiper spindle. In both cases, the potentiometer is securely fixed to the same plate as the drive motor, such that both the cogwheels on the potentiometer spindle and the motor drive shaft are in gear with a larger cogwheel. One large cogwheel is fixed to the baseplate mounted on the top of the field station, so the entire head rotates

about it. The other cogwheel has the tilting platform attached to it, so when it rotates under power from the tilt motor, there will be a corresponding change in tilt of the platform. This means that whenever the pan and tilt head moves under power from the two motors, a corresponding rotation in the potentiometer spindles will be produced. Therefore, if the potentiometers are used with a suitable supply voltage across them, the output voltage for the wiper can be used to sense the position of the platform.

4.6.2.2 Conversion of the analogue position of the pan and tilt head to a digital form.

The voltage across the potentiometers is derived from the +5 V supply in the electronics crate located in the operation console. The output from the potentiometer wipers goes to the 11-bit ADC unit in the electronics crate, via the 50 m cable harness. The ADC unit has one conversion channel dedicated to the output from each potentiometer. As both channels use the +5 V supply as a reference voltage, then the unit produces two readings from 0 to 2047 for the wiper voltage. It is based on the National Semiconductor ADC1211 i.c., which can make a 12-bit conversion in 100 microseconds. A block diagram outlining the circuit is given in Fig. 4.36.

The operation of this unit under computer control is similar that described for the 8-bit ADC, and the readout is also transmitted to the computer via the 11-bit bus controller and the GPIB. The readout process is initiated when the computer acts on the BASIC command: "READ@7,2:X$". The primary address specifies the 11-bit bus controller, which is device number 7 on the GPIB, while the secondary address selects the 11-bit ADC unit for data transfer. The microprocessor in the bus controller then activates the lines on the 11-bit address bus which specify the ADC board. As shown in Fig. 4.36, line 7 is used for two purposes. Firstly to cause a pulse to be applied to the start conversion input of the ADC, which resets the device and initiates the conversion of both channels. The digital output from each ADC goes to a pair

of tri-state hex buffers, which are used to interface the ADC to the 11-bit data bus. The connections between the buffers and the data bus are such that data lines 0 to 10 correspond to the digital outputs from LSB+1 to MSB. The LSB output is not used as the data bus is not capable of 12-bit resolution. The output from the buffers is kept in the high impedance state until the bus controller is ready to receive the data.

Secondly, line 7 is used in combination with lines 0,1 and 4 to 6, to select which one of the two channels is to put data out on the 11-bit data bus. Line 7 enables the 3-to-8 line decoder, the inputs for which are lines 4 to 6 of the address bus. These cause one of the 8 outputs from the decoder to make a high to low transition, which is used to enable the 2-to-4 line decoder. Address lines 0 and 1 are used as inputs for this decoder, with the outputs allowing any one of four channels on the board to be selected. In this case, only two channels are in use, so two outputs from the decoder are connected to the tri-state disable input on the two pairs of hex buffers. Selection of one of these output lines causes the digital data from the relevant channel to be put on the 11-bit data bus, and sent to the bus controller. The data are transferred as an ASCII string over the GPIB to the computer, with two characters being used to represent the reading from each channel. This can be converted by the computer to give the digital reading from 0 to 2047.

4.6.2.3 Generation of digital data by the computer to move the pan and tilt
head.

When the computer has read in the current position of the pan and tilt head, it compares the azimuth and zenith readings with those for the object which are stored in its memory. If either or both of the readings are not equal, the computer works out the difference and initiates the process to move the pan and tilt head so that it is pointing nearer to the object. The first stage in this sequence is to calculate how far the pan and tilt head is from

the object and the direction in which it should move. This is represented by a decimal number, which is sent out over the GPIB when the computer executes an I/O statement of the form "WBYTE@37,13:X". The primary address specifies that device number 5 on the GPIB, which is the motor controller, has been selected to act as a listener in the data transfer. The decimal number containing the information regarding the movement of the pan and tilt head is represented in the above statement as "X", and is transferred over the GPIB data lines as an 8-bit code.

4.6.2.4 Conversion of digital data from the computer to an analogue form.

The motor controller unit contains a microprocessor which is programmed to act as an interface for an 8-bit DAC unit. This unit has two conversion channels which are used to provide control voltages for the pan and tilt motors. The circuit is based on the Analog Devices AD7525, and a block diagram is given in Fig. 4.37. The two units are linked by an 8 line data bus and 4 address lines. The digital data from the motor controller enters an 8-bit bistable latch, which stores the data on the inputs to the DAC for as long as it is enabled. The motor controller uses the address lines to operate the 4-to-16 line decoder on the DAC board, which selects the channel to provide the analogue output. Two of the output lines from the decoder are used, and these are connected to the chip select pins on the two DAC's. When one of the channels is selected, the chip select input makes a high to low transition, and the DAC enters write mode, converting the digital input to an analogue voltage in the range from -12 to +12 V. When the chip select input returns to the high state, the DAC goes into hold mode, where the analogue output remains at the value corresponding to the last digital data input before the chip select line went high. The computer can then send data to the second DAC channel while the first is still generating a control voltage.

4.6.2.5 Use of the analogue voltages to drive the pan and tilt motors.

The two voltages from the DAC unit are routed to the servo controller via two switches on the main console front panel. These switches are used to select the velocity input to the servo amplifier as the voltages from the DAC when the system is under computer control, or the voltages generated by the joystick potentiometer on the servo controller for manual operation of the pan and tilt head. The servo amplifier uses the voltages to control the velocity of the motors in the pan and tilt head, and the resulting signal is sent out via the 50 m cable harness.

The data acquisition process then returns to the first step in the sequence, where the computer reads the current position of the pan and tilt head. The computer then works out how much the pan and tilt head has moved, and sends out new instructions to the DAC which alter the velocity of the pan and tilt motors.

This continues until the position of the pan and tilt head corresponds with the stored co-ordinates in the computer memory, at which point the radiometer will be pointing at the desired object. The computer then sends data to the DAC so that the analogue output goes to 0 V, and stops the movement of the pan and tilt head.

4.6.2.6 Acquisition of temperature data.

When the radiometer is correctly positioned with the object in its field of view, the computer then executes the part of the program determining the type of data to be recorded. The data format used in Durham is described in Section 4.7, but basically consists of the date and time, the reference number of the object in the specified sequence, and the readings from the contact temperature sensors and the radiometer. The autoguidance process then restarts using the next pair of co-ordinates in the sequence.

After time and temperature readings have been logged for all of the objects in the sequence, the data stored in the memory of the computer are

written on tape. The pan and tilt head is then moved so that the radiometer is pointing at the first object in the sequence again, and the computer sends signals to the DAC to stop the pan and tilt head in this position. The system waits at this point for the time interval specified by the operator when starting the autoguidance and data acquisition program. At the end of this time interval, the real time clock ROM pack signals the computer to start the data acquisition process again.

4.6.3 Operating capabilities of the autoguidance system.

The operating performance of the hardware and software described in the previous section determines two important properties for the data acquisition system: the accuracy with which the radiometer may be positioned to point at a specified object, and the rate at which temperature data for different objects can be acquired.

The method used to determine the position of the pan and tilt head was outlined in Section 4.6.2. Assuming that backlash can be ignored and that the potentiometers are not a source of error, the accuracy with which the position may be determined will depend on the resolution of the ADC. For movement in the pan direction, it is found that a change in the azimuth angle of $360°$ corresponds to a change in the output from the ADC of about 1600 bits, and similarly a change in the zenith angle of the platform of $180°$ leads to a change in the ADC reading of around 800 bits. This suggests that for both cases, the position of the pan and tilt head can be determined with a resolution of about $0.2°$. This could be improved if the gearing on the potentiometers was changed such that the movement through the maximum pan angle of $360°$ and tilt angle of $180°$, corresponded to the maximum possible change in ADC readings, which for an 11-bit device would be 2047. However, this is not necessary as the currently obtainable resolution is well within the $2°$ field of view of the radiometer.

The ultimate factor which determines the data acquisition rate is the

speed with which the computer can read the position of the pan and tilt head

and generate the appropriate control signals for the DAC. The computer can

carry out the process described in Section 4.6.2 at a rate of about 10 times

per second, which allowed a typical sequence of 30 objects at Durham

Observatory to be covered in 4 to 5 minutes. However, the rate at which

temperature data may be acquired for different objects depends mainly on their

locations relative to each other; it will obviously take longer to complete a

data acquisition sequence where the objects are widely separated than one

where they are closer together. The other factor which must be taken into

account is that the maximum angular velocity of the tilting platform is 25%

slower than that for motion in the pan direction of the pan and tilt head.

Therefore the order of the different objects in the sequence needs to be

chosen carefully in order to minimize the time taken.

4.7   Methods of data storage.

4.7.1 Short term storage of radiometer and contact temperature sensor data.

As outlined in Section 4.6, data are recorded on a standard DC300

magnetic tape cartridge in the internal tape drive of the computer for each

object in a fixed sequence. The format of the stored data is specified in the

autoguidance and data acquisition program, and is chosen so that tape usage is

minimized while all the necessary data are recorded, enabling the system to be

left unattended for suitably long periods before the tape needs to be changed.

When the equipment was in use at Durham, the storage format was altered

three times during the initial few months of operation before a final version

was decided on. This consists of a single string containing the data for each

object in the sequence, which is written to tape after the temperature

measurement for the last object in the sequence has been made. The data string

starts with the date and time at which the temperature measurement for the

first object in the sequence is made. This is read by the computer from the

real time clock ROM pack, which is set to GMT by the operator when the autoguidance and data acquisition program is started. This is followed by the reference number of the object and the readings from the 33 channels in use on the 8-bit ADC boards. The method of obtaining the ADC readings is described in Section 4.3.3, and these readings correspond in order to contact temperature sensors 1 to 31, the contact temperature sensor inside the instrument package (sensor 32), and the temperature recorded by the radiometer. The other 15 channels of the third ADC unit are not used, and are therefore not recorded. The reading for each of the channels in use is represented in the data string by an ASCII character, which has a decimal value in the range 0 to 255 corresponding to the digital output from the 8-bit ADC. The advantage of using ASCII characters is that only 33 characters are required to repesent the data, compared to 99 if the equivalent decimal numbers were used. For subsequent objects in the sequence, it was decided to restrict the recorded data to the time, reference number of the object, and readings from the sensor inside the instrument package and the radiometer. The reason for omitting the date was that it could be easily deduced from the data for the first object. The other 31 contact temperature sensor readings were also not recorded again during the scan of the sequence of objects as they were either not in use, or fixed to surfaces that were not expected to show very rapid changes in temperature.

The resulting data string is written to a file on a standard DC300 magnetic tape cartridge after the temperature of the final object in the sequence has been measured. The data are stored as a binary string, which has the advantage of requiring less storage space than the corresponding ASCII form. Typically, scanning a sequence of 30 objects with a waiting time of 10 minutes between starting successive scans, the system can record data for a week before the tape needs to be changed.

4.7.2 Long term storage of radiometer and contact temperature sensor data.

The disadvantage of permanently storing data on DC300 cartridges is their high cost and the large number being required if the data acquisition system is to be used over an extended period. The other fact to be considered is that only a small fraction of the data obtained over the period of operation at Durham were recorded under weather conditions suitable for use with the models, so the bulk of the data is not required for routine analysis. It was decided to use a standard 9-track magnetic tape for long term data storage, which has several advantages over the use of DC300 cartridges apart from being more economic. Firstly, there is a significant reduction in the size of the medium required to store the data: one standard length tape can easily contain all the data recorded at Durham, which is the equivalent of about 45 DC300 cartridges. This also means the data can be easily transported and used at other computer installations, provided a suitable storage format is selected.

The method of data transfer consists of three stages. Firstly, the binary data strings need to be converted to an ASCII format. This is easily achieved by using a BASIC program in which the computer reads from a binary data tape in the internal tape drive, and then writes the ASCII data in a file on another DC300 tape cartridge located in an external tape drive, which is connected to the computer via the GPIB. The ASCII data format differs from the binary data in two respects. Firstly, the binary data string representing the results from one complete scan of the sequence of objects is split up into several shorter data strings. The first two strings consist of the date and the data for the first object in the sequence, including all the temperature sensor readings. These are followed by one short string for each of the other objects, giving time, reference number, and readings from the sensor inside the instrument package and the radiometer. Secondly, the ASCII characters representing the readings from the contact temperature sensors and the radiometer were converted to their decimal equivalents, as certain control characters which may be present in the data would corrupt the next stage in

the process.

The ASCII data is then transferred to a host VAX 750 computer which has a 9-track tape drive available. This is achieved by using a BASIC program to read data from the internal tape drive and send it to the host computer through the data communications interface. The data can be stored temporarily as a disc file in the host computer until a suitable amount of data have been transferred. It can then be written on the 9-track tape.

When any of the data which have been stored in this way are required for later analysis, it can easily be brought back to the Tektronix computer via the data communications interface, and stored on DC300 tape cartridges again.

4.7.3 Storage of weather data.

The data available from the weather station logger have already been described in Section 4.5.3. The data were recorded every 15 minutes at Durham, and consisted of a set of 9 readings which gave the date, time and the values of 7 different weather parameters. Using the appropriate BASIC program, the data were transferred from the logger to the Tektronix computer via the data communications interface, and converted so that the results for 24 hours were combined in one long ASCII data string. This was then stored in a file on a standard DC300 tape cartridge in the internal tape drive of the computer. A standard length DC300 tape cartridge will contain all the weather data recorded over a period of about 2 months, so only 6 cartridges were needed to store all the data recorded in observations at Durham. It was therefore acceptable to keep the weather data on DC300 tape cartridges as a long term measure.

4.8   Summary of available data.

4.8.1 Radiometer data.

The data acquisition system which has been described in the previous chapters was in almost continuous operation at Durham from February 1983 to

May 1984. This has provided temperature data for a wide range of objects, with measurements generally being made every 15 minutes. Objects which have been observed include trees, bushes, grass, an unmade road, and the sandstone walls of the Observatory building. Measurements have also been made of targets on the horizon and the sky temperature at several zenith angles. The former values are used in the model to provide an idea of the temperature of the surroundings for a particular object, and the latter to give a measure of the long-wave flux from the sky.

The data are now stored on 9-track tape, as described in the previous section. However, data for periods of particular interest are kept on DC300 tape cartridges for use with the analysis programs outlined in the Appendix. In this way, the data can be reduced to either a numerical or graphical form suitable for use with the modelling programs.

4.8.2 Contact temperature sensor data.

For most of the operating period of the data acquisition system, the majority of the temperature sensors were located inside the Observatory building. One exception was the sensor which was fixed to the optical unit of the radiometer in order to measure the temperature inside the instrument package. It was decided later in the period of operation of the system to attach some sensors to objects outside the building, and a set of eight sensors were deployed on the balcony of the Observatory from April to May 1984. These were fixed to surfaces including the sandstone walls of the building and the plastic netting attached to it. The locations are descibed in more detail in Table 4.1, and were chosen as far as possible to coincide with objects being measured by the radiometer. The sensor readings were logged at the same time as the radiometer measured the temperature of the first object in the sequence, which was roughly every 15 minutes. As the sensors were calibrated before deployment, the contact temperatures recorded can be easily deduced.

It is possible to compare the measured temperature for a particular object with the predictions from the model; but as discussed in Section 4.4.2, the main problem which arises when using sensors for validation purposes is finding the most satisfactory method of attaching the sensor to the surface. It was therefore decided to use the radiometer measurements for validating the model, which are likely to more be accurate as they do not involve contact with the object.

4.8.3 Weather data.

The weather data were recorded independently of the temperature measurement apparatus, and were derived from the automatic weather station described in Section 4.5. The data recorded at Durham Observatory cover the period from February 1983 to May 1984, and are continuous apart for a gap of three weeks in July when the equipment was unserviceable. The logger was set to record the weather conditions every 15 minutes, and the parameters recorded included the date, time, average solar flux, net earth/sky radiation balance, wind speed and direction, air temperature, wet and dry bulb depression, and depth of rainfall. The data are now stored on DC300 tape cartridges, and can be analysed using the results of calibrations carried out either at Durham, or by using information supplied by the manufacturer. The data can be reduced to a numerical or graphical form using the software described in the Appendix.

4.8.4 Summary.

The data which have been recorded at Durham cover a wide range of objects and weather conditions. With careful analysis, suitable periods of stable weather conditions can be identified. The weather and temperature data can then be used for applications such as model validation exercises.

WEATHER STATION

MICRODATA
LOGGER

OFF-LINE
DATA TRANSFER

8 m

32 CONTACT
TEMPERATURE
SENSORS

MAXIMUM
DISTANCE
100 m

OPERATOR'S CONSOLE.

TO HOUSE THE TEKTRONIX
4052 COMPUTER AND THE
ELECTRONICS CRATE.

FIELD STATION.

50m CABLE HARNESS

A WEATHERPROOF ENCLOSURE
CONTAINING THE RADIOMETER
ELECTRONICS PACK. A PAN
AND TILT HEAD IS FIXED TO
THE TOP, AND CARRIES THE
INSTRUMENT PACKAGE WITH
THE RADIOMETER AND CCTV
CAMERA INSIDE.

System Outline.

Fig. 4.1.

Fig. 4.2

Operator's Console.

METER DISPLAYING TEMPERATURE RECORDED BY RADIOMETER

PRINTER

CCTV MONITOR

SWITCHES TO SELECT AUTOMATIC OR MANUAL CONTROL OF PAN AND TILT HEAD

SWITCHES FOR MAINS SUPPLY TO FIELD STATION

TELEPHONE

SERVO CONTROLLER FOR PAN AND TILT HEAD

TEKTRONIX 4052 COMPUTER

ELECTRONICS CRATE

CONNECTORS TO CABLE HARNESS AND BETWEEN UPPER AND LOWER HALVES OF THE CONSOLE

Fig. 4.3
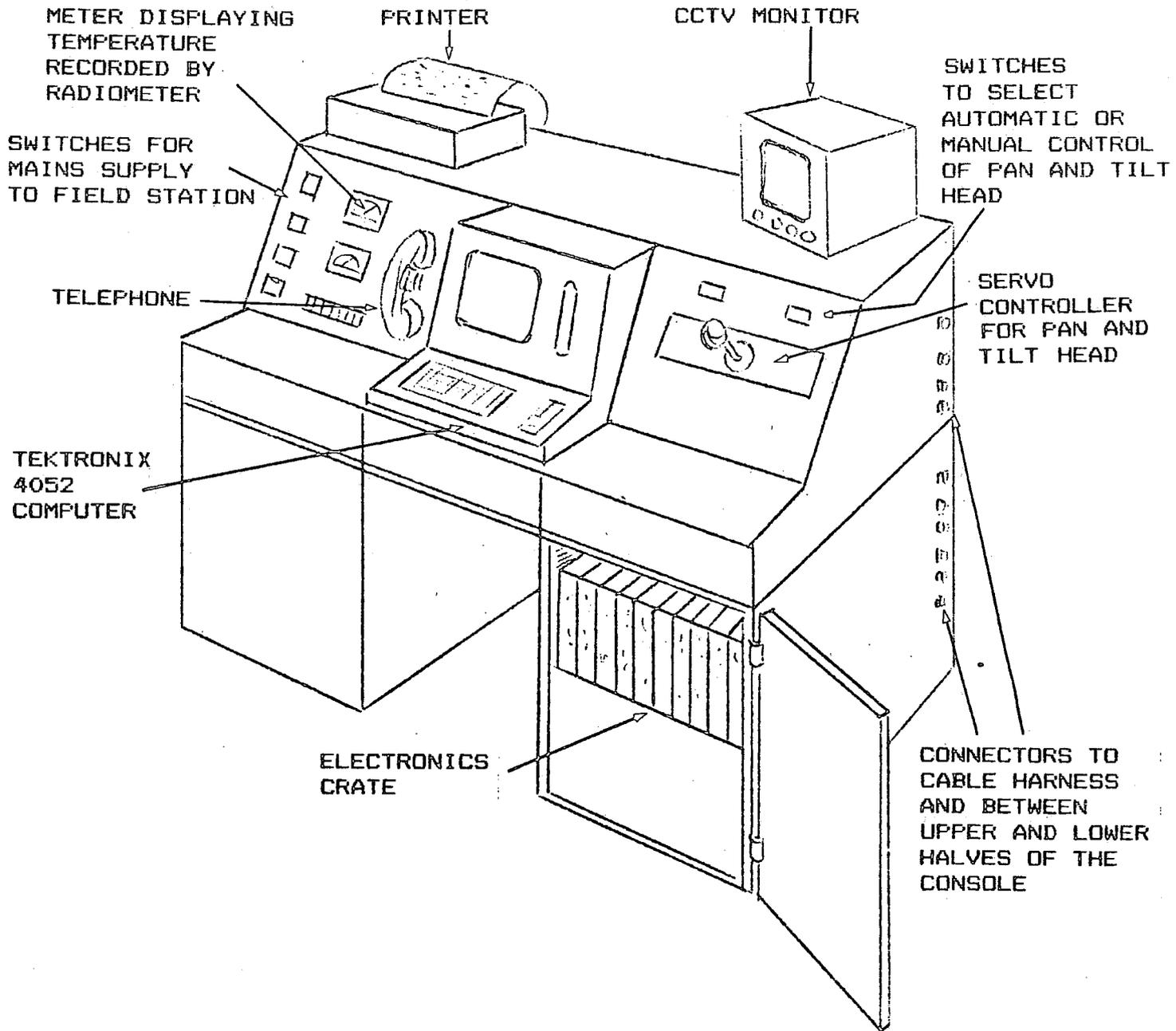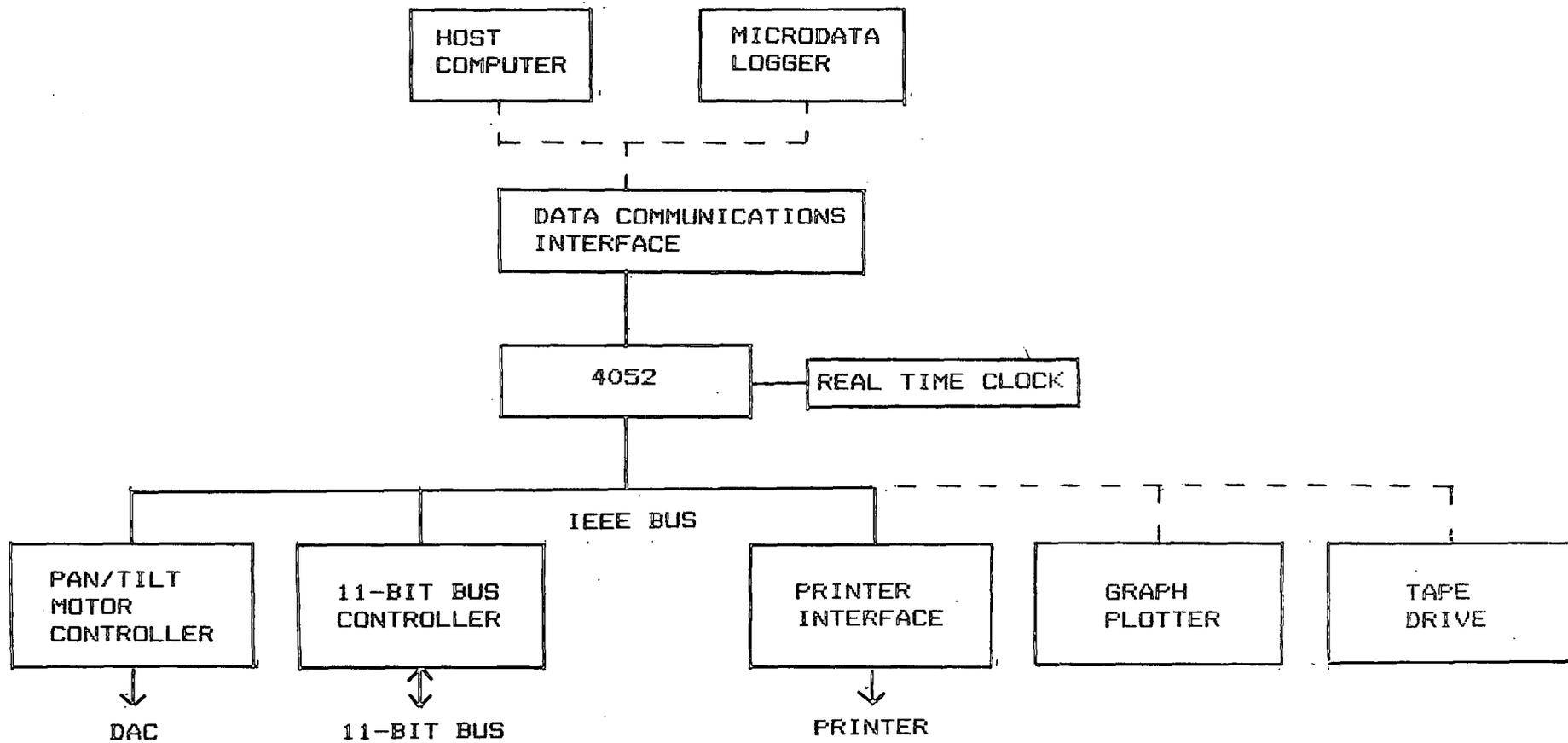
Computer Electronics Block Diagram.

Fig. 4.4

Electronics Block Diagram.

Fig. 4.5

The Instrument Package.

TV CAMERA

RADIOMETER

SIDE

VIEWING APERTURE
FOR TV CAMERA

VIEWING APERTURE
FOR RADIOMETER

FRONT

OPTICAL UNIT

TEMPERATURE CONTROLLED
REFERENCE CAVITY

OPTICAL
CHOPPER

INPUT
TARGET
RADIATION

LENS
FILTER

DETECTOR

THERMISTOR BEAD

CHOPPER
MOTOR

REFERENCE SYNC SIGNAL

MAGNETIC PICKUP

CAVITY TEMPERATURE
CONTROL SIGNAL

CAVITY TEMPERATURE
ERROR SIGNAL

PREAMPLIFIER   MAIN
SIGNAL

ELECTRONICS UNIT

CONTROL ELECTRONICS
FOR CAVITY HEATER

MAIN AMPLIFIER FOR
SIGNAL FROM DETECTOR

0-1 V
OUTPUT
SIGNAL

PANEL
METER

240 V
MAINS
INPUT

Fig. 4.6   Block Diagram of the Radiometer.

Fig. 4.7

Normalized Spectral Characteristic
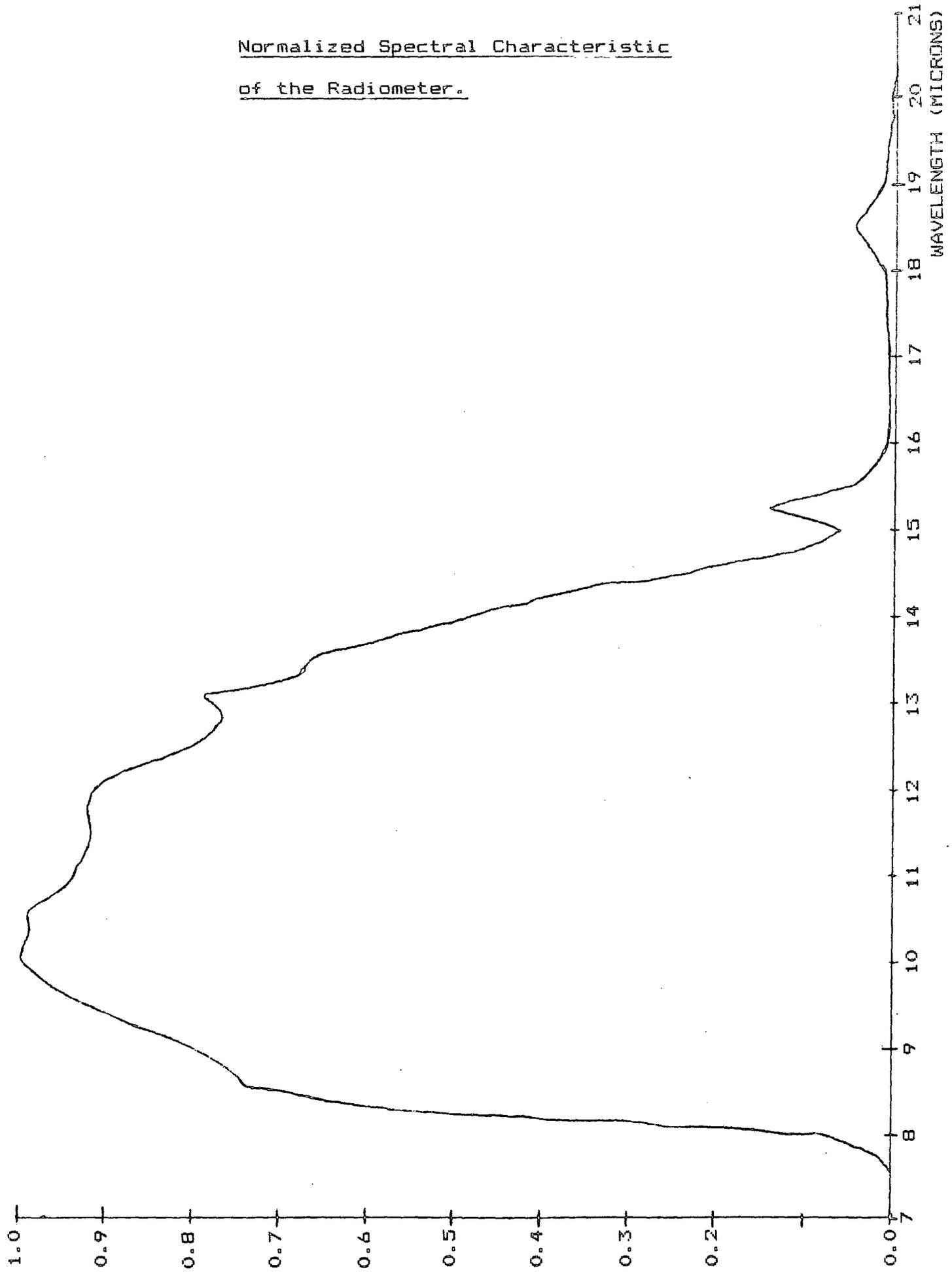
of the Radiometer.

Fig. 4.8

Extra Circuit in ADC 6 to Convert the Radiometer
Output to a 0 to 5V Level and to Drive the Panel
Meter.

TO PANEL METER
VIA 75 OHM CO-AX
CABLE

0-5V INPUT TO
CHANNEL 1 OF ADC

0-10 K

+12V

0-5 K

| 14 | 13 | 12 | 11 | 10 | 9 | 8 |

747

| 1 | 2 | 3 | 4 | 5 | 6 | 7 |

−12V

1K

0-1V OUTPUT FROM RADIOMETER
VIA 75 OHM CO-AX CABLE

ADC0816
TRISTATE
DATA
OUTPUTS

7
6
5
4
3
2
1
0

DATA

CD
4047
CLOCK

ADC0816
CLOCK
1000kHz

$t=1\times10^{-6}s$

100R

B 74121 Q

1000pF

ADC0816
START

04

ADC0816
ADDRESS
LATCH
ENABLE

GATE G2

74138
3-8 LINE
DECODER

7
6
5
4
3
2
1
0

7
6
5
4

04

SELECT BOARD
ADDRESS WITH
LINK

3
2
1
0

ADC0816
ADDRESS
INPUTS

ADDRESS

RESET

04

ADC0816
TRISTATE
CONTROL

GOES TO MSB
OF ADDRESS

Fig. 4.10

Calibration Graph for Radiometer on Low Scale

(from Manufacturer's Manual).
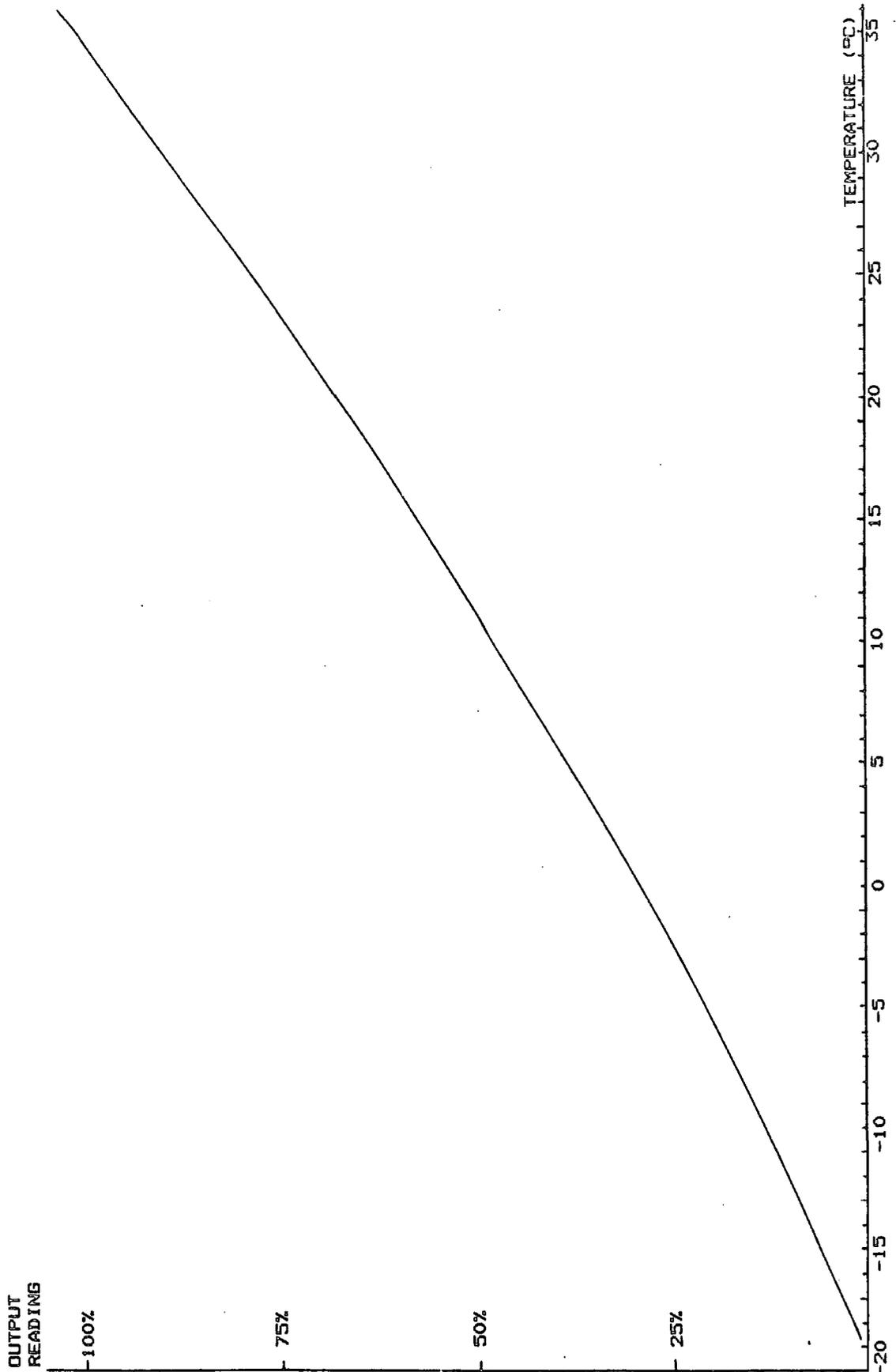
Fig. 4.11

Results of the First Calibration of the

Radiometer Using the Black Body Source.

ADC OUTPUT (BITS)
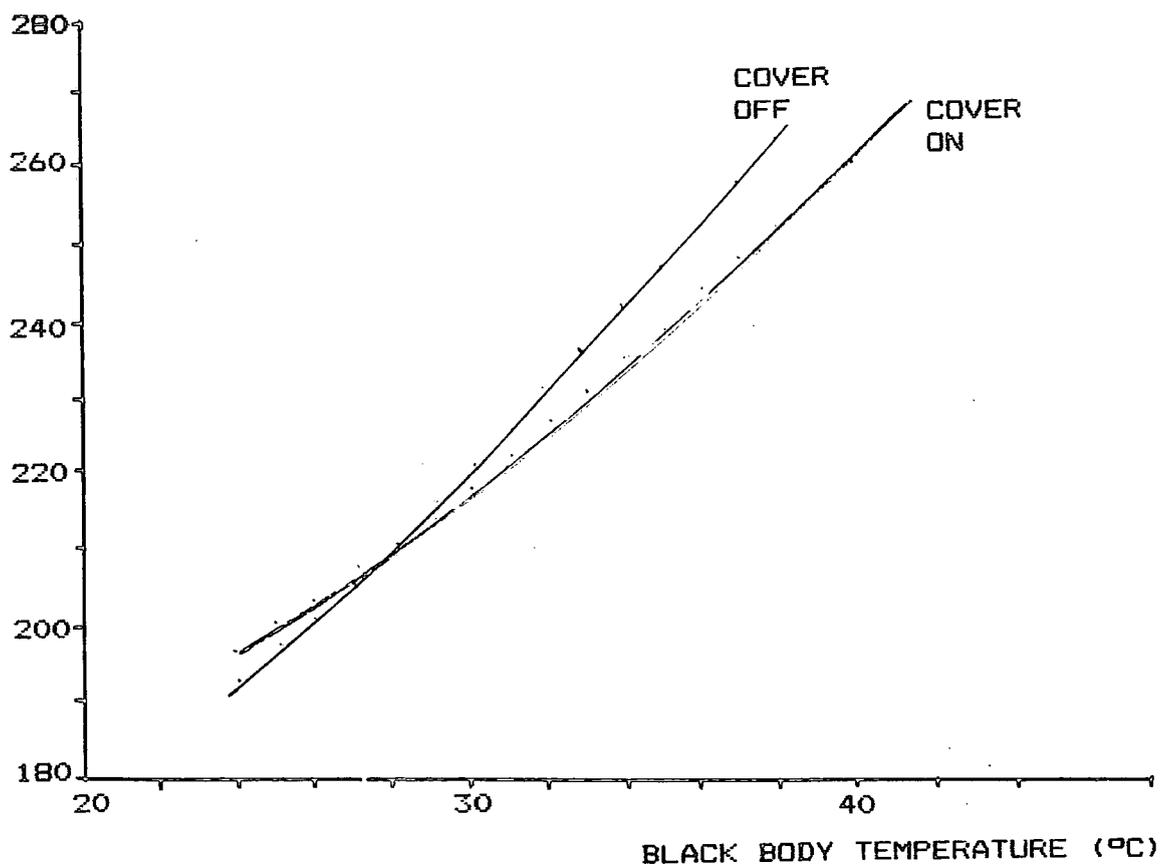
Fig. 4.12

Layout for a Set of 16 Contact Temperature Sensors

SENSORS 1-8

SENSORS 9-16

FIG 8 WIRE (50m)

15 WAY PLUG/SOCKET

9 WAY CABLE (50m)

37 WAY PLUG/SOCKET

25 WAY RIBBON CABLE

2x25 WAY PLUGS
(INPUT TO TEMPERATURE
AMPLIFIERS)
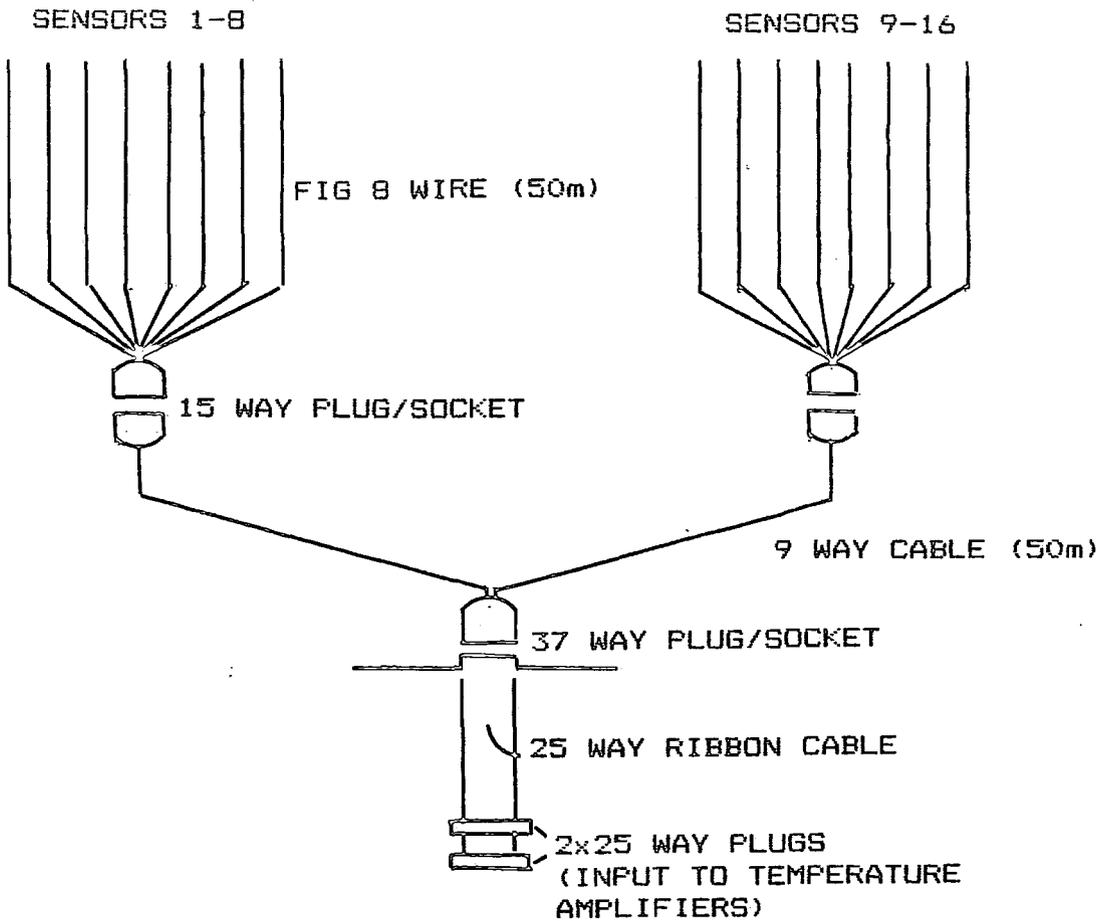
Fig. 4.13

Electronics Block Diagram.

SENSORS 9-16 → TEMPERATURE AMPLIFIER (OCTAL)

SENSORS 1-8 → TEMPERATURE AMPLIFIER (OCTAL)

16 CHANNEL 8-BIT ADC

11-BIT BUS

BUS CONTROLLER

TEK 4052

IEEE BUS
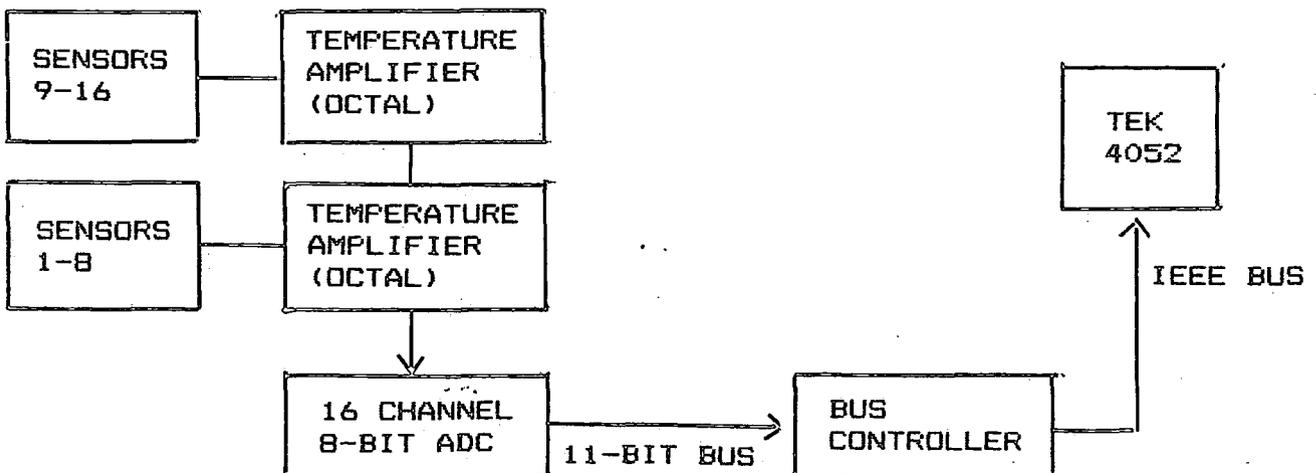
Fig. 4.14

Non Linearity of a Typical Contact Temperature
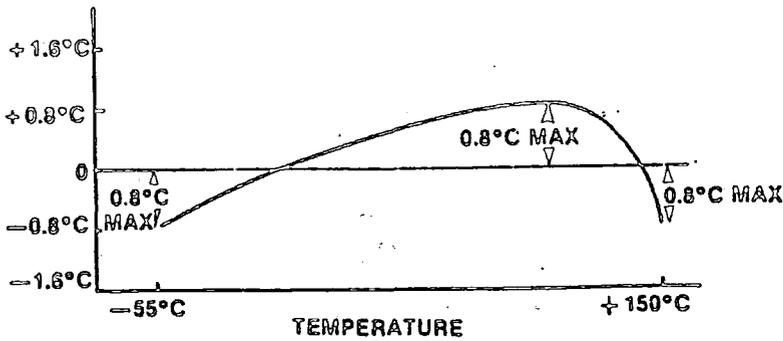
Sensor.

Fig. 4.15

Temperature Amplifier Circuit.
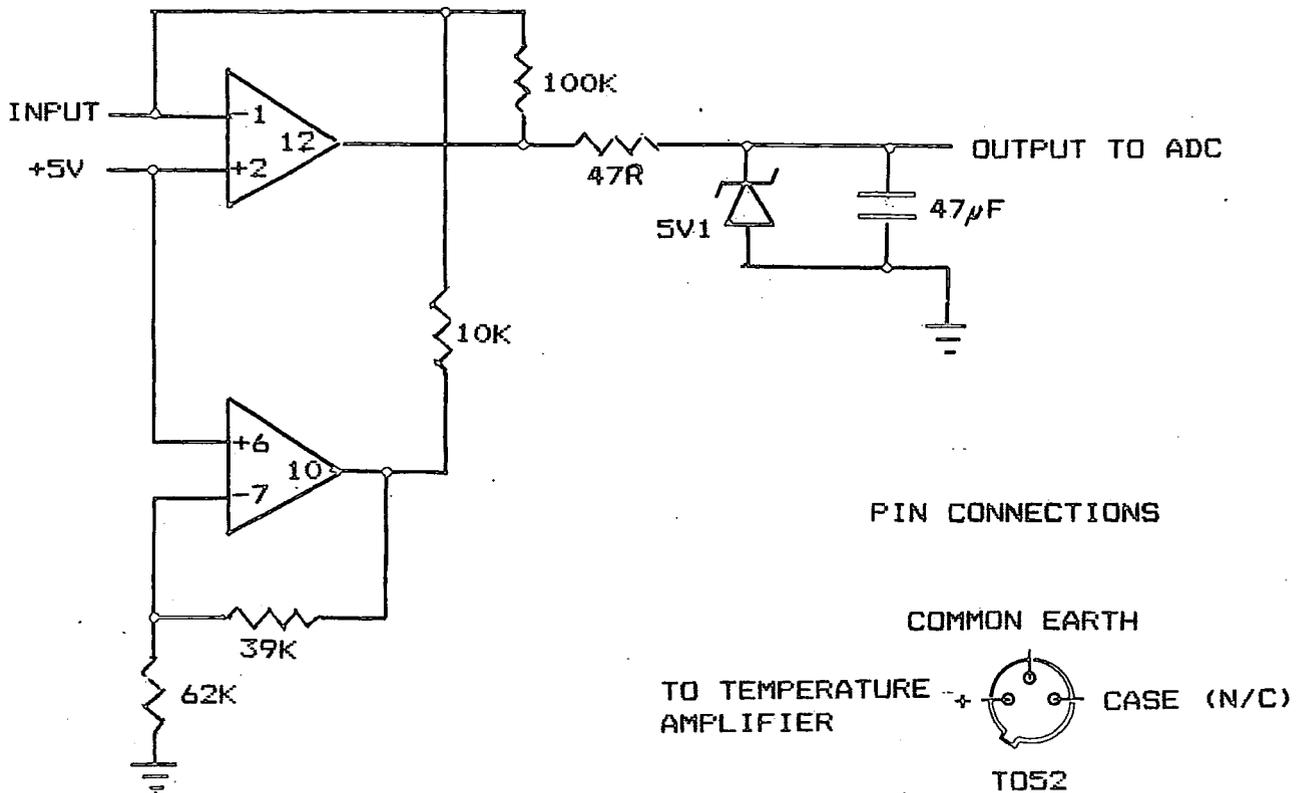
Fig. 4.16

Calibration Curve for Contact
Temperature Sensor Number 1.
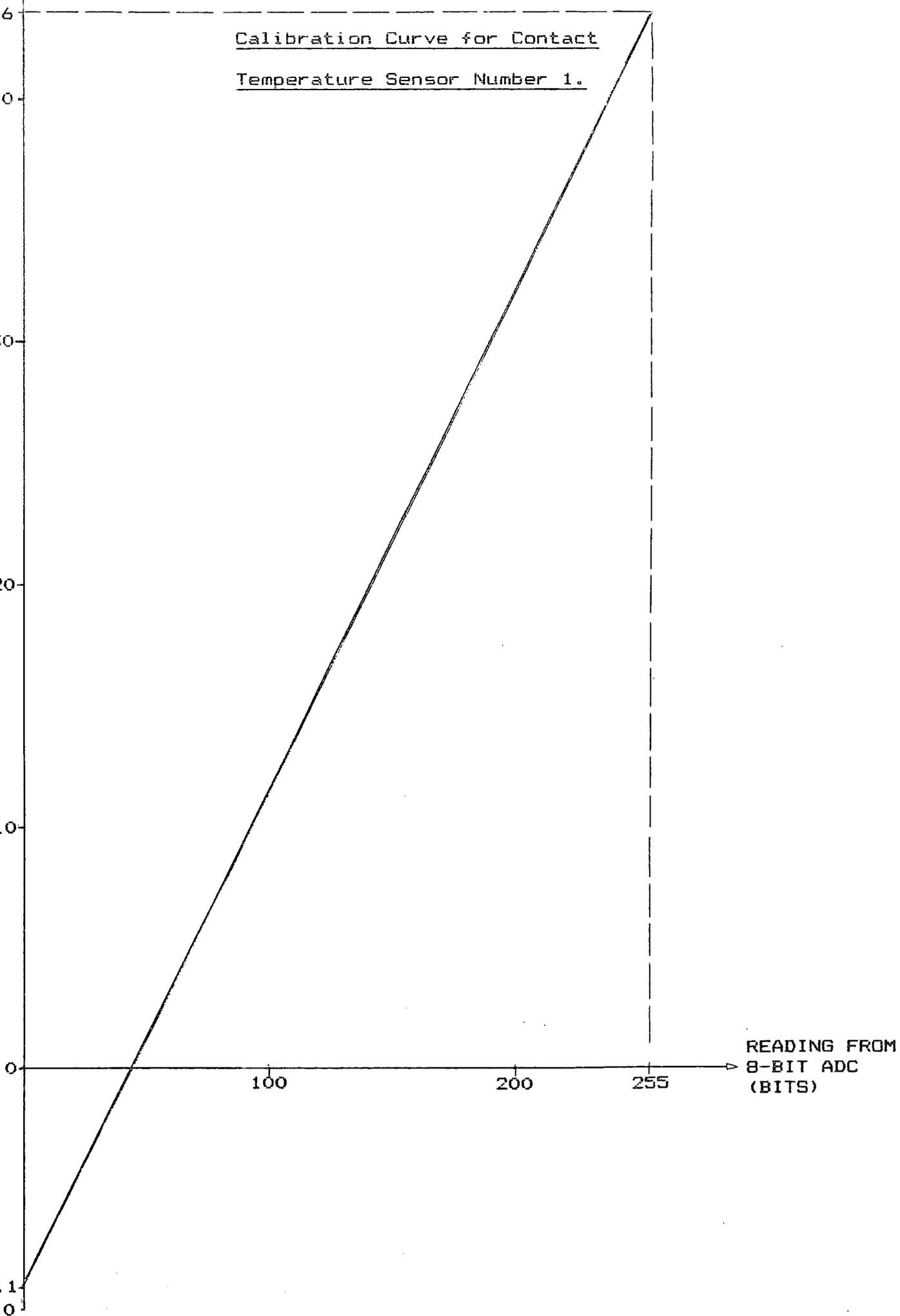
Fig. 4.17   WEATHER DATA RECORDED AT DURHAM OBSERVATORY
            AV. SOLAR RADIATION FROM 12:00 04-APR-84 TO 12:00 05-APR-84.
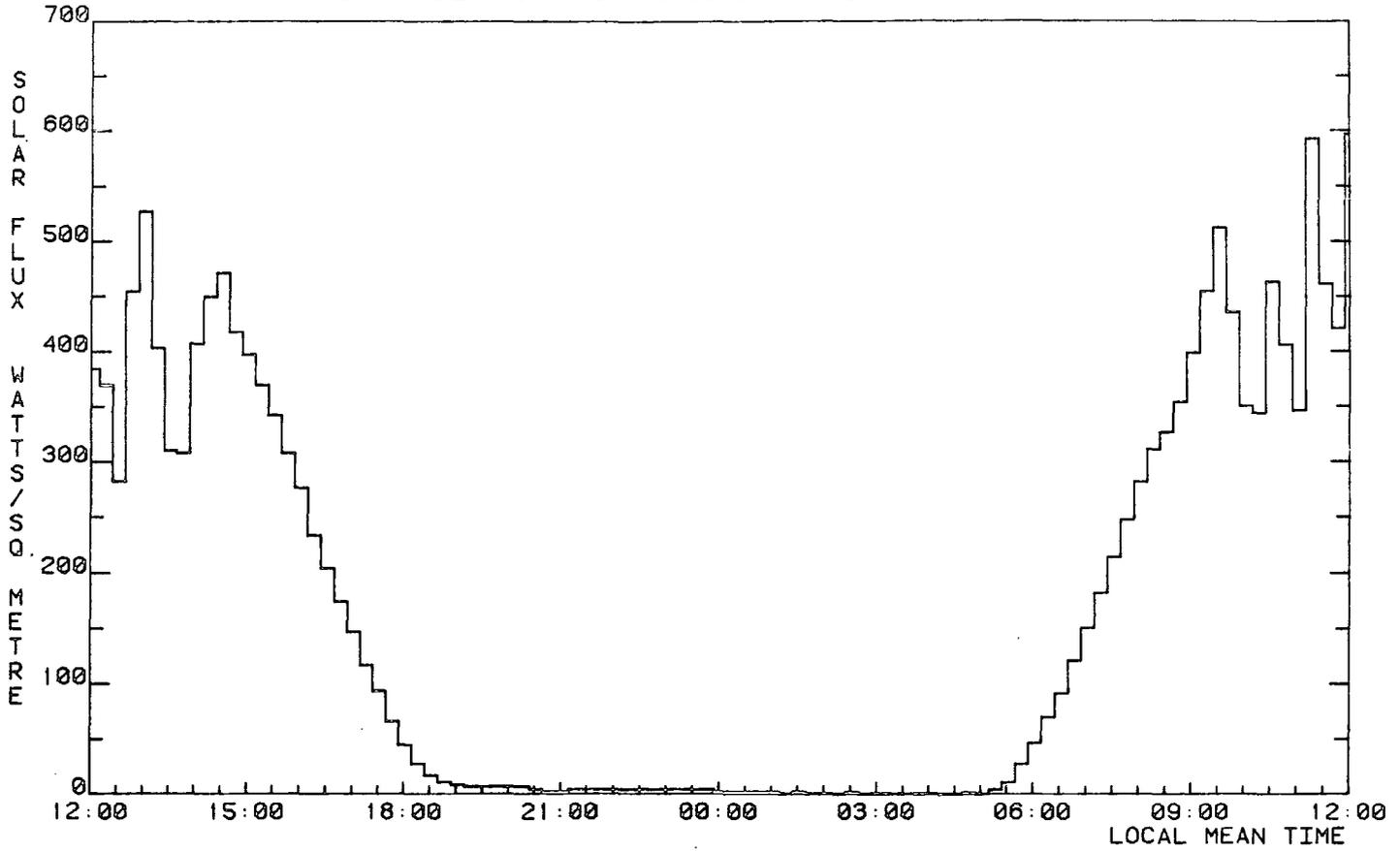
Fig. 4.18

LONG WAVE CLOUD COVER FACTOR FROM 12:00 04-APR-84 TO 12:00 05-APR-84.
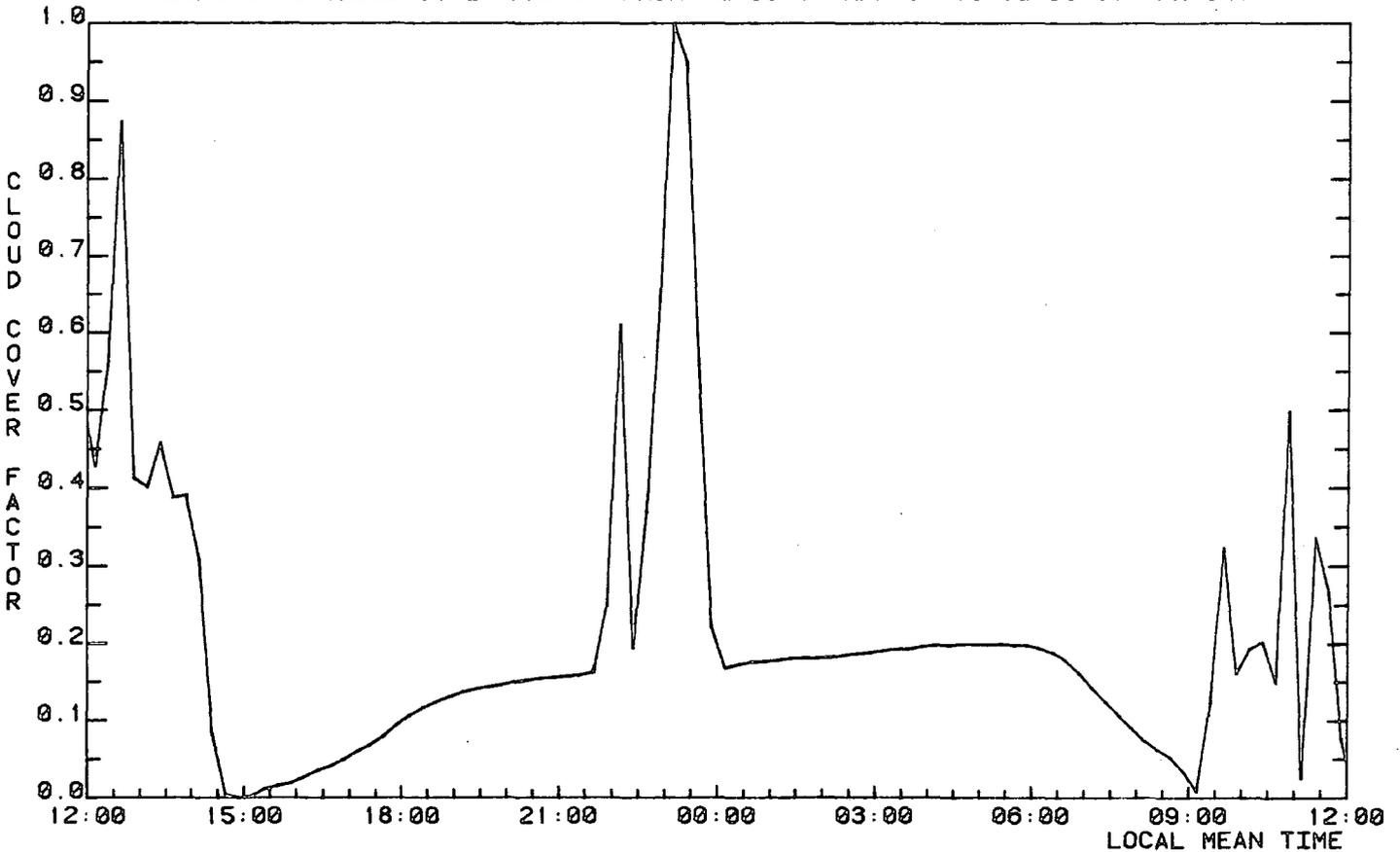
Fig. 4.19 WEATHER DATA RECORDED AT DURHAM OBSERVATORY
AV. SOLAR RADIATION FROM 12:00 05-APR-84 TO 12:00 06-APR-84.
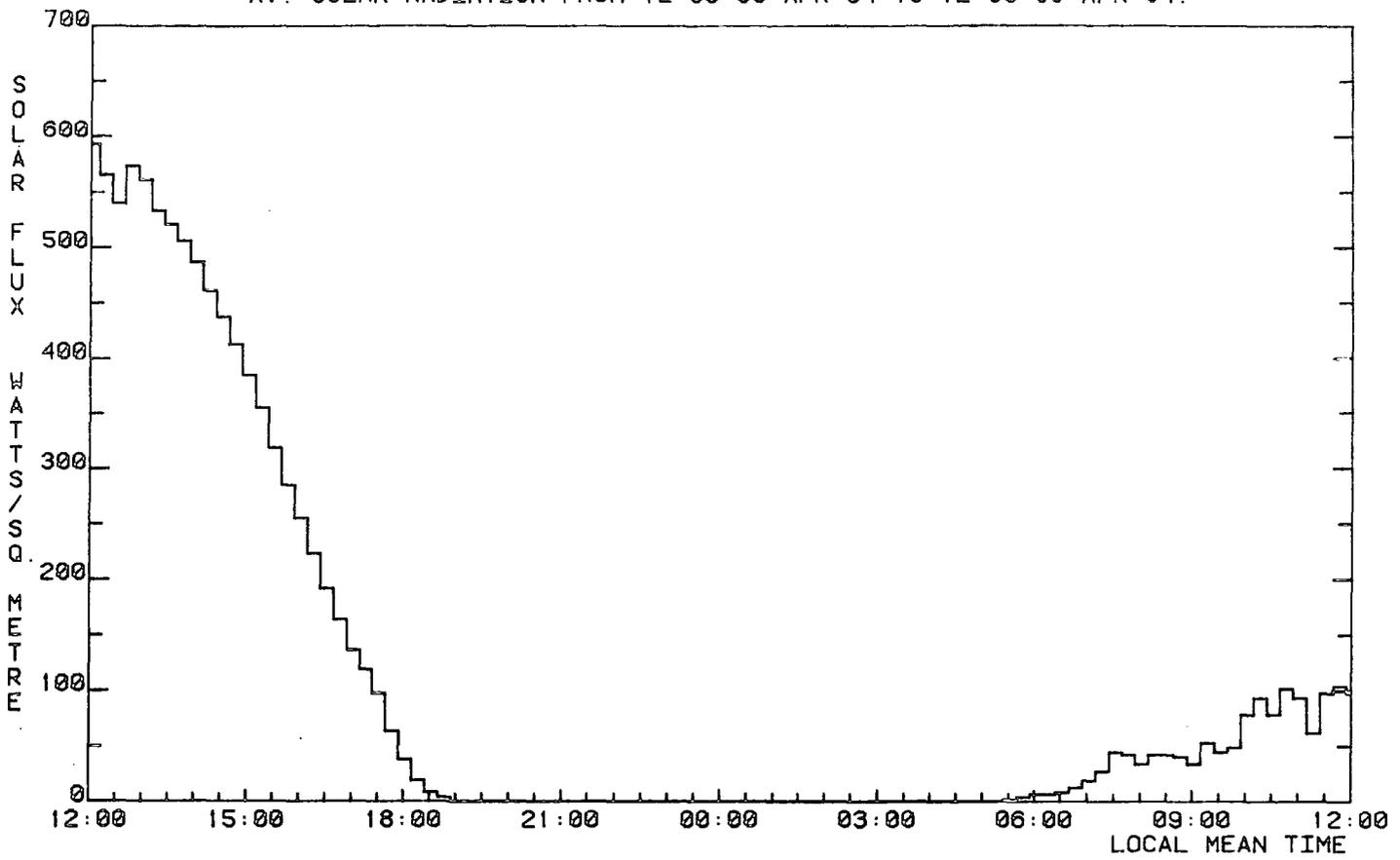
Fig. 4.20

LONG WAVE CLOUD COVER FACTOR FROM 12:00 05-APR-84 TO 12:00 06-APR-84.
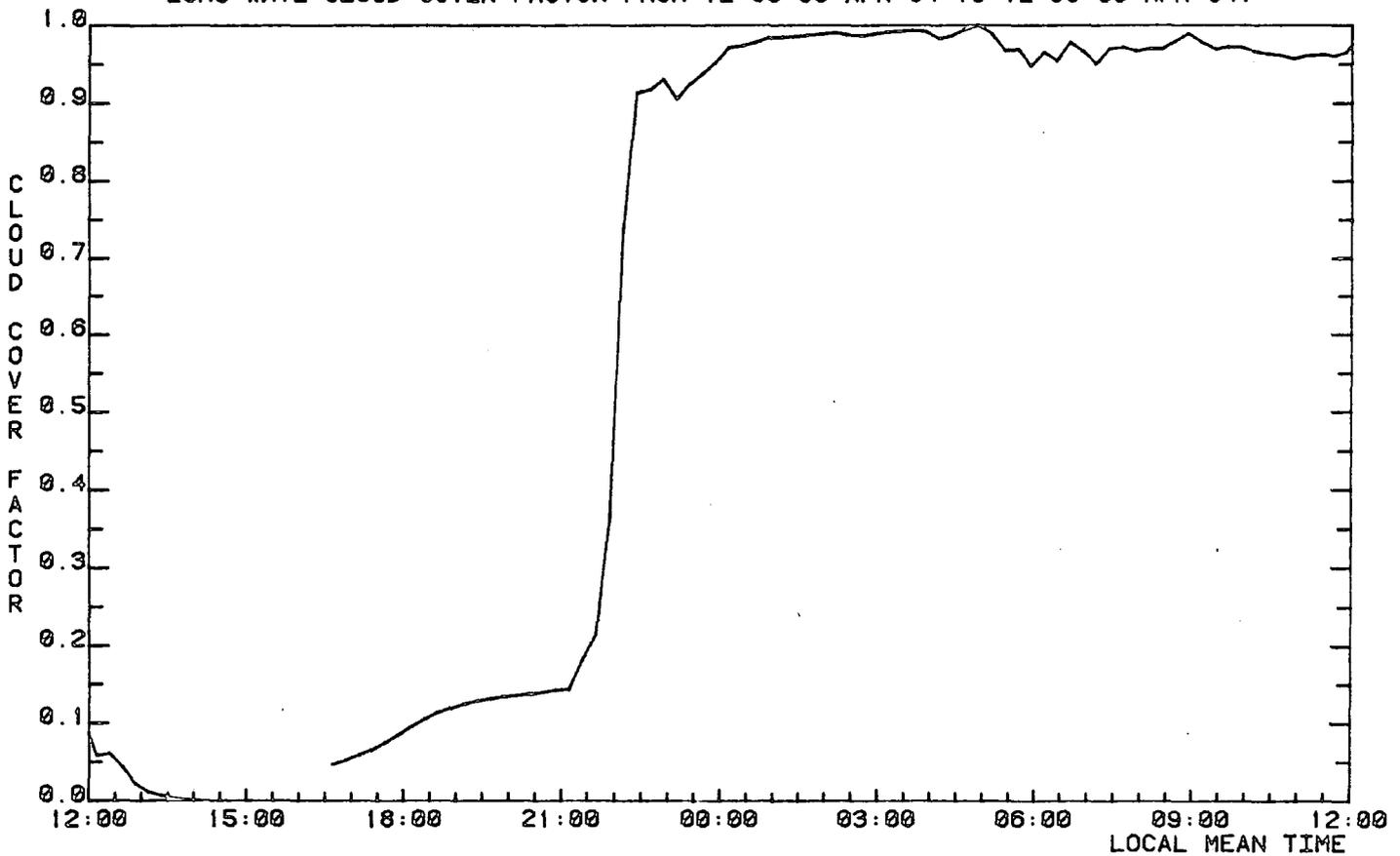
Fig. 4.21   MEASURED CONTACT AND RADIATION TEMPERATURE DATA
             FOR THE SOUTH FACING SANDSTONE WALL,
             FROM 12:00 04-APR-84 TO 12:00 05-APR-84.
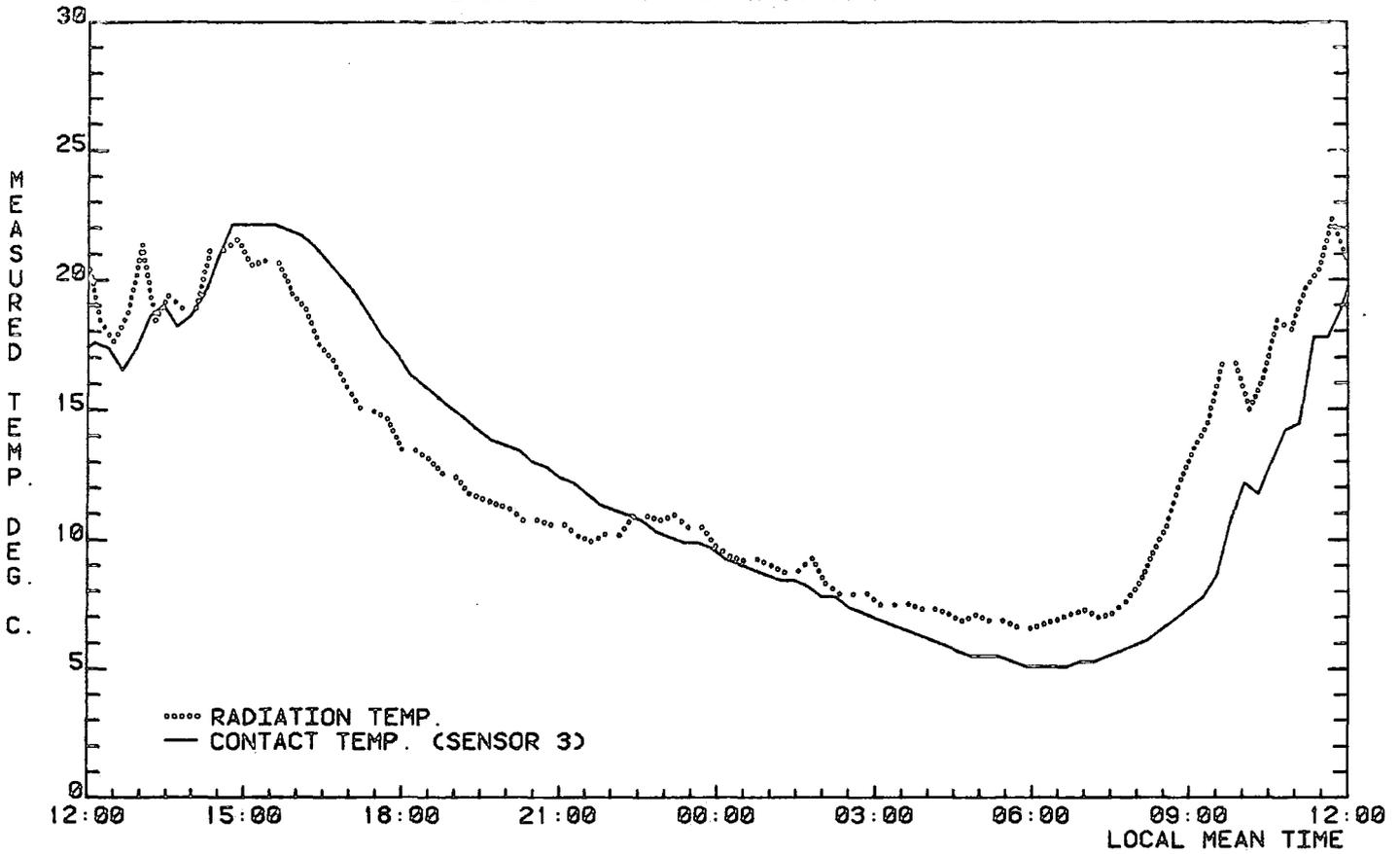
Fig. 4.22   MEASURED CONTACT AND RADIATION TEMPERATURE DATA
             FOR THE SOUTH FACING SANDSTONE WALL,
             FROM 12:00 05-APR-84 TO 12:00 06-APR-84.
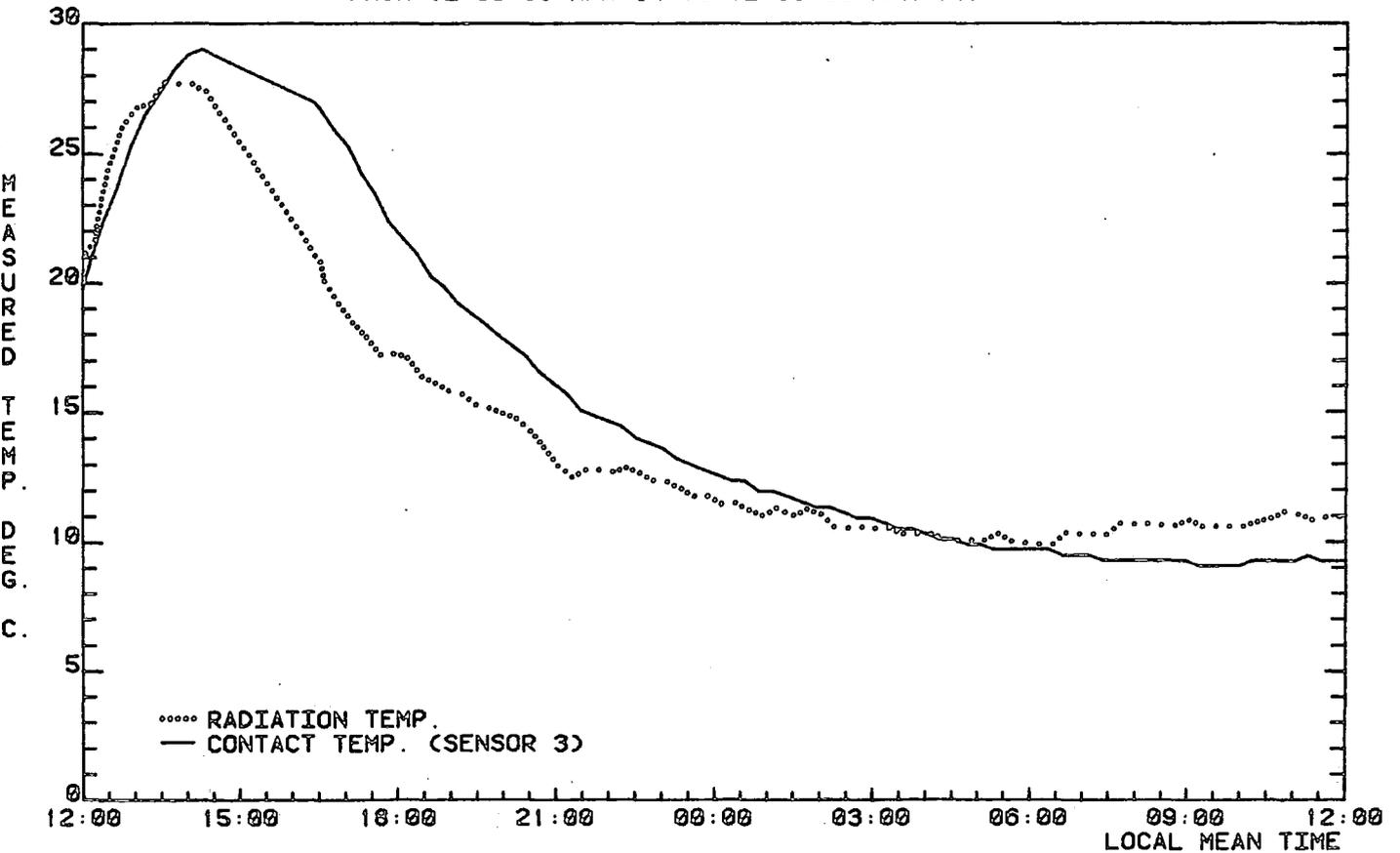
Fig. 4.23   MEASURED CONTACT AND RADIATION TEMPERATURE DATA
FOR THE SOUTH FACING SANDSTONE WALL AND NET,
FROM 12:00 04-APR-84 TO 12:00 05-APR-84.
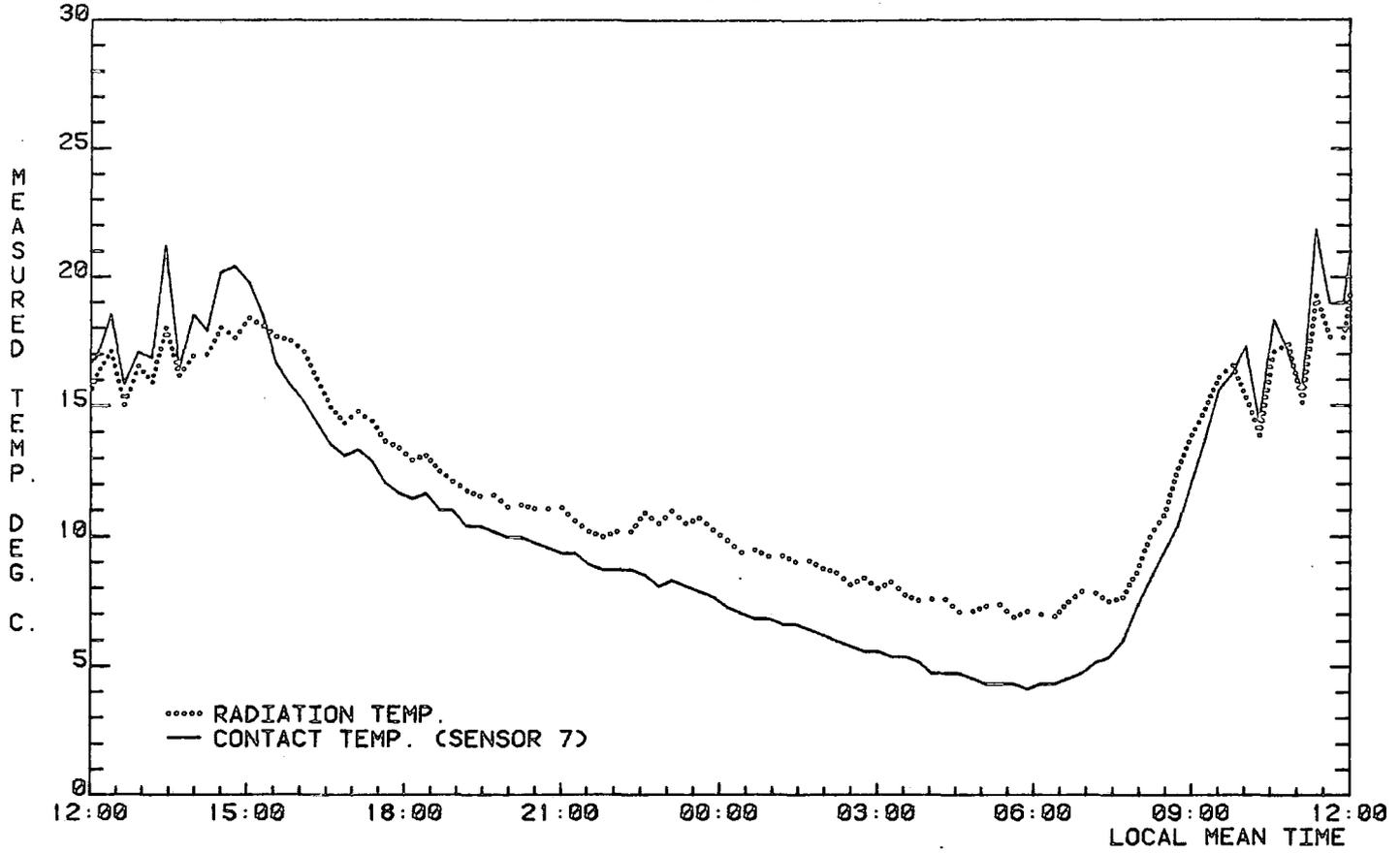
Fig. 4.24   MEASURED CONTACT AND RADIATION TEMPERATURE DATA
FOR THE SOUTH FACING SANDSTONE WALL AND NET,
FROM 12:00 05-APR-84 TO 12:00 06-APR-84.
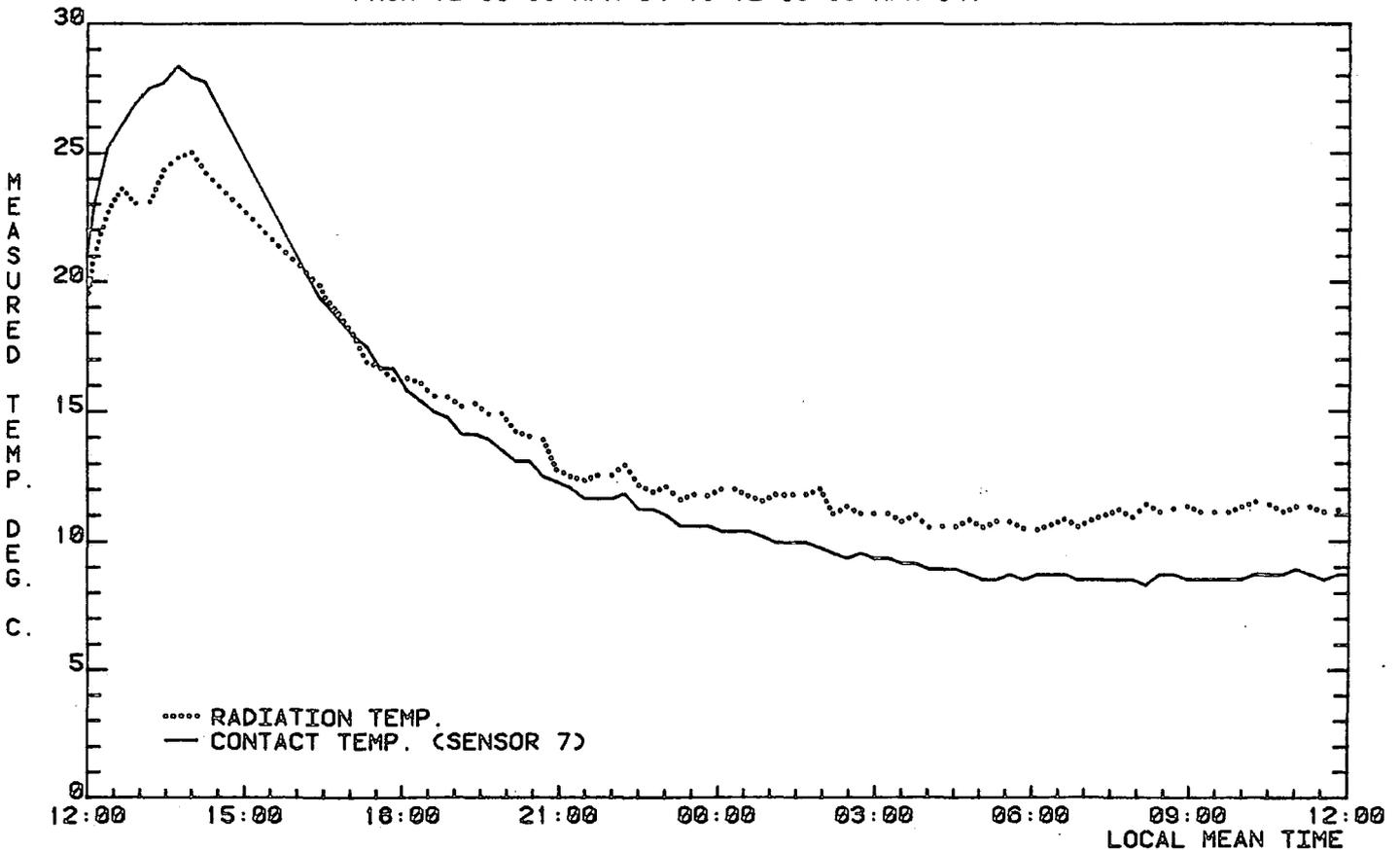
Fig. 4.25   MEASURED CONTACT AND RADIATION TEMPERATURE DATA
FOR THE WEST FACING SANDSTONE WALL,
FROM 12:00 04-APR-84 TO 12:00 05-APR-84.
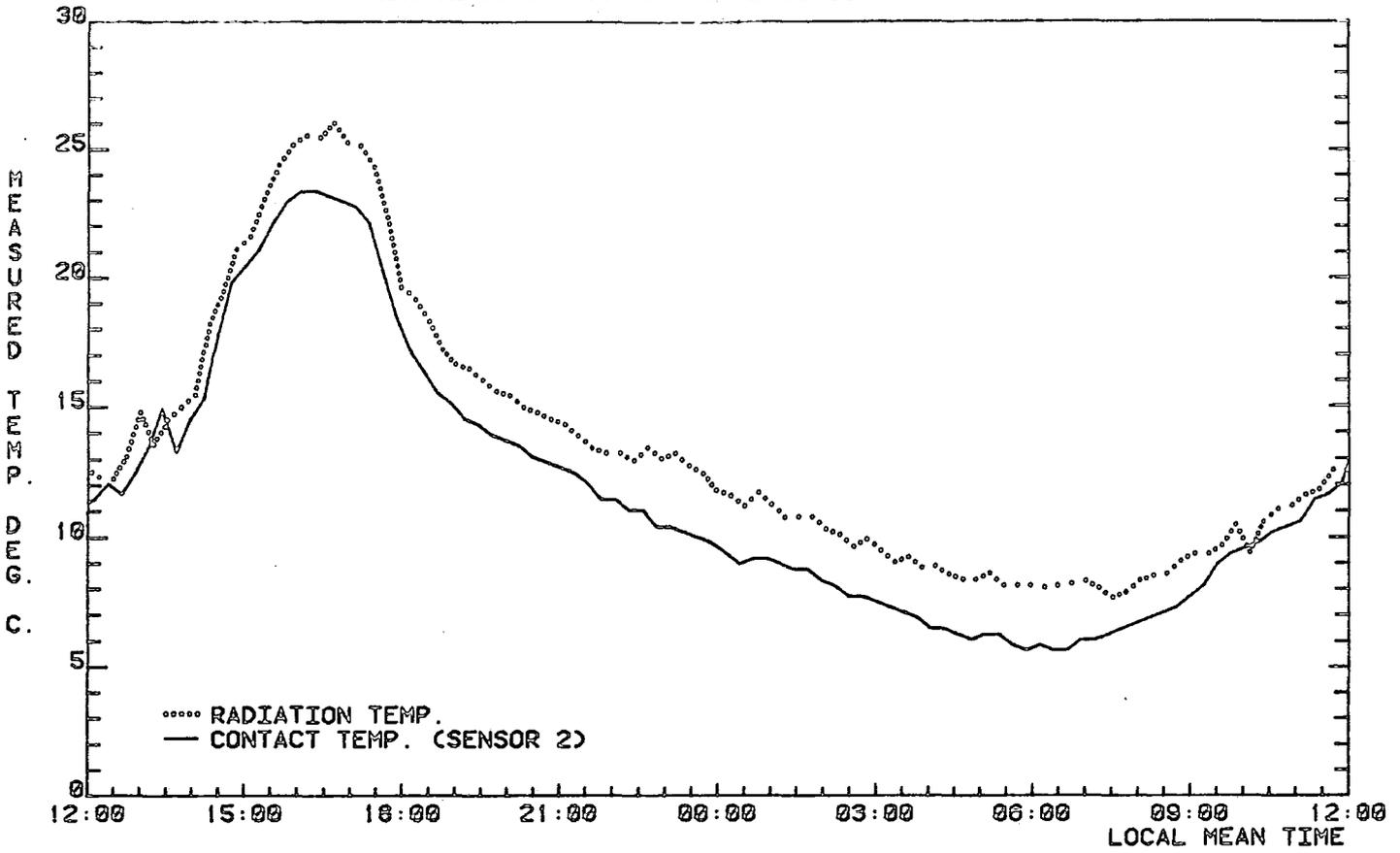
Fig. 4.26   MEASURED CONTACT AND RADIATION TEMPERATURE DATA
FOR THE WEST FACING SANDSTONE WALL,
FROM 12:00 05-APR-84 TO 12:00 06-APR-84.
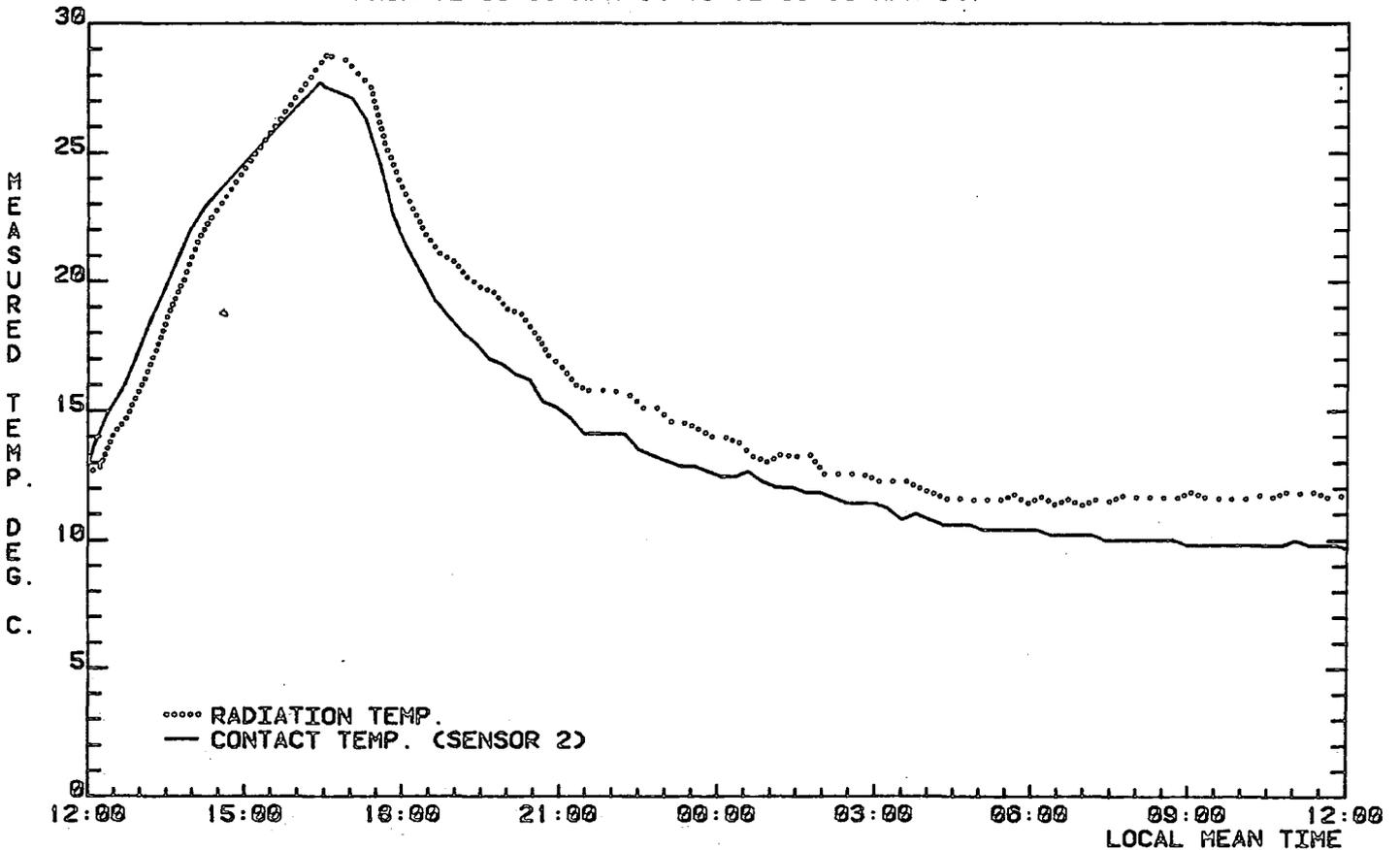
Fig. 4.27   DATA FROM CONTACT TEMPERATURE SENSOR 8, IN FREE AIR,
COMPARED WITH AIR TEMPERATURE AT DURHAM OBSERVATORY
FROM 12:00 02-APR-84 TO 12:00 03-APR-84.
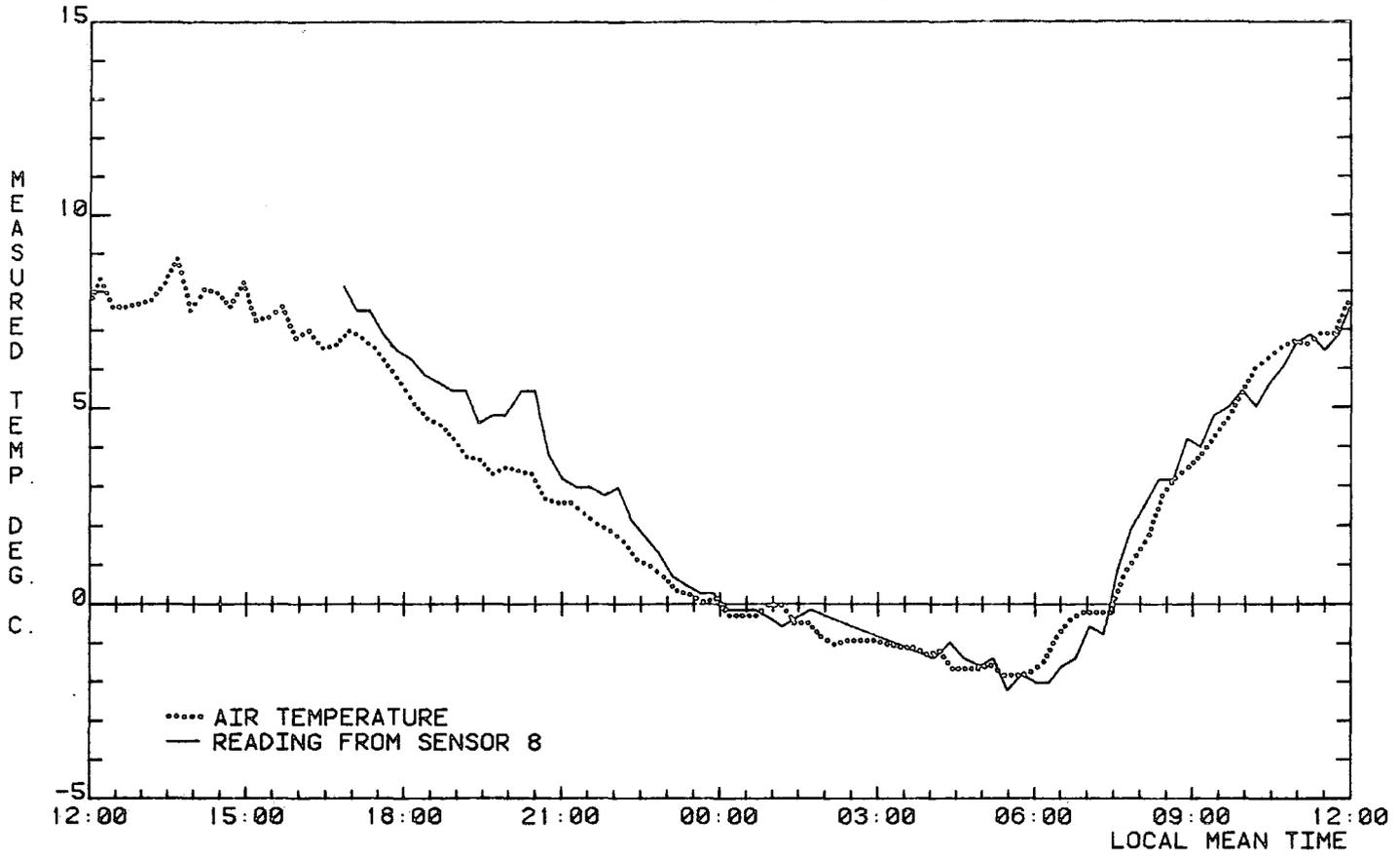
Fig. 4.28   DATA FROM CONTACT TEMPERATURE SENSOR 8, IN FREE AIR,
COMPARED WITH AIR TEMPERATURE AT DURHAM OBSERVATORY
FROM 12:00 03-APR-84 TO 12:00 04-APR-84.
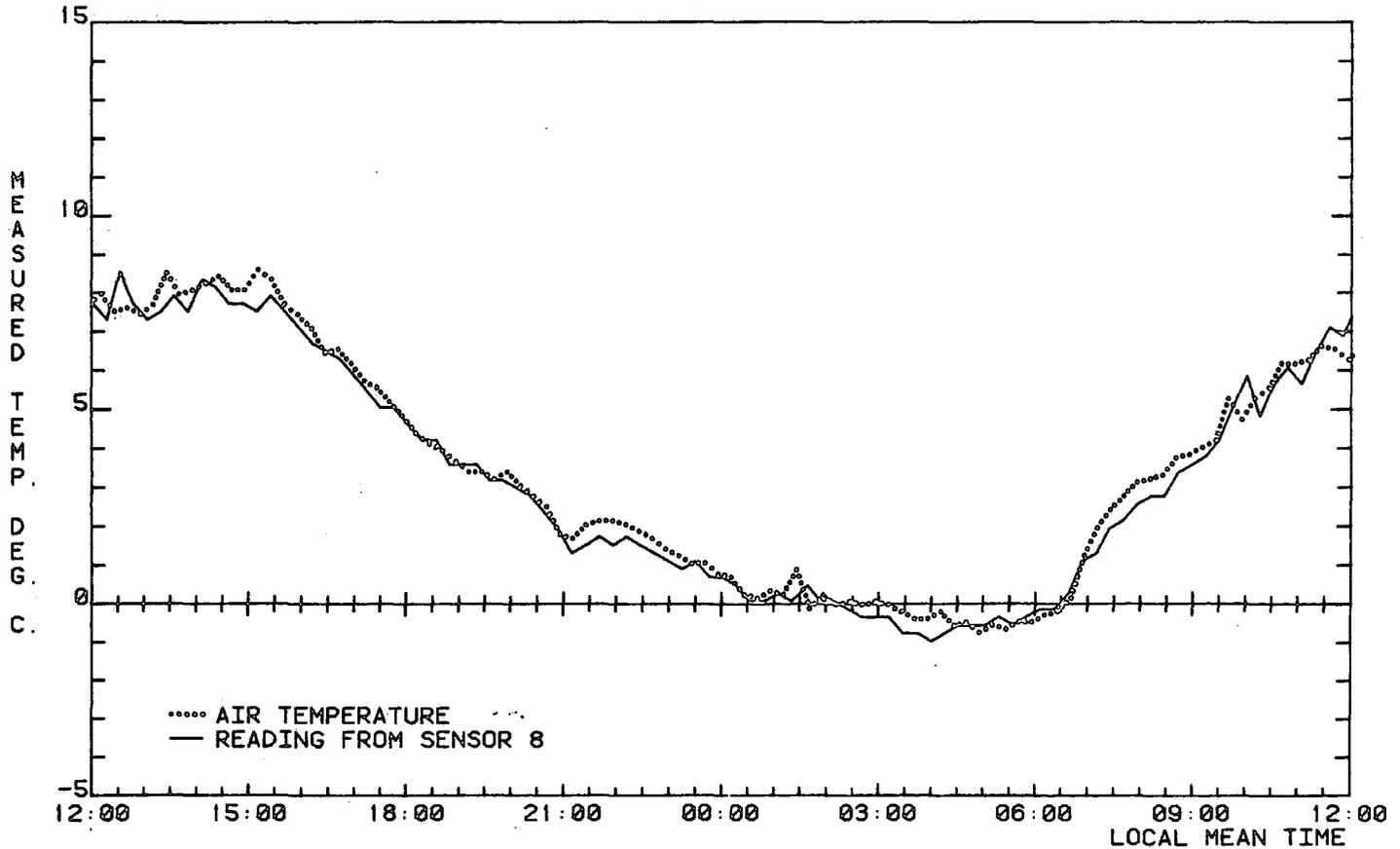
Fig. 4.29   DATA FROM CONTACT TEMPERATURE SENSOR 8, IN FREE AIR,
             COMPARED WITH AIR TEMPERATURE AT DURHAM OBSERVATORY
             FROM 12:00 04-APR-84 TO 12:00 05-APR-84.
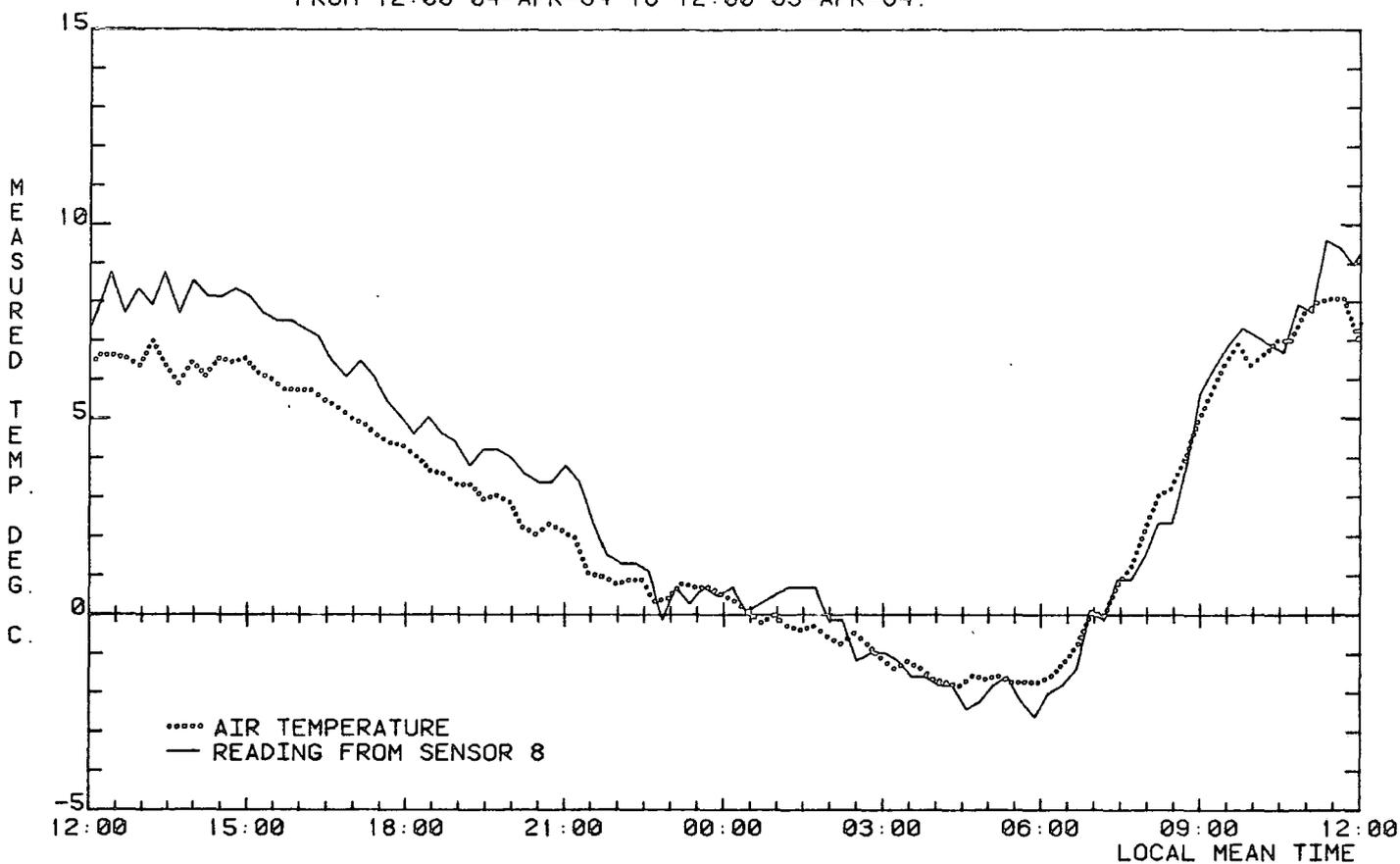
Fig. 4.30   DATA FROM CONTACT TEMPERATURE SENSOR 8, IN FREE AIR,
             COMPARED WITH AIR TEMPERATURE AT DURHAM OBSERVATORY
             FROM 12:00 05-APR-84 TO 12:00 06-APR-84.
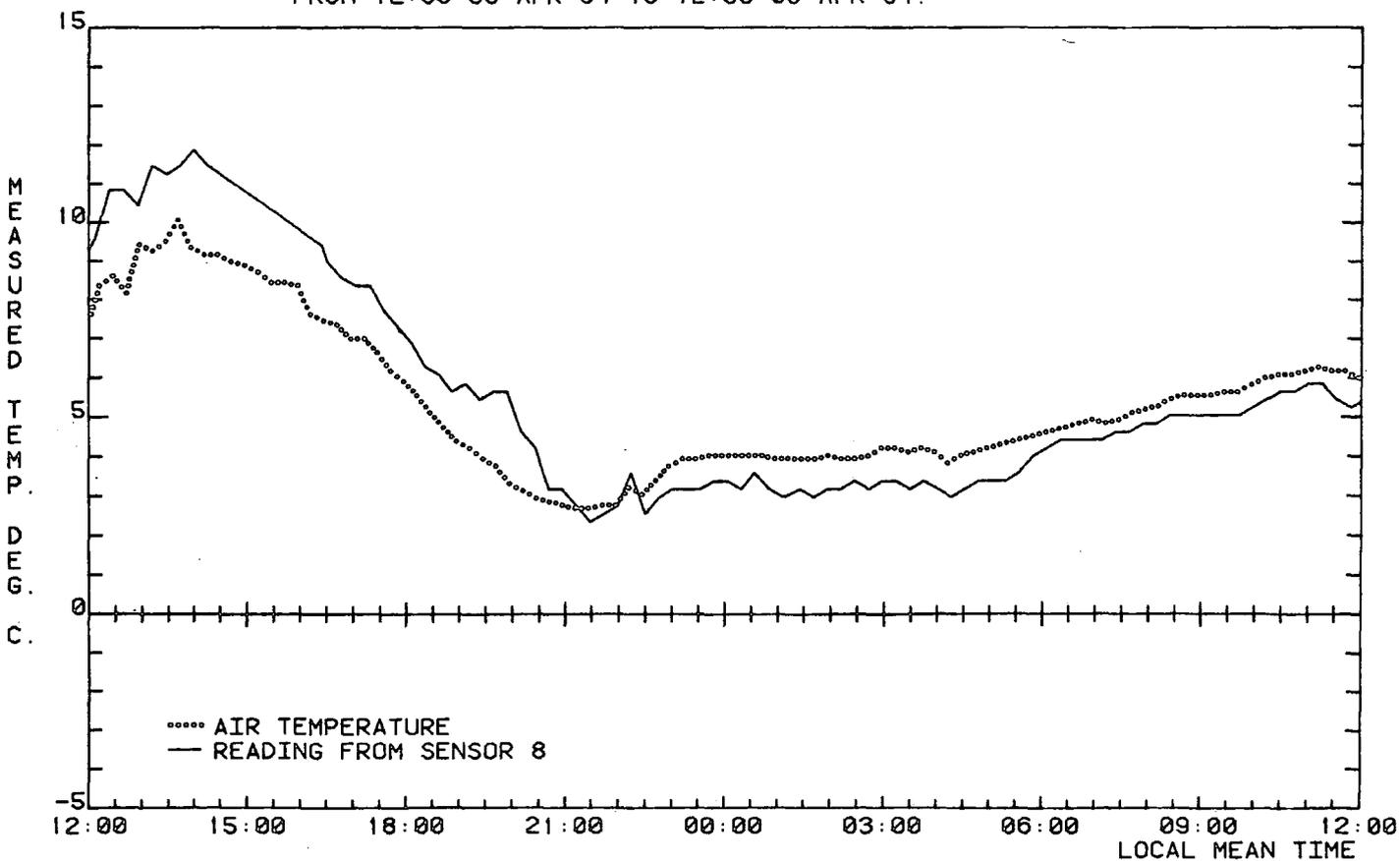
Fig. 4.31

Automatic Weather Station.

SOLARIMETER

ANEMOMETER

WIND DIRECTION
INDICATOR

TEMPERATURE SCREEN

N

JUNCTION BOX

NET RADIOMETER

TO RAINGAUGE   TO DATA LOGGER

Fig. 4.32

Pyranometer.

GLASS DOMES

RADIATION SHIELD

CONNECTOR

MAST
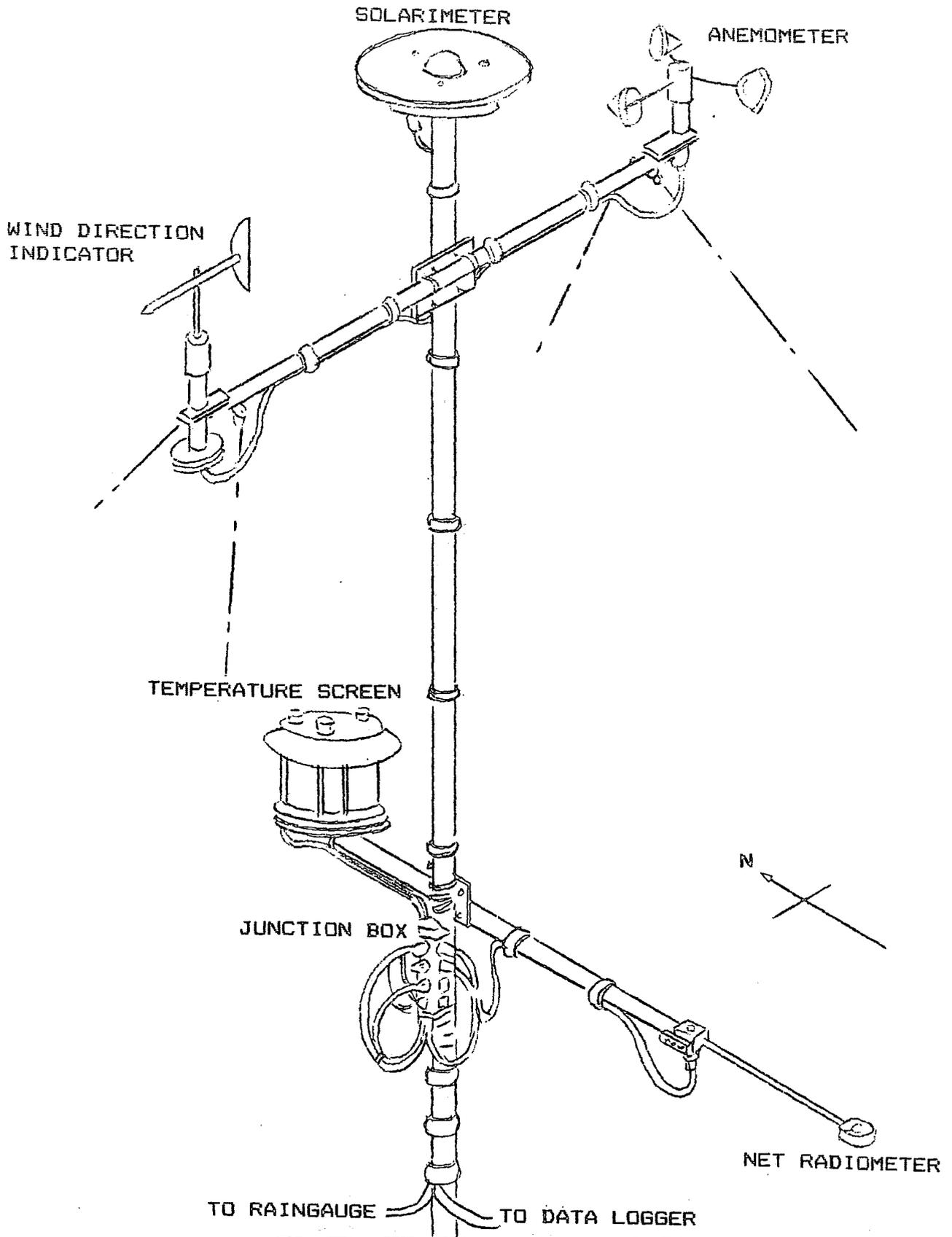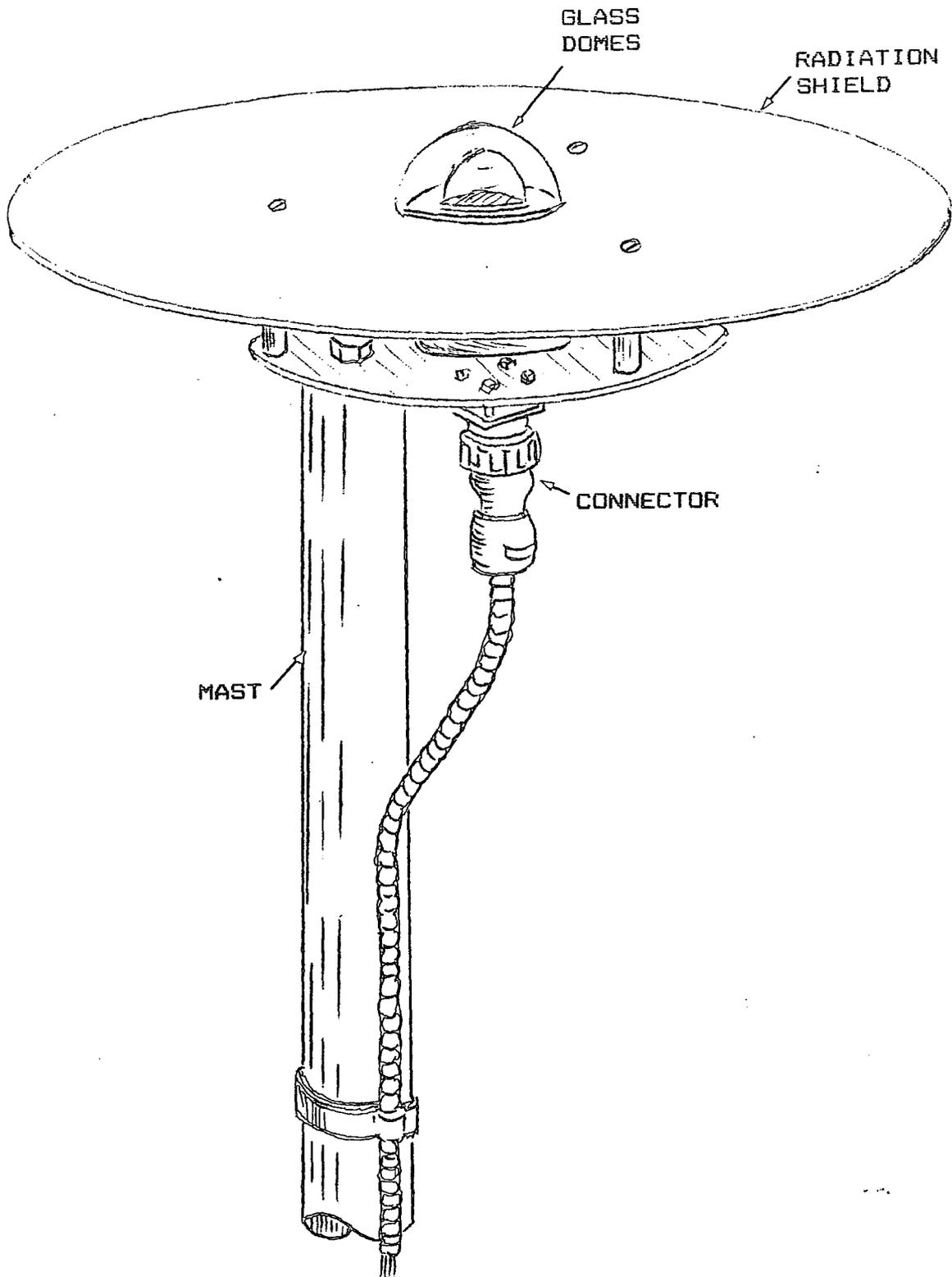
Fig. 4.33

Thermopile of a Moll-Gorczynski Pyranometer.
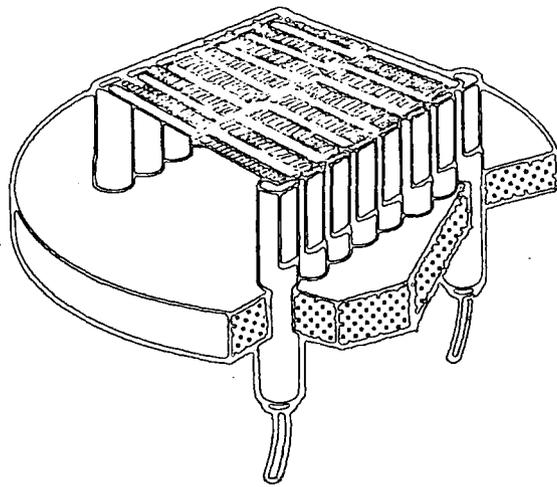
Fig. 4.34

Temperature Screen.

AIR TEMPERATURE
THERMOMETER

DRY BULB

WET BULB

WATER RESERVIOR
FOR WET BULB WICK
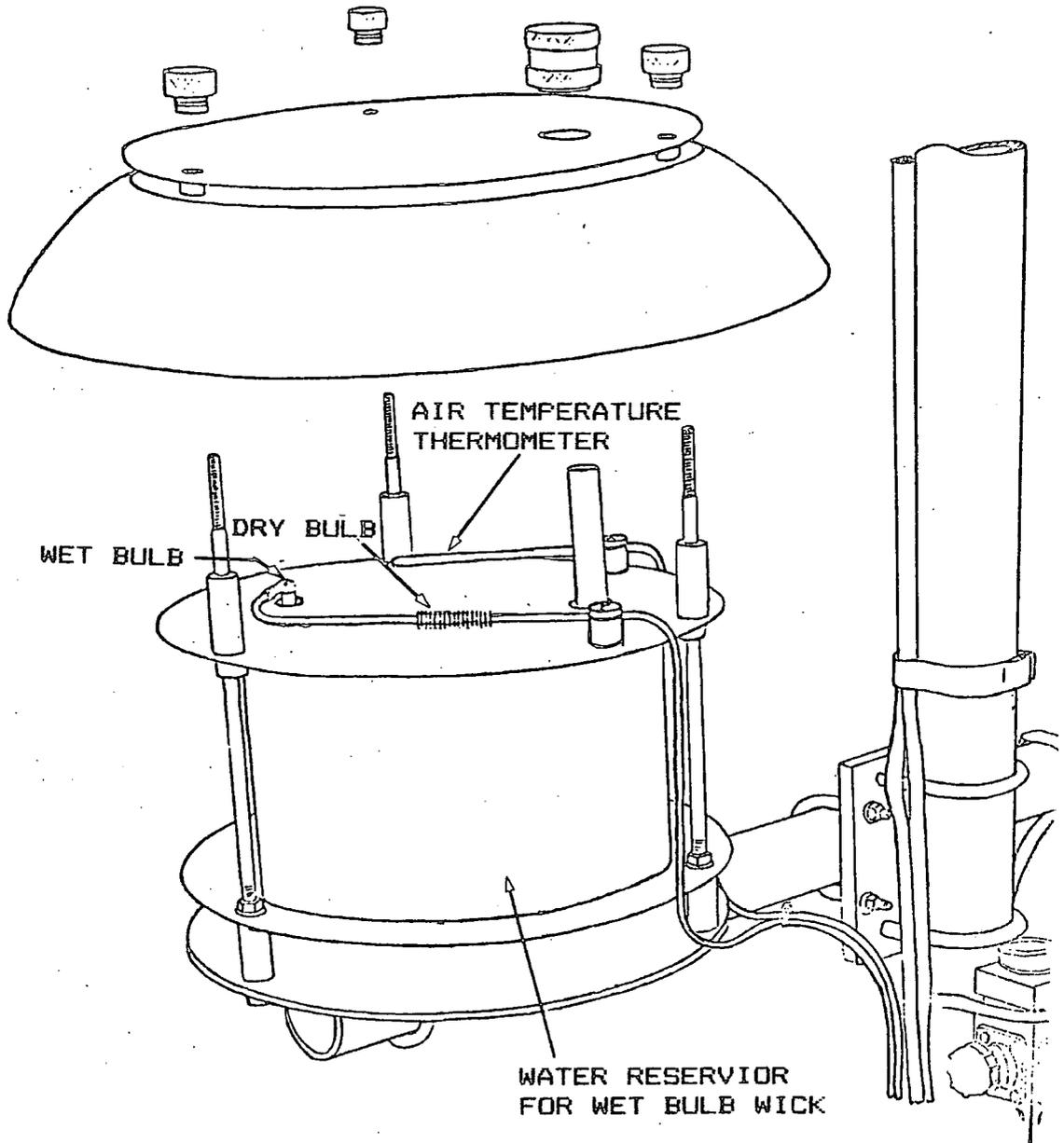
Fig. 4.35

Flowchart for the Operation of the Data Acquisition System under Computer Control.

INPUT ANALOGUE
VOLTAGE (O TO +5V)

A 74121 Q̄

t=1x10⁻⁶s

MSB   .GATE   "0"=ON

7

6

74
138

5

4

3

2

GATE   "0"=ON

1

74
.139

0

LSB

'BOARD SELECT'
LINK ONE 74138
OUTPUT TO 74139
GATE

2 SPARE OUTPUTS

CRATE DATA
HIGHWAY
ADDRESS LINES

CD4502
"DISABLE 3-STATE"

+5V

4.7 μF

START
ADC1211

CD4502
(2)

12

4.7
μF   -12V

+5V

4.7 μF

START
ADC1211

CD4502
(2)

12

12

4.7
μF   -12V

CRATE DATA
HIGHWAY

CD4047
CLOCK

125 kHz
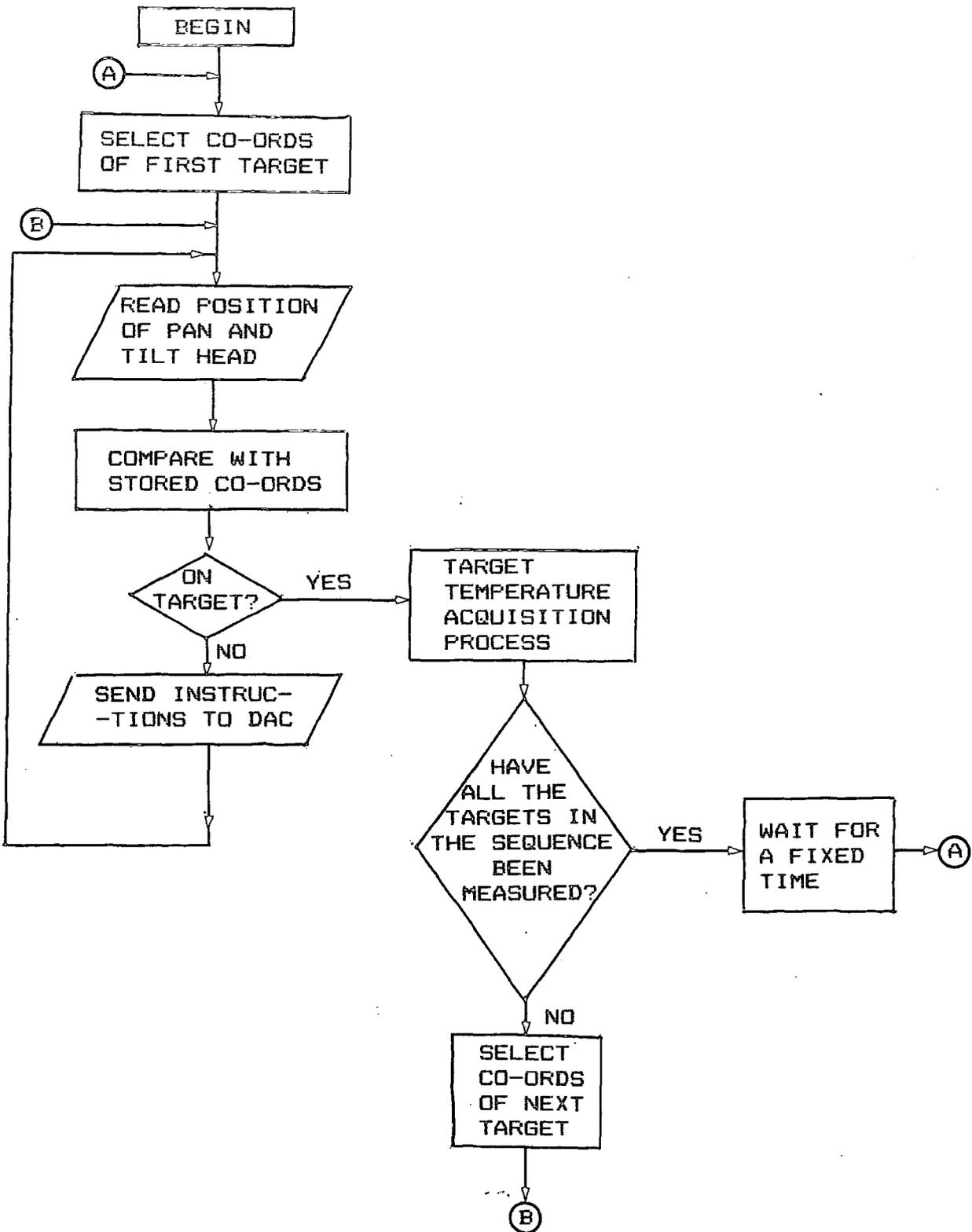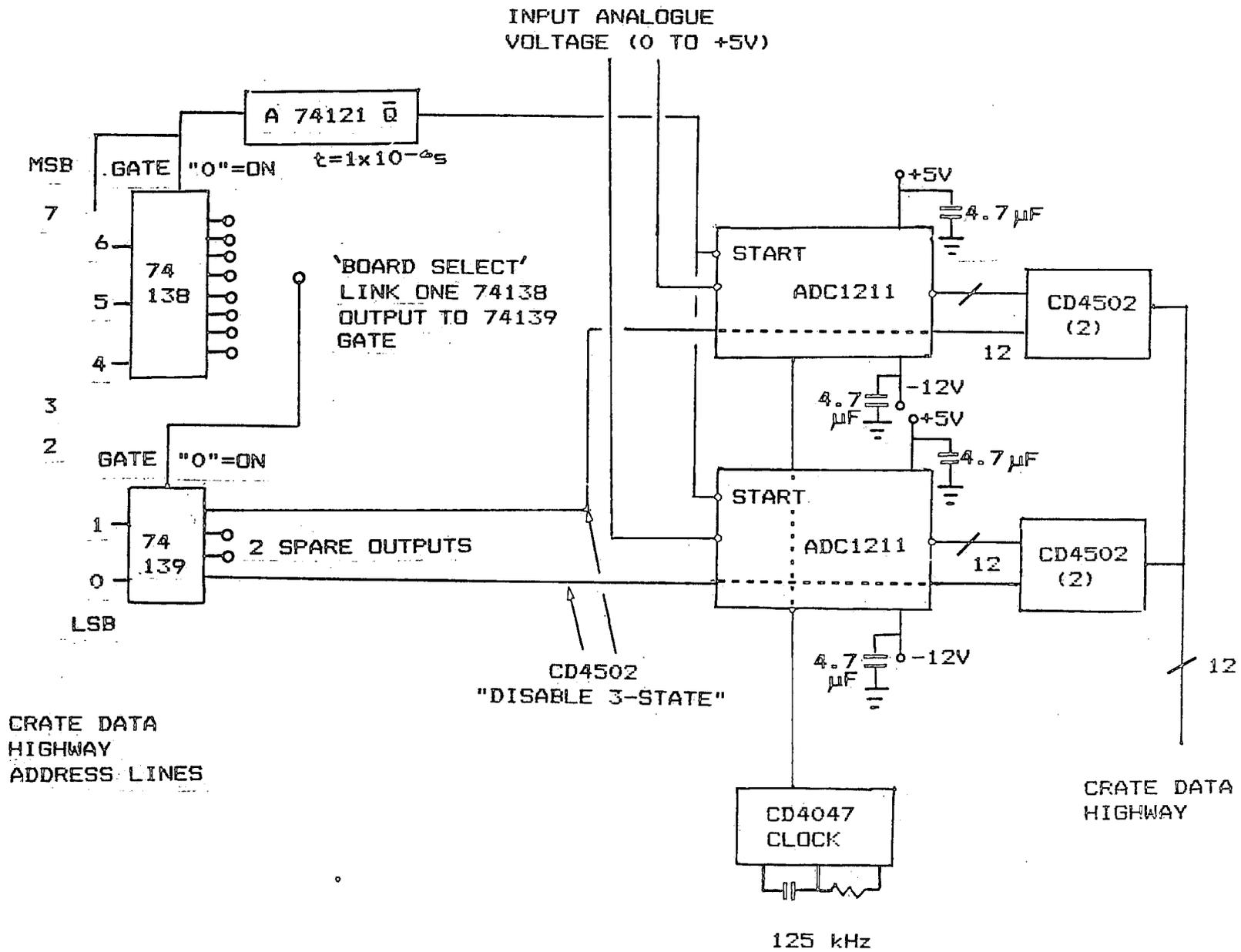
Fig. 4.36

12-Bit ADC Board.
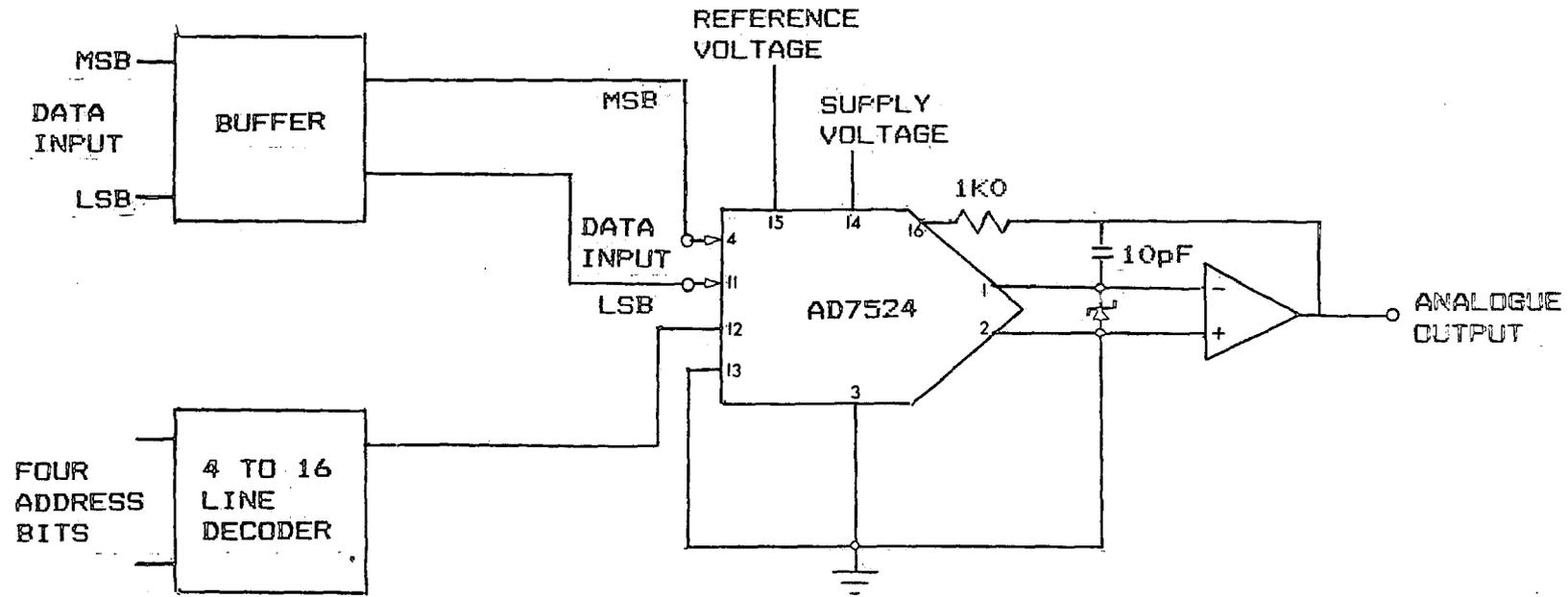
Fig. 4.37

8-Bit DAC Board.

Chapter 5   Validation of the general purpose model.

5.1 Introduction.

The method used for the validation of the mainframe computer general purpose model consisted of a direct comparison between the surface radiation temperatures measured by a radiometer and the temperatures predicted by the model for the same object under the same weather conditions. The experimental data required for the validation were obtained using the equipment described in Chapter 4 while it was in operation at Ouston, Northumberland over the period from 19th April to 25th April 1982. It was decided to use the radiometer measurements in preference to contact temperatures for reasons outlined in Section 4.4.3, which compares the two types of data.

The period over which the data were recorded consisted of a mixture of fine weather with clear skies and cloudy, overcast days. The former is most suitable for modelling applications as the presence of clouds is difficult to simulate accurately, although the cloudy periods are useful to obtain an idea of how well the model is predicting temperatures under such conditions.

The database consists of radiation temperature measurements of a wide range of surfaces, including concrete, asphalt and grass, and weather data which include the incident short-wave solar flux, air temperature, wet and dry bulb depression, and average windspeed. Both the weather data and the radiometer measurements for each surface were recorded at intervals of roughly 15 minutes. The two most suitable non-vegetated surfaces for validation purposes consisted of the concrete and asphalt covered roads and taxiways. These satisfied the two requirements needed to enable their temperatures to be predicted by the one-dimensional model. Firstly it could be reasonably assumed that the composition of the surface layer and the underlying structure were homogenous and of uniform thickness. Secondly, the transverse extent of the material was large compared to the vertical depth of the material influenced by the diurnal temperature wave.

In the next section the methods used for determining the input data for the model are described. This is followed by a comparison between the surface temperature predictions of the model and the radiometer measurements of the concrete and asphalt surfaces. Finally, the validation data are used to investigate the ability of the model to predict temperature contrasts between the two different surfaces.

5.2 Input data required for the validation of the model.

5.2.1 Site characteristic parameters.

The relevant parameters for the site at Ouston, Northumberland where temperature data were recorded are given in Table 5.1. Both the concrete and asphalt surfaces were located in exposed positions and were not shaded from direct solar radiation at any time during the day.

Table 5.1   Site characteristics.

Location .... Ouston, Northumberland.

Latitude .... $55°$ 1' N.

Longitude .... 1° 53' W.

Altitude .... 133 m.

5.2.2 Surface parameters.

The initial values of these parameters are given in Table 5.2. The albedo and emissivity are from measurements made on similar types of surfaces by Balick et al., 1981.

The average ground albedo was set to a typical value of 0.2. However, as the results of the sensitivity analysis showed, this parameter is not important for the prediction of temperatures for horizontal surfaces.

As there was no rainfall during the period over which data were recorded, the surfaces were assumed to remain dry. Therefore the moisture factor, representing the state of saturation of the surface, was set to zero.

Table 5.2 Surface parameters.

Material	Vertical Emissivity	Vertical Albedo
Concrete	0.97	0.30
Asphalt	0.96	0.20

5.2.3 Material parameters.

The layered structures with concrete and asphalt surfaces assumed for use with the model are shown in Figures 5.1 and 5.2. The exact thickness of the different layers of material could not be determined at the site, so the values shown on the diagrams are estimates of what might be reasonably expected. These estimates were arrived at after considering the results of the sensitivity analysis carried out on this model. The sensitivity of the model to layer thickness depends to a large extent on the thermal conductivity of the layer, with higher conductivities causing the model to be less sensitive to changes in thickness. However, as the sensitivity analysis was carried out on a structure identical to that with the concrete surface in Fig. 5.1, and very similar to that with the asphalt surface in Fig. 5.2, the results of the analysis may be directly applied to this validation of the model. The sensitivity analysis showed that the model predictions were only sensitive to changes in thickness of the top layer, provided the thickness of the second layer was not greatly reduced. The results also showed that the predictions were much more sensitive to a decrease rather than an increase in the thickness of the top layer. It was therefore clear that provided reasonable values were assumed for the thickness of the layers, then these input data should not constitute a major source of error.

The values used for the thermal conductivities and diffusivities of the layers comprising the two composite structures are shown in Table 5.3. These are also obtained from measurements made on similar types of materials by Balick et al., 1981. The values for soil represent a mixture containing equal proportions of sand and clay soil types.

The use of the values obtained by Balick et al. can be justified when the results of the sensitivity analysis for the material parameters are considered. In the case of thermal diffusivity, it was found that the temperature predictions of the model were only sensitive to large changes in the diffusivity of the top layer. Variations in the thermal conductivity of the top layer were found to have more effect on the temperature predictions, with changes of $\pm$ 30% leading to a maximum change of 1 °C. However, variations as large as these would only be achieved in practice by a change in the type of material from which the layer was composed. The model was found to be much less sensitive to changes in the conductivity of the second layer and insensitive to changes in the value for the third layer. It is therefore possible to assume that a reasonable estimate of the conductivities and diffusivities is acceptable. This is particularly useful in the case of the concrete layer for two reasons. Firstly, because it is not possible to determine the type or proportions of the materials from which the concrete was made, and secondly, because the thermal characteristics at different positions in the layer of the concrete are likely to show variations depending on the composition and uniformity of the mixture.

Table 5.3   Material parameters.

Material	Thermal Conductivity	Thermal Diffusivity
Concrete	1.54 $Wm^{-1}K^{-1}$	7.20×10^{-7} m^2s^{-1}
Asphalt	0.70 $Wm^{-1}K^{-1}$	3.67×10^{-7} m^2s^{-1}
Gravel	2.50 $Wm^{-1}K^{-1}$	8.00×10^{-7} m^2s^{-1}
Soil	0.70 $Wm^{-1}K^{-1}$	4.70×10^{-7} m^2s^{-1}

5.2.4 Initial temperature profile and lower boundary condition.

The total depth below the surface to which temperatures were predicted by the model was 1 m. This was chosen as it represents the extent of the depth of subsurface material whose temperature is influenced by the diurnal temperature

wave, so allowing the approximation of a constant temperature to be used for the lower boundary condition. As subsurface temperatures were not measured at Ouston, the initial temperature profile and temperature at the lower boundary had to be estimated.

The temperature at the lower boundary was obtained from measurements made at a depth of 1 m at the Observatory, Durham, over the period in April when the validation data were being recorded. The use of data recorded at a site several miles from Ouston may be justified by consideration of the results described in Section 3.3.4.2 of the sensitivity analysis. These imply that the predictions of the model are insensitive to large variations of the temperature at the lower boundary, provided the depth of material being modelled is suitably large and the thermal conductivity of the material is not excessively high. The other reason why it was felt acceptable to use these data was that as the lower boundary was at sufficient depth to be unaffected by the diurnal temperature wave, then the variation in soil temperature between different sites was unlikely to be very great.

The initial temperature profile was obtained by the procedure which was outlined in Section 3.2.1. Firstly the temperature profile throughout the composite structure was set at a constant value, arbitrarily chosen to be the same as the temperature at the lower boundary. The stable profile within the structure was then obtained by running the modelling program, using the data recorded during the period of generally cloud free weather from 12:00 19th April to 12:00 20th April. The resulting temperature profiles for the two composite structures at the start of the validation period at 12:00 19th April are shown in Figures 5.3 and 5.4.

5.2.5 Meteorological parameters.

The weather data required as input for the model were recorded by the weather station, the operation of which is described in Section 4.5. The data were recorded at 15 minute intervals almost continuously over the period from

19th to 25th April. However, there are some short gaps corresponding to when the Microdata logger was transferring data to the Tektronix computer. The data required as input for the model consisted of the average windspeed and the average incident short-wave solar flux over the 15 minute interval, and the values of the air temperature and wet and dry bulb depression as measured instantaneously at the end of the 15 minute interval. These data are plotted in Figures 5.5 to 5.28.

5.2.6 Radiometer data.

While the data logging equipment was in operation at Ouston, the temperatures of many objects were measured at roughly 15 minute intervals. The temperature data are nearly continuous over the validation period, with gaps occuring where the equipment was unserviceable. There are three potential uses for the temperatures measured by the radiometer. Firstly, the radiation temperatures of the concrete and asphalt surfaces are used for comparison with the predictions of the model to determine how well the model is simulating the behaviour of the measured temperature.

The second use of the data is to calculate the value of the function "TREP", which is the average temperature of distant objects which may obscure part of the sky as viewed from the surface under investigation. The function is used in the model in the calculation of the net long-wave radiative flux incident on the surface. However, in this case the surfaces are horizontal and have a completely unimpeded view of the sky. Therefore the value of the function was set to an arbitrary value of 0 °C and the relevant parameters in the data file were set to indicate that the surfaces were unobscured and the value of "TREP" was to be ignored in the calculation of the net long-wave radiative flux

The other use of the radiometer data is in the calculation of the long-wave cloud cover factor, "CLFAC", which is used to obtain a measure of the downward long-wave radiation flux due to the clouds. This factor is

derived from the temperatures measured by the radiometer while pointing vertically upwards at the sky. These measurements were made several times during the routine scan of the surfaces under investigation. Calculation of the value of this factor was carried out by an off-line data analysis program, which is described in Section A.3.1.2 of the Appendix. This program starts by finding the maximum and minimum sky temperatures over the 24 hour period to be modelled. These are then chosen to represent conditions of total cloud cover and clear sky respectively, with cloud cover factors of 1 and 0. Intermediate values are then calculated by assuming a linear correspondence of cloud cover factor against recorded sky temperature, between the upper and lower limits of the factor as evaluated above. The cloud cover factors calculated from the data recorded over the validation period are plotted in Figures 5.29 to 5.34.

5.3 Method of validation of the model.

The model was run using the data file for the first 24 hour period from 12:00 19th April to 12:00 20th April, using the input data described in the previous paragraphs. The final temperature profile predicted at the end of the period was then used as the starting profile in the data file for the next 24 hour period. This was repeated until temperatures had been predicted up to the end of the validation period at 12:00 25th April.

The next stage of the procedure was to compare the temperatures predicted by the model with those measured by the radiometer. This was most easily accomplished by a comparison of plots of measured and predicted surface radiation temperatures over the period being modelled. Initially there was found to be fairly good agreement between the two plots for the concrete surface, although for the asphalt surface the measured and predicted temperatures showed the same type of behaviour but were not in as good agreement. The results for the asphalt could be explained by two possible reasons. Firstly, the model was not suitable for simulating surface temperatures of asphalt, or secondly, there had been an incorrect choice of

one or more of the values of the parameters used in the input data file for the model. The results for the concrete surface suggested that the model was capable of producing satisfactory simulations of temperatures of non-vegetated surfaces, so the latter possibility was investigated. The results of the sensitivity analysis were used to decide which parameters should be varied to bring the predicted and measured temperatures into better agreement. As the weather data were measured by the weather station, it was not possible to alter their values. Therefore, the parameters to which the model was most sensitive, and whose values it was acceptable to vary, were the vertical emissivity and albedo of the surface. It was also acceptable to vary the properties of the materials comprising the composite structure, including thermal conductivities and diffusivities and the thicknesses of the layers. Reasonable bounds on the magnitude of the variations that were allowable were provided by the results of the sensitivity analysis, and also obtained bearing in mind the ranges of possible values quoted by Balick et al., 1981.

The period from 12:00 19th April to 12:00 20th April was chosen to observe the effects of variation of these parameters, as this represented a fine weather period with the advantage that it was generally cloud free. The method used was to firstly vary the emissivity of the surface slightly in order to cause the predicted and measured overnight temperatures to coincide. Secondly, the albedo of the surface could be changed if necessary to account for any disagreement that might still exist between predicted and measured temperatures during the hours of daylight. Thirdly, the emissivity could be varied again if it was thought that it would lead to an improvement. If these alterations were insufficient, then the material parameters could be varied, although their effect on the predictions would be much smaller.

Once the best agreement between the predicted and measured temperatures had been found, the parameters were then kept fixed at their optimal values. A new stable temperature profile for the first 24 hour period was then determined by the method described previously, and the model run for the

remainder of the validation period after the data files had been suitably modified. A comparison of the measured and predicted temperatures over the entire validation period was then made for both surfaces. It was found that the agreement between measurements and predictions was equally good for subsequent periods where the weather conditions were similar to those in existence over the initial 24 hours, which suggested that the variation of the parameter values as described above had been justified.

When the model was used to simulate the behaviour of the composite structure with the concrete surface, it was found that it was only necessary to alter the value for the emissivity of the surface slightly to obtain the best agreement between measured and predicted temperatures. In the case of the structure with the asphalt surface, it was found that the value of the emissivity of the surface needed to be increased, while the original choice of the value for the albedo from the range of values suggested by Balick et al., 1981, could not be improved. Table 5.4 gives the values of emissivity and albedo for the two surfaces, which were finally used for the validation.

Table 5.4 Optimal values for surface parameters.

Material	Vertical Emissivity	Vertical Albedo
Concrete	0.98	0.30
Asphalt	0.985	0.20

5.4 Results of the validation of the model.

The results of the validation over the six 24 hour periods from 12:00 19th April to 12:00 25th April are displayed in Figures 5.35 to 5.46. These graphs compare the temperature measured by the radiometer with that predicted by the model for the asphalt and concrete surfaces. The results are discussed in more detail in the following paragraphs.

5.4.1 Results from 12:00 19th April to 12:00 20th April 1982.

This was the first 24 hour period for which validation data were available. As described previously, this period was used to determine the optimal values for certain parameters in the input data files for the model, which resulted in the best agreement between the predicted and measured temperatures.

Weather data acquisition began on the morning of the 19th, and conditions were initially cloudy. By 12:00 it was clear and sunny, and the sky stayed clear for the rest of the afternoon. This behaviour can be seen in the plots of incident solar radiation and long-wave cloud cover factor (Figures 5.5 and 5.29 respectively). The radiometer was switched on at 13:00 on the 19th, and after a warming up period data were collected over the remainder of the 24 hour period.

The plots of measured and predicted radiation temperatures against time are given in Figures 5.35 and 5.36 for the concrete and asphalt surfaces. The temperature profiles shown in Figures 5.3 and 5.4 were used as the initial profiles in the data file for the model. In the clear and sunny weather of the afternoon of the 19th, the measured and predicted temperatures are in good agreement, as is also the case overnight. The morning of the 20th was initially bright and clear, although some thin cloud appeared as the morning progressed. This is reflected in the plot of incident solar flux, and in the slightly uneven behaviour of the measured and predicted temperatures in Figures 5.35 and 5.36.

5.4.2 Results from 12:00 20th April to 12:00 21st April 1982.

This period is not very useful for validation purposes as the radiometer was out of service for a large proportion of the day. There is also a gap in the weather data from 16:30 to 17:15 on the 20th. The comparisons between the predicted temperatures and the available measurements are shown in Figures 5.37 and 5.38.

Over the period from 12:00 to 16:15 on the 20th, agreement between measured and predicted temperatures is not very good. This is possibly due to poor simulation of the cloudy conditions on the afternoon of the 20th. The presence of cloud is clearly reflected on the plot of the long-wave cloud cover factor in Fig. 5.30, and the plot of the incident solar flux for this period, which is shown in Fig. 5.9. If the graph showing the solar flux is compared with the temperatures for the asphalt and concrete surfaces, it is possible to see the correspondence between peaks in the flux where the sky cleared, and peaks in the measured temperature of the target. This behaviour can be easily seen at around 14:30 and 16:00 on the 20th.

The loss of weather data from 16:15 to 17:15 results in the predictions starting to diverge from the measured temperatures. The values for the weather parameters missing from the data file are calculated by the model, using linear interpolation between the last data at 16:15, and the next data at 17:15. The divergence of the measured and predicted temperatures is mainly due to the interpolated values of the incident solar flux readings being incorrect. It is possible to estimate the flux by considering the geographical characteristics of the site, the orientation of the surfaces, and the time of year at which the measurements were made. However, this calculation is unlikely to produce very accurate results, especially if the sky is not clear and there are insufficient data available to estimate the type and amount of cloud cover.

No radiometer data are available from 18:30 on the 20th until early the next day. The morning of the 21st was sunny, with only a few traces of high altitude cloud in the sky. This is confirmed by the plot of incident solar flux shown on Fig. 5.9. On the basis of the results for the previous 24 hour period, good agreement would be expected between the measured and predicted surface temperatures under these weather conditions. As can be seen in Figures 5.37 and 5.38, for the short period from 09:30 to 11:00 on the 21st where the radiometer data were available again, the agreement between the two

temperatures is as good as that on the previous day.

5.4.3 Results from 12:00 21st April to 12:00 22nd April 1982.

The first 12 hours of this period represent clear and sunny weather conditions, which were very similar to those on the afternoon of the 19th. As might therefore be expected, there is good agreement between the measured and predicted temperatures, as shown in Figures 5.39 and 5.40. The sky remained clear until around 04:30 on the 22nd, and the formation of cloud at this time can be seen in the behaviour of the long-wave cloud cover factor, as shown in Figure 5.31. In Figures 5.39 and 5.40, the appearance of cloud can clearly be seen where the measured temperatures of the two surfaces rise by a few degrees above the almost constant overnight value. As expected, the peak temperature occurs at about 04:30, and afterwards the temperatures gradually fall until sunrise. This is also reflected in the predictions of the model, although the agreement with the measured temperatures is slightly better for the asphalt surface than for the concrete.

The available solarimeter data plotted in Figure 5.13 suggests that the morning of the 22nd is mainly sunny, but with a short cloudy period at about 06:00. However, the long-wave cloud cover factor shows a clear sky at this time, which is possibly due to the radiometer being pointed at a clear patch in an otherwise overcast sky. This may explain why the predicted temperatures for the concrete surface at this time are lower than those measured, although there is still good agreement between measurements and predictions for the asphalt surface. The remainder of the morning was generally clear, but with a gradual increase in the amount of cloud cover, consisting of fair weather cumulus. There were no further weather data recorded after 08:45, and as mentioned previously, the loss of the solarimeter data in particular means that the predicted temperatures will be much less accurate.

5.4.4 Results from 12:00 22nd April to 12:00 23rd April 1982.

The afternoon of the 22nd became progressively more cloudy, and was overcast with thick grey cloud by 17:30. However, there were a few brief bright periods, as shown by the plots of incident solar flux in Figure 5.17 and long-wave cloud cover factor in Figure 5.32.

The measured and predicted temperatures for the two surfaces are shown in Figures 5.41 and 5.42. It is immediately apparent that although the behaviour of the predicted and measured temperatures are similar, they are separated by a roughly constant amount. This occurs over the period from 14:00 on the 22nd, when the weather data started to be available again, until 09:30 on the 23rd. The effect is due to a thin plastic cover being placed over the viewing aperture of the radiometer in order to prevent rain from entering the detector. Unfortunately, the radiometer was not calibrated against a blackbody with the plastic cover in place, so it is not possible to allow for the effect of the cover in the analysis of the radiometer data. However, a qualitative comparison of the measured and predicted temperatures for the concrete and asphalt surfaces can be used to obtain a general idea of how the radiometer measurements are affected by the presence of the cover. Firstly, it appears that the cover causes the measured temperature to be higher than would be produced by the radiometer if it was uncovered, by an amount which stays roughly constant. Secondly, while the behaviour of the measured and predicted temperatures are basically the same, the measured temperatures show a larger variation between maxima and minima, suggesting that the cover does not affect the capability of the radiometer to detect small changes in the temperature of the surface under investigation. This can be seen in Figures 5.41 and 5.42, where there are clear minima and maxima at 14:45 and 16:00 respectively. However, as this period consists of cloudy weather, this effect may also be partially due to inaccuracies in the type and amount of cloud cover in the input data file for the model.

The sky cleared around 24:00 on the 22nd, and this was accompanied by a

fall in the measured and predicted temperatures. The morning of the 23rd was generally sunny, as indicated by the graph of incident solar flux, although the plot of the long-wave cloud cover factor shows the presence of small amounts of cloud. This was observed to consist of high altitude cirrus clouds. There was also a strong westerly wind, reaching a maximum average speed of 19 ms^{-1} by 09:00. The cover over the radiometer viewing aperture was removed at 09:15, and it can be seen on both Figures 5.41 and 5.42 that the measured and predicted temperatures are then in good agreement once again.

5.4.5 Results from 12:00 23rd April to 12:00 24th April 1982.

The afternoon of the 23rd was cloudy, but with some brief sunny periods. The plot of solar flux in Figure 5.21 and the plot of the long-wave cloud cover factor in Figure 5.33 show three short periods with high incident solar flux, which occur at 13:15, 14:15, and 15:30. These three peaks can also be seen in the measured and predicted temperatures for the two surfaces, which are shown in Figures 5.43 and 5.44, and up to 17:45 on the 23rd, measurements and predictions are in good agreement. The cover was then replaced over the viewing aperture of the radiometer, which caused the radiometer reading to behave in a similar manner to that observed in the previous 24 hour period.

It was cloudy overnight, but there were two short, clear periods at 01:00 and 04:00, which can be seen on the graph showing the long-wave cloud cover factor. As expected, the fall in temperature of the surfaces when the sky clears is shown by both the measured and predicted temperatures. The morning of the 24th was cloudy and no radiometer data are available between 04:45 and 11:00.

5.4.6 Results from 12:00 24th April to 12:00 25th April 1982.

This was the final period over which data were recorded. The recorded weather data end at 06:43 on the 25th, and the radiometer data end shortly afterwards.

The afternoon of the 24th was initially cloudy, but cleared by 14:30 when the sky was blue with a low proportion of cirrus cloud cover. This is reflected in the plots of temperatures in Figures 5.45 and 5.46, which start unevenly with distinct peaks and then become smoother as the sky clears. Overnight, there was no cloud and there is good agreement between the measured and predicted temperatures. On the graph showing the long-wave cloud cover factor it can be seen that cloud started to form at around 04:00, and after this time the measured and predicted temperatures appear to start diverging. This is probably due to an inaccurate representation of the amount of cloud present. The divergence between the temperatures becomes larger after sunrise, although this due to inaccuracies in the predictions resulting from the loss of weather data after 06:30.

5.5 Results of a comparison of predicted and measured temperature contrast between the asphalt and concrete surfaces.

The temperature data discussed in the previous section were also used to investigate the ability of the model to predict the difference in the radiation temperatures of two different surfaces at a given time. The predicted and measured temperature contrasts between the asphalt and concrete surfaces were calculated by subtracting the surface radiation temperature for the asphalt from that of the concrete. The results are shown in Figures 5.47 to 5.52, and cover the validation period from the 19th to the 25th April 1982.

On the first graph, it can be seen that for the clear, sunny weather on the afternoon of the 19th, there is very close agreement between measurements and predictions. The results for the next morning do not show quite as good agreement, although the temperatures are still within about 1 °C of each other. The two peaks in the measured data at 08:30 and 10:30 can also be seen to correspond fairly well with the predictions.

There is only a limited amount of data available for comparisons to be

made over the next 24 hour period, and this is plotted in Figure 5.48. This shows that the measured and predicted temperatures are in agreement to within the same limits as before and show a similar type of variation.

The interesting feature on Figure 5.49 is the poor correspondence between the predicted and measured temperature contrasts from about 21:00 on the 21st until the end of the 24 hour period. Figures 5.39 and 5.40 compare the predicted and measured temperatures for each of the surfaces and it is evident that the poor agreement in the contrast after 21:00 results from the failure of the model temperature predictions to closely follow the uneven behaviour of the measured temperature of the concrete surface. As mentioned in the analysis of these results, this is possibly due to a poor simulation of the cloud cover which was present. However, the good agreement between the smoother predicted and measured temperature curves for the asphalt surface over the same period, and the plot of the long-wave cloud cover factor in Figure 5.31, would rather tend to suggest that the sky was reasonably clear. There were no weather data available after 08:45, and as discussed in Section 5.4.2, predicted temperatures are therefore likely to be much less accurate. This explains the poor correspondence between the predicted and measured temperature contrast after 08:45, as shown in Figure 5.49.

The results for the 22nd to the 23rd April are shown in Figure 5.50. This period consisted of a mixture of clear and cloudy weather which is reflected in the behaviour of the temperature curves. In general, the predicted and measured contrast agree to within 1.5 °C. It is also interesting to note that the cover was placed over the viewing aperture of the radiometer until 09.30 on the 23rd. This may be the reason for the measured and predicted contrast being separated by a small, but roughly constant, amount until the two curves converge at the time corresponding to when the cover was removed. This assumption can be justified if the results of Figures 5.41 and 5.42 are considered. Here it can be seen that for the measured temperatures of both the asphalt and concrete surfaces, the effect of the cover was to cause the

temperature recorded by the radiometer to be higher than would be expected if it was uncovered, and by an amount which stays roughly constant. The curves diverge again after 10:30 although this could be due to errors in the predicted temperatures, perhaps caused by an incorrect representation of the cloud cover being used in the input data file for the model.

The results for the next 24 hour period are shown in Figure 5.51. The afternoon of the 23rd was cloudy and up to around 18:00 there is good agreement between measurements and predictions. The cover was then replaced over the viewing aperture of the radiometer and, as seen in the previous 24 hour period, this is probably the cause of the fairly constant difference between the measured and predicted temperatures.

Figure 5.52 shows the remaining data up to the end of the validation period, which was early on the morning of the 25th. Agreement between measurements and predictions is very close on the afternoon of the 24th and to within about 1 °C until the recorded data end.

5.6 Conclusion.

The validation results discussed in Section 5.4 were based on a comparison between the temperatures of the concrete and asphalt surfaces measured by the radiometer and those predicted by the model. It was found that there was generally good agreement between predicted and measured temperatures, and that the agreement was best when the sky was clear. When clouds appeared the difficulty of determining the cloud type and amount of the sky which was covered resulted in the predictions becoming less accurate, although in general it was found that the predictions for cloudy weather still followed the behaviour of the measured temperatures quite well.

It is important to note that these results do not imply that all of the parameterisations used in the model are producing accurate values of the quantities which they are supposed to simulate. These quantities, which

include the heat fluxes at the surface for example, were not directly measured at Duston, and so it is not possible to compare predictions with measurements. However, in many cases the most important result from the model is the prediction of the surface temperature of the object of interest and this relies on the model as a whole producing accurate predictions rather than individual parameterisations. Of course, if some of these parameterisations are inaccurate, then it is likely that the model will fail to produce realistic surface temperature predictions under certain weather conditions or if materials with certain physical properties are studied. Therefore, the main conclusion which can be drawn from the validation is that the model is able to realistically simulate the behaviour of the surface radiation temperature of the two composite structures considered, over the range of weather conditions in existence while the validation data were being recorded.

The validation data were also used to investigate the ability of the model to simulate the temperature contrast between two different surfaces. The results are described in Section 5.5, and in general it was found that the predicted and measured temperature contrasts between the asphalt and concrete surfaces were in agreement to within 1.5 °C. This is perhaps not surprising, as provided the calibration of the instrument does not vary while measurements are being made, then the measurement of a temperature difference means that the radiometer does not have to be accurately calibrated against a reference source. Therefore the measurement of the important quantity, temperature contrast, will be less subject to error than the measurement of an absolute surface temperature using the radiometer. One of the main problems of using the data recorded from the 19th to the 25th April 1982 for the validation is that part of the radiometer measurements were made with a plastic cover over the viewing aperture, and it was not possible to calibrate the radiometer against a suitable reference source while the cover was in place. It would therefore be reasonable to expect that the temperature difference measured by the radiometer with the cover in place would be approximately the same as that

which would be measured if the cover was removed. However, difficulties arise as the cover will emit radiation at its own temperature, and if the effect of the cover is to be ignored, then the temperature of the cover has to stay constant. Fortunately, the two surfaces were located close together and there was a minimal time delay between taking the two temperature measurements, so there are unlikely to be radical changes in the radiation emitted by the cover under most conditions. This means that the contrasts measured with the cover in place can be compared with the temperature predictions of the model, although the accuracy of the measurements may be much lower than those obtained with the cover removed. The results discussed in Section 5.5 show that there is agreement to within about 1.5 °C, so the above assumptions are justified.

In summary, the mainframe general purpose model is capable of producing a good simulation of the surface radiation temperatures of the asphalt and concrete surfaces, and also the temperature contrast between the two surfaces, under the weather conditions experienced during the validation period.
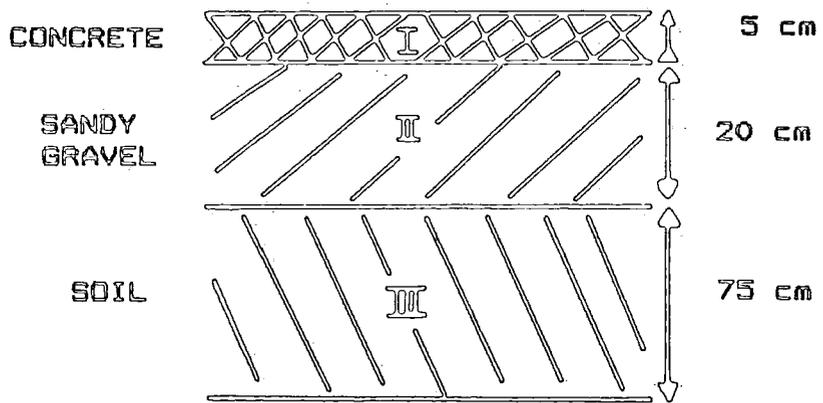
CONCRETE   I   5 cm

SANDY GRAVEL   II   20 cm

SOIL   III   75 cm

<u>Fig. 5.1</u>   <u>Thickness and composition of the layers</u>

     <u>comprising the one-dimensional</u>

     <u>structure with the concrete surface.</u>

ASPHALT   I   3 cm

SANDY GRAVEL   II   25 cm

SOIL   III   72 cm
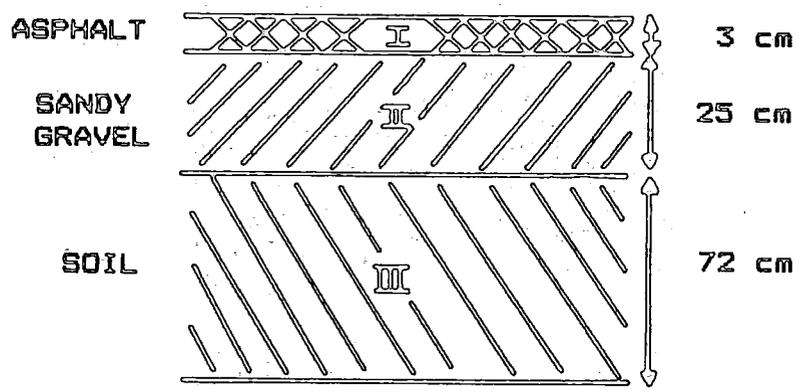
<u>Fig. 5.2</u>   <u>Thickness and composition of the layers</u>

     <u>comprising the one-dimensional</u>

     <u>structure with the asphalt surface.</u>

Fig. 5.3
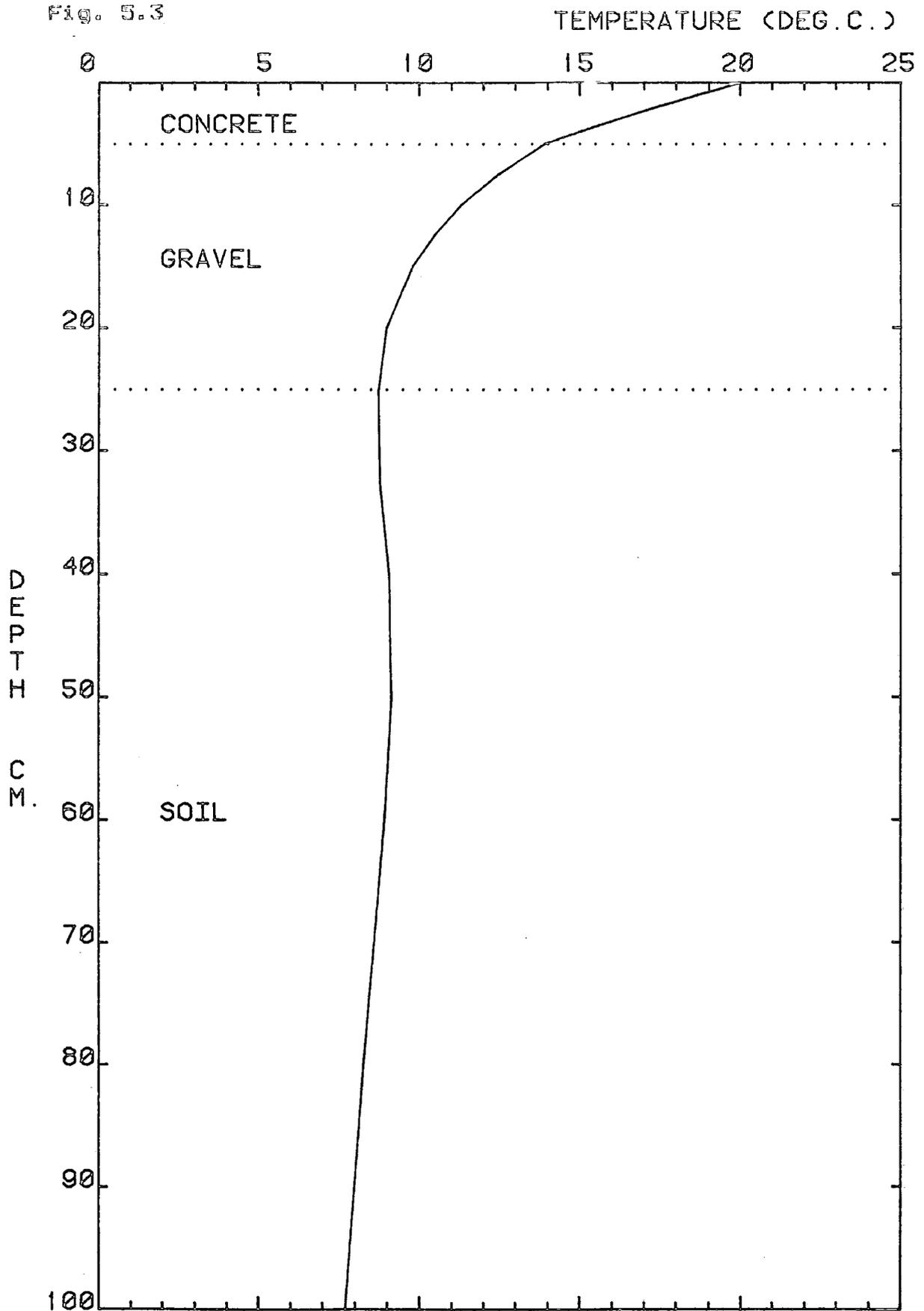
INITIAL TEMPERATURE PROFILE AT 12:00 ON 19/4/82,
FOR THE STRUCTURE WITH THE CONCRETE SURFACE.

Fig. 5.4
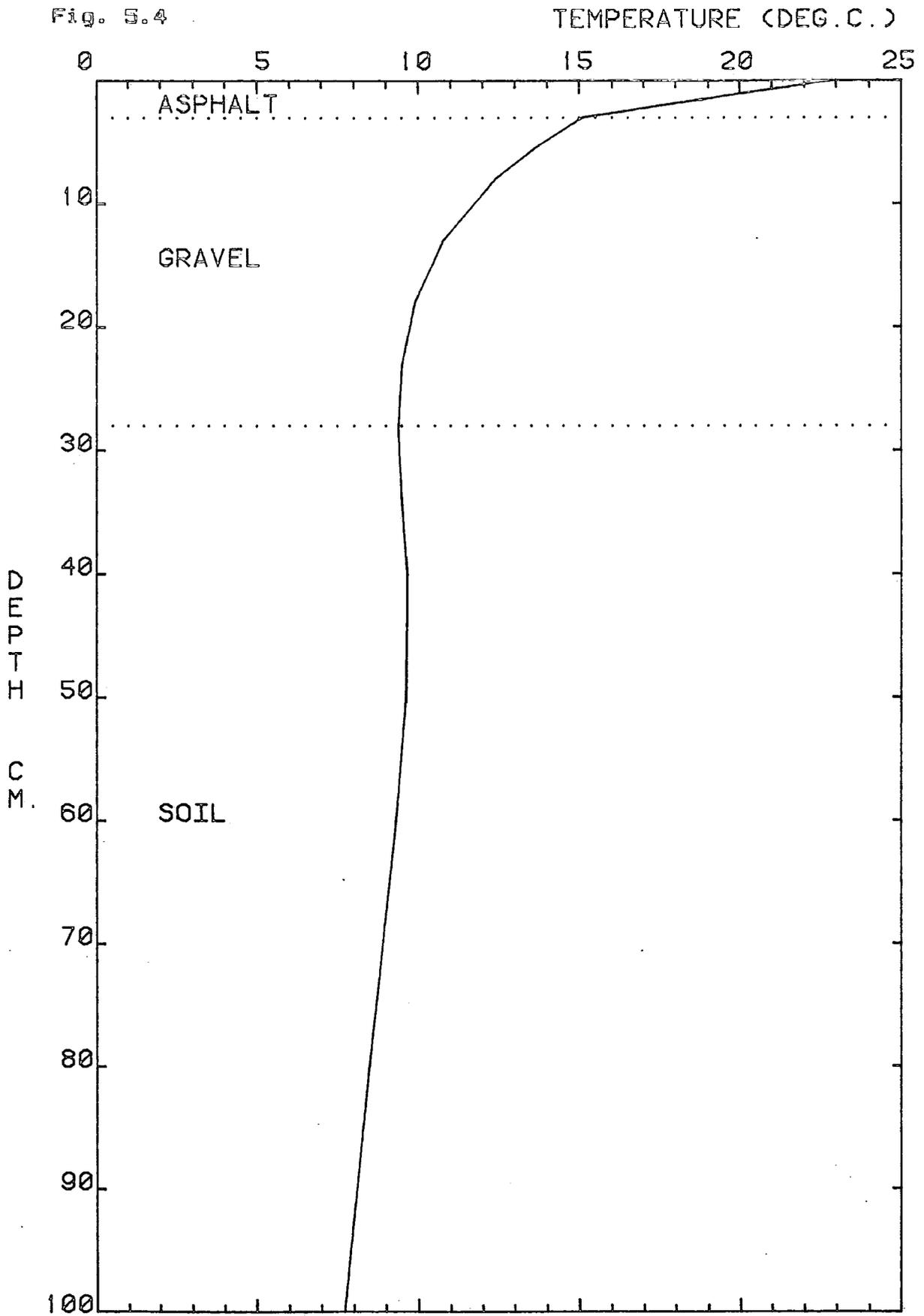
INITIAL TEMPERATURE PROFILE AT 12:00 ON 19/4/82,
FOR THE STRUCTURE WITH THE ASPHALT SURFACE.

Fig. 5.5   WEATHER DATA RECORDED AT OUSTON, NORTHUMBERLAND
            AV. SOLAR RADIATION FROM 12:00 19-APR-82 TO 12:00 20-APR-82.
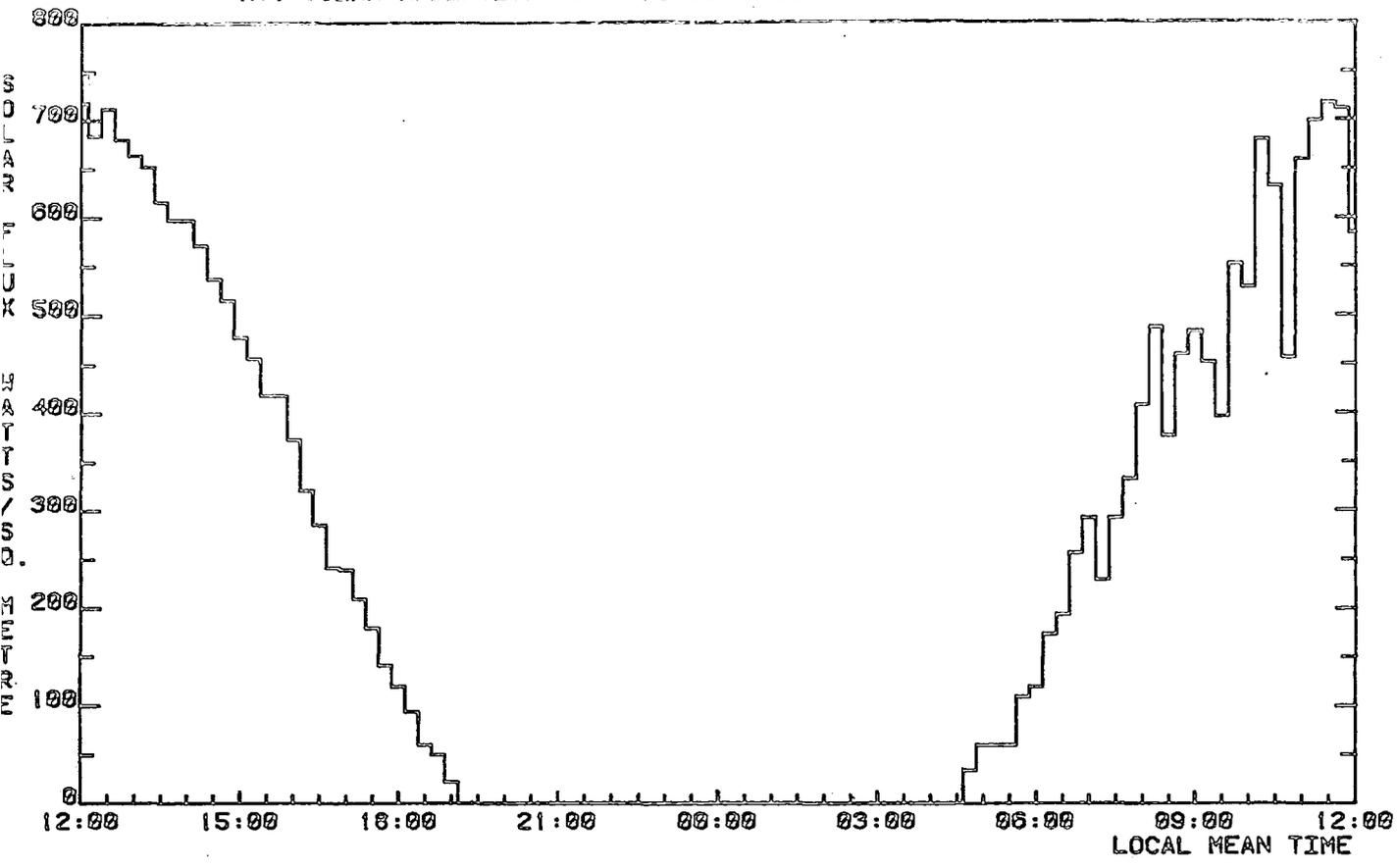
Fig. 5.6   WEATHER DATA RECORDED AT OUSTON, NORTHUMBERLAND
            AV. WINDSPEED FROM 12:00 19-APR-82 TO 12:00 20-APR-82.
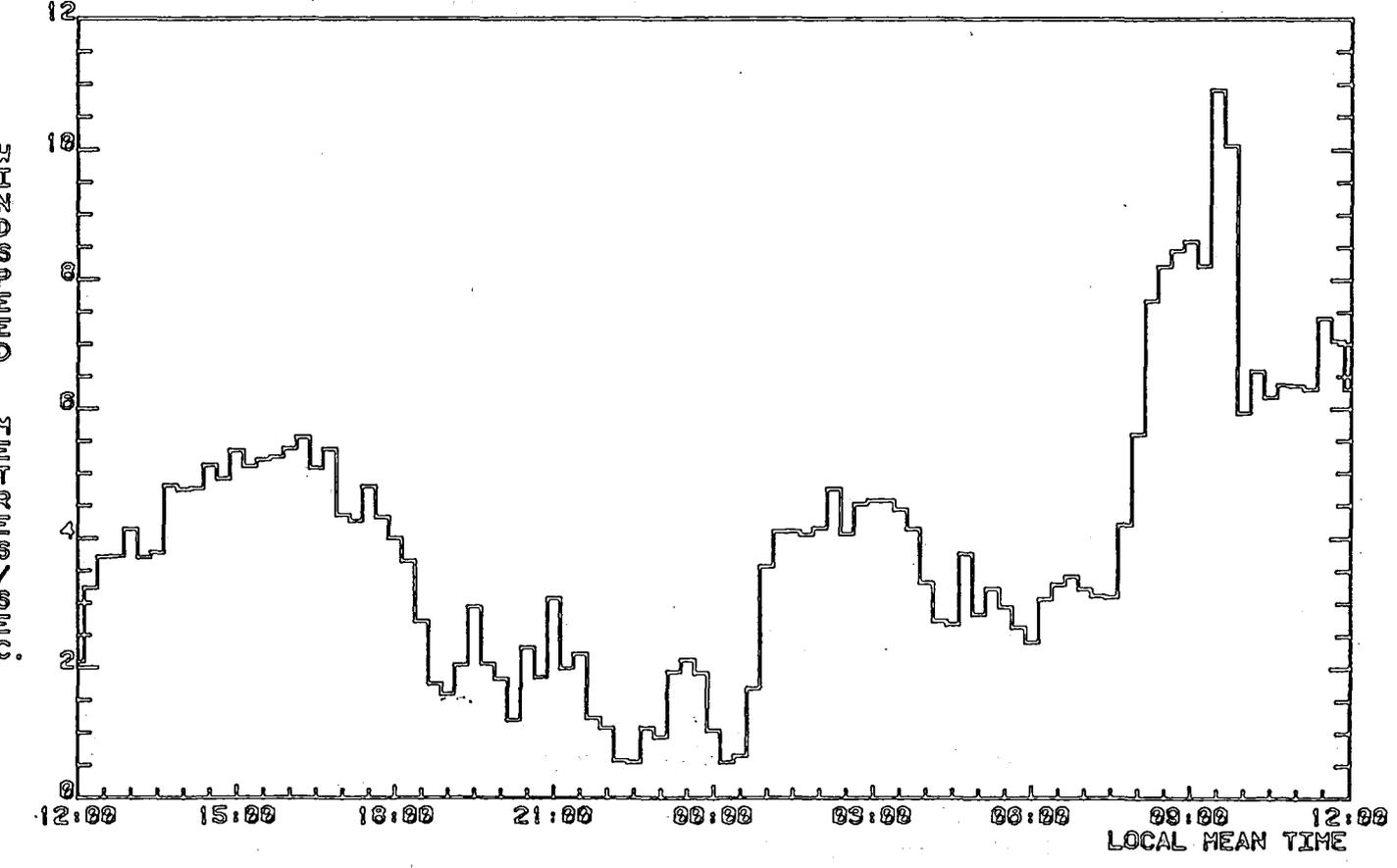
Fig. 5.7   WEATHER DATA RECORDED AT OUSTON, NORTHUMBERLAND
            AIR TEMPERATURE FROM 12:00 18-APR-82 TO 12:00 20-APR-82.
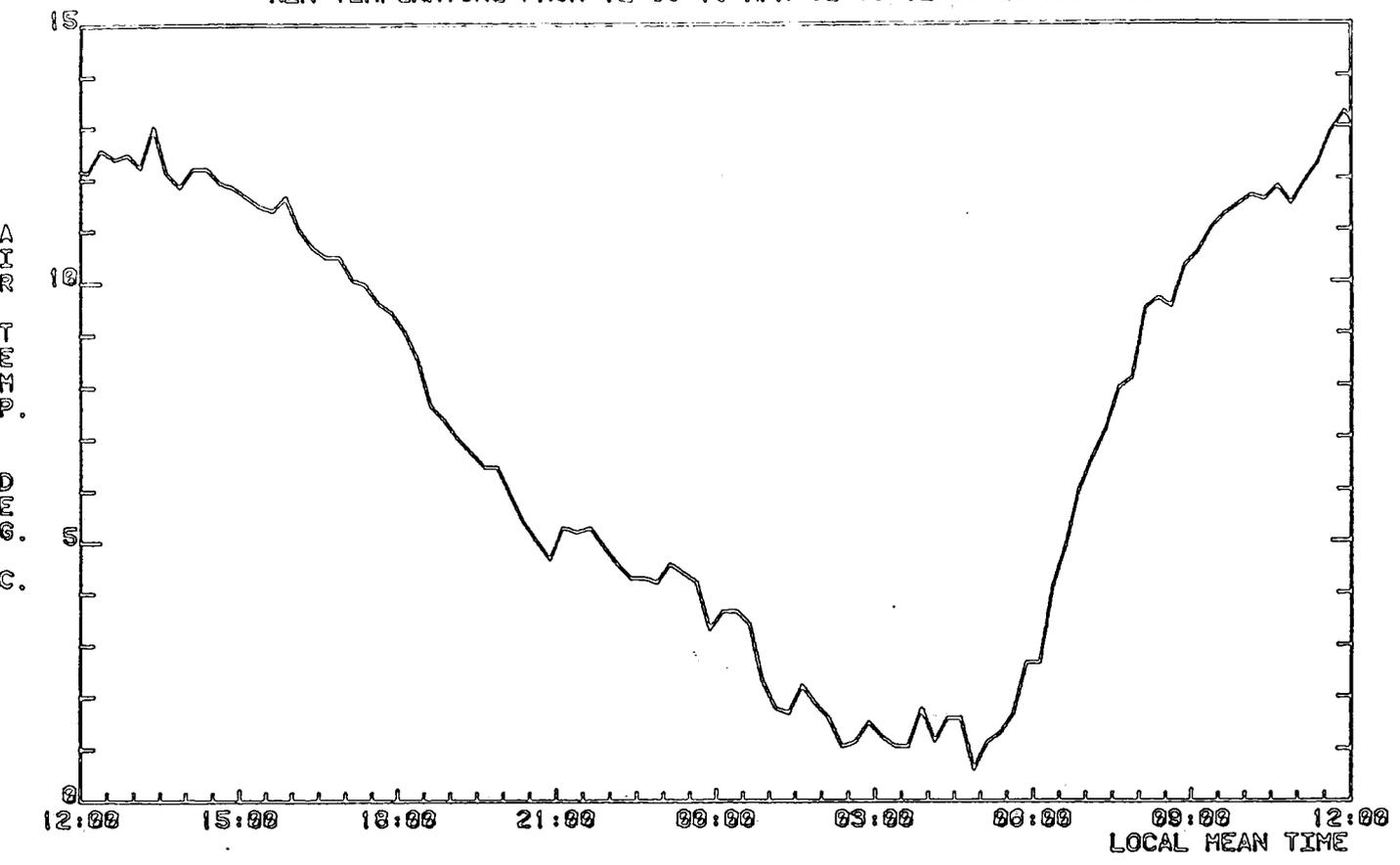
Fig. 5.8   WEATHER DATA RECORDED AT OUSTON, NORTHUMBERLAND
            WET/DRY BULB DEPRESSION FROM 12:00 18-APR-82 TO 12:00 20-APR-82.
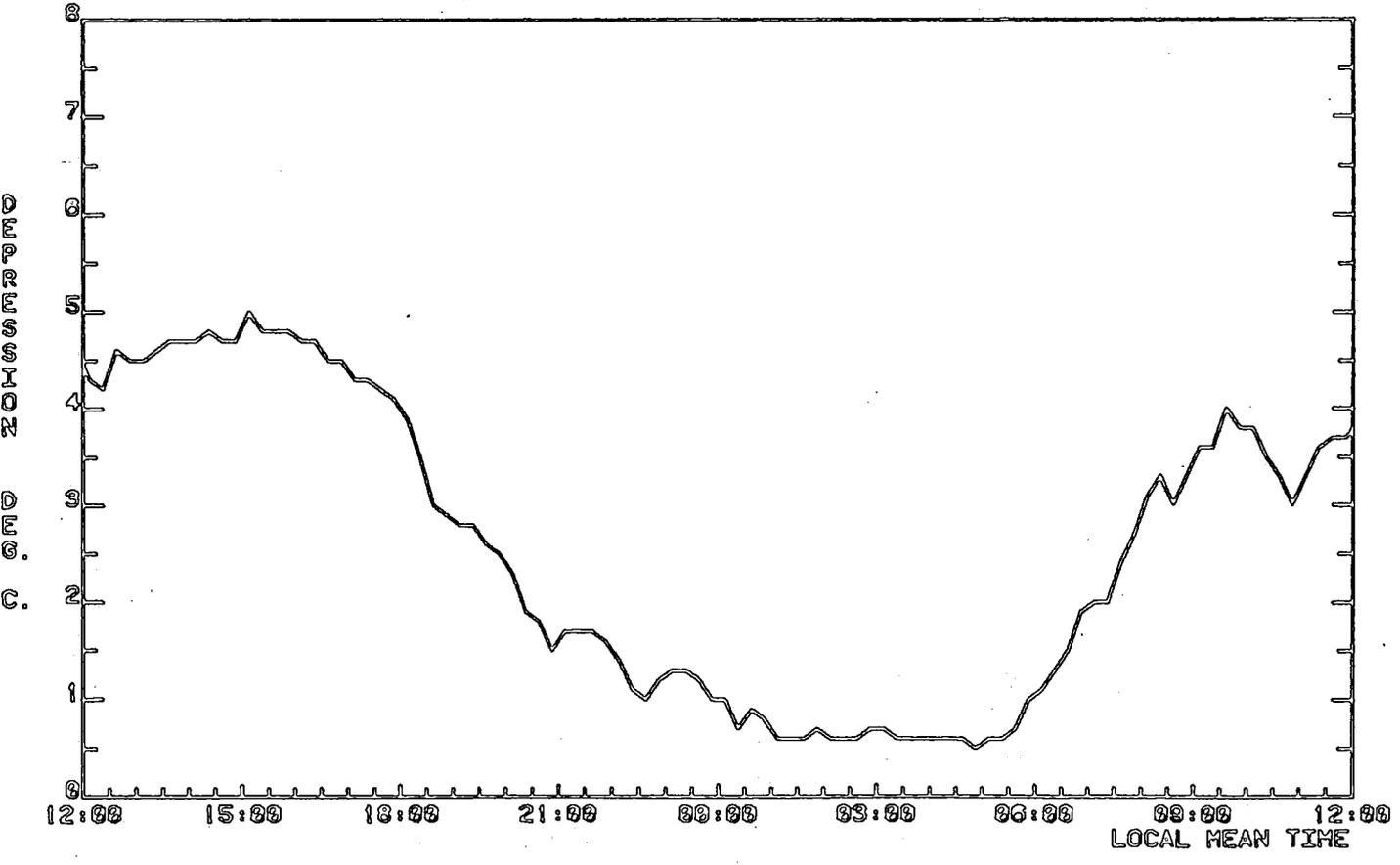
Fig. 5.9   WEATHER DATA RECORDED AT OUSTON, NORTHUMBERLAND
            AV. SOLAR RADIATION FROM 12:00 20-APR-82 TO 12:00 21-APR-82.
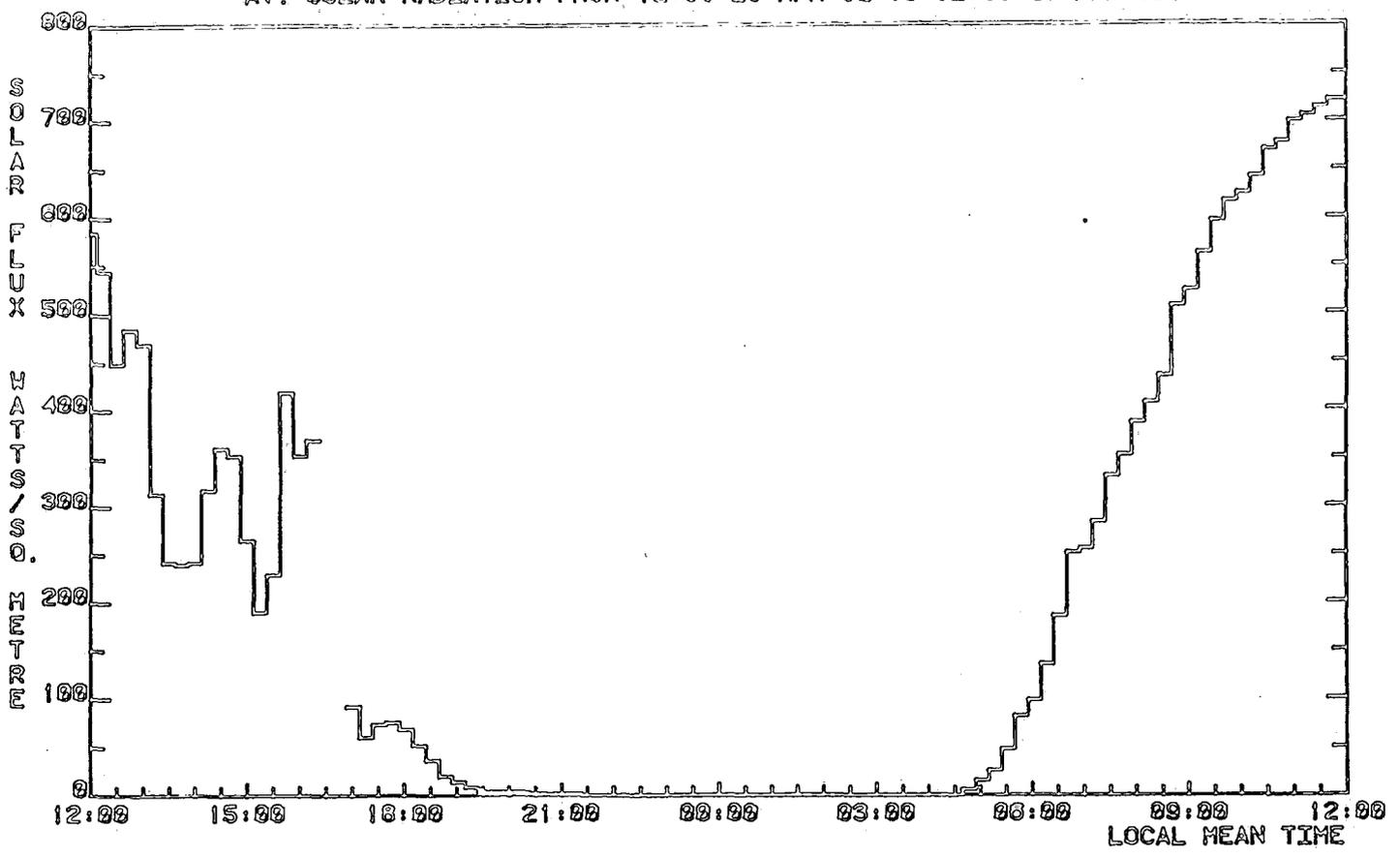
Fig. 5.10   WEATHER DATA RECORDED AT OUSTON, NORTHUMBERLAND
             AV. WINDSPEED FROM 12:00 20-APR-82 TO 12:00 21-APR-82.
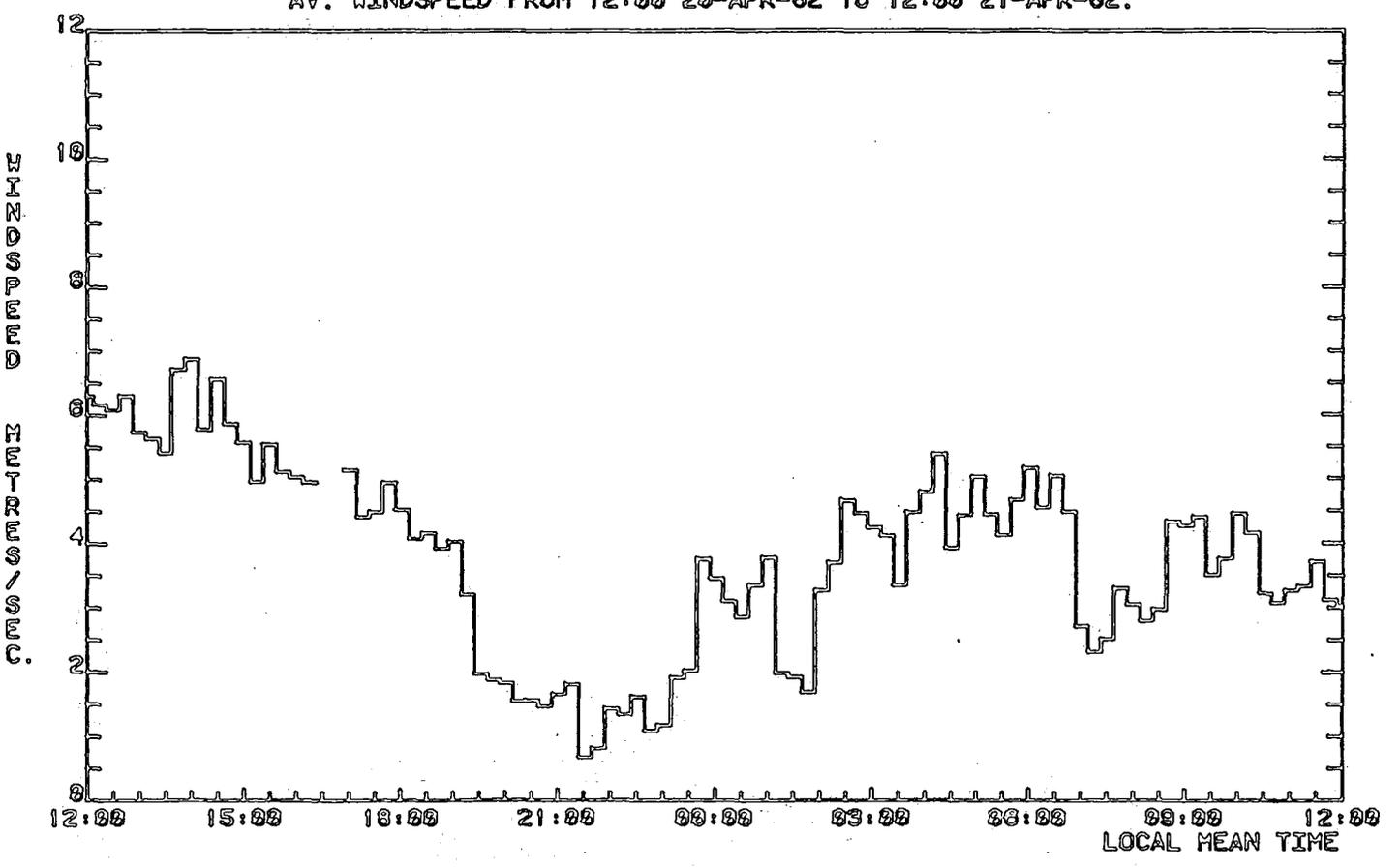
Fig. 5.11   WEATHER DATA RECORDED AT OUSTON, NORTHUMBERLAND
AIR TEMPERATURE FROM 12:00 20-APR-82 TO 12:00 21-APR-82.
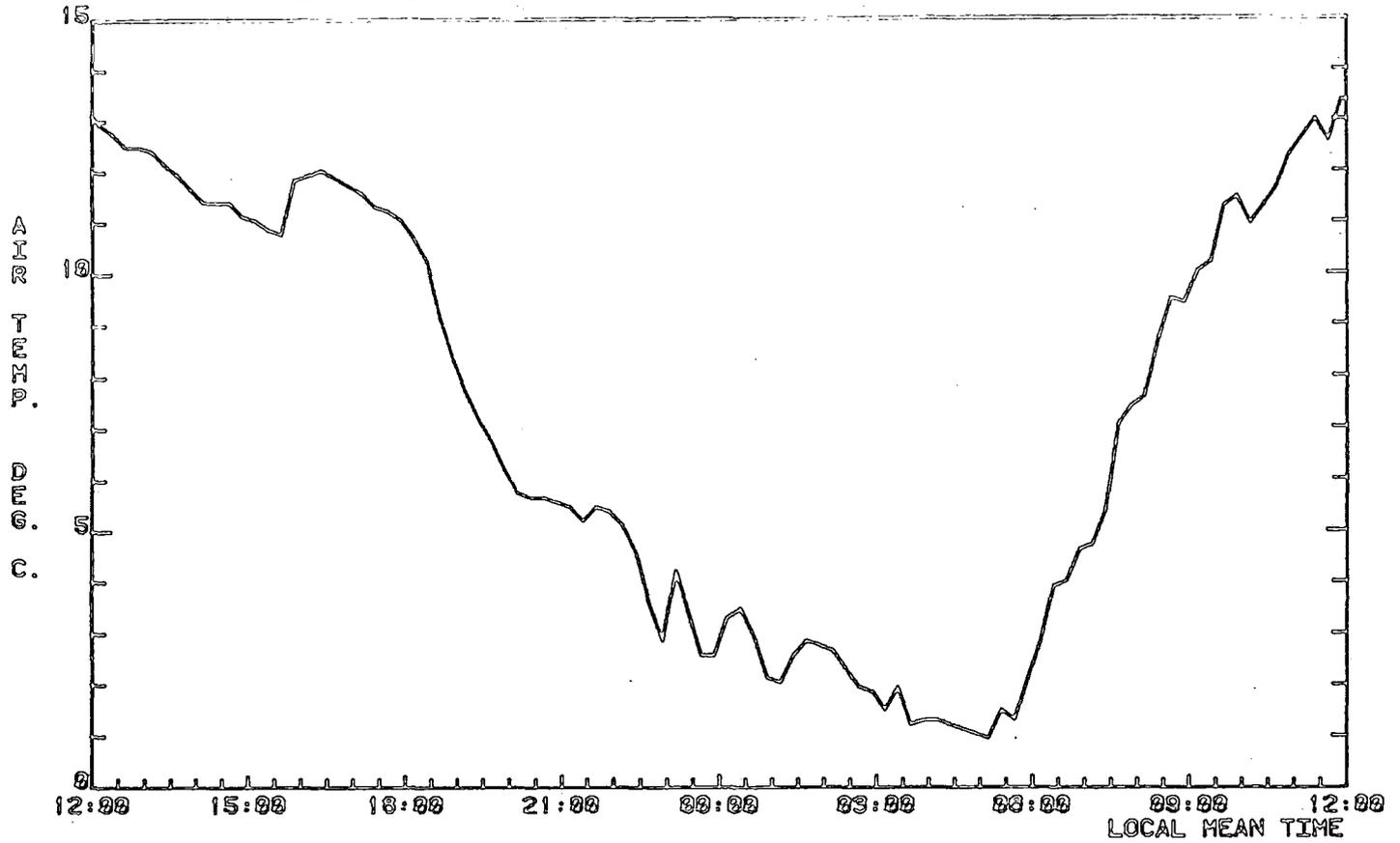
Fig. 5.12   WEATHER DATA RECORDED AT OUSTON, NORTHUMBERLAND
WET/DRY BULB DEPRESSION FROM 12:00 20-APR-82 TO 12:00 21-APR-82.
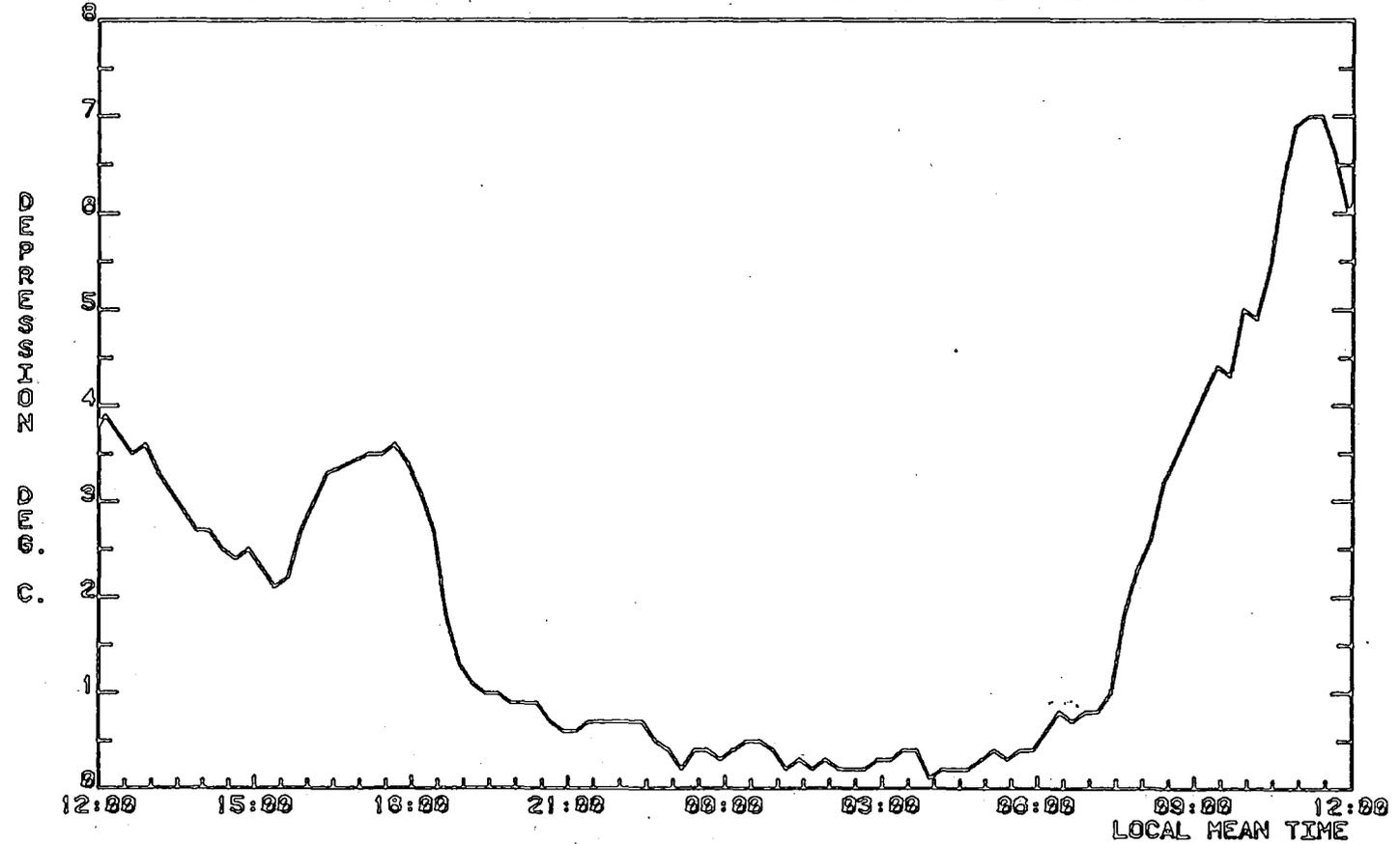
Fig. 5.13   WEATHER DATA RECORDED AT OUSTON, NORTHUMBERLAND
             AV. SOLAR RADIATION FROM 12:00 21-APR-82 TO 12:00 22-APR-82.
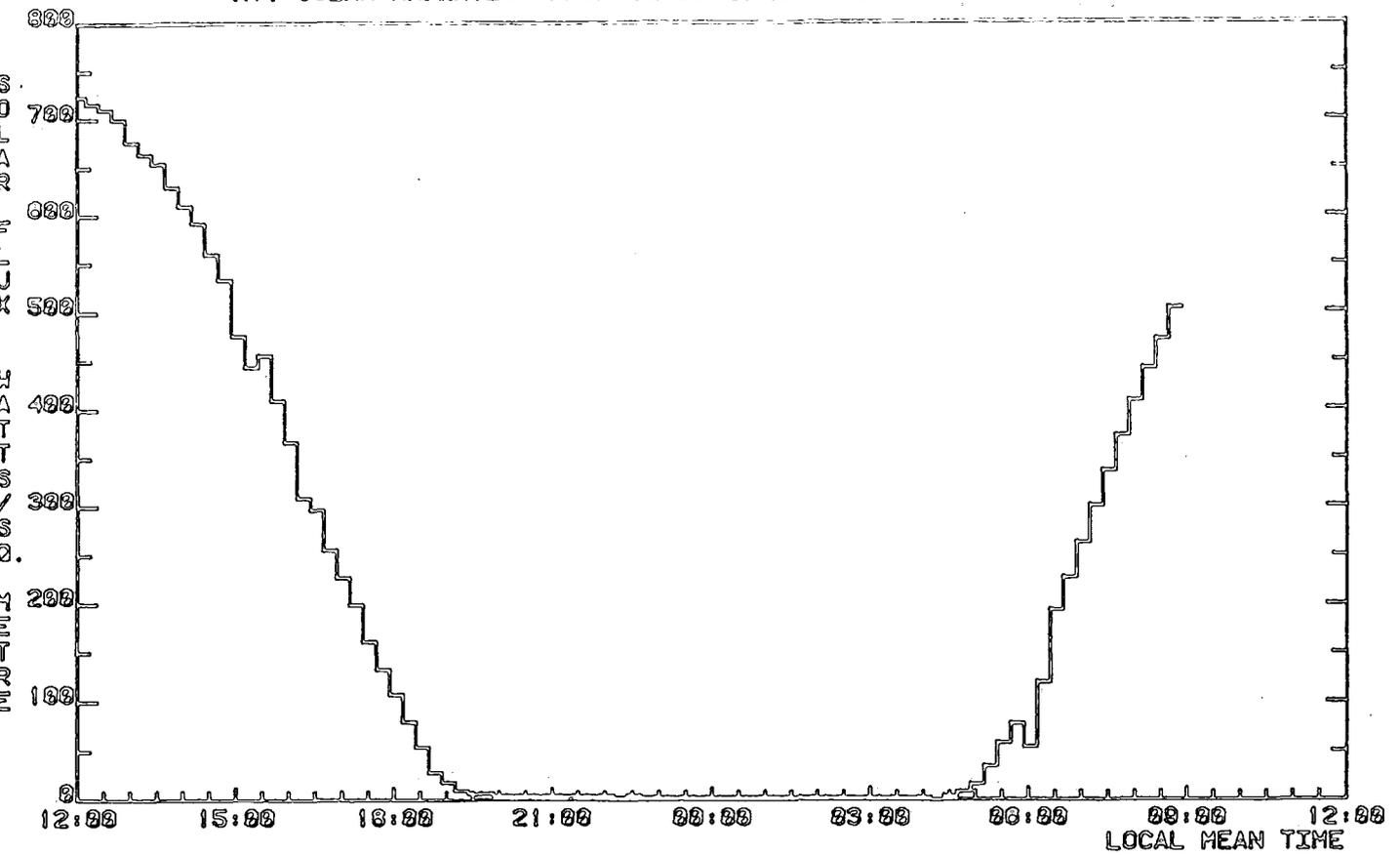
Fig. 5.14   WEATHER DATA RECORDED AT OUSTON, NORTHUMBERLAND
             AV. WINDSPEED FROM 12:00 21-APR-82 TO 12:00 22-APR-82.
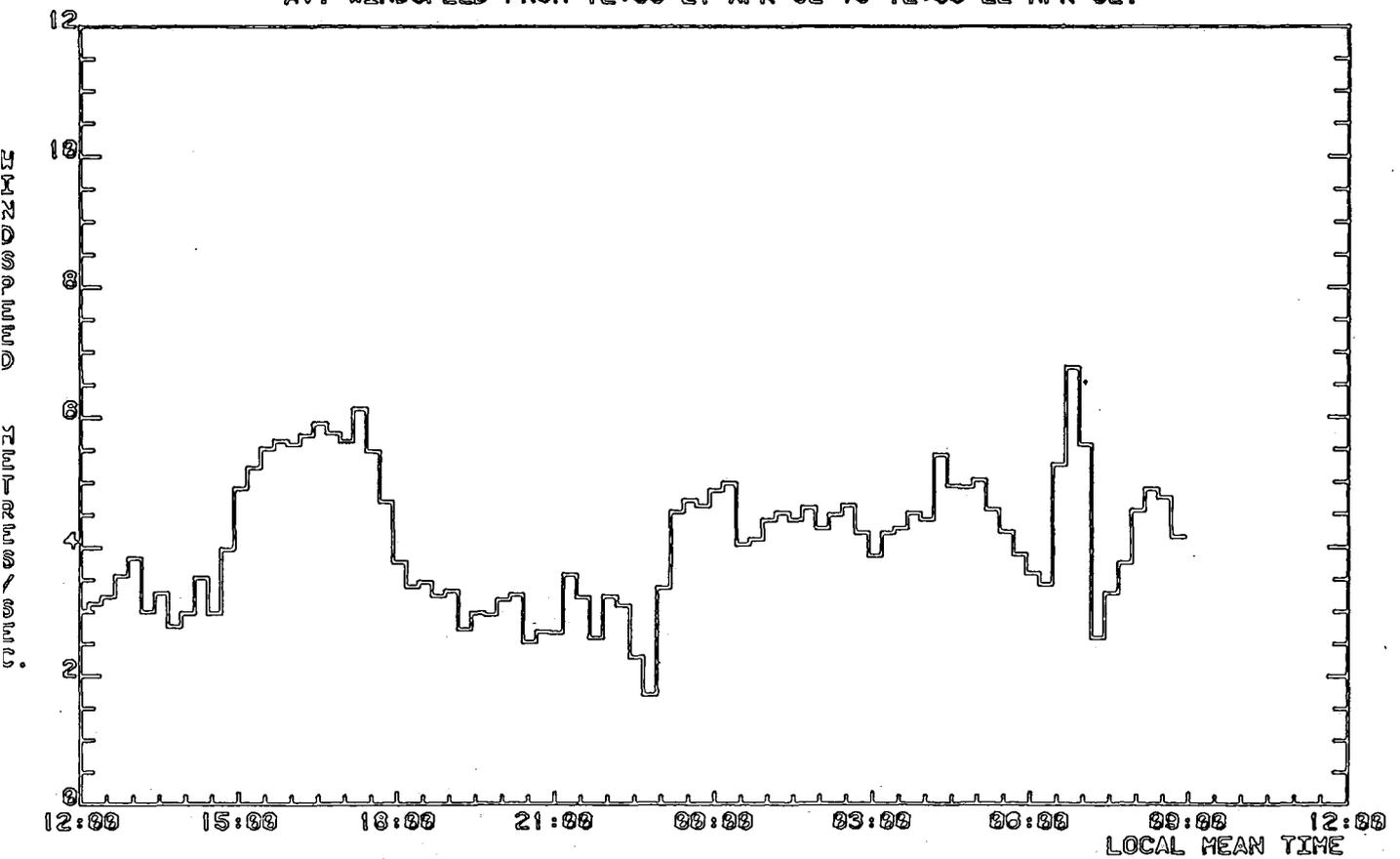
Fig. 5.15   WEATHER DATA RECORDED AT OUSTON, NORTHUMBERLAND
            AIR TEMPERATURE FROM 12:00 21-APR-82 TO 12:00 22-APR-82.
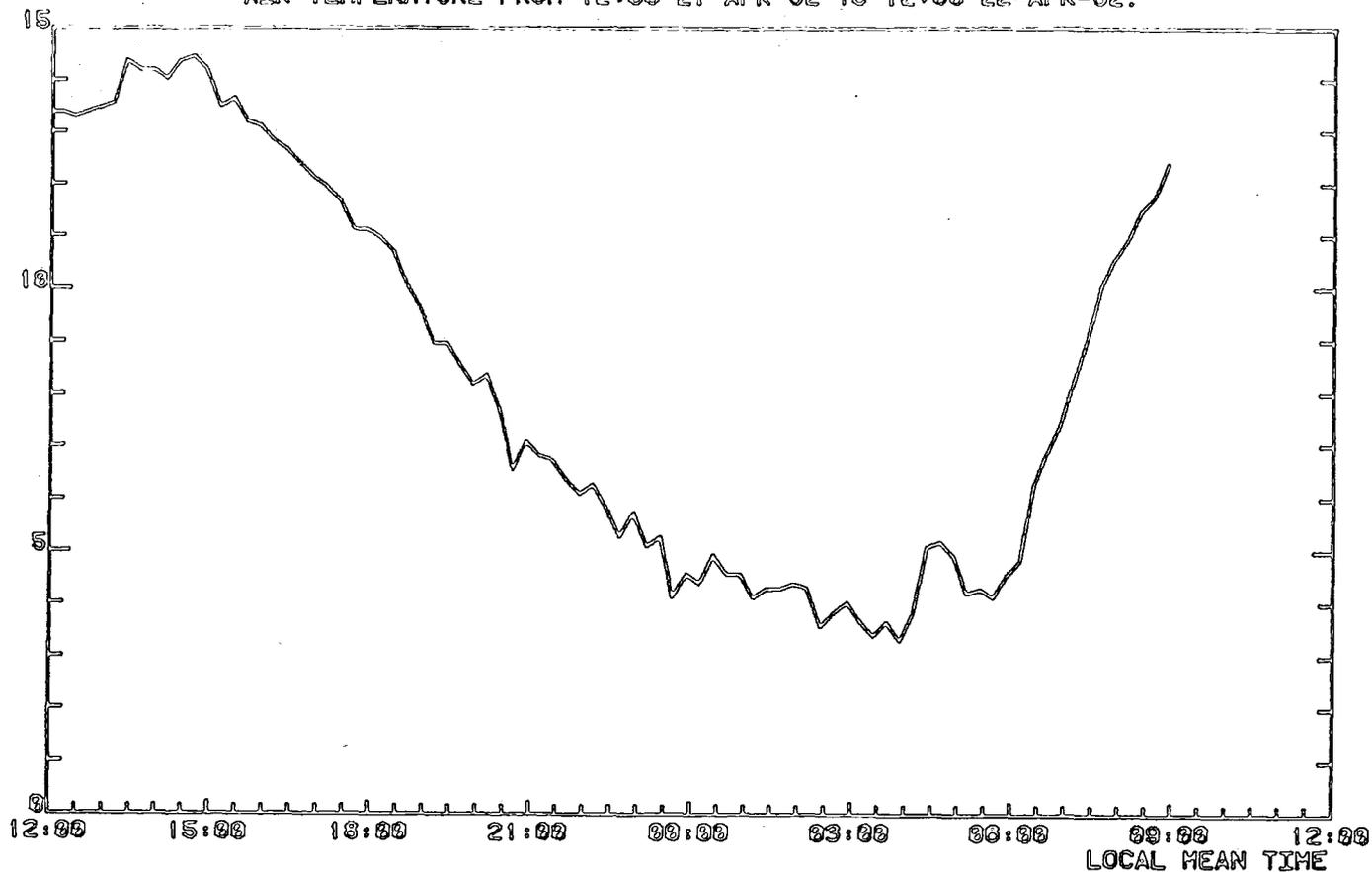
Fig. 5.16 WEATHER DATA RECORDED AT OUSTON, NORTHUMBERLAND
          WET/DRY BULB DEPRESSION FROM 12:00 21-APR-82 TO 12:00 22-APR-82.
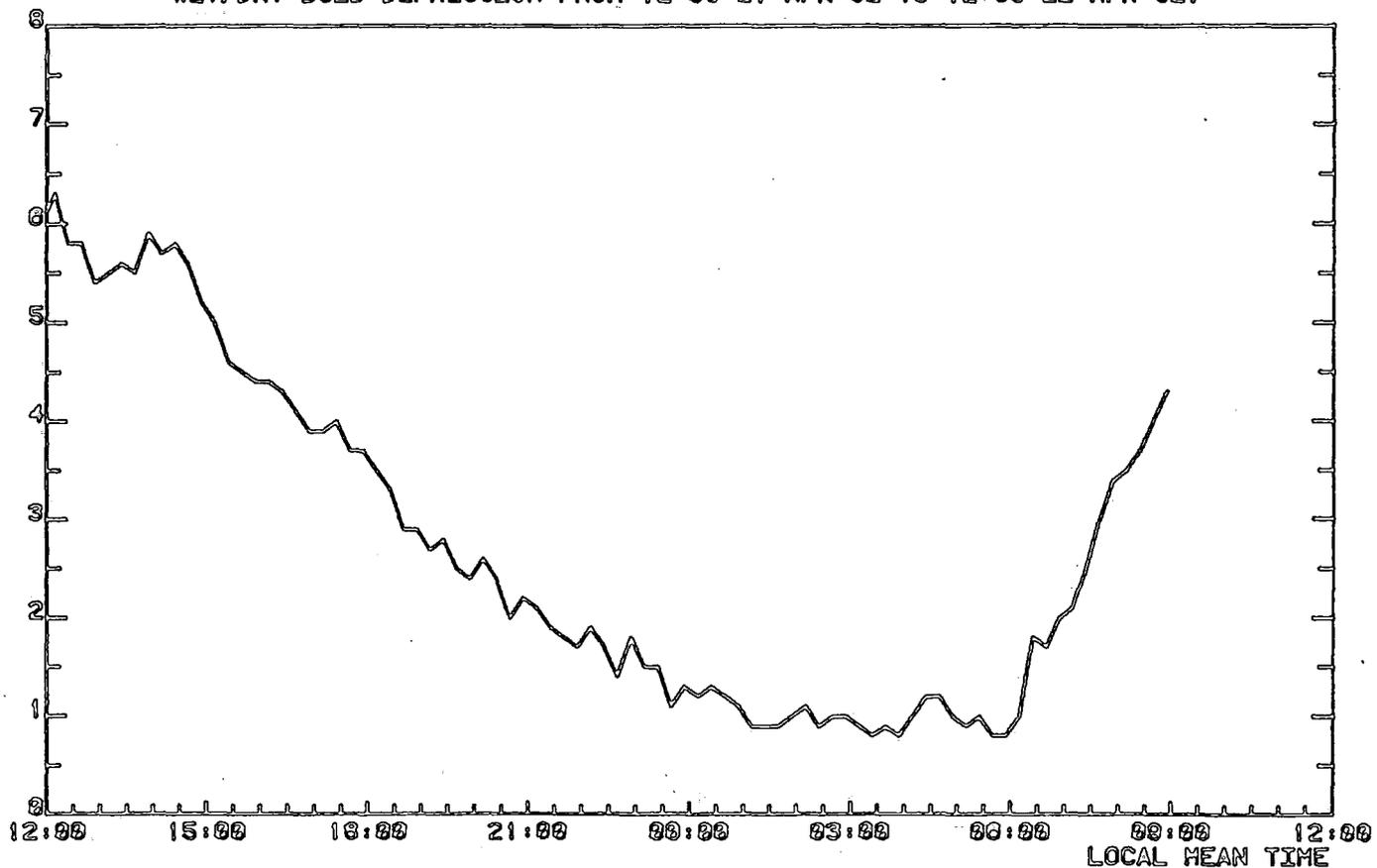
Fig. 5.17   WEATHER DATA RECORDED AT OUSTON, NORTHUMBERLAND
AV. SOLAR RADIATION FROM 12:00 22-APR-82 TO 12:00 23-APR-82.
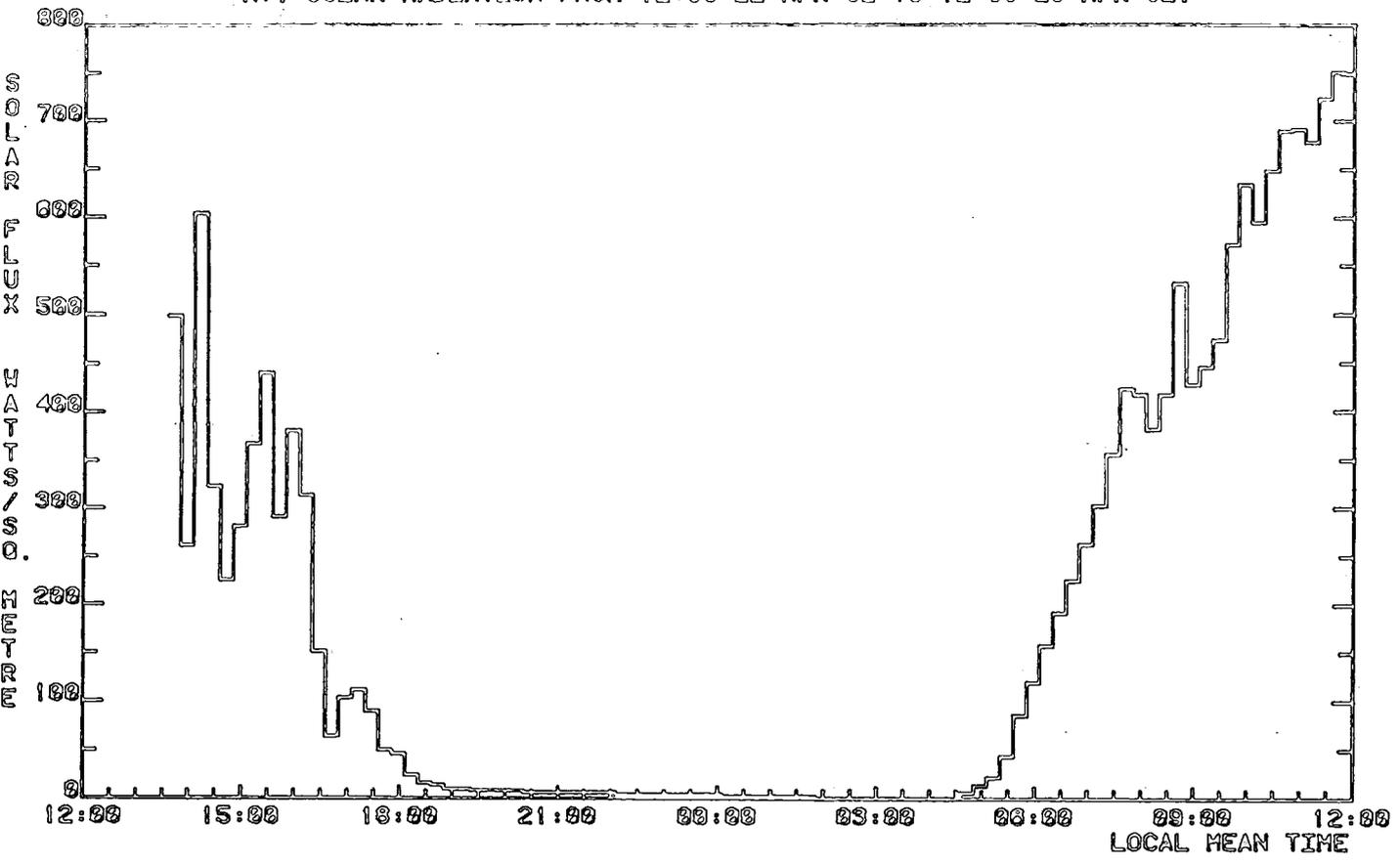
Fig. 5.18   WEATHER DATA RECORDED AT OUSTON, NORTHUMBERLAND
AV. WINDSPEED FROM 12:00 22-APR-82 TO 12:00 23-APR-82.
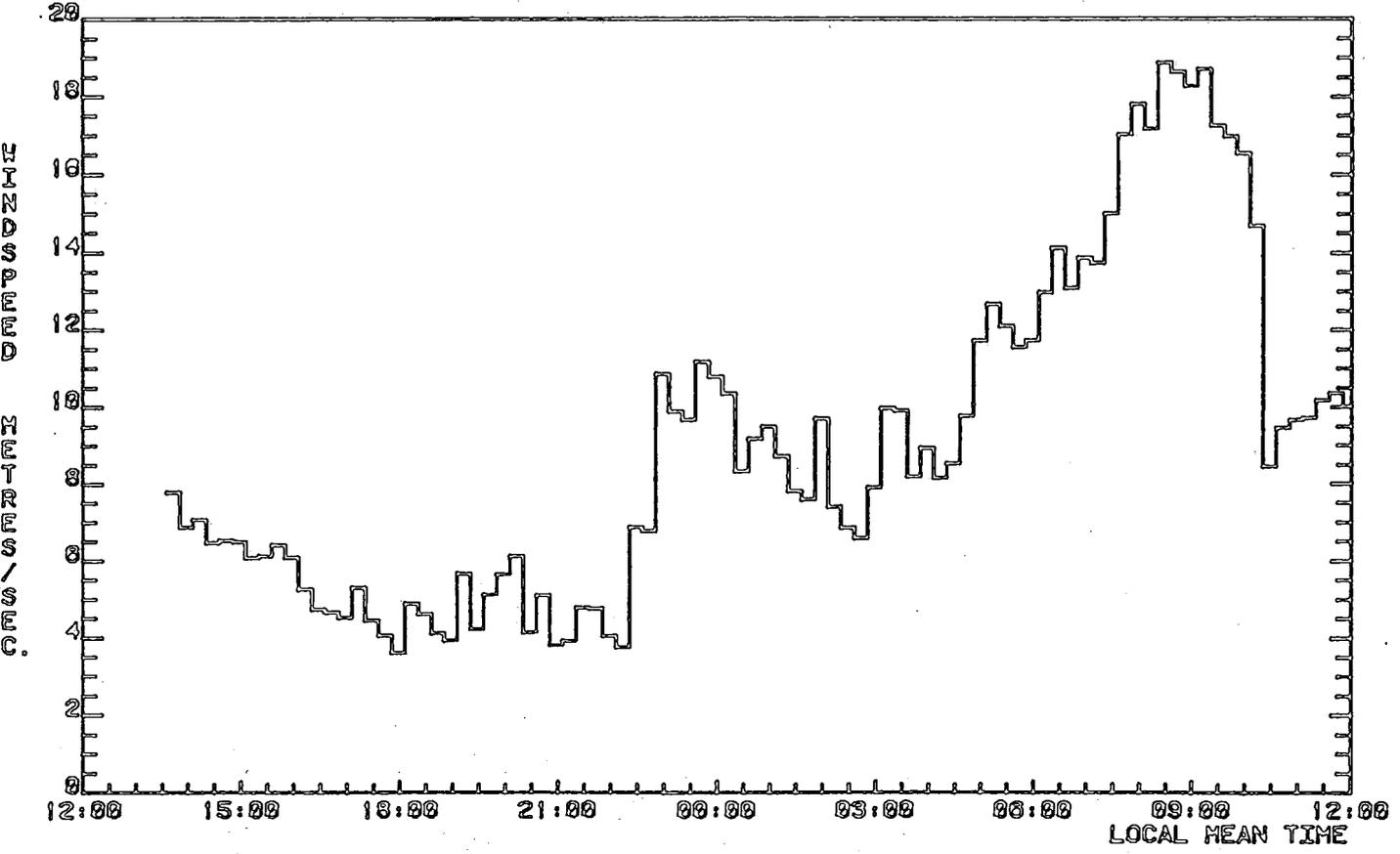
Fig. 5.19 WEATHER DATA RECORDED AT OUSTON, NORTHUMBERLAND
AIR TEMPERATURE FROM 12:00 22-APR-82 TO 12:00 23-APR-82.
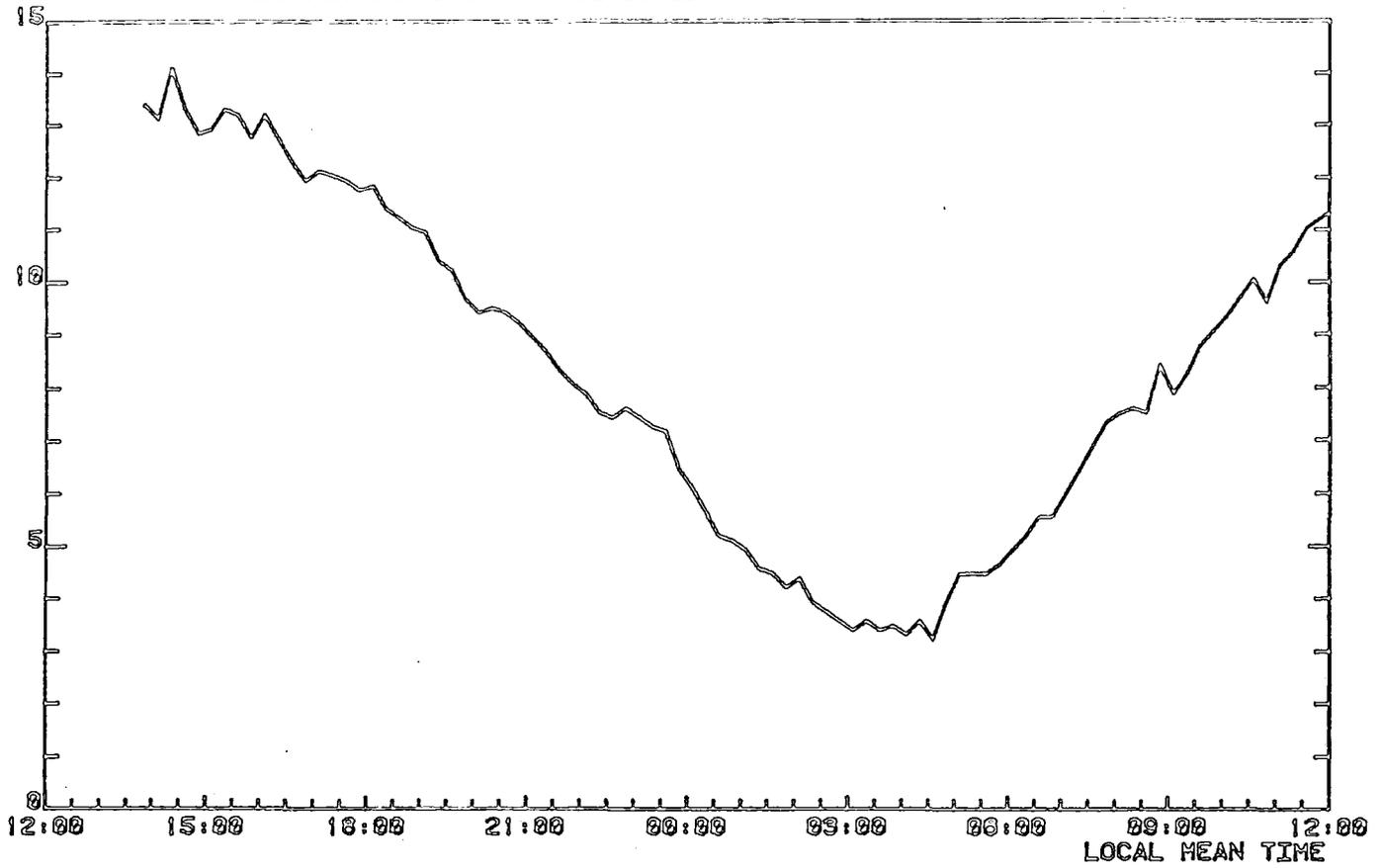
Fig. 5.20 WEATHER DATA RECORDED AT OUSTON, NORTHUMBERLAND
WET/DRY BULB DEPRESSION FROM 12:00 22-APR-82 TO 12:00 23-APR-82.
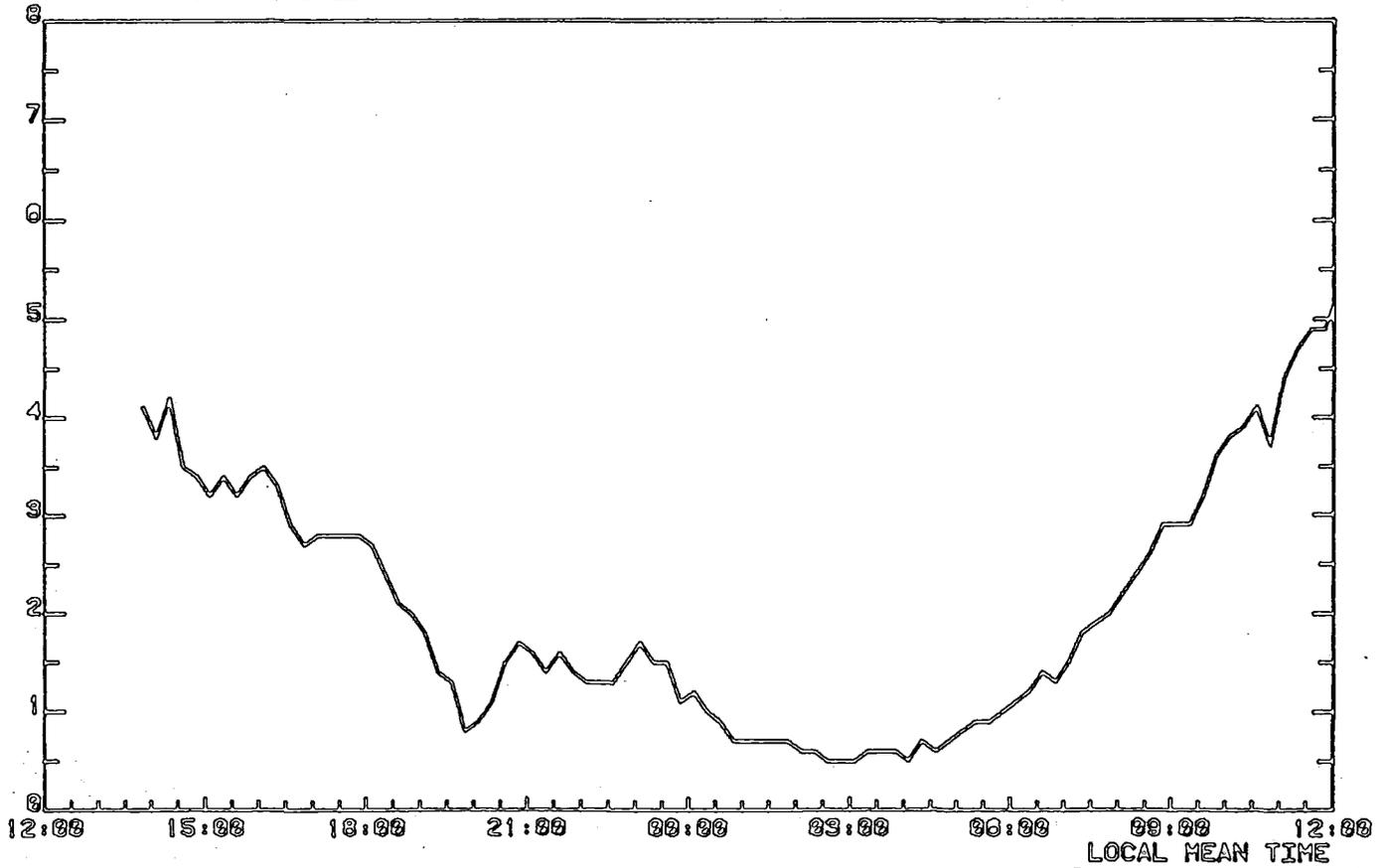
Fig. 5.21   WEATHER DATA RECORDED AT OUSTON, NORTHUMBERLAND
             AV. SOLAR RADIATION FROM 12:00 23-APR-82 TO 12:00 24-APR-82.
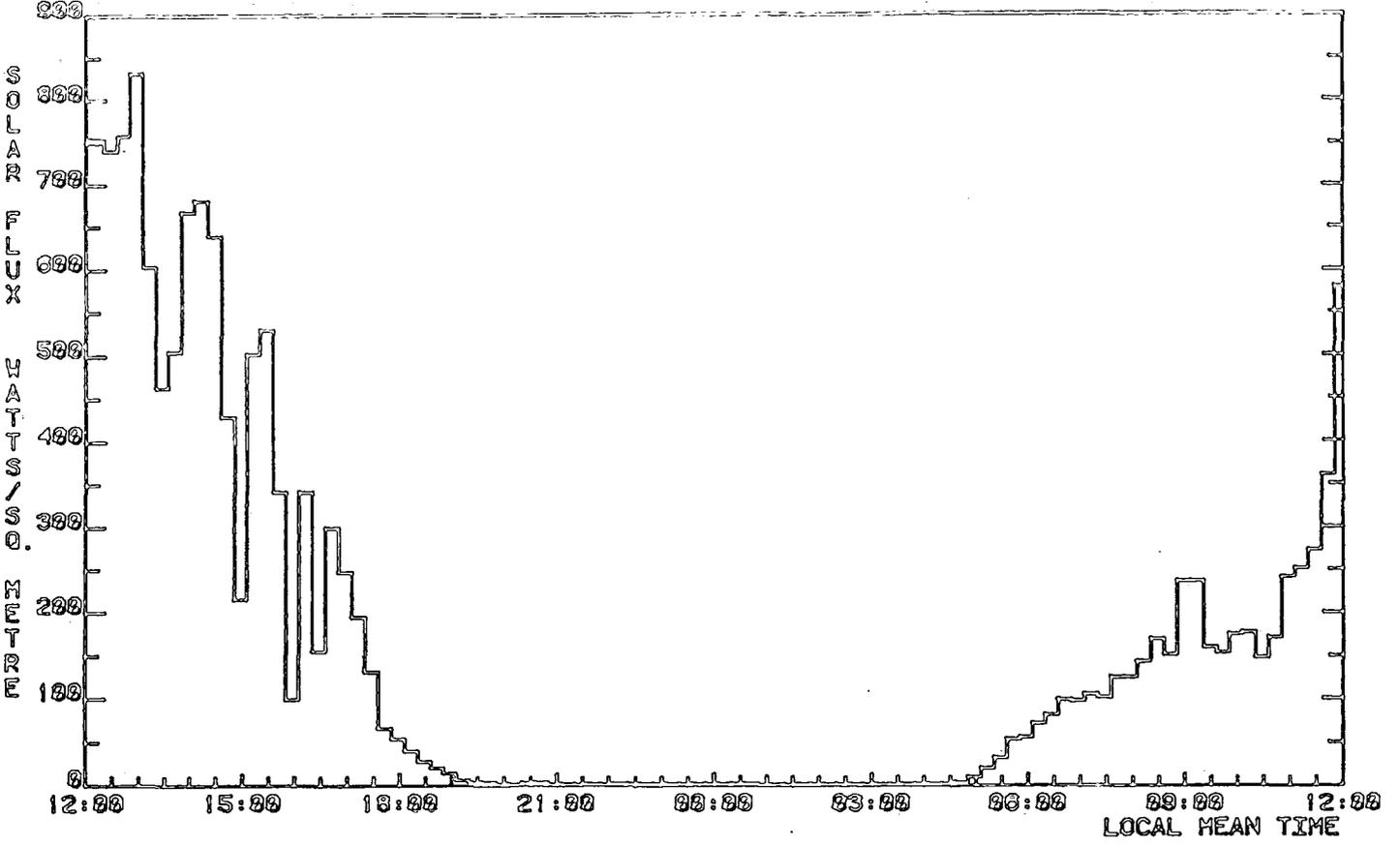
Fig. 5.22   WEATHER DATA RECORDED AT OUSTON, NORTHUMBERLAND
             AV. WINDSPEED FROM 12:00 23-APR-82 TO 12:00 24-APR-82.
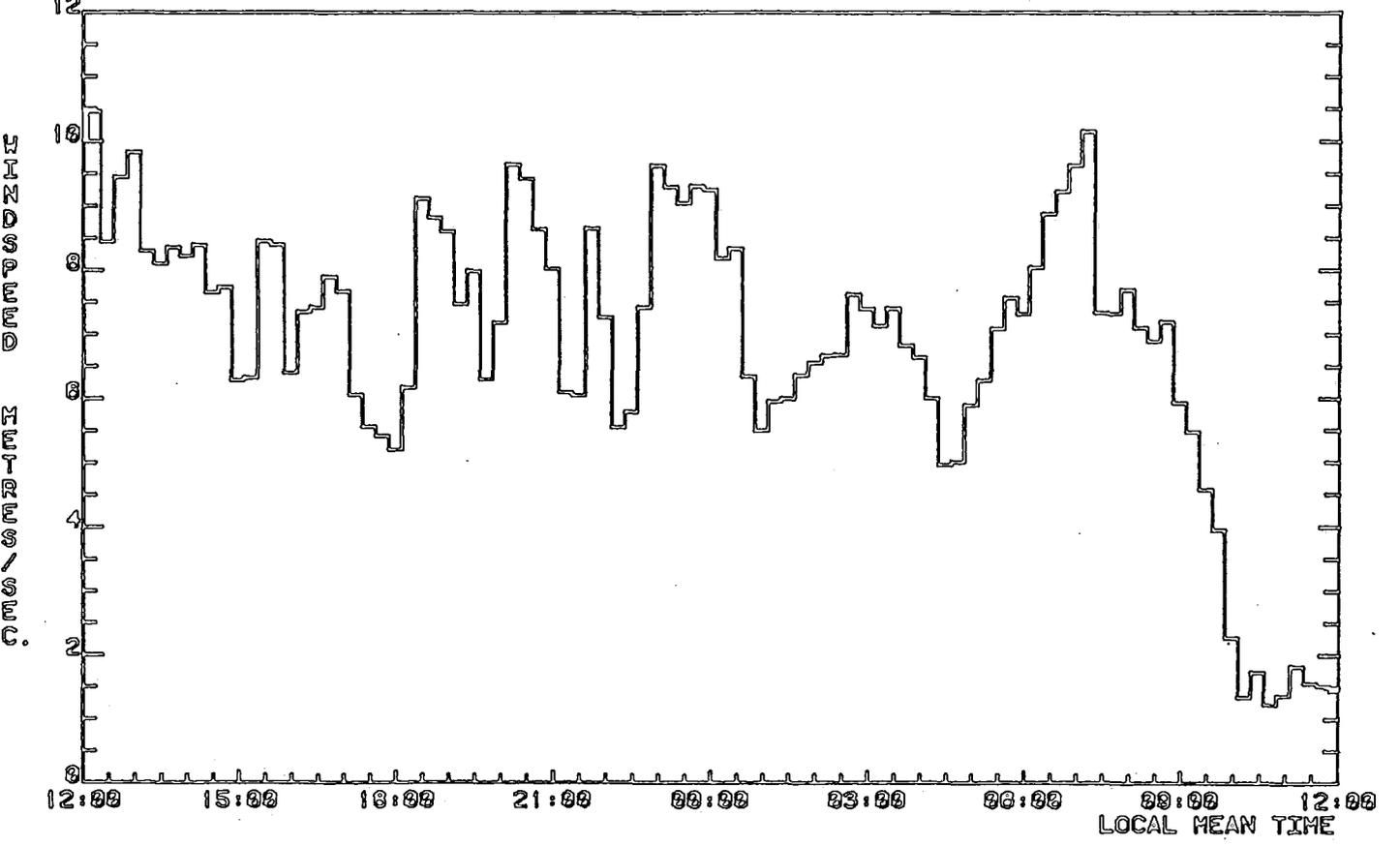
Fig. 5.23   WEATHER DATA RECORDED AT OUSTON, NORTHUMBERLAND
             AIR TEMPERATURE FROM 12:00 23-APR-82 TO 12:00 24-APR-82.
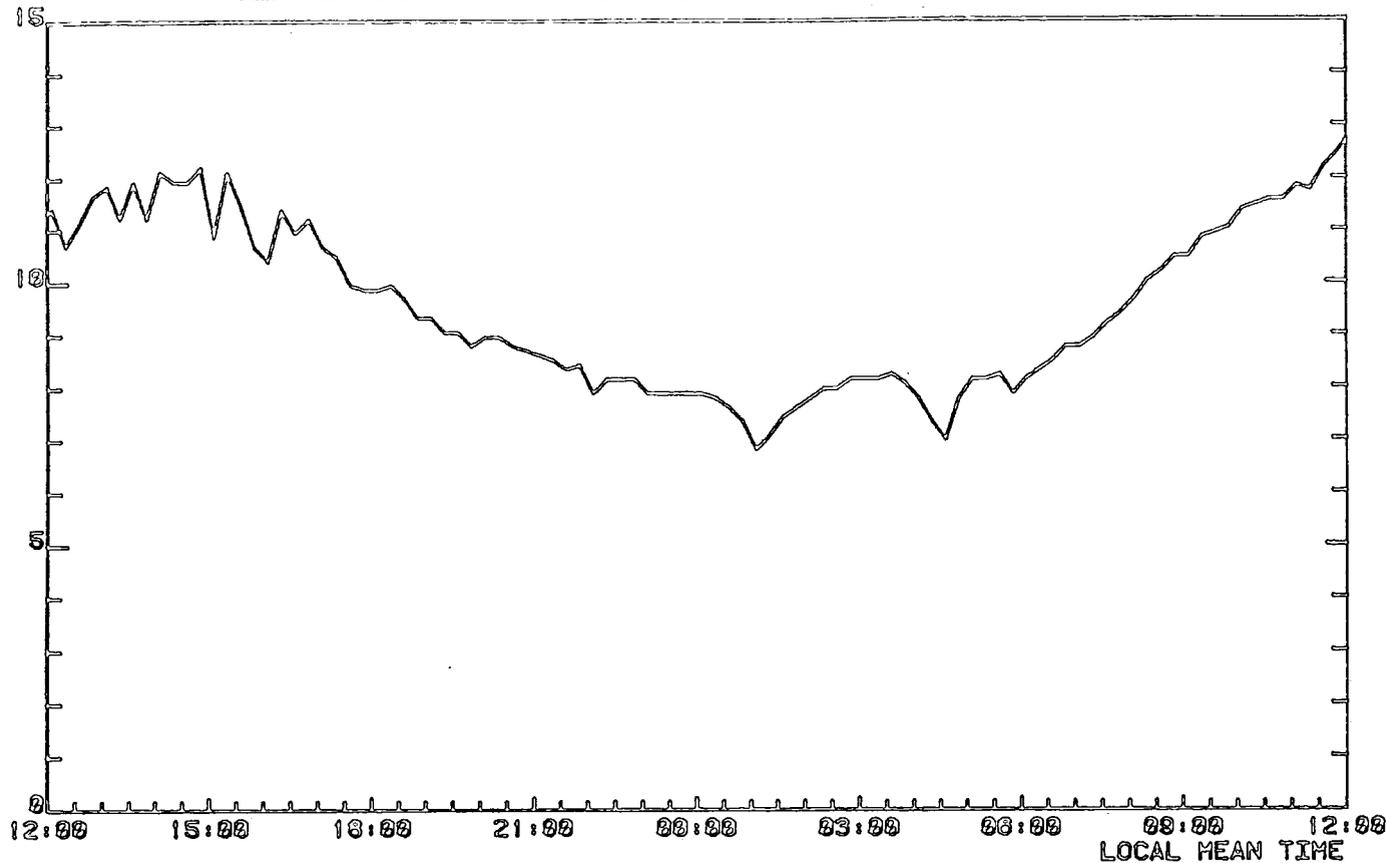
Fig. 5.24 WEATHER DATA RECORDED AT OUSTON, NORTHUMBERLAND
           WET/DRY BULB DEPRESSION FROM 12:00 23-APR-82 TO 12:00 24-APR-82.
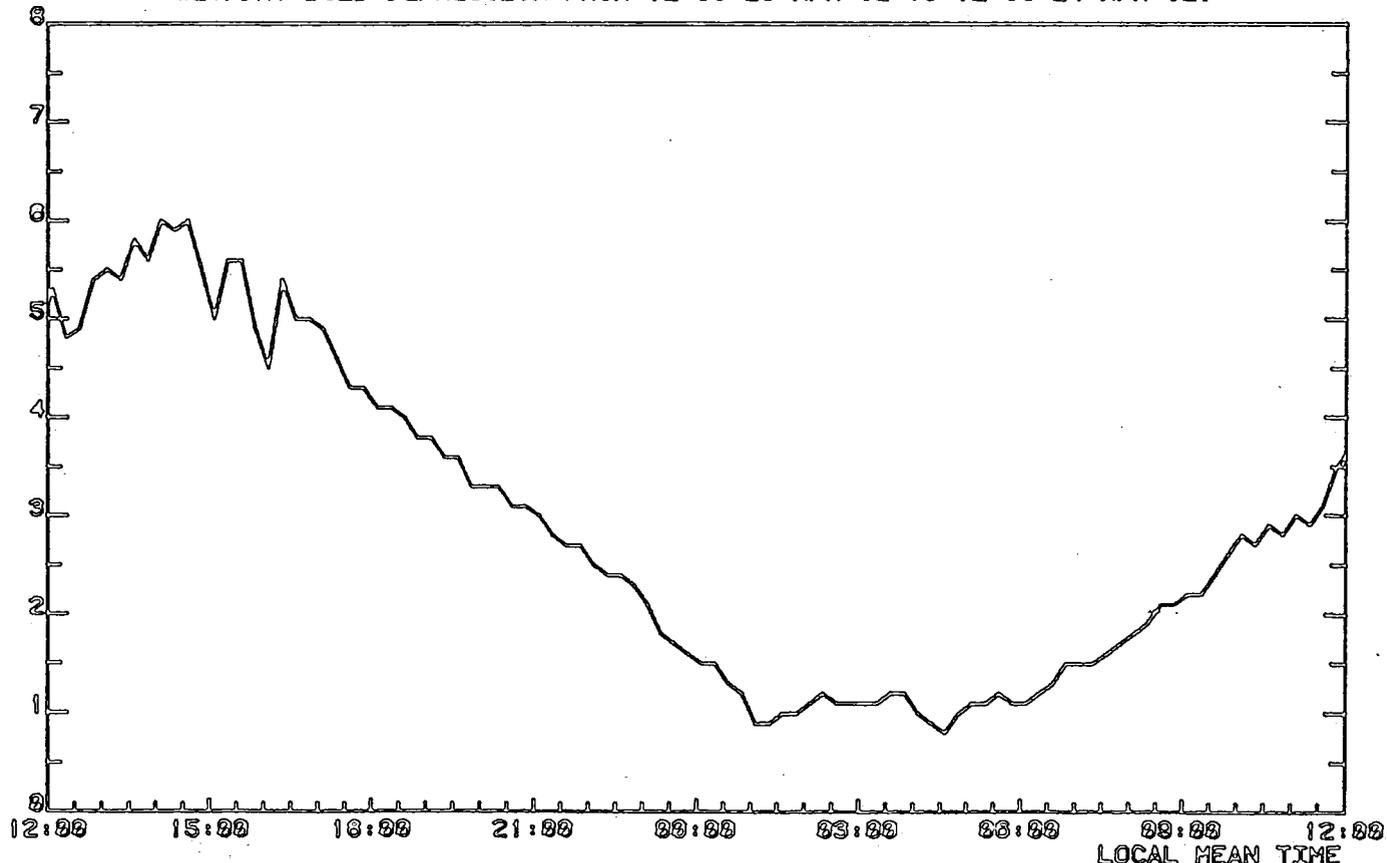
Fig. 5.25   WEATHER DATA RECORDED AT OUSTON, NORTHUMBERLAND
AV. SOLAR RADIATION FROM 12:00 24-APR-82 TO 12:00 25-APR-82.
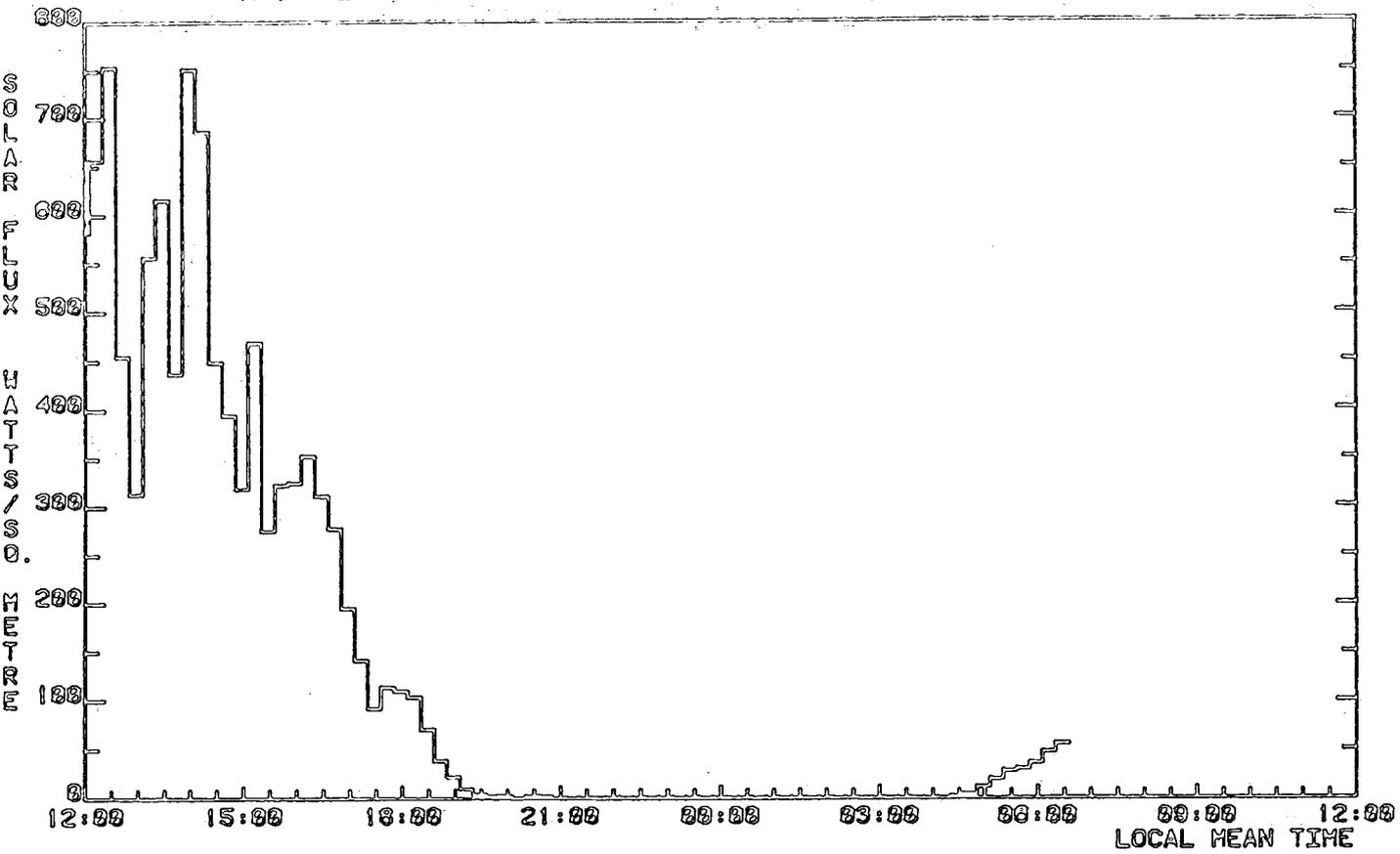
Fig. 5.26   WEATHER DATA RECORDED AT OUSTON, NORTHUMBERLAND
AV. WINDSPEED FROM 12:00 24-APR-82 TO 12:00 25-APR-82.
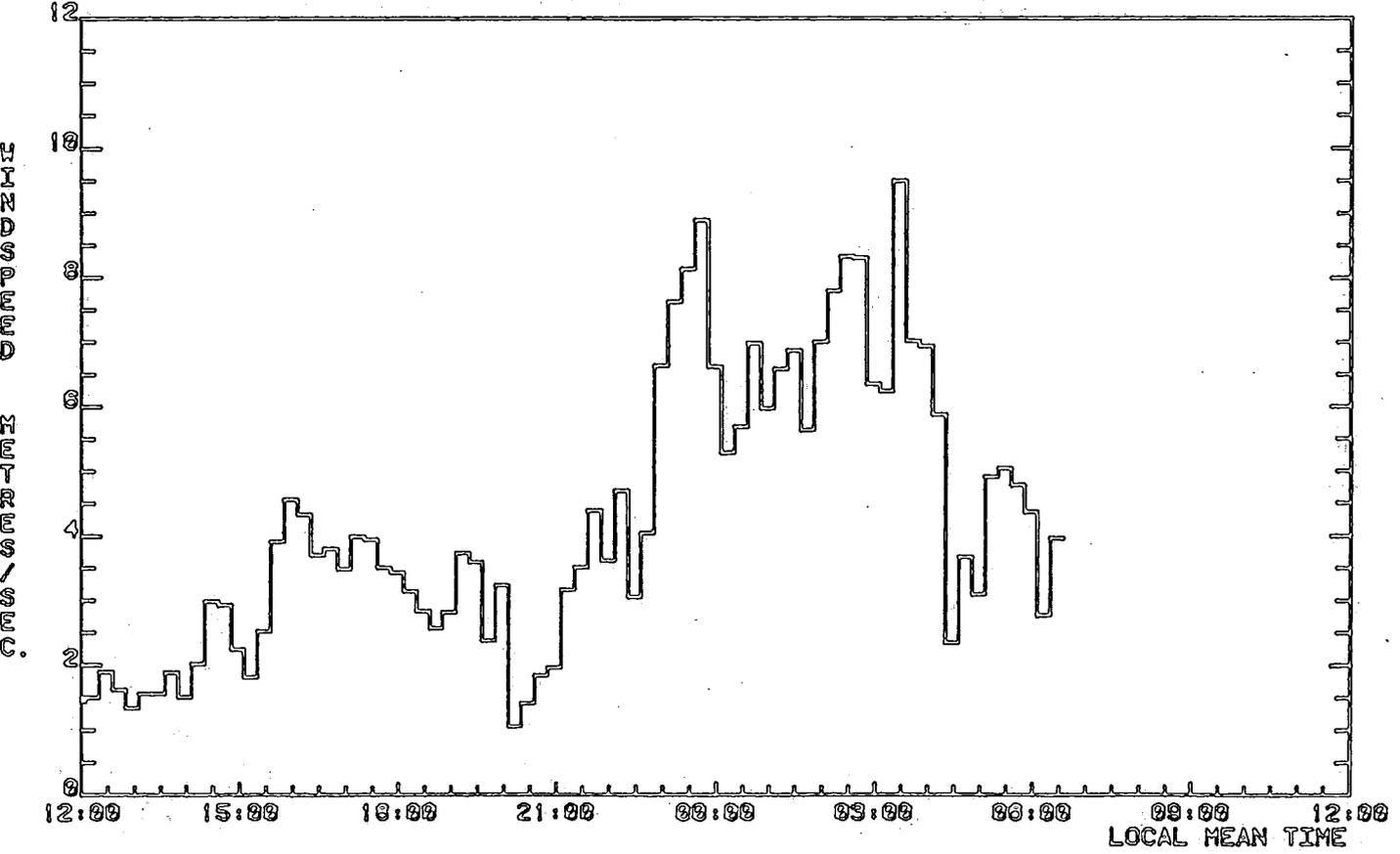
Fig. 5.27 WEATHER DATA RECORDED AT OUSTON, NORTHUMBERLAND
AIR TEMPERATURE FROM 12:00 24-APR-82 TO 12:00 25-APR-82.
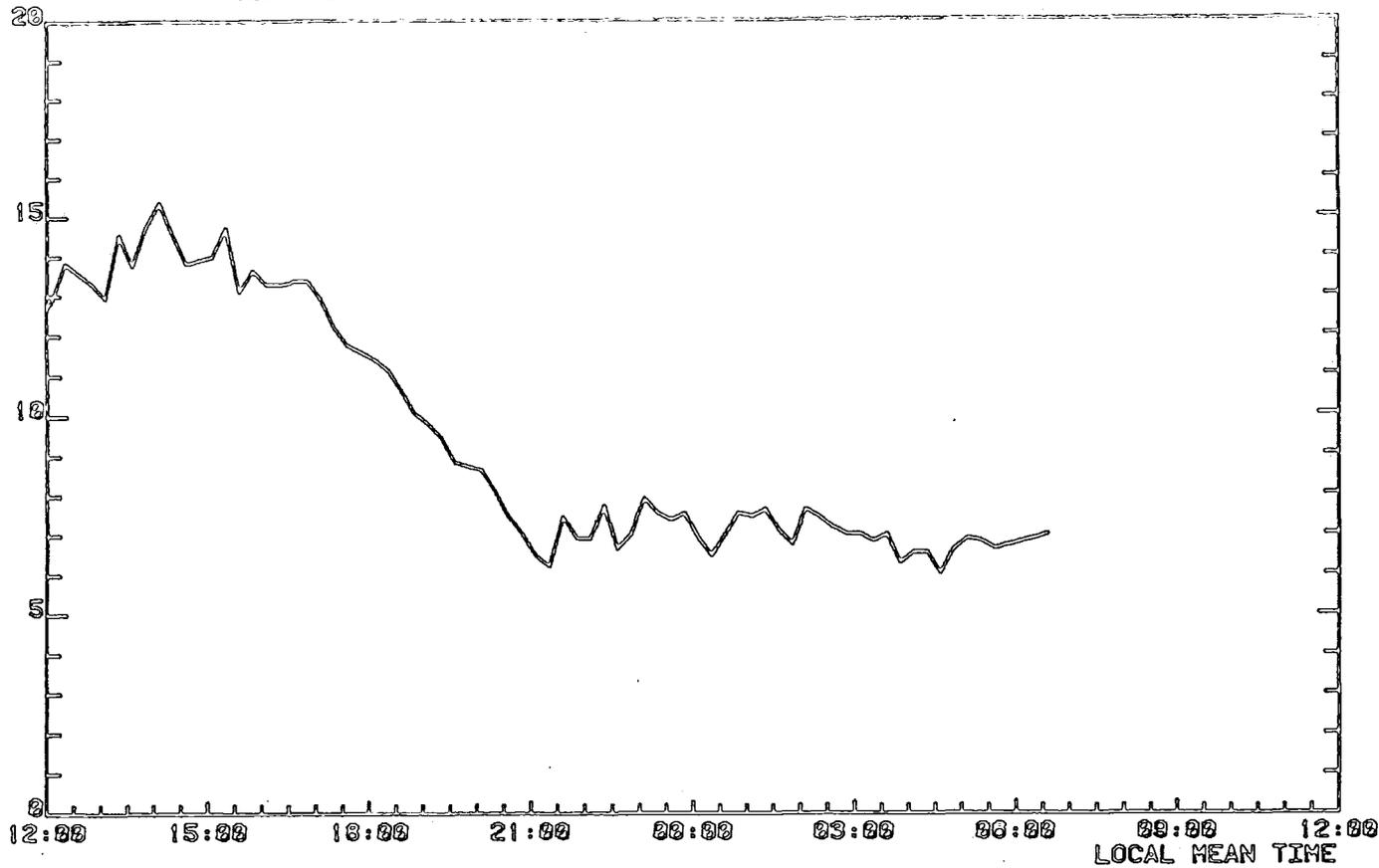
Fig. 5.28 WEATHER DATA RECORDED AT OUSTON, NORTHUMBERLAND
WET/DRY BULB DEPRESSION FROM 12:00 24-APR-82 TO 12:00 25-APR-82.
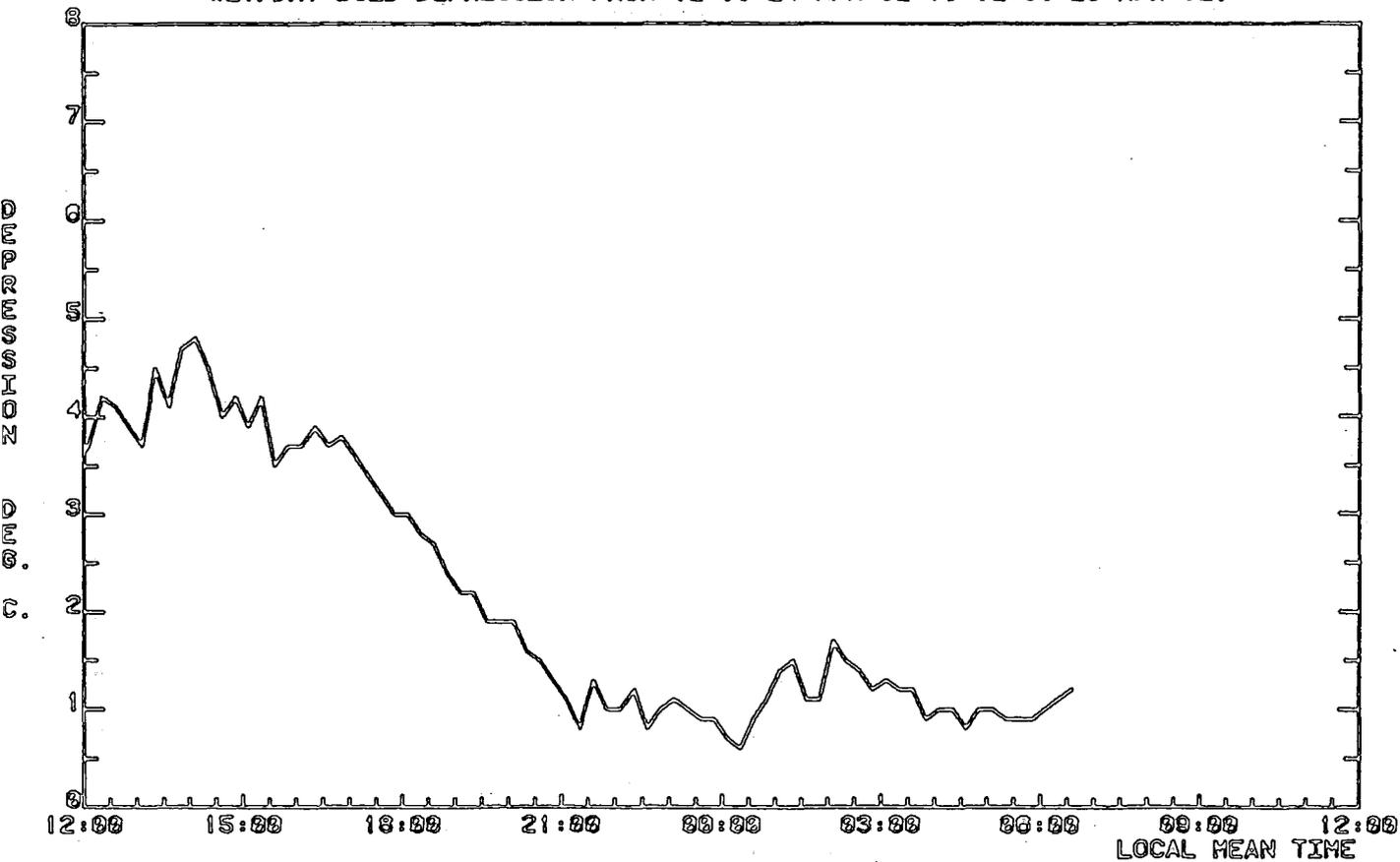
Fig. 5.29

LONG WAVE CLOUD COVER FACTOR FROM 12:00 19-APR-82 TO 12:00 20-APR-82.
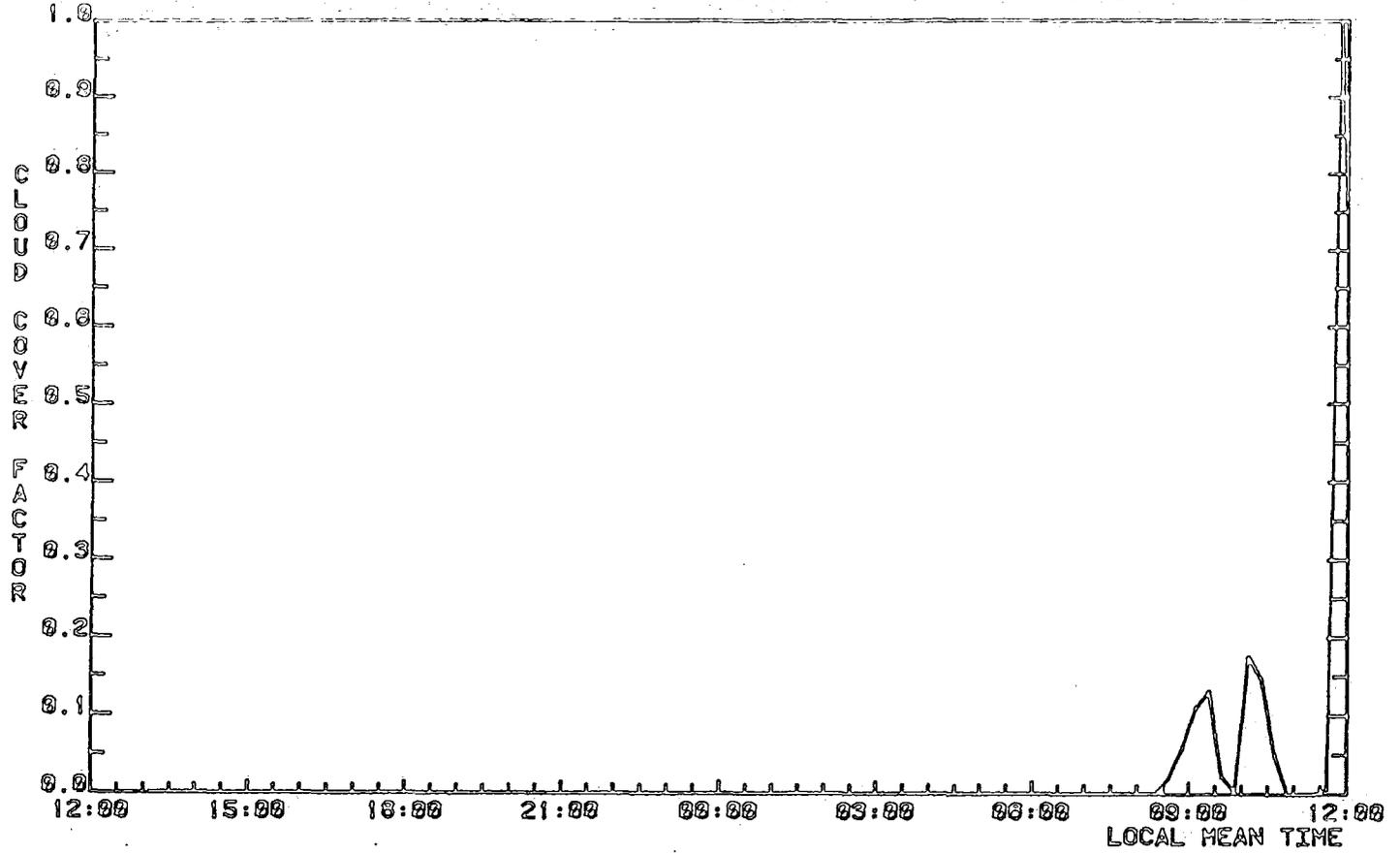
Fig. 5.30

LONG WAVE CLOUD COVER FACTOR FROM 12:00 20-APR-82 TO 12:00 21-APR-82.
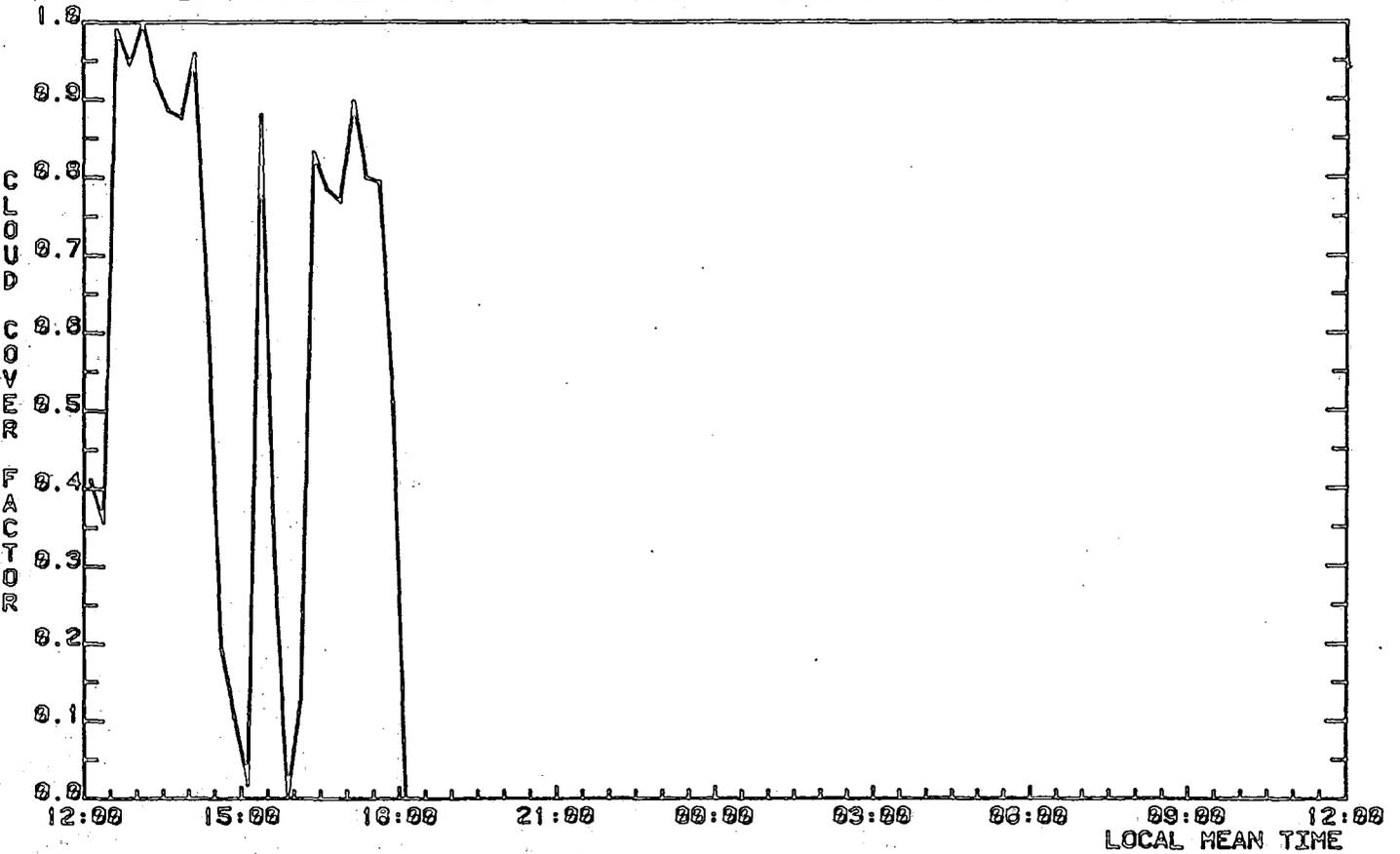
Fig. 5.31.

LONG WAVE CLOUD COVER FACTOR FROM 12:00 21-APR-82 TO 12:00 22-APR-82.
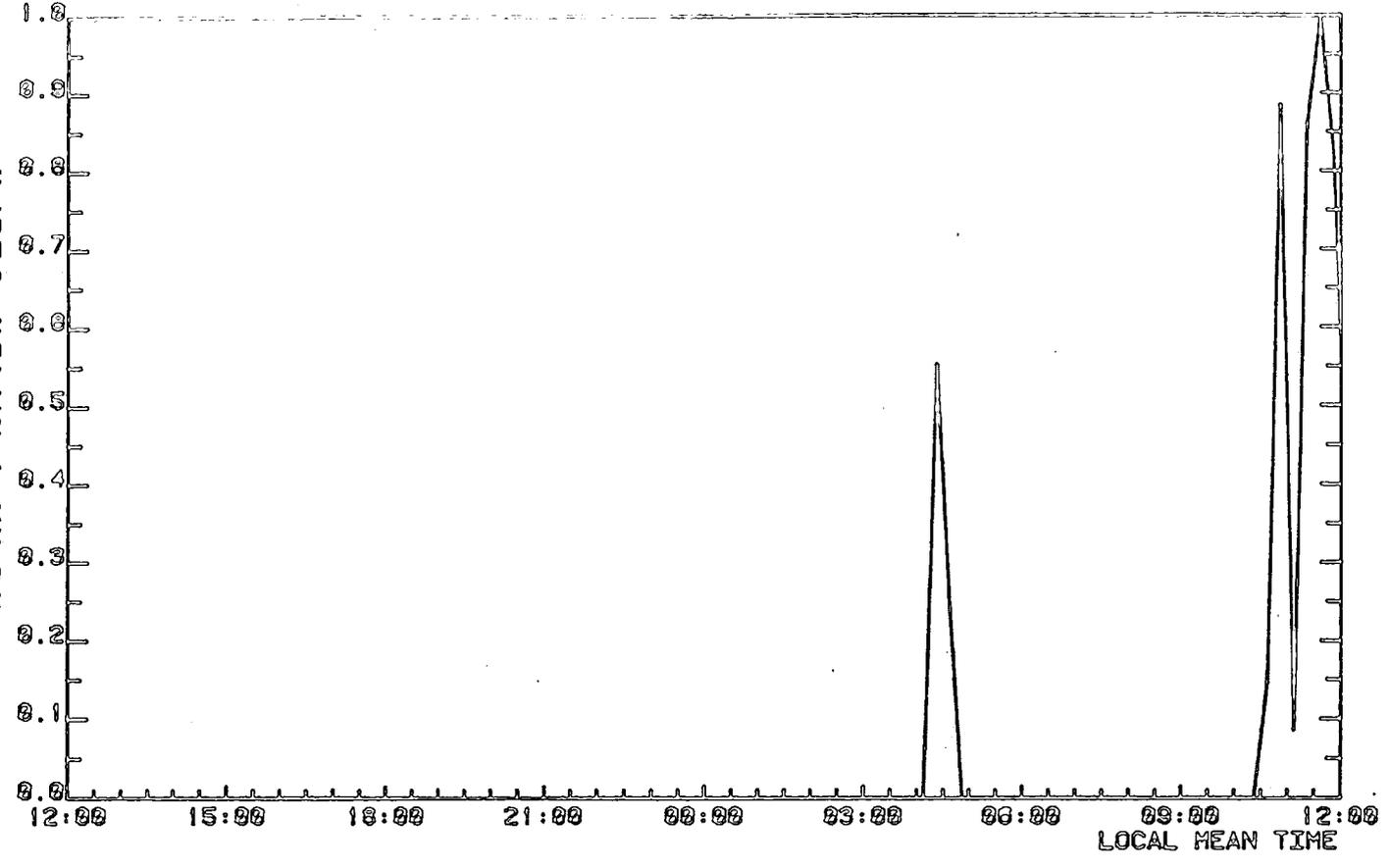
Fig. 5.32

LONG WAVE CLOUD COVER FACTOR FROM 12:00 22-APR-82 TO 12:00 23-APR-82.
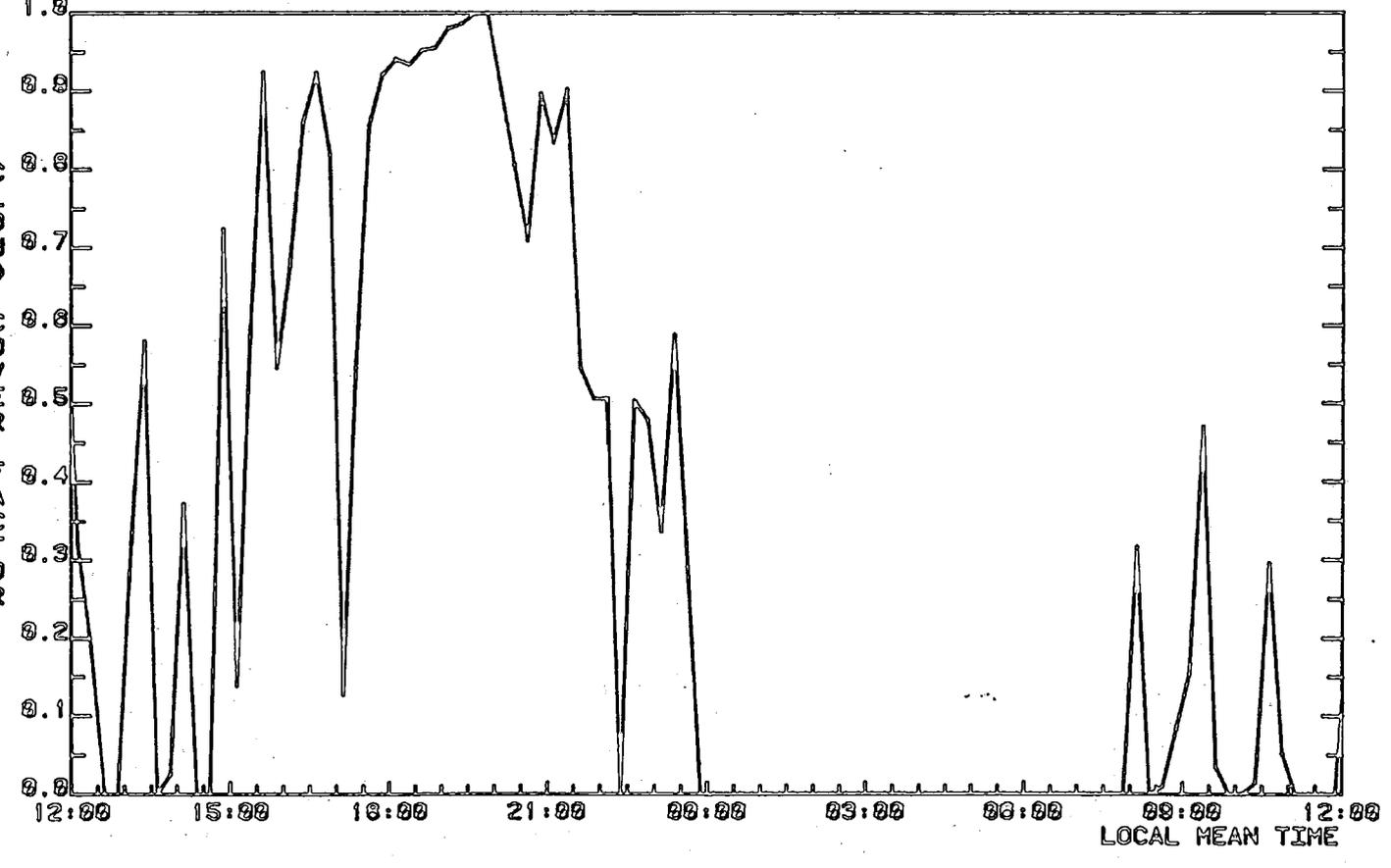
Fig. 5.33

LONG WAVE CLOUD COVER FACTOR FROM 12:00 23-APR-82 TO 12:00 24-APR-82.
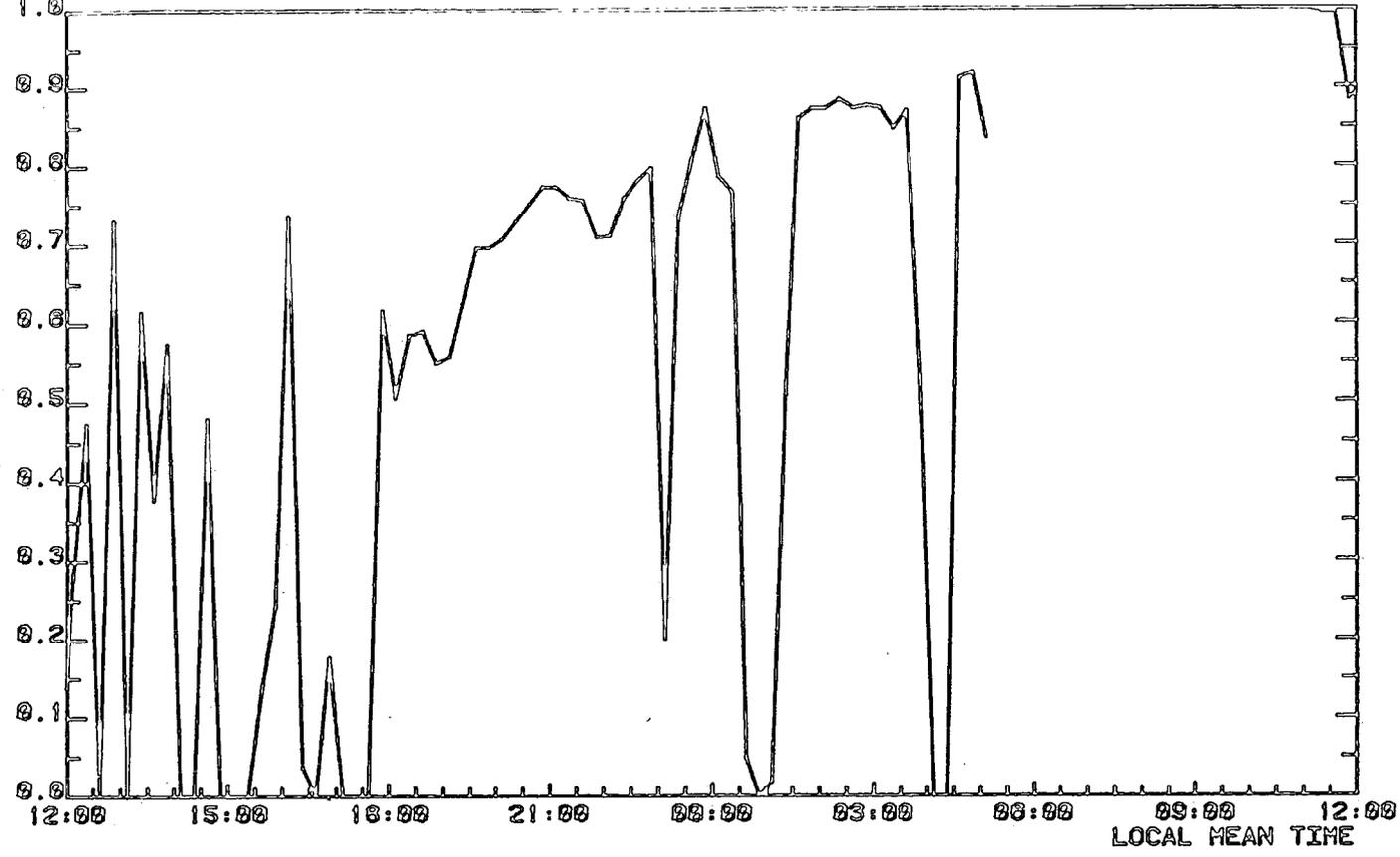
Fig. 5.34

LONG WAVE CLOUD COVER FACTOR FROM 12:00 24-APR-82 TO 12:00 25-APR-82.
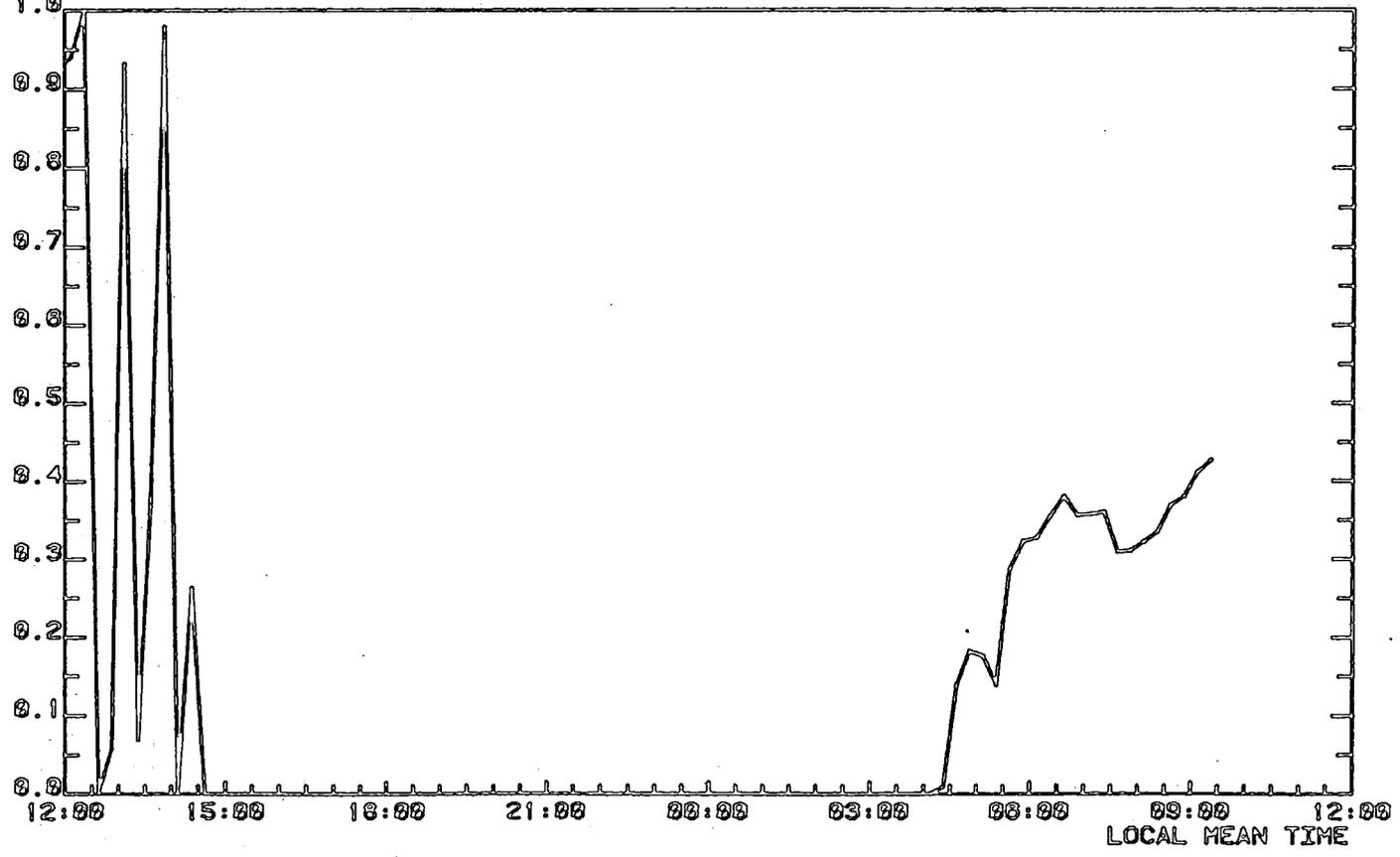
Fig. 5.35   PREDICTED & MEASURED RADIANT TEMPS. FOR THE CONCRETE SURFACE
             DURING THE PERIOD FROM 12:00 19/4/82 TO 12:00 20/4/82.
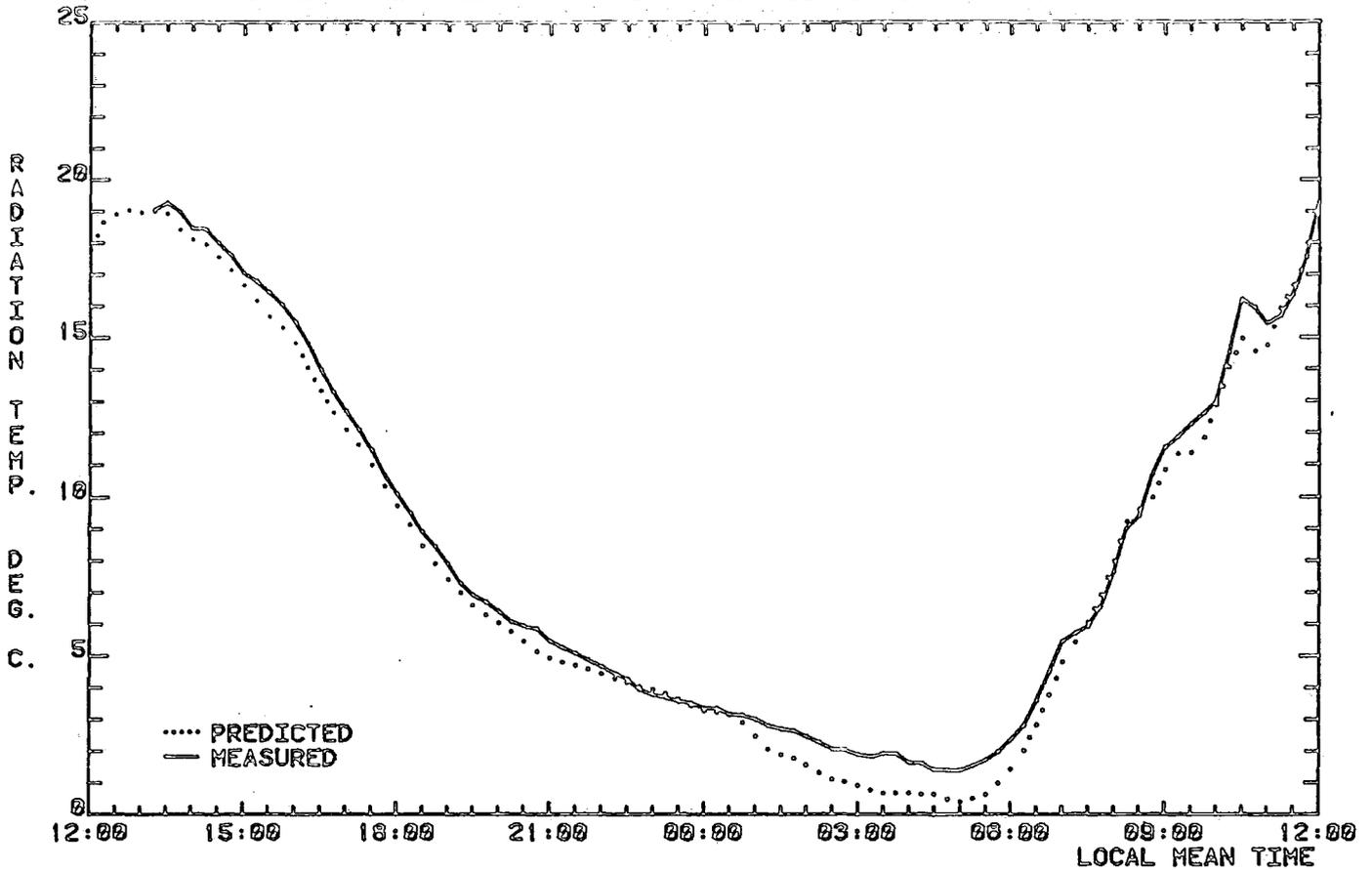
Fig. 5.36   PREDICTED & MEASURED RADIANT TEMPS. FOR THE ASPHALT SURFACE
             DURING THE PERIOD FROM 12:00 19/4/82 TO 12:00 20/4/82.
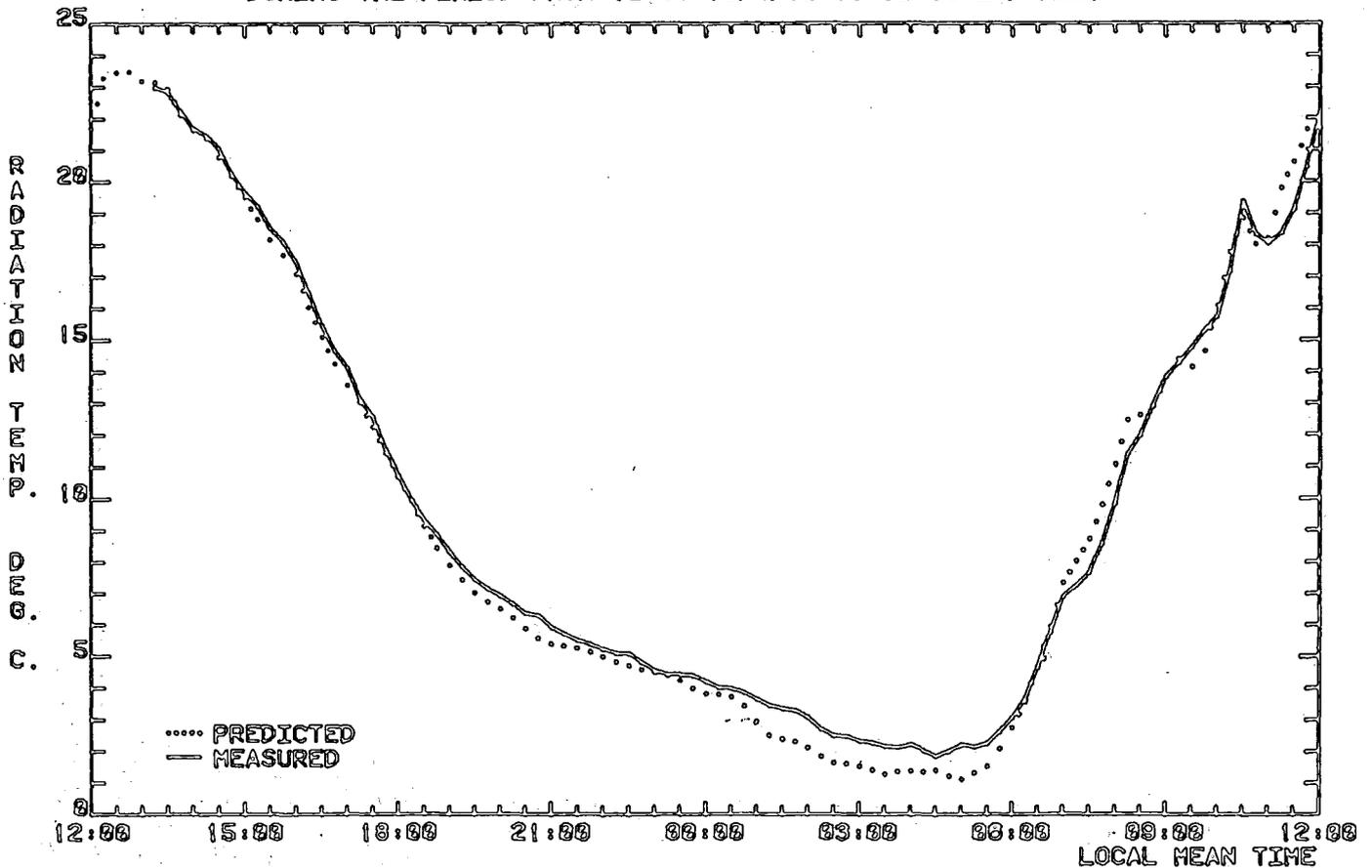
Fig. 5.37   PREDICTED & MEASURED RADIANT TEMPS. FOR THE CONCRETE SURFACE
             DURING THE PERIOD FROM 12:00 20/4/82 TO 12:00 21/4/82.
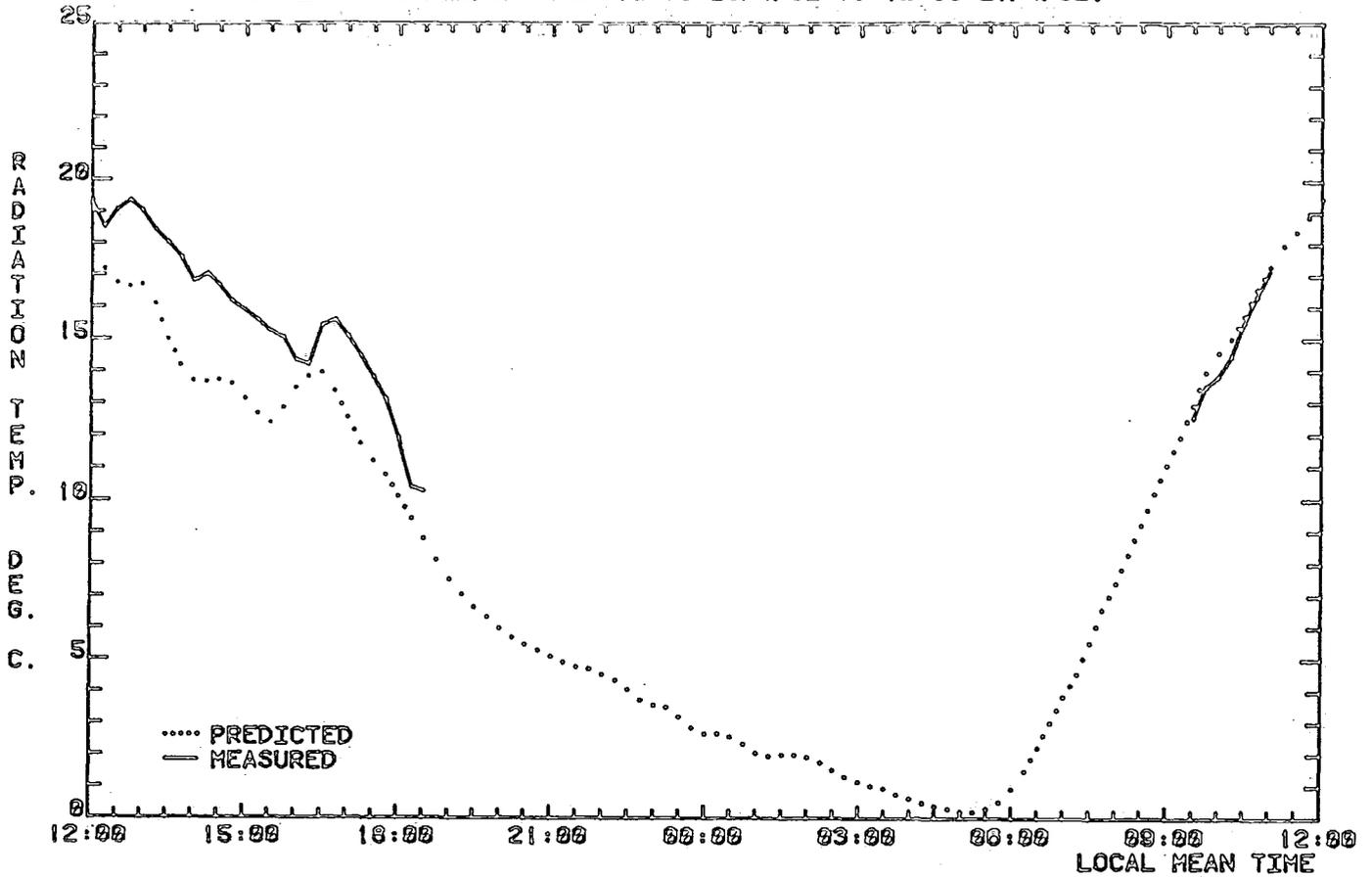
Fig. 5.38   PREDICTED & MEASURED RADIANT TEMPS. FOR THE ASPHALT SURFACE
             DURING THE PERIOD FROM 12:00 20/4/82 TO 12:00 21/4/82.
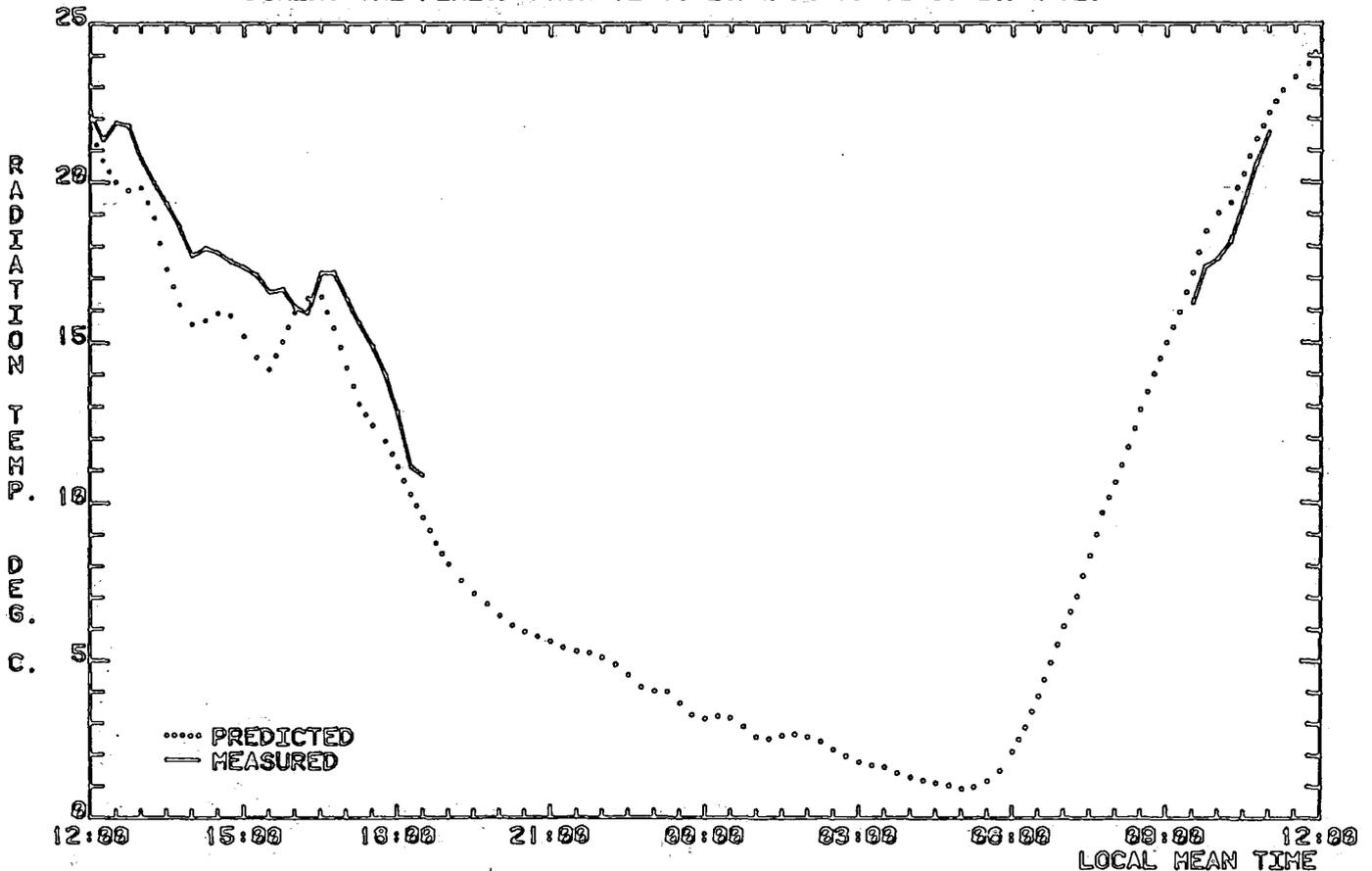
Fig. 5.39   PREDICTED & MEASURED RADIANT TEMPS. FOR THE CONCRETE SURFACE
DURING THE PERIOD FROM 12:00 21/4/82 TO 12:00 22/4/82.
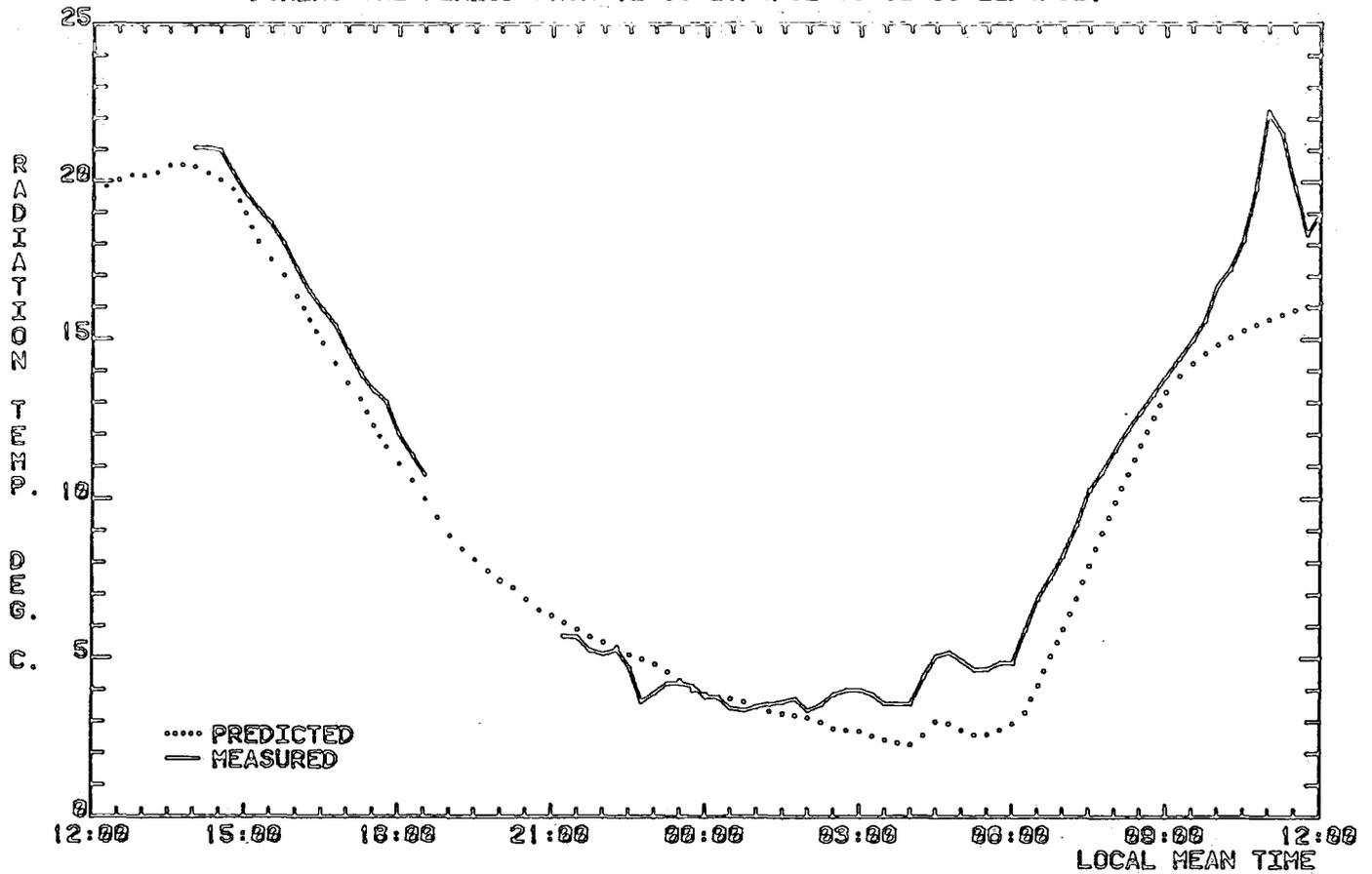
Fig. 5.40   PREDICTED & MEASURED RADIANT TEMPS. FOR THE ASPHALT SURFACE
DURING THE PERIOD FROM 12:00 21/4/82 TO 12:00 22/4/82.
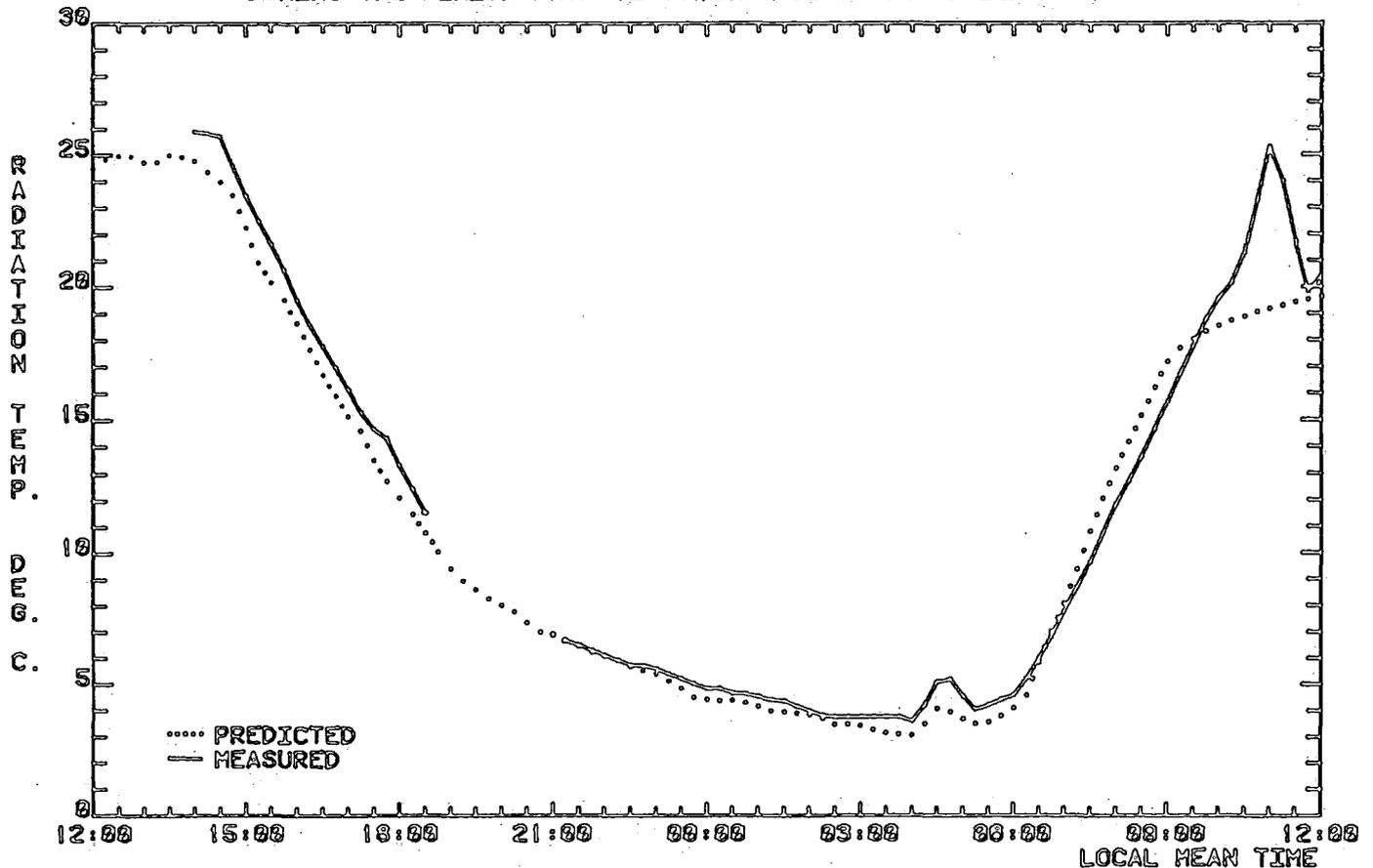
Fig. 5.41 PREDICTED & MEASURED RADIANT TEMPS. FOR THE CONCRETE SURFACE DURING THE PERIOD FROM 12:00 22/4/82 TO 12:00 23/4/82.
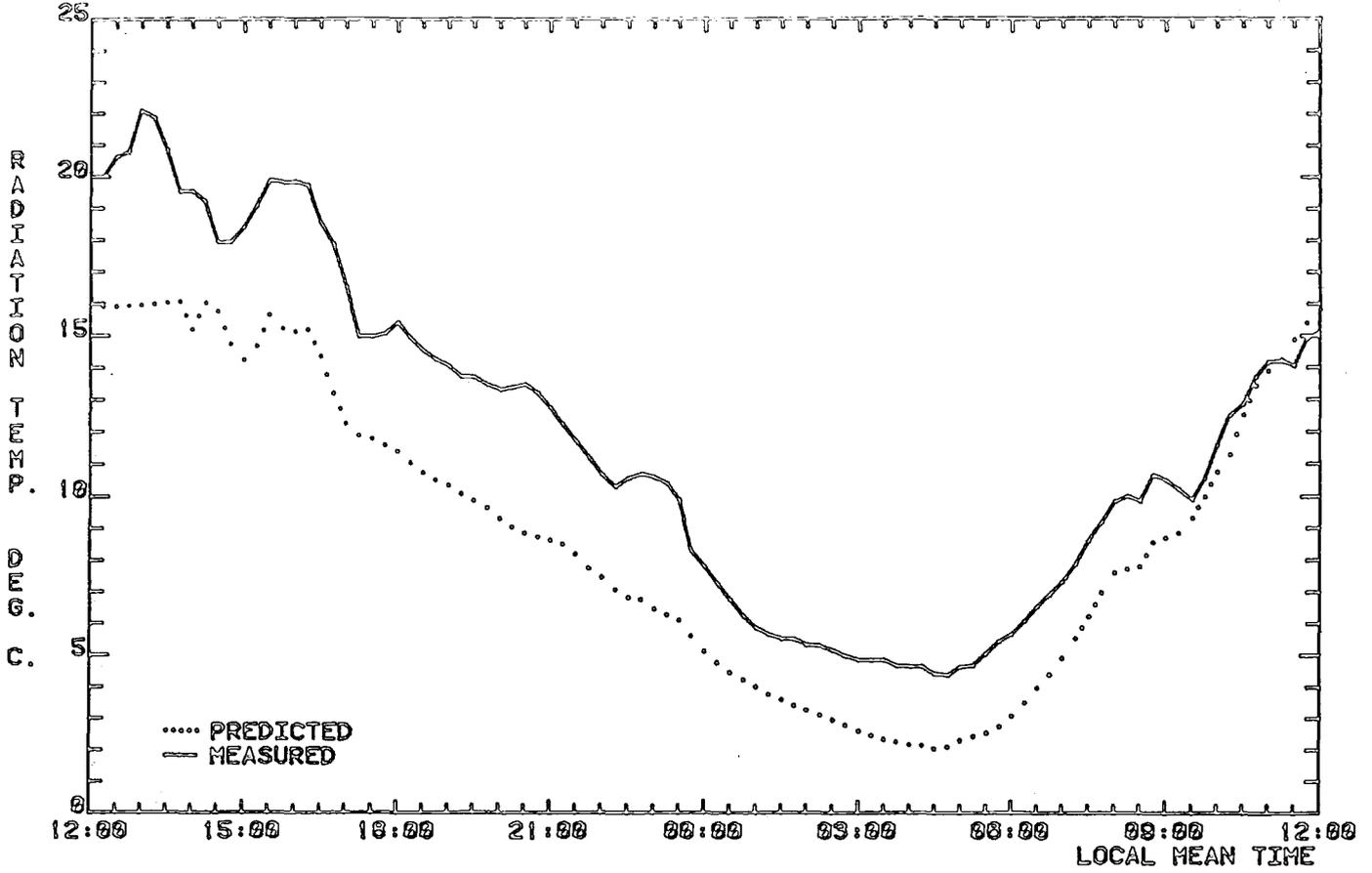
Fig. 5.42 PREDICTED & MEASURED RADIANT TEMPS. FOR THE ASPHALT SURFACE DURING THE PERIOD FROM 12:00 22/4/82 TO 12:00 23/4/82.
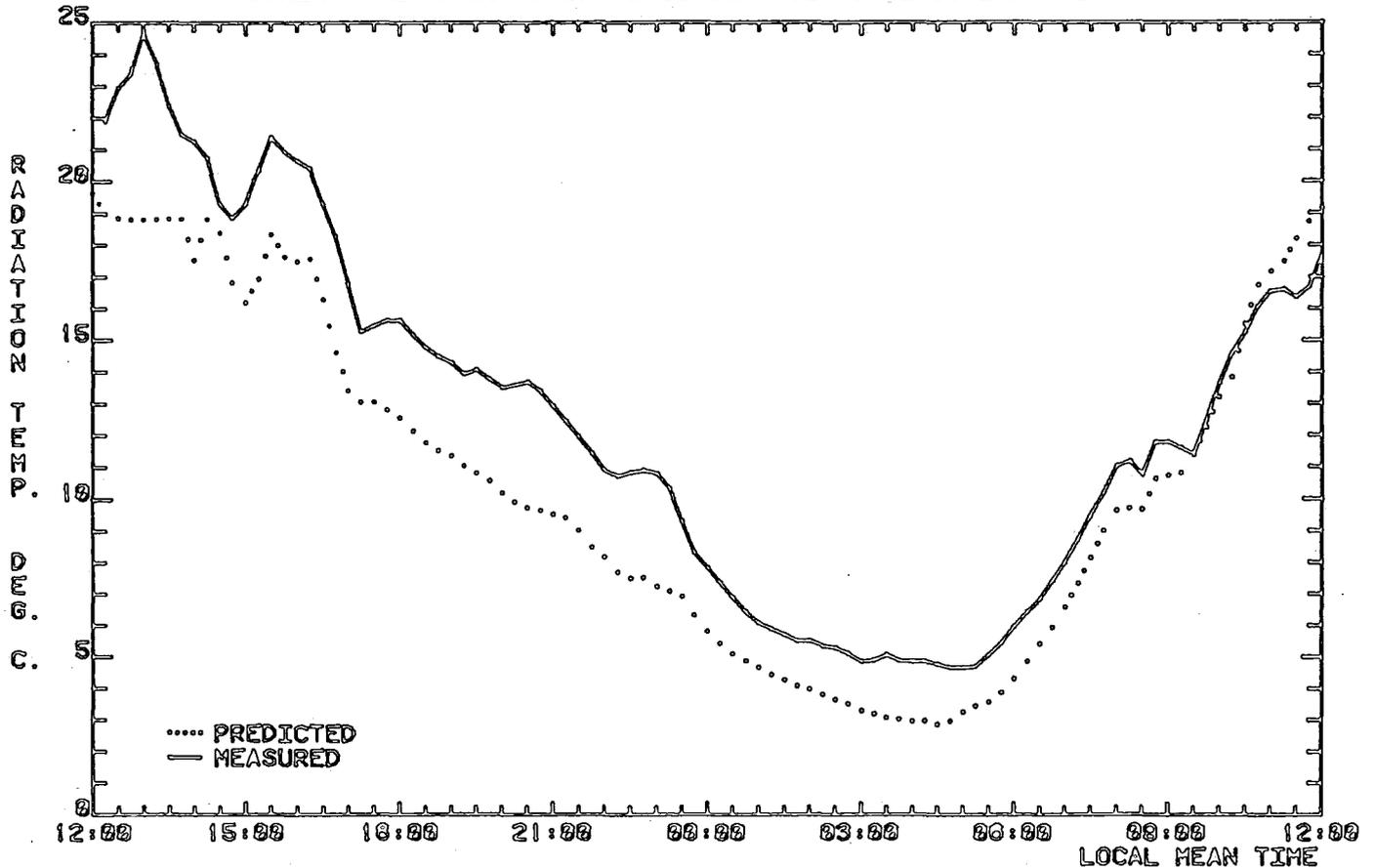
Fig. 5.43   PREDICTED & MEASURED RADIANT TEMPS. FOR THE CONCRETE SURFACE
DURING THE PERIOD FROM 12:00 23/4/82 TO 12:00 24/4/82.
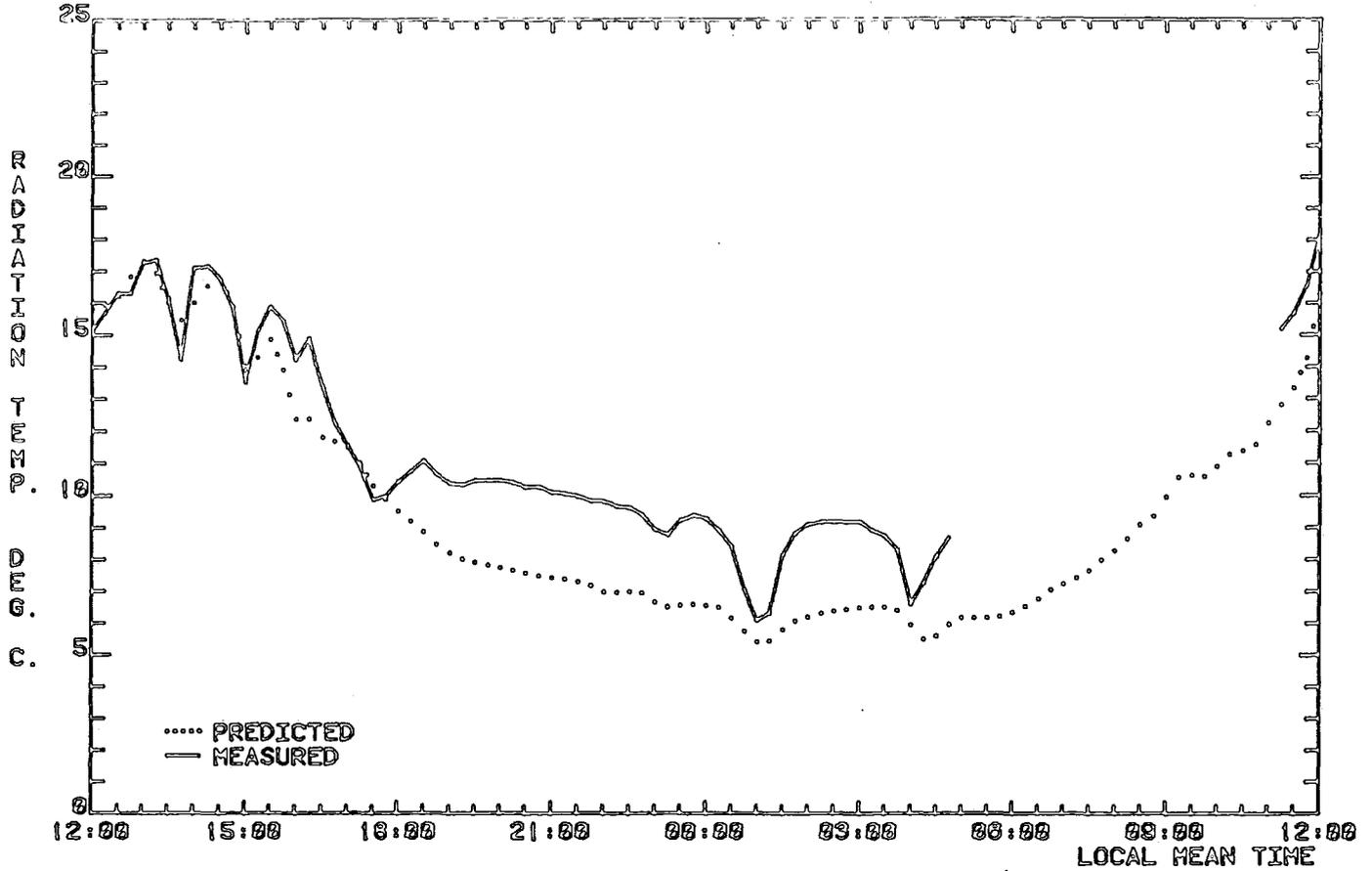
Fig. 5.44   PREDICTED & MEASURED RADIANT TEMPS. FOR THE ASPHALT SURFACE
DURING THE PERIOD FROM 12:00 23/4/82 TO 12:00 24/4/82.
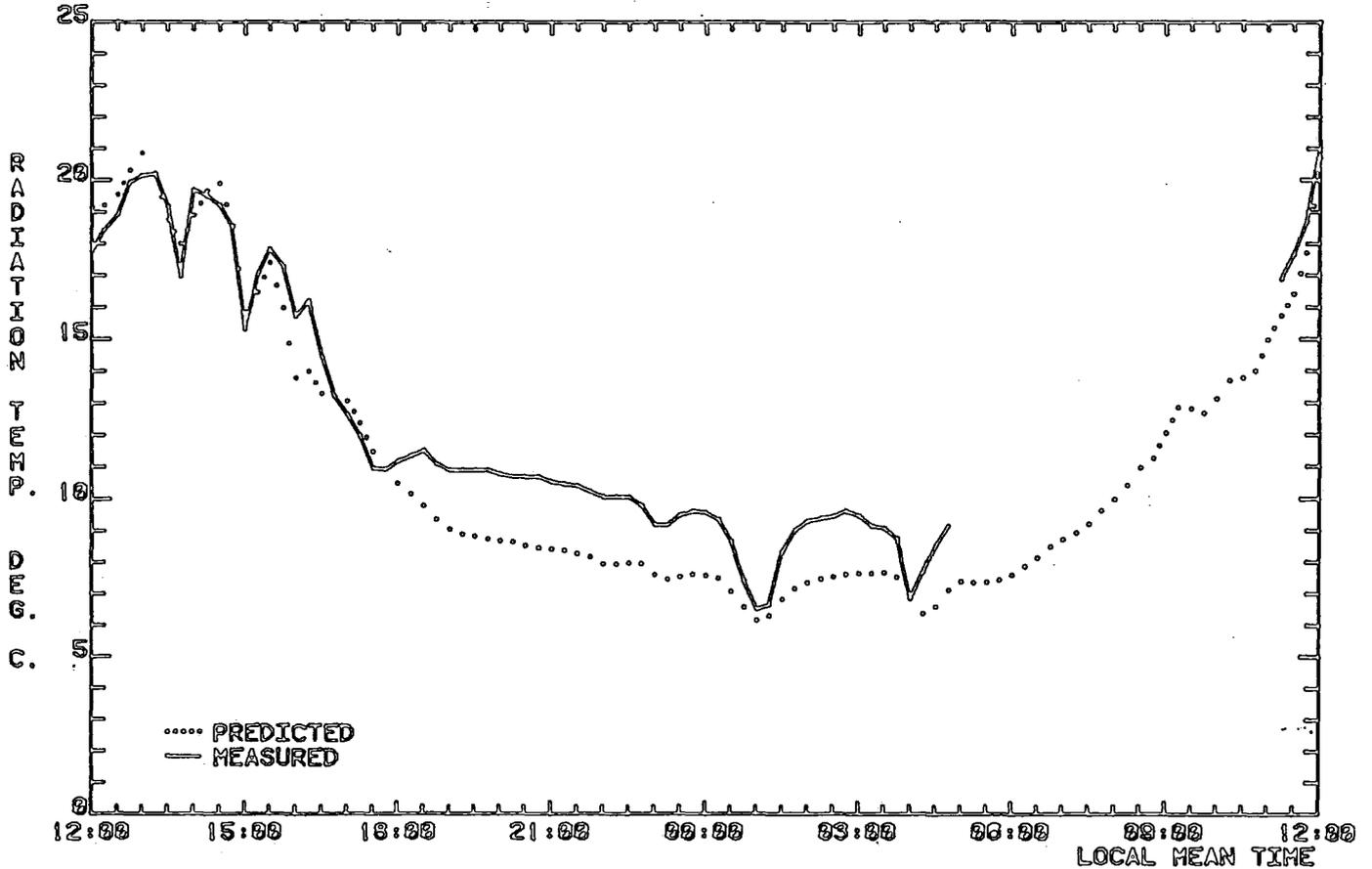
Fig. 5.45   PREDICTED & MEASURED RADIANT TEMPS. FOR THE CONCRETE SURFACE
            DURING THE PERIOD FROM 12:00 24/4/82 TO 12:00 25/4/82.
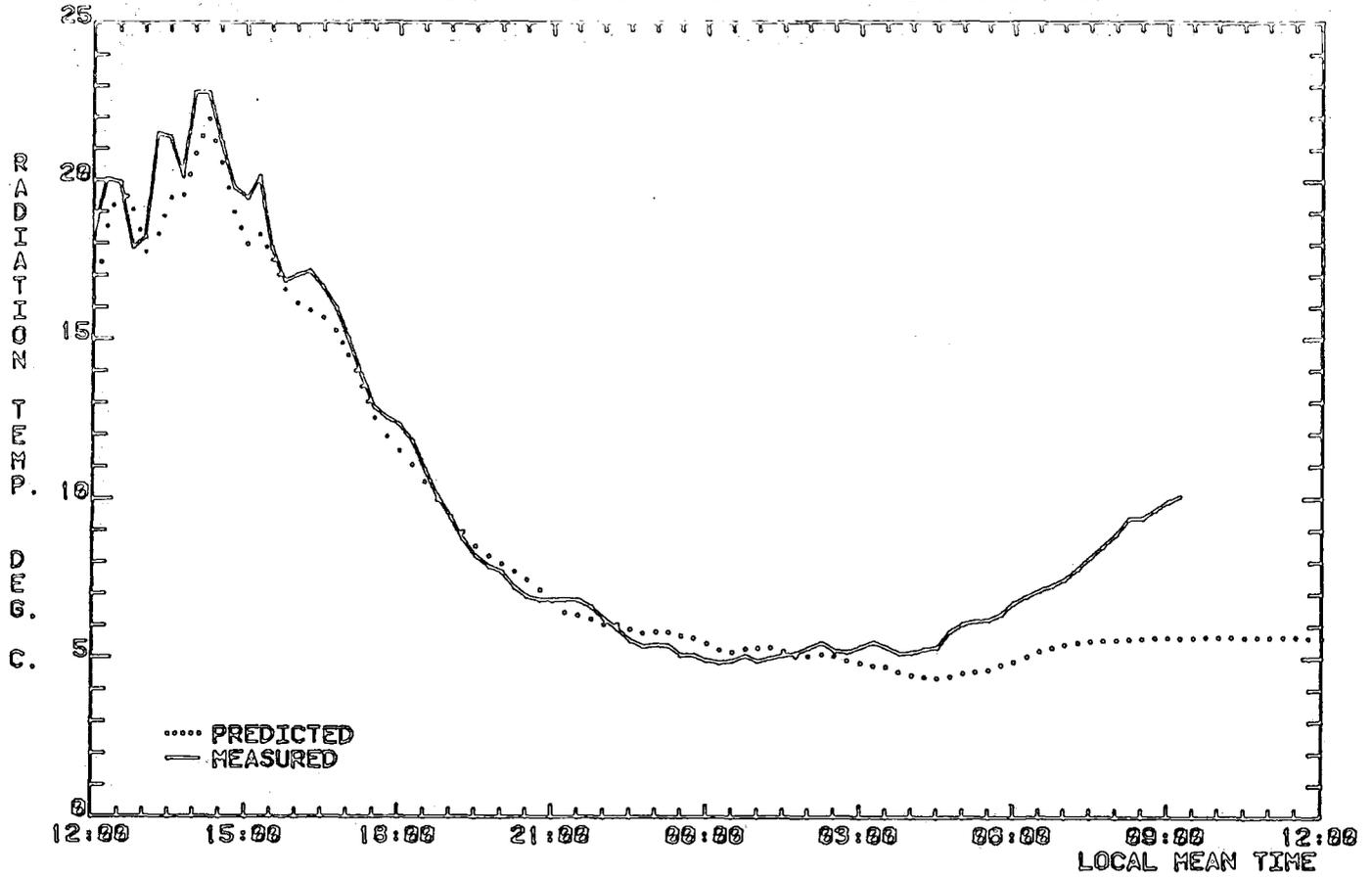
Fig. 5.46   PREDICTED & MEASURED RADIANT TEMPS. FOR THE ASPHALT SURFACE
            DURING THE PERIOD FROM 12:00 24/4/82 TO 12:00 25/4/82.
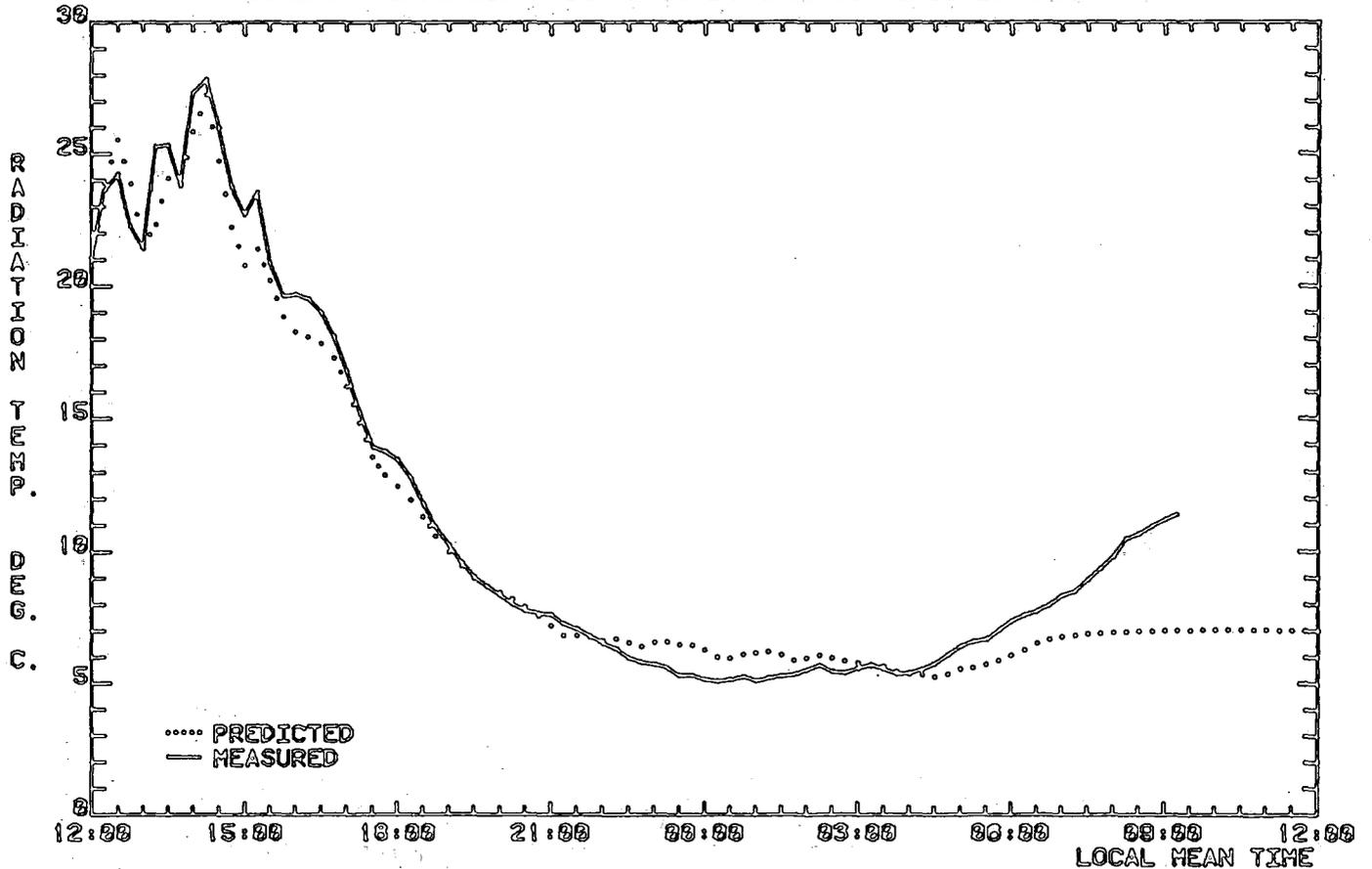
Fig. 5.47 PREDICTED & MEASURED RADIATIVE TEMPERATURE CONTRAST
BETWEEN THE ASPHALT AND CONCRETE SURFACES,
DURING THE PERIOD FROM 12:00 19/4/82 TO 12:00 20/4/82.
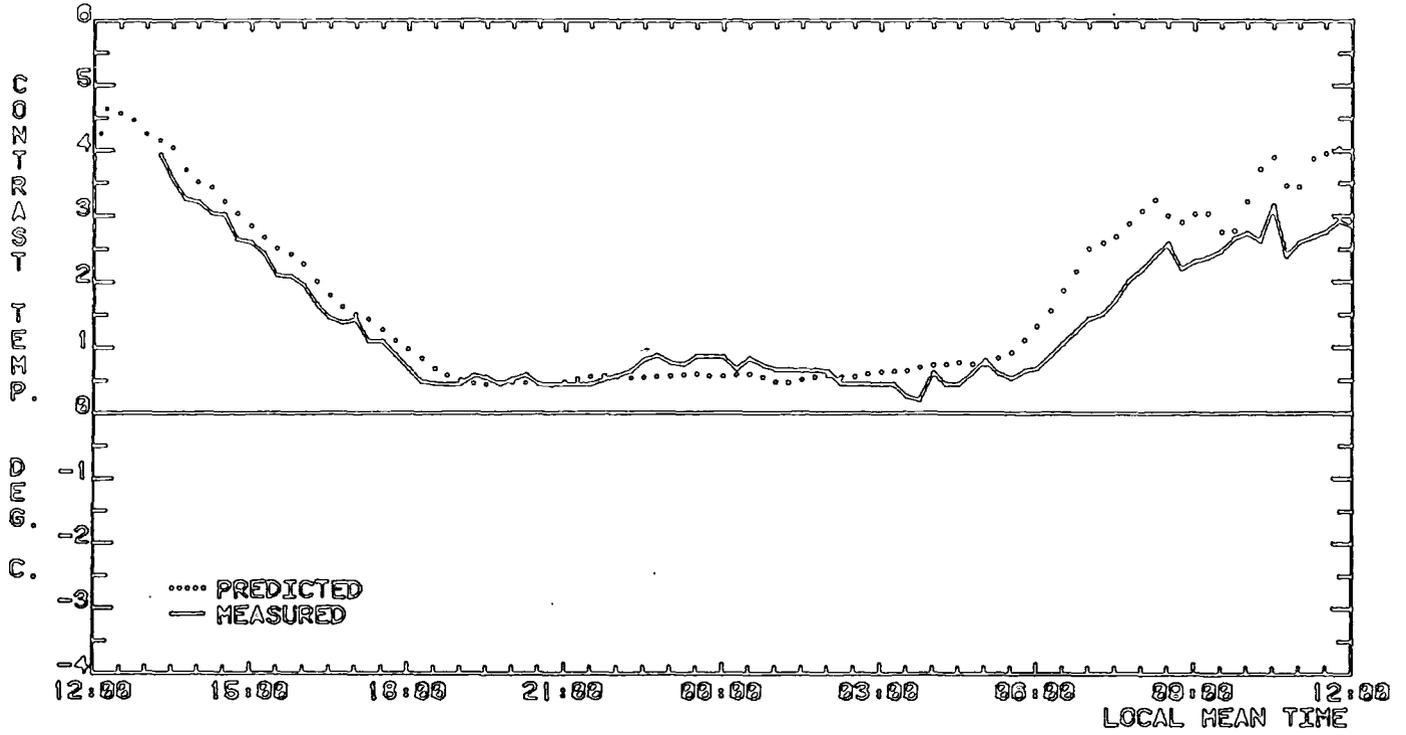
Fig. 5.48 PREDICTED & MEASURED RADIATIVE TEMPERATURE CONTRAST
BETWEEN THE ASPHALT AND CONCRETE SURFACES,
DURING THE PERIOD FROM 12:00 20/4/82 TO 12:00 21/4/82.
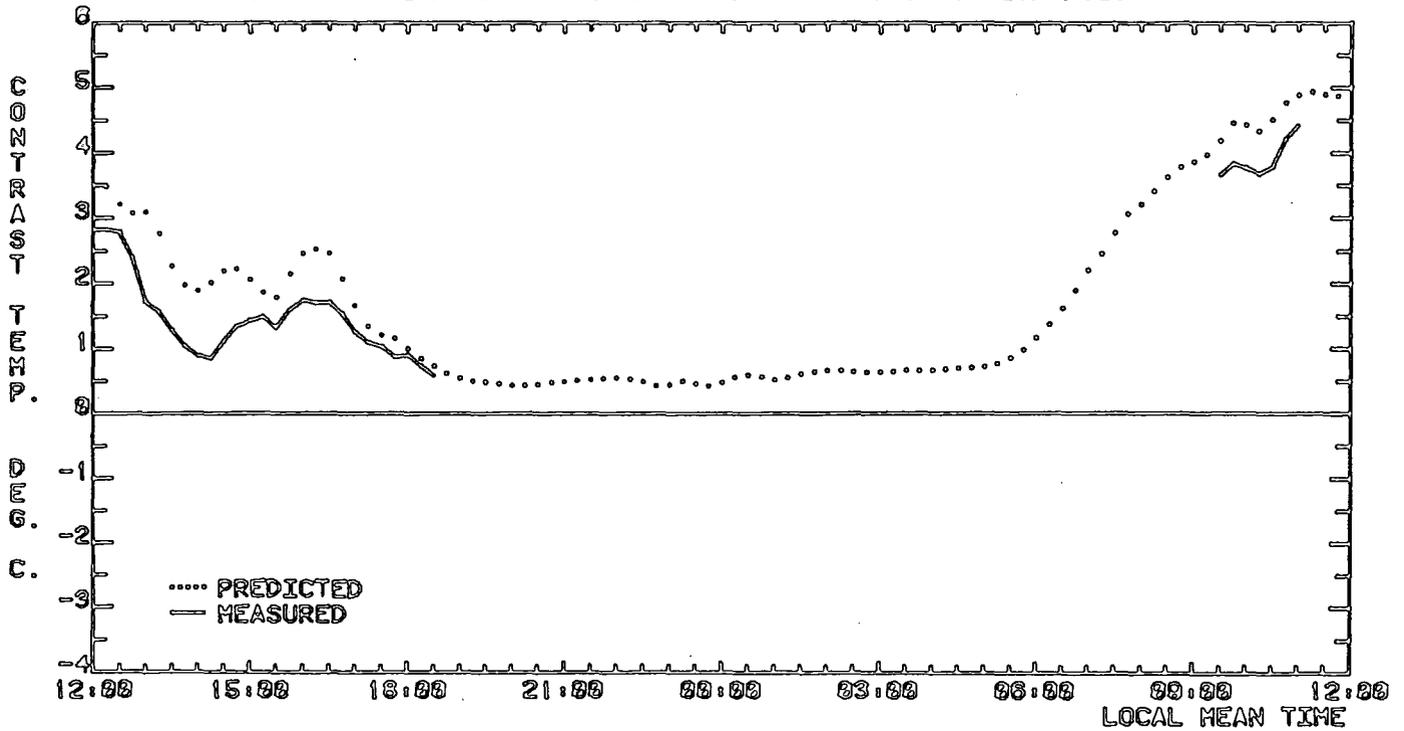
Fig. 5.49   PREDICTED & MEASURED RADIATIVE TEMPERATURE CONTRAST
              BETWEEN THE ASPHALT AND CONCRETE SURFACES,
              DURING THE PERIOD FROM 12:00 21/4/82 TO 12:00 22/4/82.
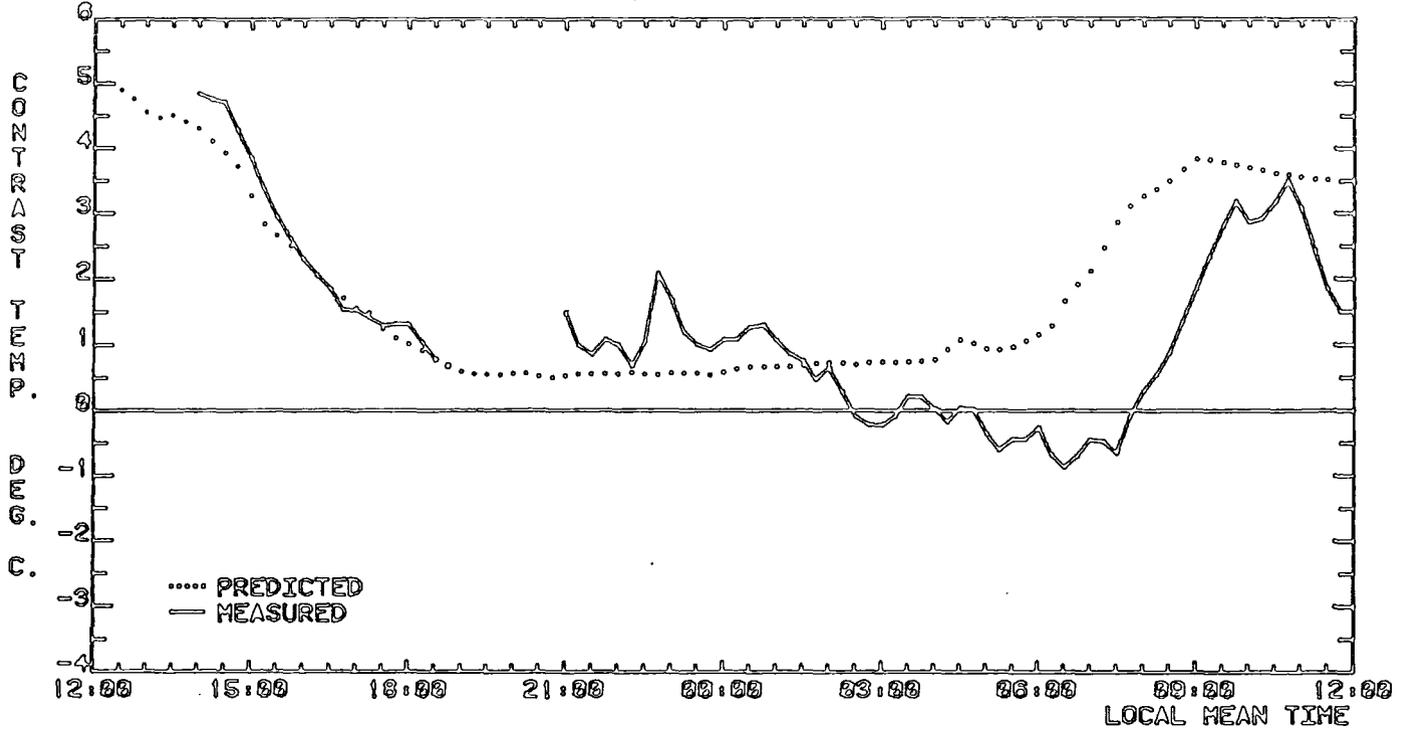
Fig. 5.50   PREDICTED & MEASURED RADIATIVE TEMPERATURE CONTRAST
              BETWEEN THE ASPHALT AND CONCRETE SURFACES,
              DURING THE PERIOD FROM 12:00 22/4/82 TO 12:00 23/4/82.
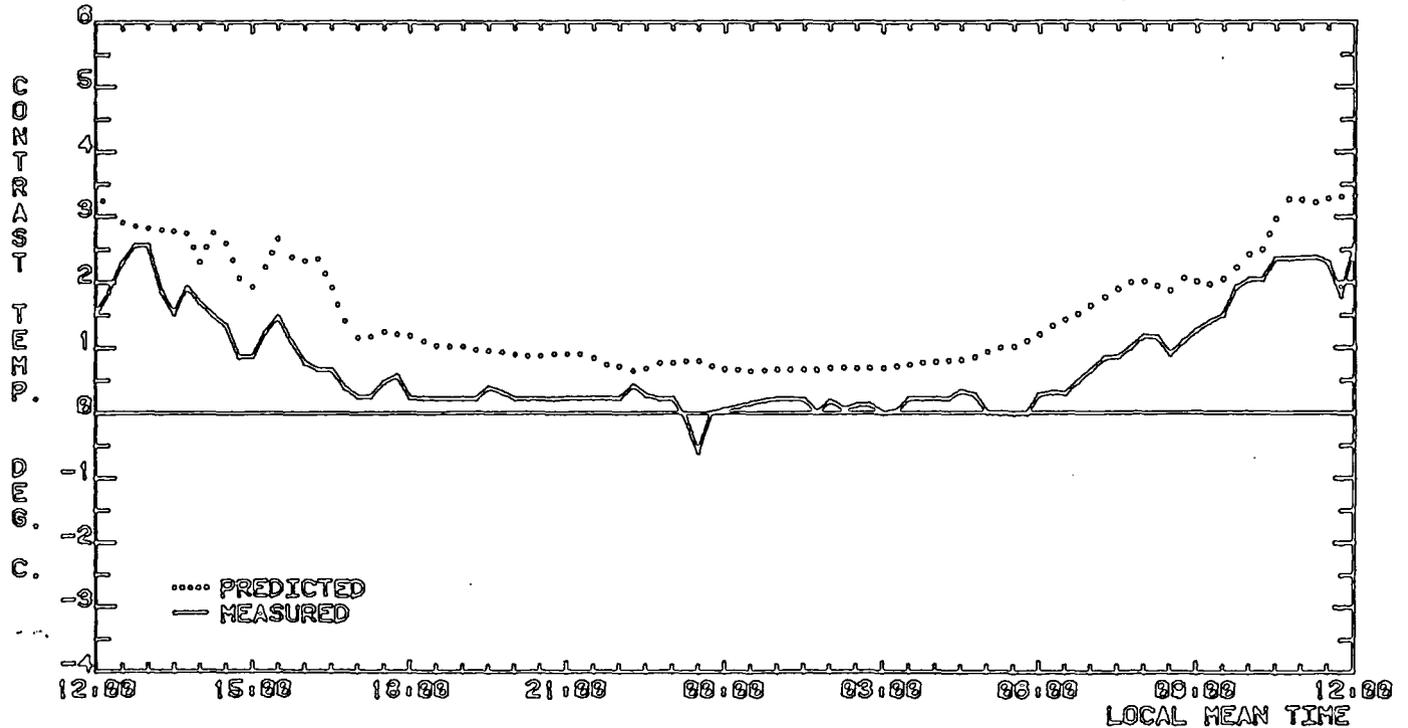
Fig. 5.51 PREDICTED & MEASURED RADIATIVE TEMPERATURE CONTRAST
BETWEEN THE ASPHALT AND CONCRETE SURFACES,
DURING THE PERIOD FROM 12:00 23/4/82 TO 12:00 24/4/82.
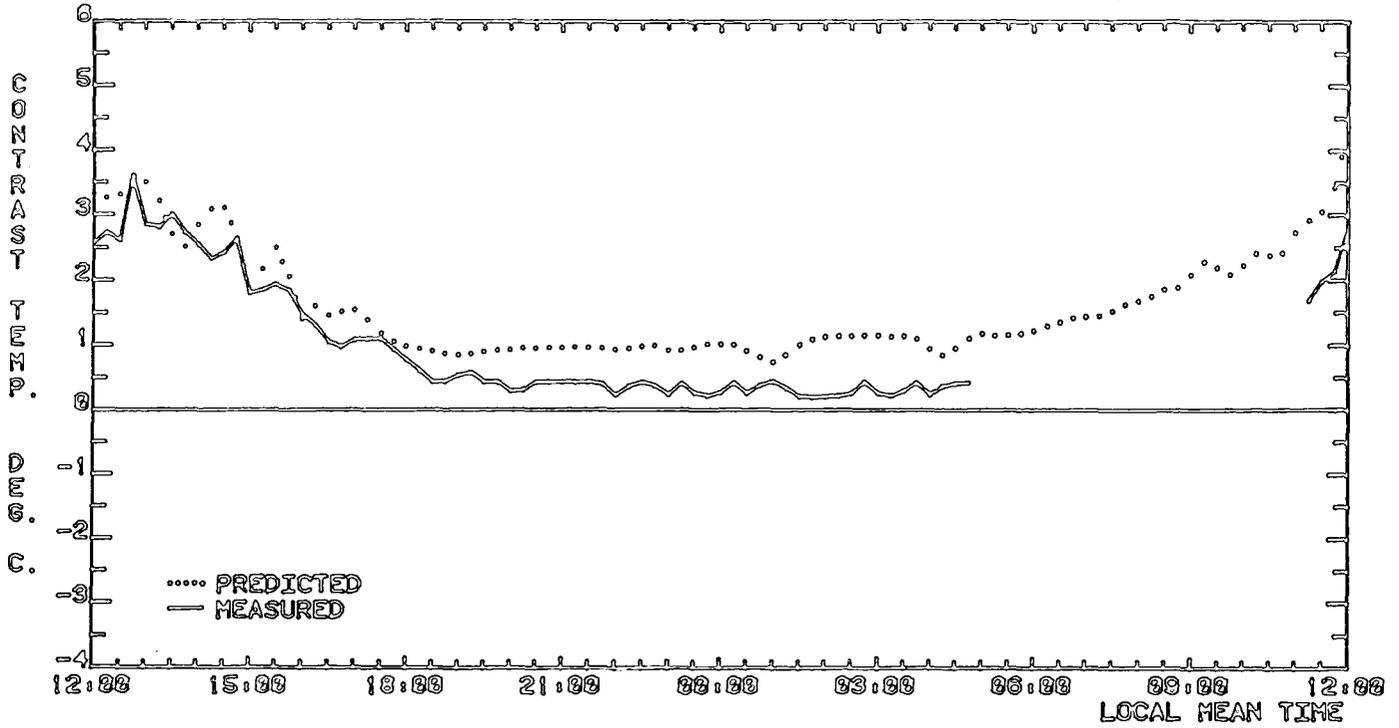
Fig. 5.52 PREDICTED & MEASURED RADIATIVE TEMPERATURE CONTRAST
BETWEEN THE ASPHALT AND CONCRETE SURFACES,
DURING THE PERIOD FROM 12:00 24/4/82 TO 12:00 25/4/82.
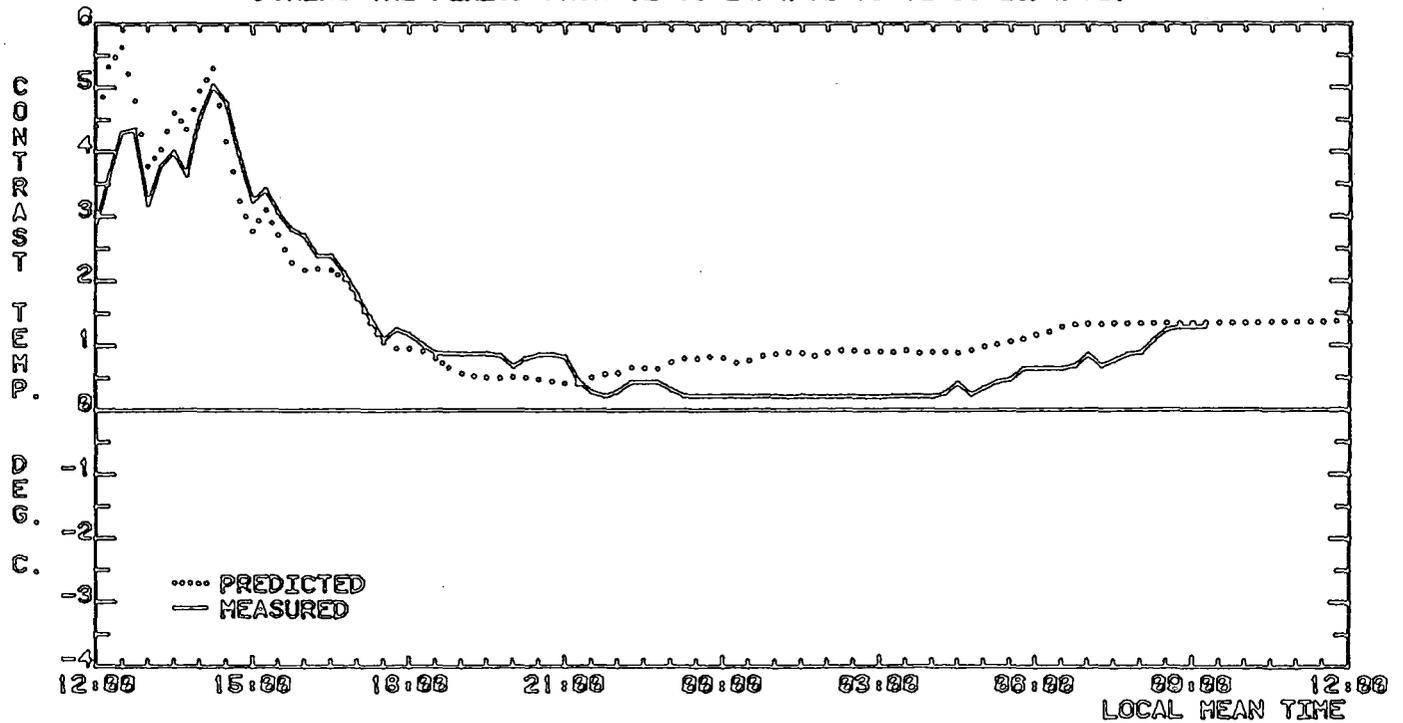
Chapter 6   Use of the general purpose model to simulate the temperature

profile in a south facing vertical sandstone wall.

6.1 Introduction.

Temperature measurements of a south facing sandstone wall at the
Observatory in Durham were routinely made by the equipment described in
Chapter 4. It was decided to attempt to simulate the observed surface
radiation temperatures over a period of fine weather in August 1983 by using
the general purpose model. In the next section, the construction and location
of the wall and the determination of the values of the parameters required to
run the model are discussed in more detail. This is followed by the results
obtained by running the model, and a discussion of how the correspondence
between the measured and predicted temperatures may be improved.

6.2   Input data required for the model.

6.2.1 Site characterisitic parameters.

The relevant parameters which specify the location of the Observatory and
the orientation of the wall are given in Table 6.1. The wall forms one of the
outer walls of the Observatory building, and is approximately 50 cm thick. The
area observed by the radiometer was located at a height of about 4.75 m above
ground level, and it was estimated that 60% of the field of view of the sky
from this point was obscured by other terrestrial objects. Figure 6.1 shows
the location of the south facing wall with respect to the rest of the
building. The west facing wall which projects out 1 m from the south facing
wall causes the area observed by the radiometer to remain in shadow for a
short period after sunrise, although the time that the south facing wall last
receives direct solar radiation is not affected by its surroundings. It was
therefore necessary to develop a modified version of the general purpose model
to take this shading effect into account. The first stage in the procedure was
to find out how long the area of interest on the wall remained in shadow after

sunrise. It was assumed that the point of temperature measurement on the south facing wall would first receive direct solar radiation at the same time an imaginary wall shown by the dotted line in Fig. 6.1, and the standard version of the general purpose model was then run for the period from 12:00 5th August to 12:00 6th August to determine the time of sunrise on this imaginary wall. The incident direct solar flux was calculated within the program assuming a cloud-free day, and the diffuse solar flux was permanently set to zero to show the sunrise time more clearly. The other meteorological parameters were set to typical constant values. The surface and material parameters were set to the values given in Sections 6.2.2 and 6.2.3, and the values for the azimuth and inclination of the imaginary wall were calculated from Fig. 6.1. The resulting temperature prediction showed that the imaginary wall, and hence the point of temperature measurement on the south facing wall, would first receive direct solar flux at 07:45. A comparison with the results obtained from running the model with the azimuth angle set to the correct value for the south facing wall, but assuming an unobstructed view of the sun, showed that the effect of the projecting west facing wall would therefore be to shield the point of temperature measurement on the south facing wall from direct solar radiation between 06:00 and 07:45. The section of the model where the measured solar flux was split up into direct and diffuse components was then modified so that no direct solar flux could be received by the wall between 06:00 and 07:45.

Table 6.1   Site characteristics of the sandstone wall.

Location .... Durham Observatory.

Latitude .... 54° 46' N.

Longitude .... 1° 35' W.

Altitude .... 100 m.

Angle of inclination of wall .... 90° 00'.

Angle of azimuth of wall .... 348° 20'.

Fraction of field of view of the sky unobscured .... 40%.

6.2.2 Surface parameters.

A summary of the initial values used for the parameters is given in Table 6.2, and these were obtained from Balick et al., 1981. The average ground albedo represents the surroundings of the wall, which consist of the asphalt floor of the balcony, the projecting west facing sandstone wall, and various trees and bushes. The moisture factor is zero as the wall was dry over the modelling period.

Table 6.2   Surface parameters.

Vertical emissivity 0.94

Vertical albedo 0.35

Average ground albedo 0.20

Surface moisture factor 0.00

6.2.3 Material parameters.

The initial values for these parameters were also derived from the results of Balick et al., 1981, and are given in Table 6.3. The wall was constructed from large sandstone blocks, so the material properties were assumed to be independent of depth or location.

Table 6.3   Material parameters.

Thermal conductivity .... 3.78 W m^{-1} K^{-1}

Thermal diffusivity .... 1.30 x 10^{-6} m^2 s^{-1}

6.2.4 Initial temperature profile and lower boundary condition.

The thickness of the wall was measured to be 50 cm, and it was decided to predict temperatures to this depth by using the model. The lower boundary was therefore located on the interface between the sandstone wall and the interior

room in the Observatory building. This was the room used to house the Tektronix computer which controlled the pan and tilt head carrying the radiometer. The contact temperature sensors which had not been deployed were also stored in this room, so it was possible to determine how the temperature inside the room varied by using the data recorded from these sensors. It was found that the difference between maximum and minimum temperatures over a 24 hour period was typically less than 1.5 °C. This is probably due to the relatively thick walls insulating the interior of the building from the more extreme variations of the outside air temperature. Other factors which contribute to the stable interior temperature of the room are the lack of artificial heat sources and the small window area. After considering the results of the sensitivity analysis, which suggested that the temperature predictions of the model were not very sensitive to changes in the lower boundary temperature, it was felt reasonable to assume that the temperature at the lower boundary was constant, and so the one-dimensional general purpose model could be applied.

The initial temperature profile was obtained by the same procedure as described in Section 3.2.1. In this case the temperature throughout the wall was initially set to the temperature at the lower boundary, and the data recorded over the fine weather period from 12:00 5th August to 12:00 6th August were used to obtain a stable initial temperature profile. The final version of this profile, which was obtained by using the optimal values for the surface and material parameters given in Section 6.3 is shown in Fig. 6.2.

6.2.5 Meteorological parameters.

The automatic weather station was located on the lawn in front of the Observatory and weather data were recorded at 15 minute intervals. The data required for modelling purposes are plotted in Figures 6.3 to 6.34.

6.2.6 Radiometer data.

Radiation temperature data were recorded every 15 minutes, and as stated in Section 5.2.6, are used in three ways.

Firstly, the temperature measurements of the sandstone wall are used for comparison with the predictions of the model.

Secondly, the data are used to calculate the value of the function "TREP", which is used in the calculation of the net long-wave radiative flux incident on the wall. The function represents the average temperature of the objects which obscure the field of view of the sky from the area of temperature measurement on the surface of the wall. These objects include the asphalt floor of the balcony, the west facing sandstone wall which projects out from the south facing wall, and various trees and bushes. Their temperatures were routinely measured by the radiometer, and the importance of their individual contribution to the average temperature was obtained by estimating the relative proportion of the sky obscured by each type of object. A program was developed for the Tektronix computer to calculate the average temperature, and this is described in the Appendix.

The third use of the radiometer data is to calculate the long-wave cloud cover factor. The procedure is exactly the same as previously described for the data recorded at Ouston, and the cloud cover factors calculated from the data are plotted in Figures 6.35 to 6.42.

6.3 Optimization of parameters.

Initially the model was run for the period from 12:00 5th August to 12:00 6th August 1983 using the values for the parameters given in the previous sections. As described for the validation of the model in Section 5.3, the optimum values for the surface and material parameters were obtained by comparing the predicted and measured radiation temperatures for the wall over the first 24 hour period, and adjusting the values of the parameters to obtain the best agreement. These values are shown in Table 6.4.

Table 6.4 Optimal values for surface parameters.

Vertical emissivity 0.99

Vertical albedo 0.20

Thermal conductivity .... 3.82 W m^{-1} K^{-1}

Thermal diffusivity .... 1.30 x 10^{-6} m^2 s^{-1}

6.4 Results of the simulation of the temperature profile in a south facing vertical sandstone wall.

After the stable temperature profile had been set up for the first 24 hour period using the optimal values for the material and surface parameters, the model was run using the data recorded at the Observatory over the corresponding period. This mainly consisted of fine weather with long, sunny periods and no recorded rainfall. The results obtained are presented as a comparison between the surface radiation temperatures of the wall predicted by the model and those measured by the radiometer.

6.4.1 Results from 12:00 5th August to 12:00 6th August 1983.

This was the first 24 hour period considered, and was used to obtain the optimum values for the surface and material parameters for the wall. The predictions of the model are compared with measured temperatures in Fig. 6.43, which shows that there is initially poor agreement between the temperature data. This is due to the use of an unrepresentative temperature profile within the wall at 12:00 on August 5th, which resulted from the effects of the weather conditions over the 24 hour period on the method used to calculate the profile. The method is described in Section 3.2.1, and calculates a stable temperature profile within the material such that when the model is run using this value at 12:00 5th August, the resulting predicted temperature profile at 12:00 6th August will be in agreement with the first to within about 0.1 °C. This is acceptable provided that certain important weather conditions, such as the air temperature and the level of cloud cover, have similar values at the

beginning and end of the 24 hour period. However, Figures 6.3 and 6.35 show that the weather was cloudy from 12:00 5th August up to when the sky cleared at 06:00 on the morning of the 6th, giving warmer, sunny weather. Consequently the stable temperature profile calculated using the method described above is more representative of the sunny conditions on the morning of the 6th than the cooler weather on the afternoon of the 5th. It is therefore reasonable to assume that the surface temperatures predicted by the model will be higher than the measurements when this temperature profile is used at the start of the modelling period, and that the predictions would slowly converge with the measurements as the temperature profile within the wall is updated by the model using the data recorded under the cloudy conditions. This is clearly shown in Fig. 6.43, and it can also be seen that the predicted and measured temperatures are in good agreement later in the evening and overnight.

On the morning of the 6th, the predicted temperatures rise sharply at about 07:45, when it was calculated that the area of temperature measurement would first receive direct solar radiation. However, the measured temperatures show only a small increase at this time before rising more rapidly at around 08:15 and crossing over the predictions at 10:00. Afterwards the predicted temperatures are slightly low although they still show the drop in temperature at 11:30 where thick cloud obscures the sun for a short period.

6.4.2 Results from 12:00 6th August to 12:00 7th August 1983.

There was variable cloud cover in the afternoon and evening of the 6th, which is reflected in the plots of the solar flux and long-wave cloud cover factor. The predicted and measured temperatures are shown in Fig. 6.44, and it can be seen that the predictions are significantly lower than the measurements.

The morning of the 7th was mainly cloudy, but with some short sunny periods. It can be seen in Fig. 6.44 that the predicted temperature rises sharply at 07:45, which was also observed in the results for the morning of

the 6th. The measured temperature shows a similar effect an hour later when
the sky clears for a brief period. The cloud soon returns and the measured and
predicted temperatures then level out at similar values. The sky starts to
clear again at around 10:00, and this is accompanied by a rise in the measured
and predicted temperatures, with both behaving similarly from then until the
end of the 24 hour period.

6.4.3 Results from 12:00 7th August to 12:00 8th August 1983.

The predicted and measured temperatures are plotted in Fig. 6.45, and
their behaviour is very similar to that observed for the afternoon and evening
of the previous 24 hour period. This is not surprising as the weather
conditions were virtually identical, consisting of sunny spells and variable
cloud cover. One interesting feature of the graph is that the sharp peaks in
the measured temperatures do not appear in the plot of the predictions. The
two peaks which occur at 22:00 and 03:00 are rises in temperature, and may be
due to the cloud thickening. At 08:15, the sudden fall in temperature may be
due to the cloud breaking and then quickly reforming. However, the plot of the
long-wave cloud cover factor for this period does not suggest that such rapid
changes in the cloud formations occured. Alternatively, the behaviour of the
measured temperatures may be due to sudden variations in the air temperature
and windspeed, although the weather data in Figures 6.12 and 6.13 would tend
to suggest that this was unlikely. It is therefore not clear which physical
process is responsible for these temperature variations, and the fact that the
predictions of the model do not behave similarly suggests that it may be due
to local variations of weather conditions around the wall which were not
detected by the weather station.

There was complete cloud cover on the morning of the 8th, as shown by the
plots of incident solar flux and long-wave cloud cover factor in Figures 6.11
and 6.37. This results in only a slight increase in the predicted temperatures
at sunrise, while there is virtually no change in the measured temperatures.

6.4.4 Results from 12:00 8th August to 12:00 9th August 1983.

The results for this 24 hour period are plotted in Fig. 6.46, which is very similar to the previous results in Fig. 6.45. This is again due to the similarity in the weather conditions, which is well illustrated by a comparison of the plots of the incident solar flux (Figures 6.11 and 6.15) and long-wave cloud cover factor (Figures 6.37 and 6.38).

6.4.5 Results from 12:00 9th August to 12:00 10th August 1983.

The afternoon and evening of the 9th were the same as observed in the past three 24 hour periods, and the behaviour of the predicted and measured temperatures in Fig. 6.47 is therefore as might be expected. Unfortunately, radiometer data were not recorded after 04:00 on the 10th due to equipment failure, so the predicted temperatures for the remainder of the 24 hour period are not very useful. However, it is interesting to note that the sudden rise in incident solar flux after 09:00 on the 10th is also clearly shown in the behaviour of the predicted temperature for the wall.

6.4.6 Results from 12:00 10th August to 12:00 11th August 1983.

This period marks a definite improvement in the weather, with less cloud and higher incident solar fluxes than in the past few days. This can clearly be seen in Figures 6.23 and 6.40. The predicted and measured temperatures for the 24 hour period are shown in Fig. 6.48, and the radiometer data for the wall are available again after 17:00 on the 10th. The behaviour of the predicted temperatures is similar to that observed previously, with the predictions being too low during the afternoon and slowly converging with the measurements overnight.

The morning of the 11th was clear and sunny, and the sharp increase in both measured and predicted temperatures at sunrise is clearly shown in Fig. 6.48. These weather conditions are the same as on the morning of the 6th, and a comparison with the results in Fig. 6.43 shows that the predicted

temperatures behave in an identical manner.

6.4.7 Results from 12:00 11th August to 12:00 12th August 1983.

The first part of the afternoon of the 11th was cloudy with short periods of sun. The sky cleared after 15:00, and this is reflected in the behaviour of the measured temperature in Fig. 6.49. The behaviour of the predicted temperatures is the same as that observed for previous periods of similar weather conditions. The morning of the 12th was initially dull, but became brighter later on. The characterisitic rise in the predicted temperature of the wall at 07:45 is clearly shown in Fig. 6.49, and as shown for example in the graph of the results for the previous 24 hour period, Fig. 6.48, the predictions start to rise rapidly above the measured temperatures. However, after 09:00 the rate of increase in the predicted temperatures slows down, and they appear to approach a constant value towards the end of the modelling period. This occurs because no weather data were recorded by the weather station from 09:00 until the end of the 24 hour period. The most important of these is the incident short-wave solar flux, which is used by the model to calculate the flux which would be received by the wall. When the data are not available, the flux is assumed to stay constant at the last recorded value, which results in the predicted temperature of the wall becoming very inaccurate.

6.4.8 Results from 12:00 12th August to 12:00 13th August 1983.

This was the final 24 hour period for which the model was run as the weather started to become much more cloudy in the afternoon of the 13th. The weather conditions over this 24 hour period were warm and sunny, with only a small amount of cloud at high altitude. This is reflected in the plots of incident solar flux in Fig. 6.31 and the long-wave cloud cover factor in Fig. 6.42. The predicted and measured temperatures are plotted in Fig. 6.50, and it can be seen that the predictions are initially much lower than the

measured temperatures. This is because the initial temperature profile at 12:00 on the 12th was not as high as would be expected, due to the loss of the incident solar flux data towards the end of the previous 24 hour period. In the evening and during the night the predicted temperatures slowly approach the measurements, as has been observed previously. On the morning of the 13th, the predicted temperatures rise sharply before falling below the measured temperatures after 09:00.

6.5 Discussion of results.

The agreement between the surface temperatures predicted by the model and those measured by the radiometer for the south facing sandstone wall was not as good as was found for the concrete and asphalt surfaces described in Chapter 5. The failings of the model can be seen in most of the graphs showing results including the initial 24 hour period from 12:00 5th August to 12:00 6th August. The results of the first 24 hour period are not particularly useful to evaluate the capability of the model to simulate the temperature profile within the wall, as during this period the surface and material parameters were altered to achieve as close a correspondence between the measured and predicted temperatures as possible. These results, however, do show the main times when disagreement between predictions and measurements occurs. In subsequent 24 hour periods it can be seen from the graphs that significant disagreement between predicted and measured temperatures occurs at roughly the same times, and this is most evident if the results for days when there was little cloud cover, for example Figs. 6.48 and 6.50, are considered. In the morning, a sharp increase in the predicted temperatures occurs at the calculated time of sunrise on the wall at 07:45, which results in the predictions rising above the measured temperatures. The measured temperatures appear to rise more slowly at sunrise, although after a short while the measurements and predictions are in reasonable agreement. However, the rate of

increase in temperature of the predictions then starts to fall below that observed in the measurements and the predicted temperatures are too low by noon. In the afternoon and into the evening, the predictions slowly converge with the measurements, and co-incide at night for most of the 24 hour periods considered.

There are possibly two main reasons why the predicted and measured temperatures are not in good agreement. Firstly, the choice of material and surface parameters may not be as close to the actual values as was expected. It was not possible to make direct measurements of the values of these parameters, and so they had to be obtained by repeatedly running the model for the first 24 hour period until the best agreement between the predicted and measured temperatures was found. This method was considered suitable as the weather conditions on the 5th to the 6th August were not significantly different from those recorded on later days, and it was therefore reasonable to suppose that if generally good agreement between the predicted and measured temperatures could be obtained on one typical day, then good agreement would also be expected for subsequent periods of similar weather conditions.

The second possible reason is that the values used for the meteorological conditions at the surface of the wall were unrepresentative of the actual conditions. This may arise because the weather station which supplied the meteorological data was situated some distance away from the wall, on an exposed area of the lawn in front of the building. The effect on the temperature predictions of the model resulting from differences between the data recorded by the weather station and the actual conditions close to the wall can be determined by refering to the results of the sensitivity analysis. Although the predictions of the model were found to be insensitive to variations in the wet and dry bulb depression, the values used for the air temperature, windspeed and incident solar flux are much more influential. Of these three parameters, probably the smallest error arises from assuming that the air temperature is roughly the same close to the wall as at the weather

station. Evidence for this may be obtained by reference to Section 4.4.4 in Chapter 4, where the air temperature measured by a sensor in free air on the balcony of the Observatory is compared with data from the weather station. The results showed that both temperatures behaved similarly, with a maximum difference of around 2 °C, although this may have been due to radiative and convective heat exchanges between the sensor and its surroundings.

The windspeed at the wall surface will probably be significantly different from the value measured by the weather station due to the complicated nature of the surroundings of the wall giving rise to gusts and eddies. However, this would be very difficult to measure accurately, as the presence of anemometers close to the wall would cause changes in the conditions that were to be measured.

It is likely that the greatest source of error was due to an incorrect calculation within the model for the value of the incident solar flux received by the wall, which is obtained from the value of the incident solar flux on a horizontal surface measured by the solarimeter. The way in which the solarimeter readings are split into the direct and diffuse components fluxes is described in Section 2.3.1.2. The diffuse flux is assumed to be isotropic and is calculated by using Equation 2.8, which was given by Khale, 1977. The direct flux component incident on the solarimeter is calculated by subtracting the value of the diffuse component from the total measured incident flux, as it is assumed that the reflected short-wave radiation received by the solarimeter is negligible. The direct flux incident on the sandstone wall is related to the component at the horizontal surface through the ratio of the zenith angles of the sun from the two surfaces. The value of this flux is set to zero when the sun is not visible from the wall, which corresponds to short periods after sunrise and before sunset. The former is due to the shading effect of the west facing sandstone wall, and the program was modified to take account of this as explained in Section 6.2.1. At sunset, the direct component becomes zero when the zenith angle of the sun relative to the wall is greater

than 90°. The representation in the model of the total flux received by the wall therefore becomes;

$$Total flux = Direct flux + (Diffuse flux \times f)$$

$$+ Reflected flux from surroundings \qquad (6.1)$$

where "f" is the fraction of the sky which is unobscured as viewed from the area on the wall for which temperatures are to be predicted.

If the model was used for simple cases where no clouds are present, then the above equation should provide a good estimate of the total flux incident on the wall. However, when the sun is obscured by cloud, the diffuse component will increase due to scattering within the cloud and the direct component will be attenuated. Except under conditions of extremely thick cloud, the diffuse flux will not be isotropic and the wall will receive more diffuse flux from the direction of the sun than from other angles. The total flux arriving at the surface of the vertical wall can therefore only be obtained from the measured flux arriving at a solarimeter on a horizontal plane if the angular distribution function of the diffuse flux is known. The magnitude of the diffuse flux arriving at the wall is then given by integrating the distribution function over the area of the sky unobscured as viewed from the surface of the wall, and the diffuse flux that would be received on the horizontal plane is obtained by integrating the distribution function over the whole hemisphere. The direct component incident on the solarimeter is obtained in the same way as described in the previous paragraph, and the direct flux component received by the sandstone wall can be found by multiplying this value by the ratio of the zenith angles of the sun from the two surfaces.

Unfortunately, the distribution function for the diffuse flux is not known, so it is necessary to find an alternative method of determining the direct and diffuse components of the solar flux incident on the wall. However, it is possible to get an idea of the upper and lower limits of the incident

flux by the following simple analysis. Firstly, the total flux received by the wall is assumed to be given by,

$$\text{Total flux} = \text{Measured flux} - (\text{Diffuse flux from sky not}$$
$$\text{visible from wall}) \qquad (6.2)$$

The measured flux is simply the reading from the solarimeter, while the second term on the right hand side of the equation can be determined in two ways. Firstly, the diffuse flux can be calculated using Equation 2.8 as before, and then multiplied by the fraction of the sky which is not visible from the wall.

$$\text{Diffuse flux} = S_D \times (1-f) \qquad (6.3)$$

This represents a lower limit on the diffuse flux that the wall would receive, so on substitution into Equation 6.2 will give the likely upper limit for the total flux incident on the wall.

A lower limit for the total flux incident on the wall may be calculated by assuming that when the sun is obscured by cloud, all the flux received by the wall is diffuse and the direct flux component is zero. This corresponds to what would be expected for conditions of extremely thick cloud. Hence, assuming the diffuse flux distribution is isotropic, the total flux received by the wall becomes,

$$\text{Total flux} = \text{Measured flux} \times (1-f) \qquad (6.4)$$

It was decided to try to obtain a broad understanding of the effects on the temperature predictions of the model which would be caused by the use of the two equations to calculate the upper and lower limits of the total flux received by the wall. The main problem was how to determine when the sun was obscured by clouds, as viewed from both the wall and the solarimeter. As these

data were not available, it was assumed for simplicity that both were in shadow at the same time, and the long-wave cloud cover factor was used to estimate the amount of cloud in the sky. The period from 12:00 12th August to 12:00 13th August was chosen as it consisted of generally fine weather. The results obtained by using the lower limit to the flux are shown in Fig. 6.51 and those for the upper limit in Fig 6.52. It can be seen that significantly different predicted temperatures over the 24 hour period were produced, and it is clear that if material parameters such as the surface albedo of the wall were varied, then it should be possible to adjust the upper and lower limits of the predicted temperatures so that the measured surface temperatures lie between them.

In conclusion, the results of this analysis would tend to suggest that for modelling problems of this type, either the general purpose model will have to be modified to calculate more accurate values for the direct and diffuse fluxes, or else measurements of the fluxes received by the wall will be required as input data for the model.

Fig. 6.1

Diagram showing the location of the south facing sandstone wall at Durham Observatory.
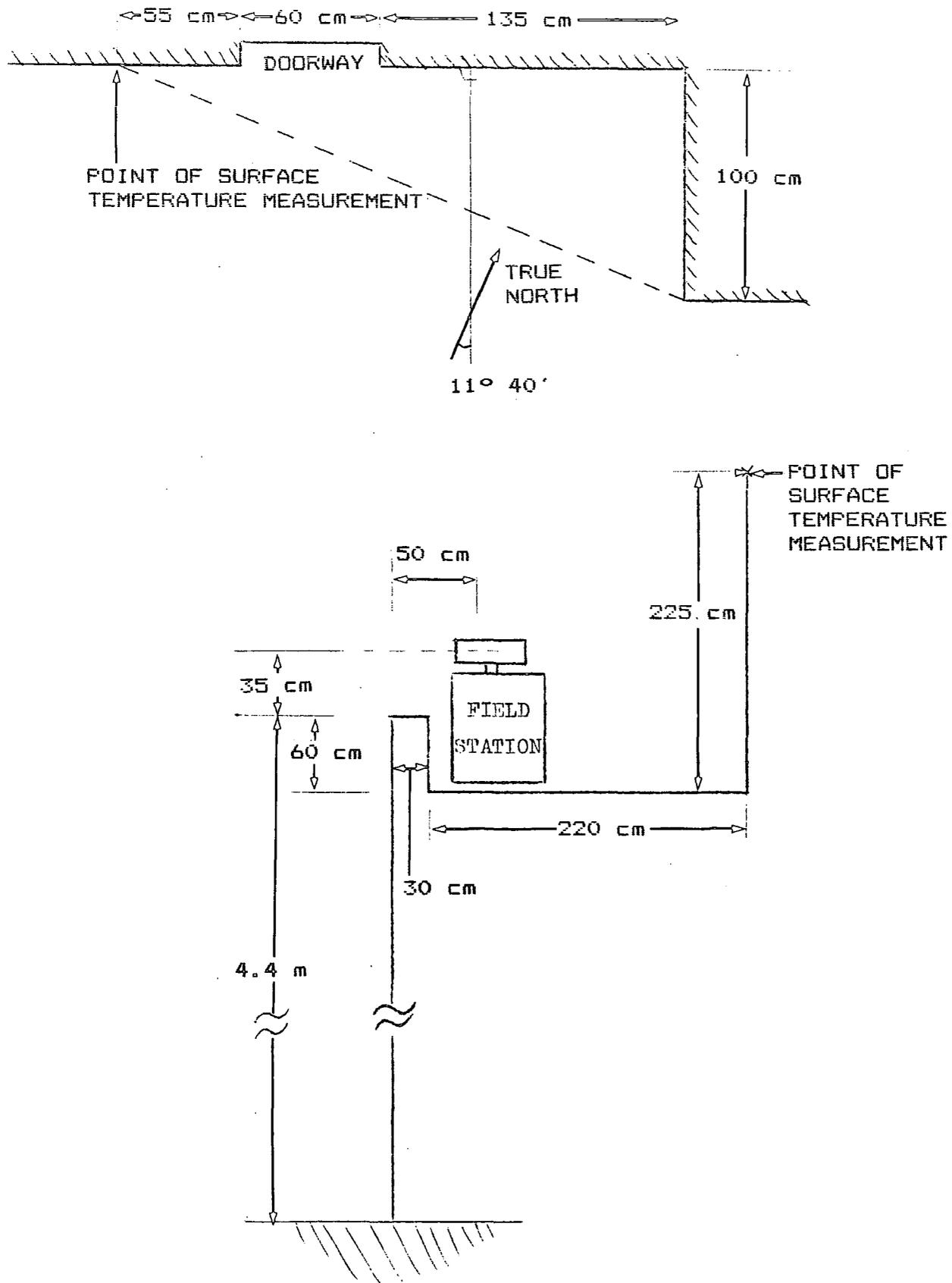
Fig. 6.2
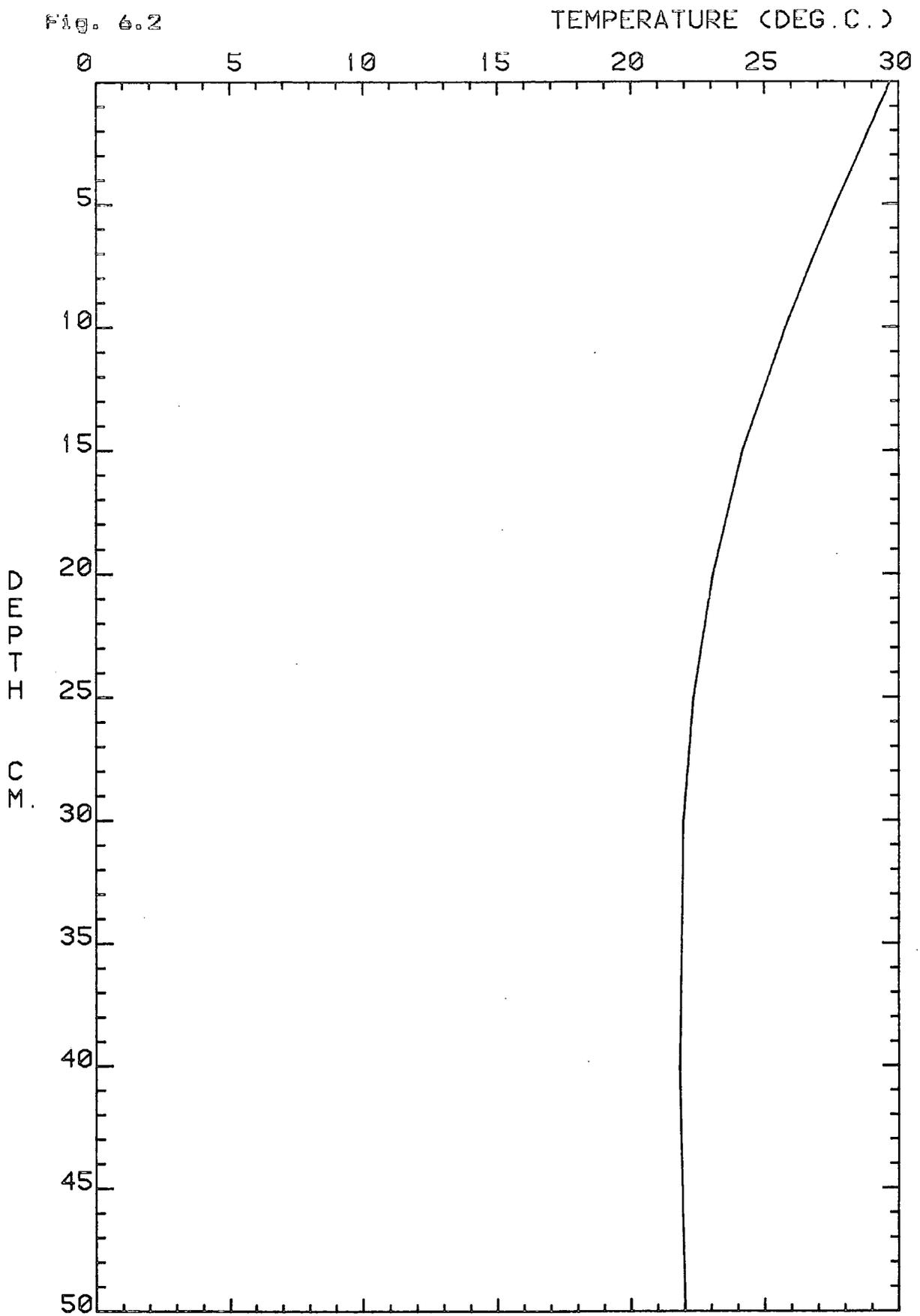
INITIAL TEMPERATURE PROFILE IN THE SOUTH
FACING SANDSTONE WALL AT 12:00 ON 5/8/83.

Fig. 6.3   WEATHER DATA RECORDED AT DURHAM OBSERVATORY
            AV. SOLAR RADIATION FROM 12:00 5-AUG-83 TO 12:00 6-AUG-83.

LOCAL MEAN TIME
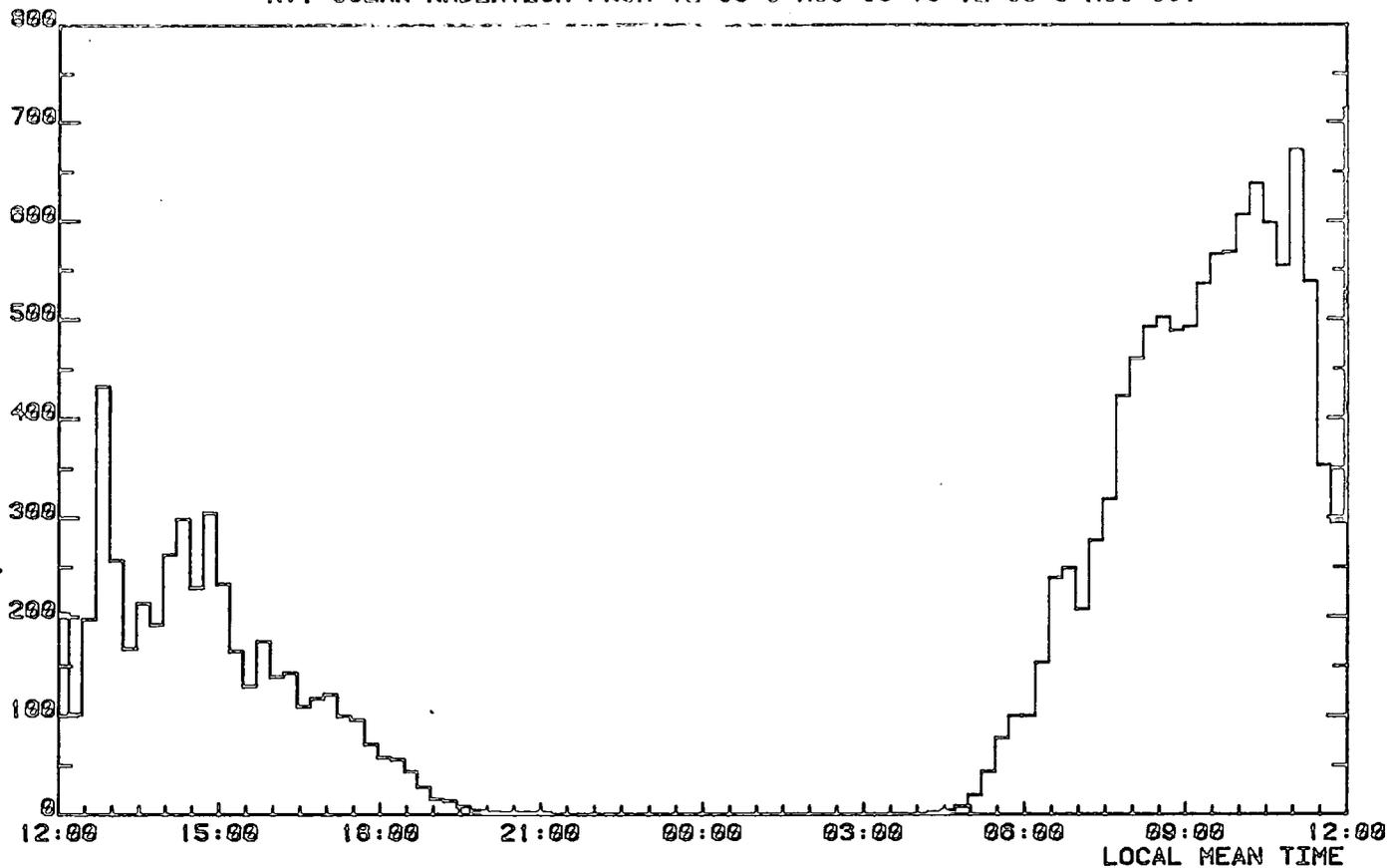
Fig. 6.4   WEATHER DATA RECORDED AT DURHAM OBSERVATORY
            AV. WINDSPEED FROM 12:00 5-AUG-83 TO 12:00 6-AUG-83.

LOCAL MEAN TIME
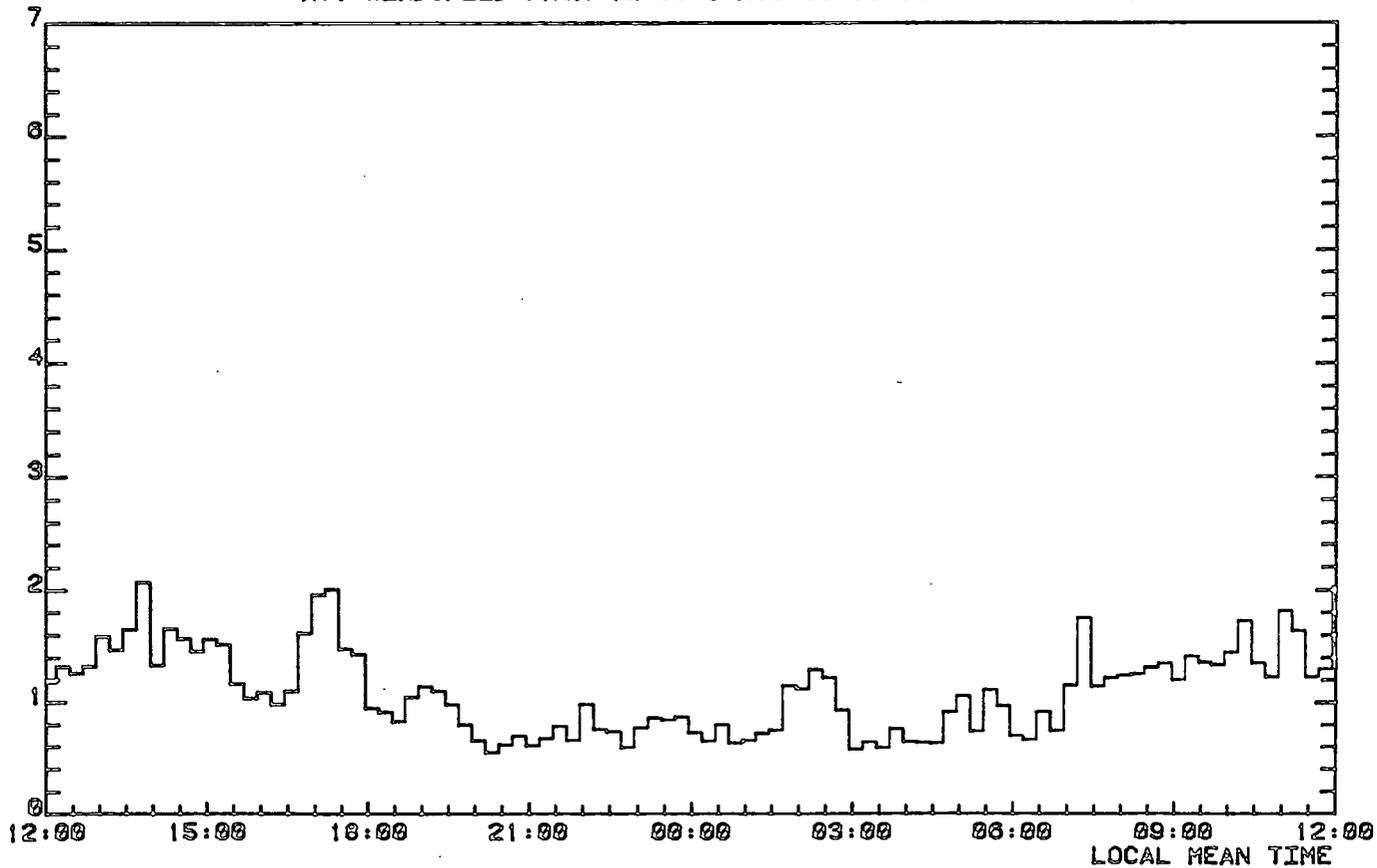
Fig. 6.5   WEATHER DATA RECORDED AT DURHAM OBSERVATORY
            AIR TEMPERATURE FROM 12:00 5-AUG-83 TO 12:00 6-AUG-83.
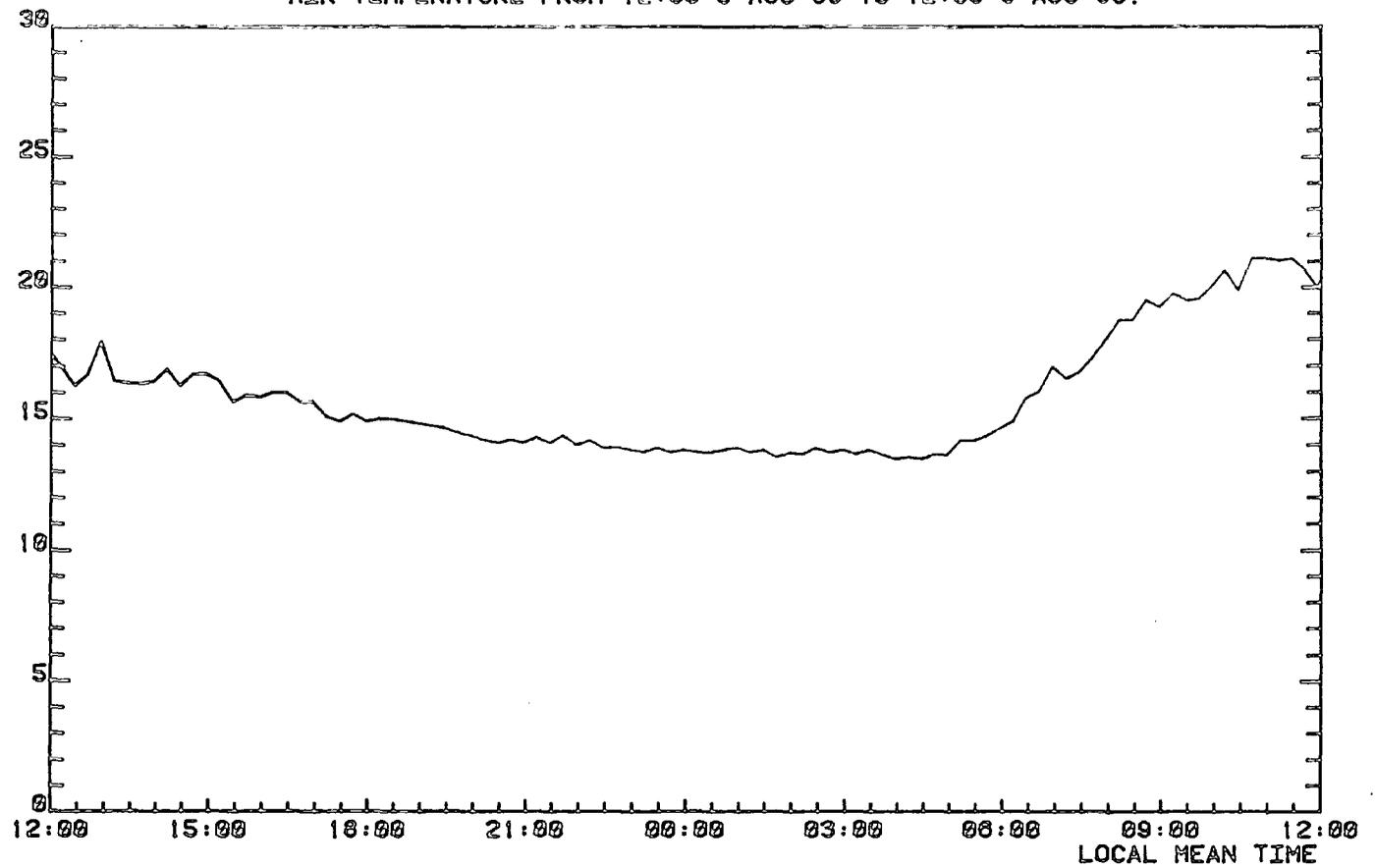
Fig. 6.6   WEATHER DATA RECORDED AT DURHAM OBSERVATORY
            WET/DRY BULB DEPRESSION FROM 12:00 5-AUG-83 TO 12:00 6-AUG-83.
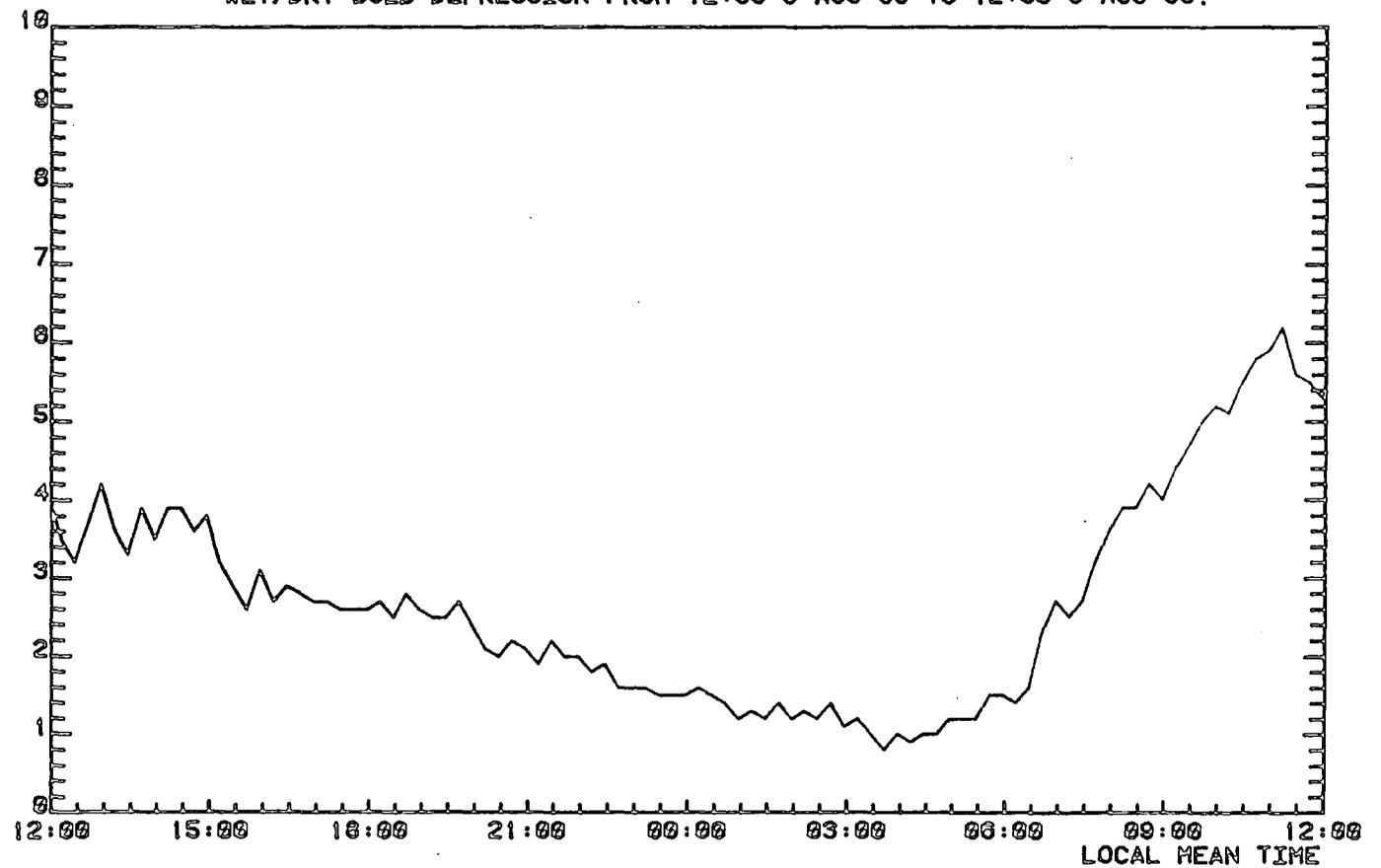
Fig. 6.7 WEATHER DATA RECORDED AT DURHAM OBSERVATORY
AV. SOLAR RADIATION FROM 12:00 6-AUG-83 TO 12:00 7-AUG-83.
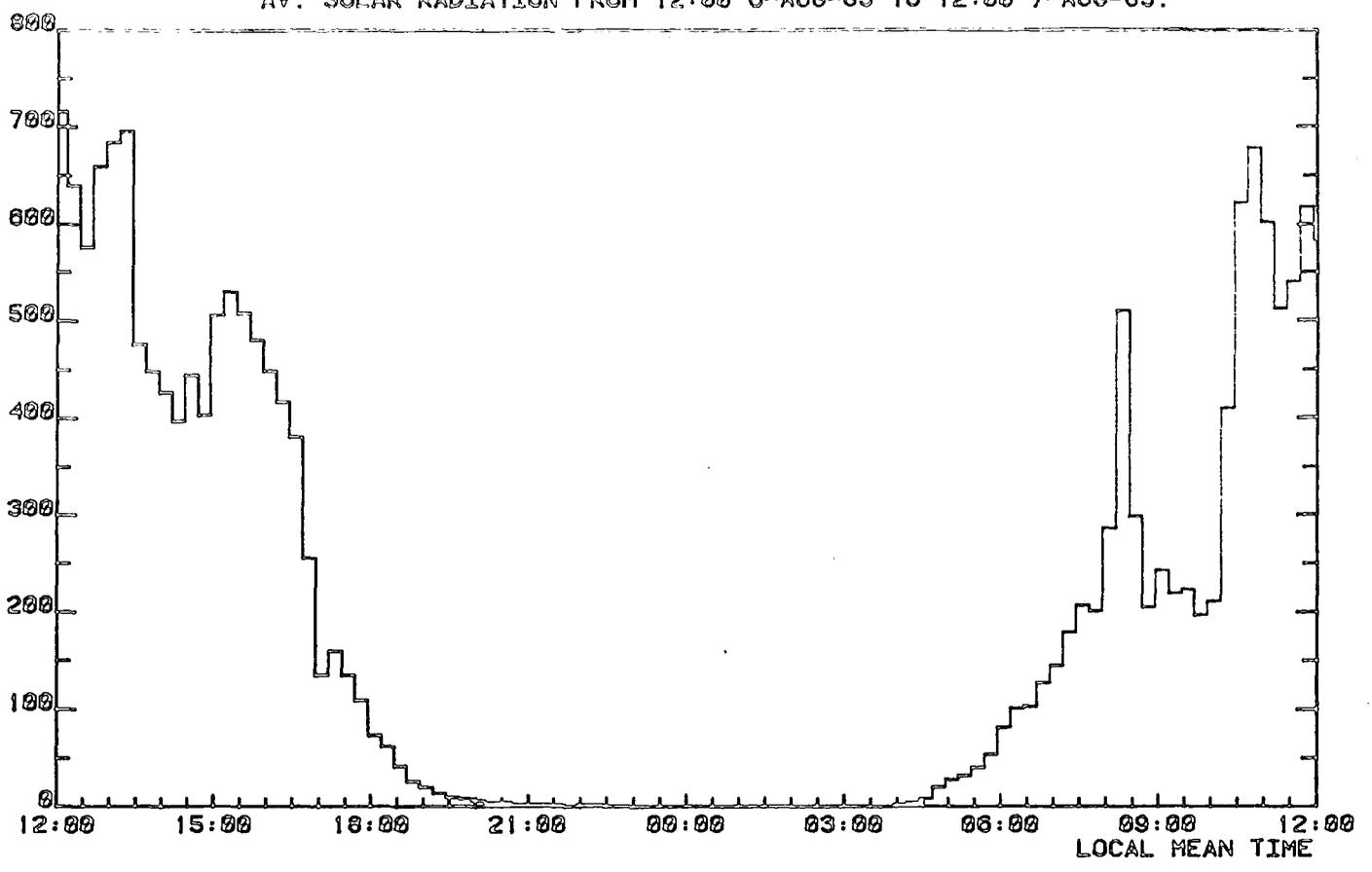
Fig. 6.8 WEATHER DATA RECORDED AT DURHAM OBSERVATORY
AV. WINDSPEED FROM 12:00 6-AUG-83 TO 12:00 7-AUG-83.
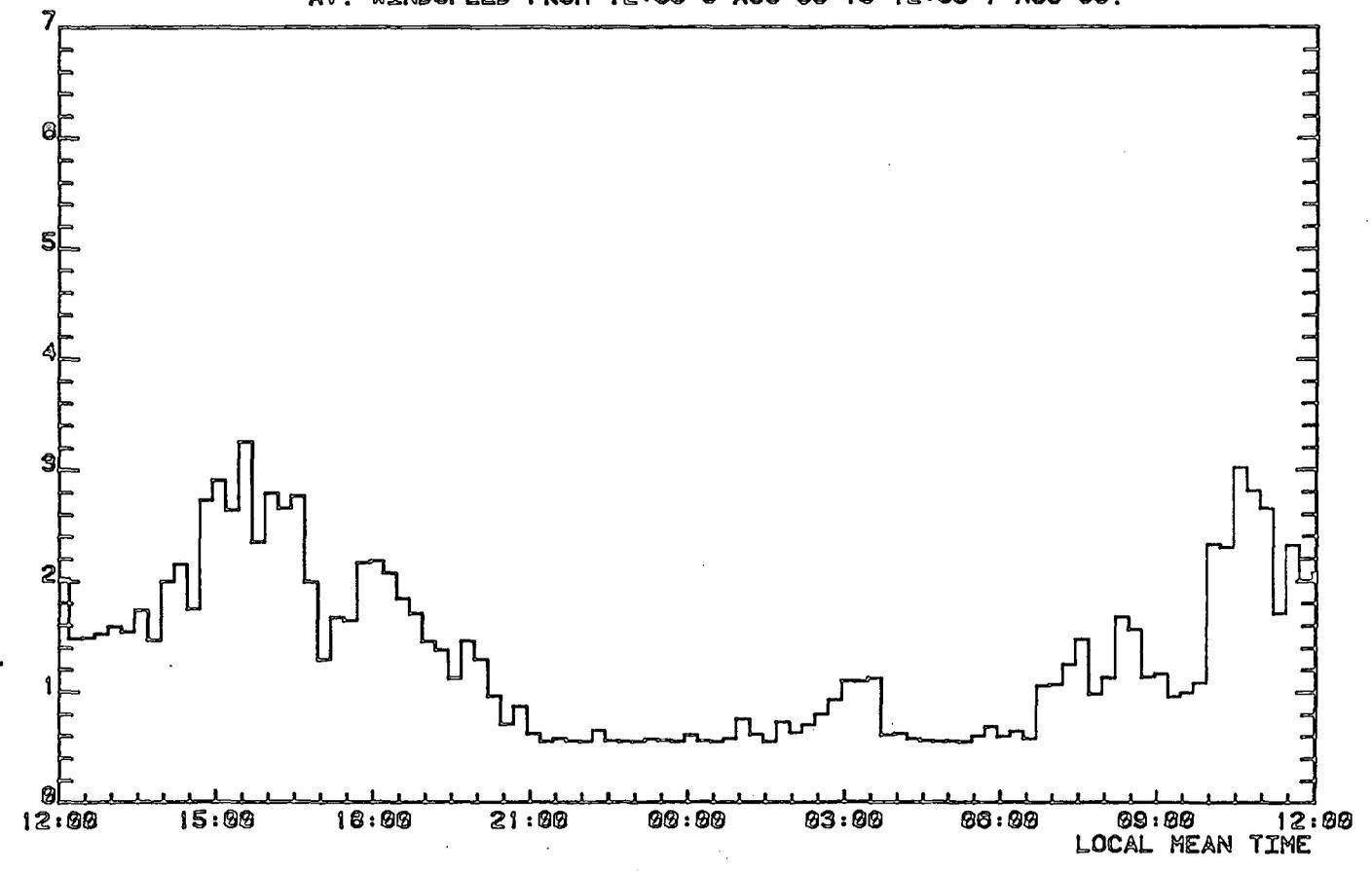
Fig. 6.9   WEATHER DATA RECORDED AT DURHAM OBSERVATORY
            AIR TEMPERATURE FROM 12:00 6-AUG-83 TO 12:00 7-AUG-83.
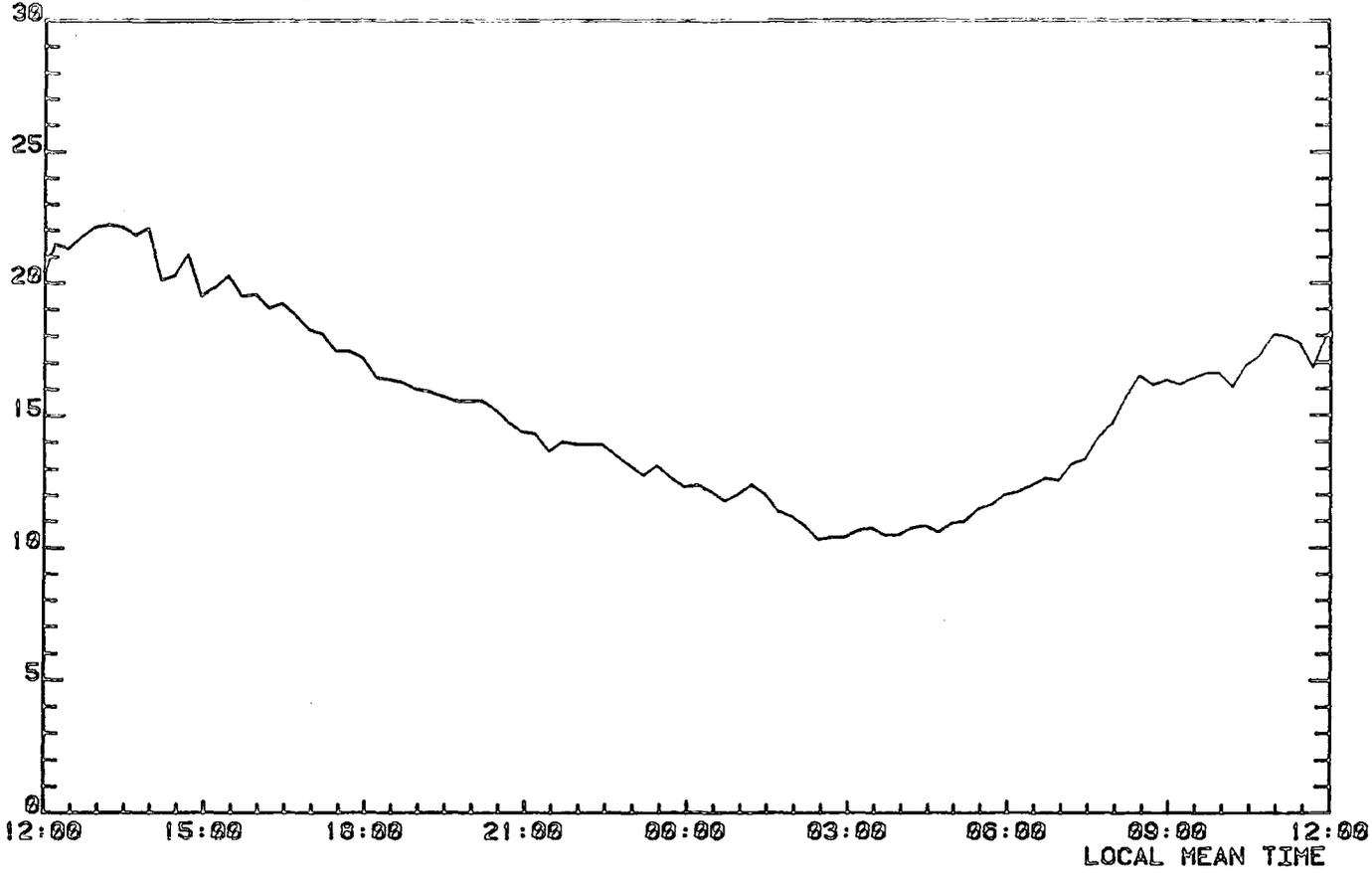
Fig. 6.10   WEATHER DATA RECORDED AT DURHAM OBSERVATORY
            WET/DRY BULB DEPRESSION FROM 12:00 6-AUG-83 TO 12:00 7-AUG-83.
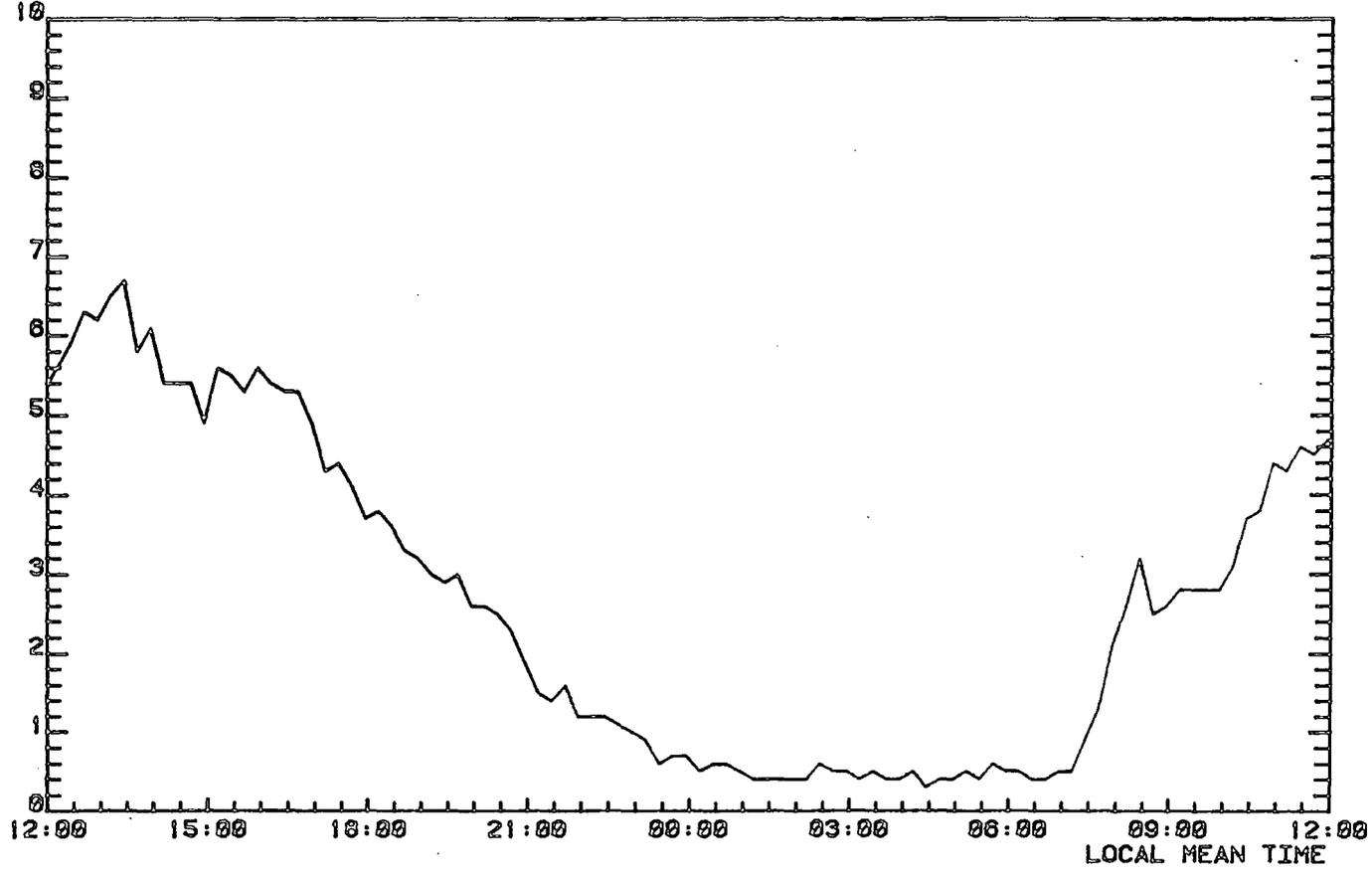
Fig. 6.11　　　WEATHER DATA RECORDED AT DURHAM OBSERVATORY
　　　　　　　AV. SOLAR RADIATION FROM 12:00 7-AUG-83 TO 12:00 8-AUG-83.
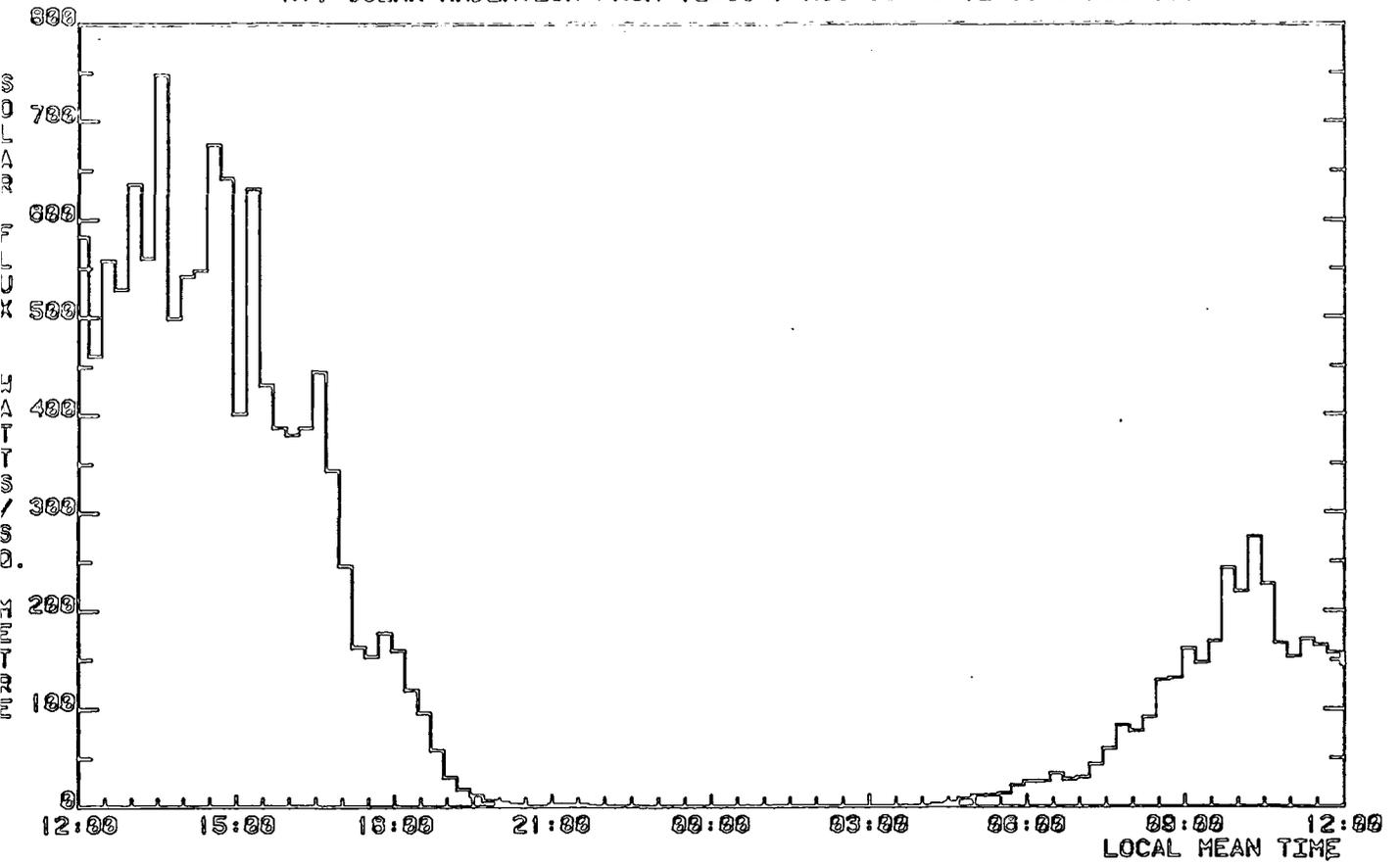
Fig. 6.12　　　WEATHER DATA RECORDED AT DURHAM OBSERVATORY
　　　　　　　AV. WINDSPEED FROM 12:00 7-AUG-83 TO 12:00 8-AUG-83.
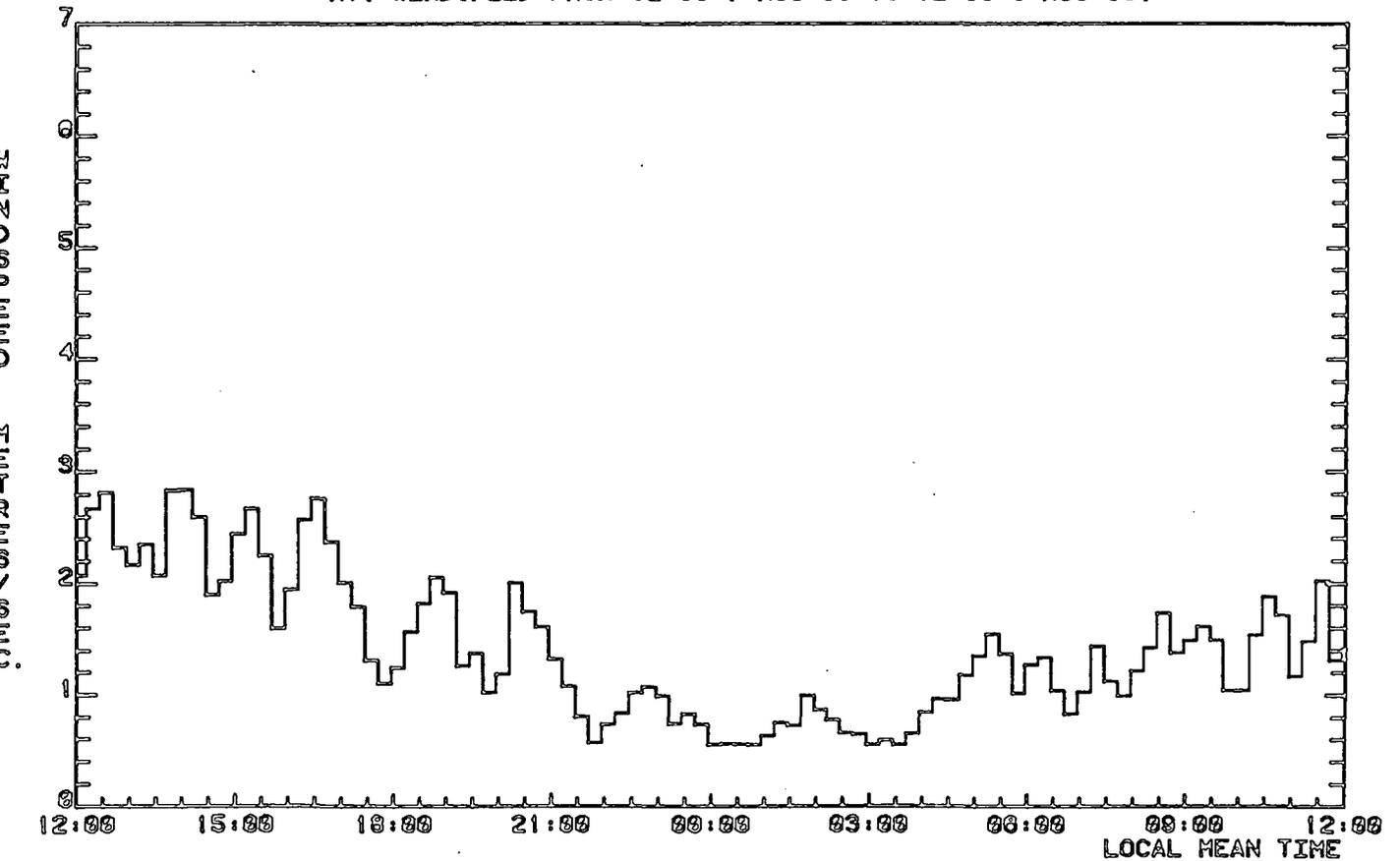
Fig. 6.13   WEATHER DATA RECORDED AT DURHAM OBSERVATORY
AIR TEMPERATURE FROM 12:00 7-AUG-83 TO 12:00 8-AUG-83.
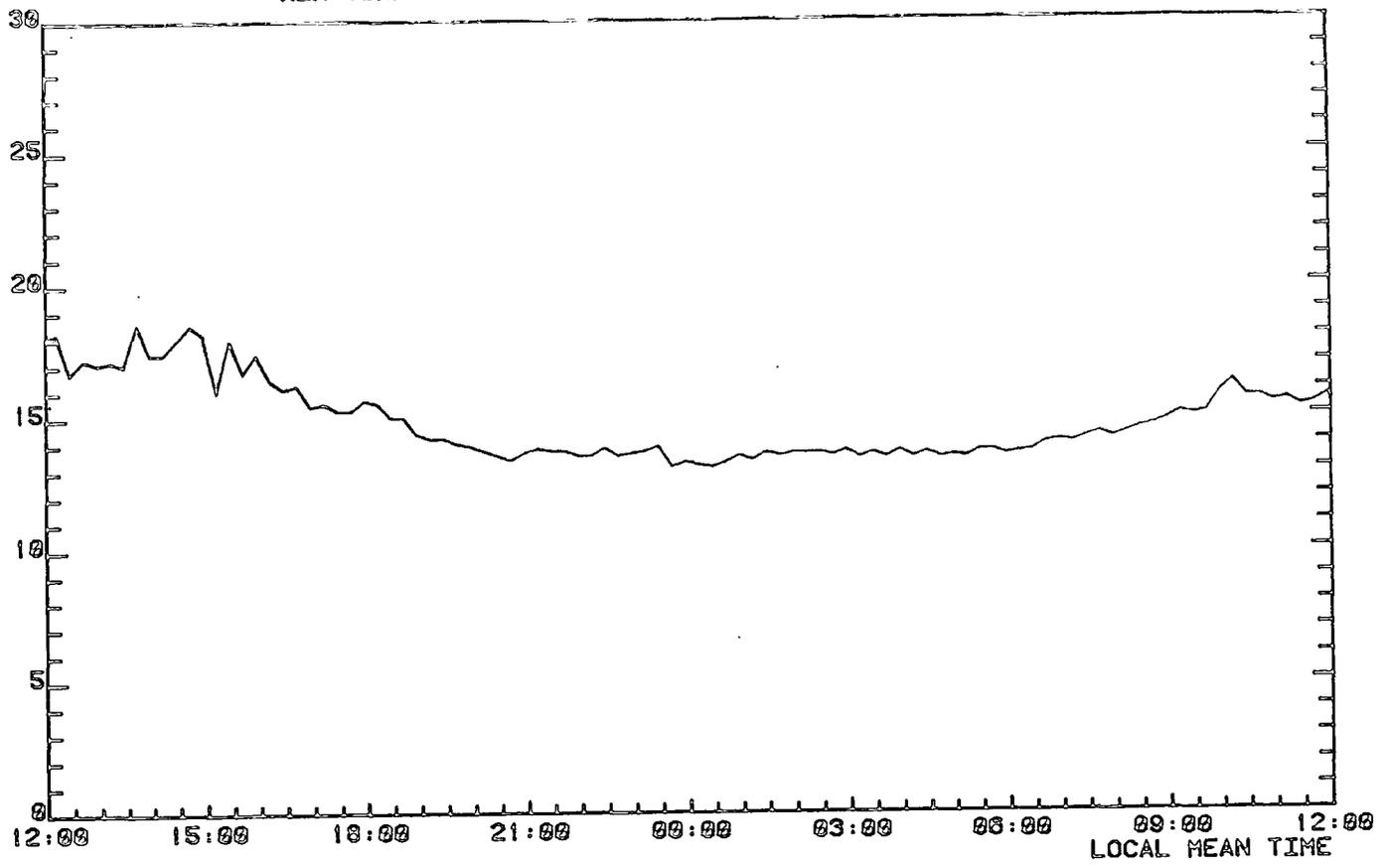
Fig. 6.14   WEATHER DATA RECORDED AT DURHAM OBSERVATORY
WET/DRY BULB DEPRESSION FROM 12:00 7-AUG-83 TO 12:00 8-AUG-83.
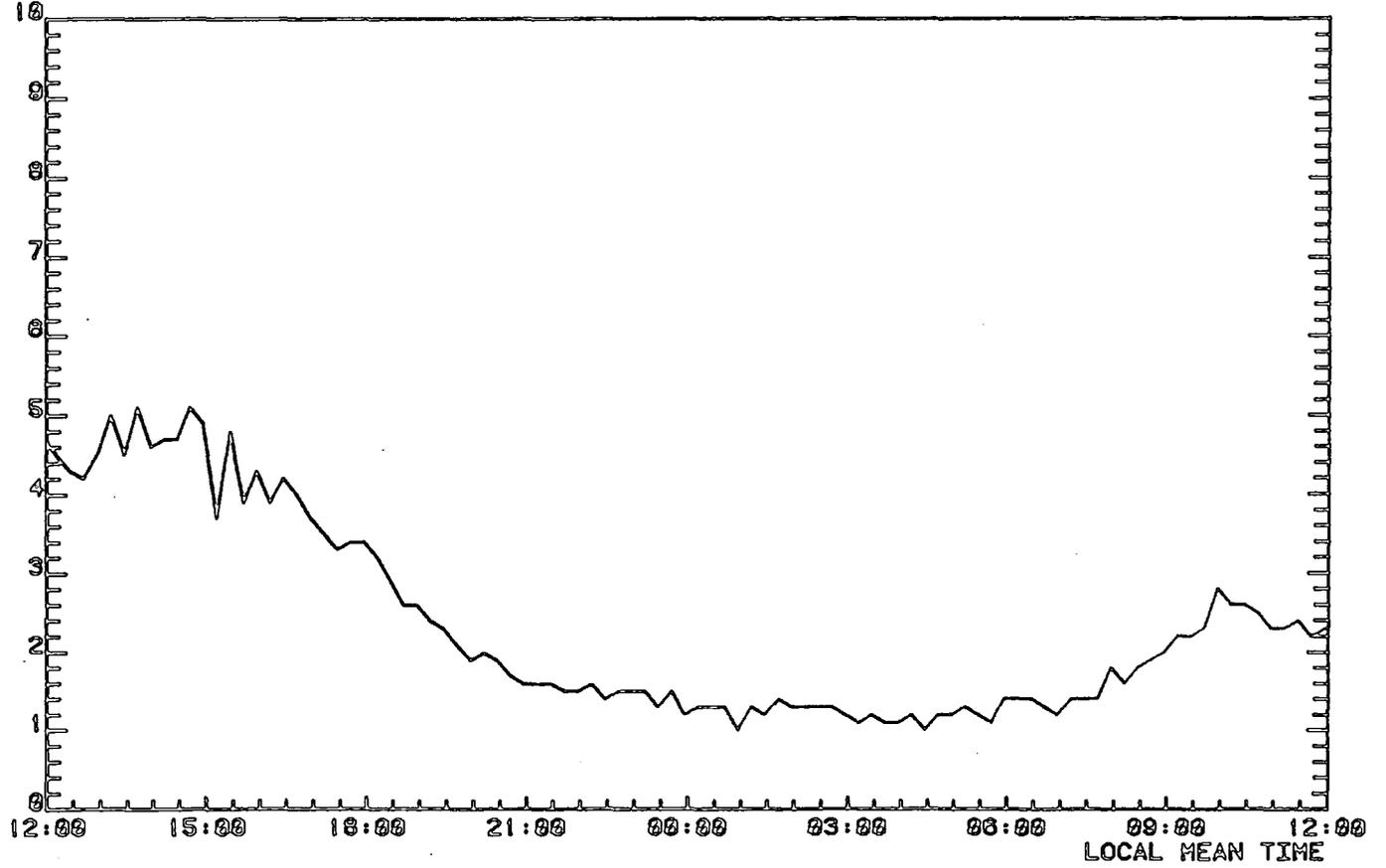
Fig. 6.15   WEATHER DATA RECORDED AT DURHAM OBSERVATORY
             AV. SOLAR RADIATION FROM 12:00 8-AUG-83 TO 12:00 9-AUG-83.
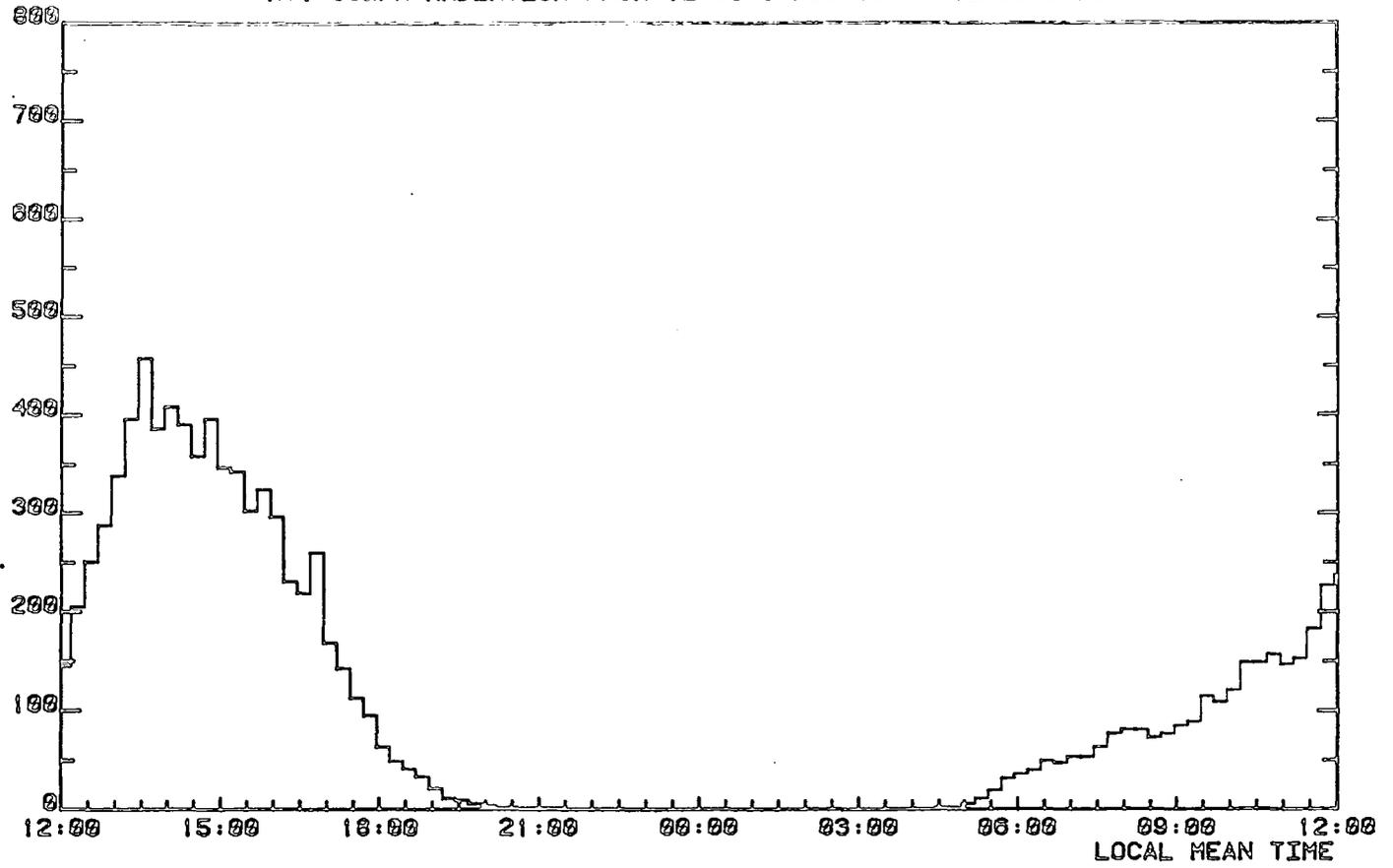
Fig. 6.16   WEATHER DATA RECORDED AT DURHAM OBSERVATORY
             AV. WINDSPEED FROM 12:00 8-AUG-83 TO 12:00 9-AUG-83.
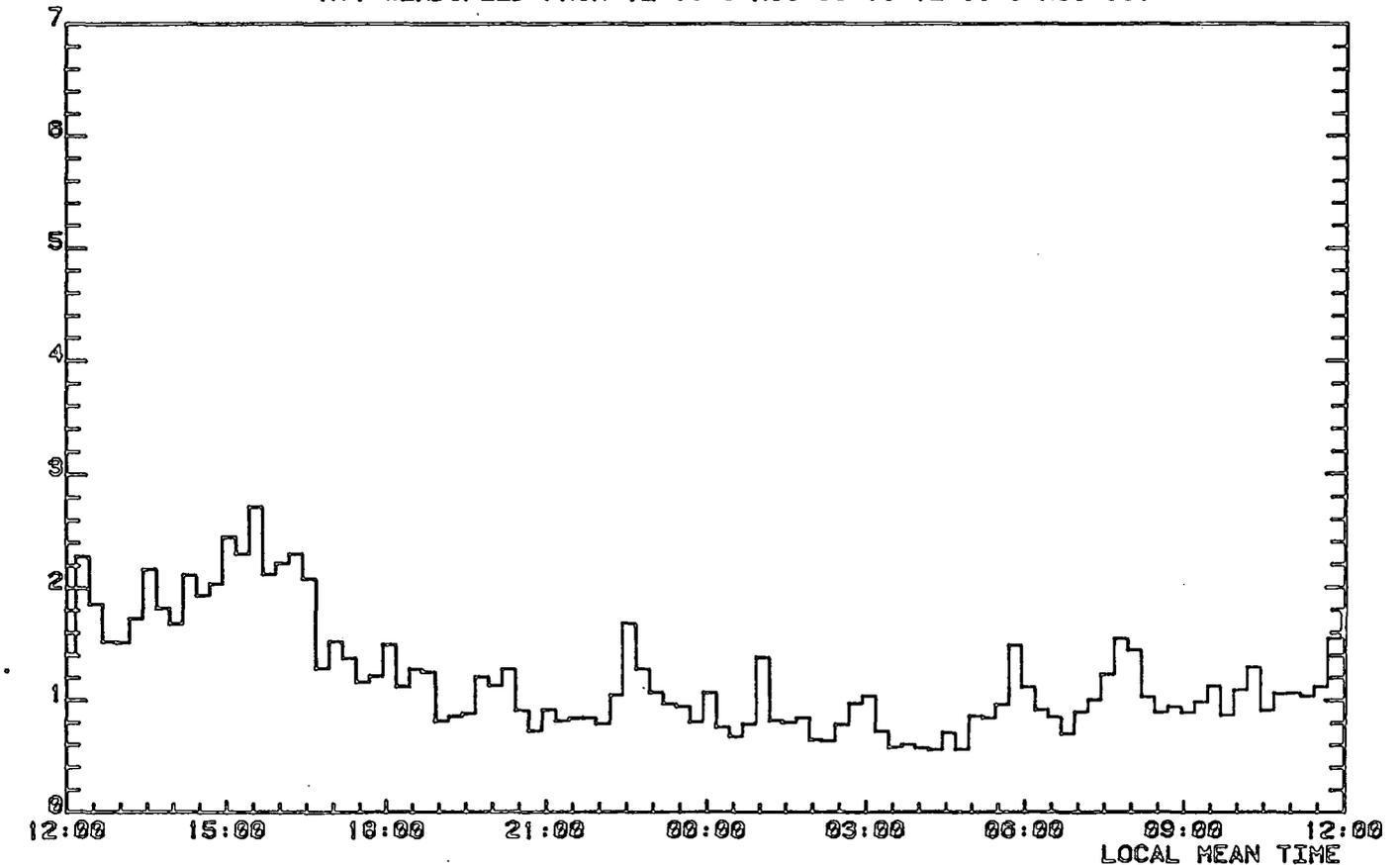
Fig. 6.17   WEATHER DATA RECORDED AT DURHAM OBSERVATORY
             AIR TEMPERATURE FROM 12:00 8-AUG-83 TO 12:00 9-AUG-83.

LOCAL MEAN TIME
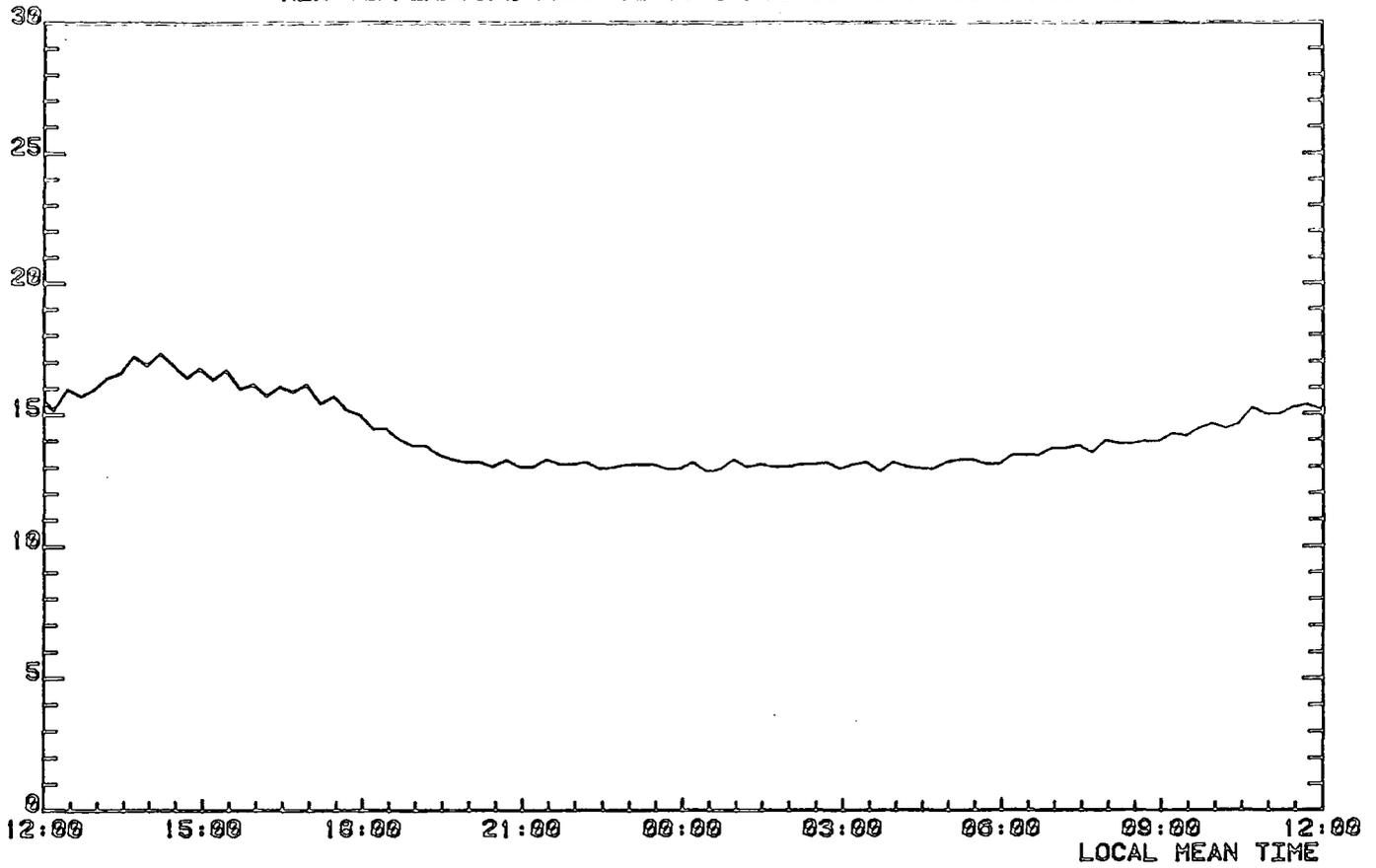
Fig. 6.18   WEATHER DATA RECORDED AT DURHAM OBSERVATORY
             WET/DRY BULB DEPRESSION FROM 12:00 8-AUG-83 TO 12:00 9-AUG-83.

LOCAL MEAN TIME
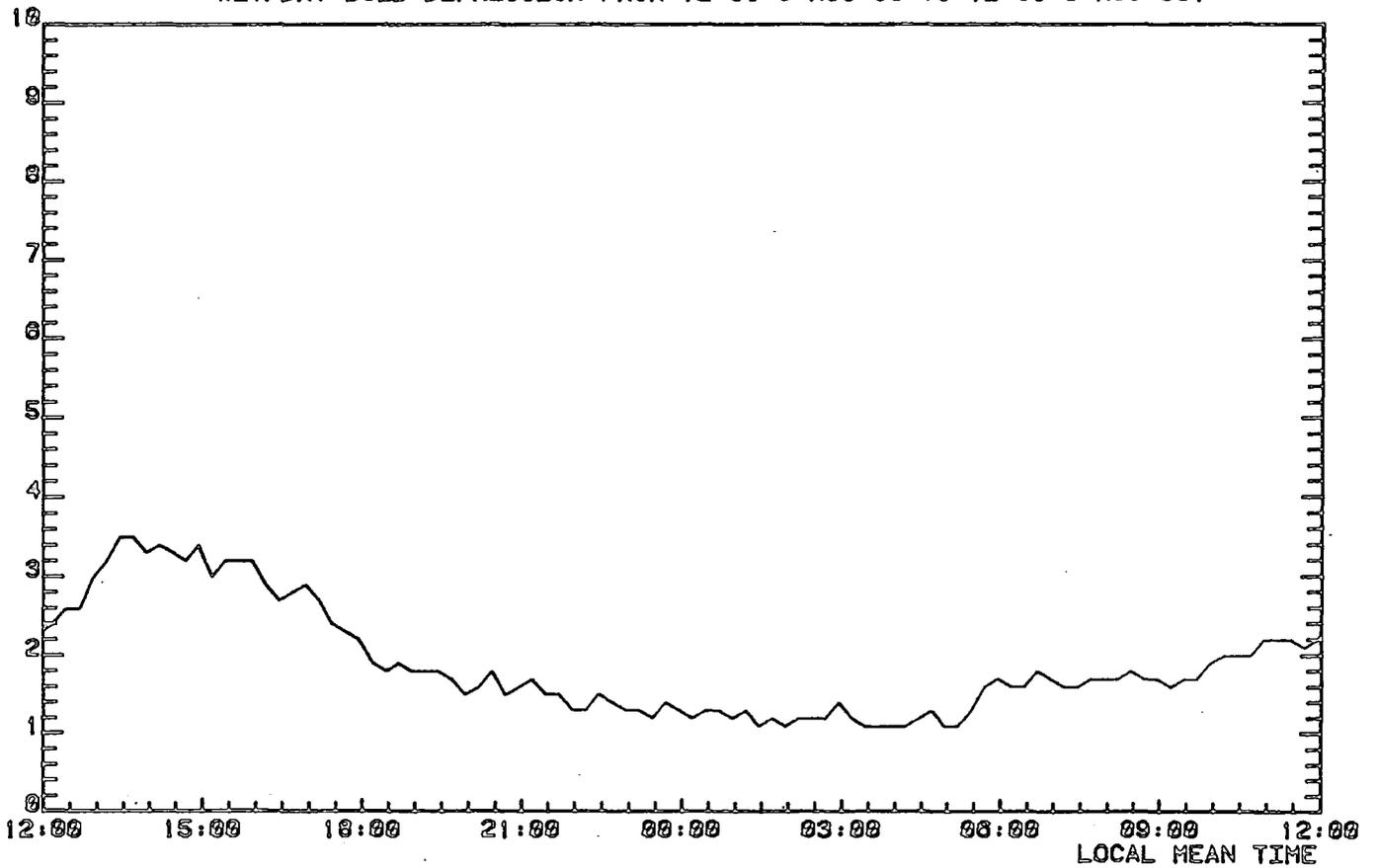
Fig. 6.19   WEATHER DATA RECORDED AT DURHAM OBSERVATORY
             AV. SOLAR RADIATION FROM 12:00 8-AUG-83 TO 12:00 10-AUG-83.
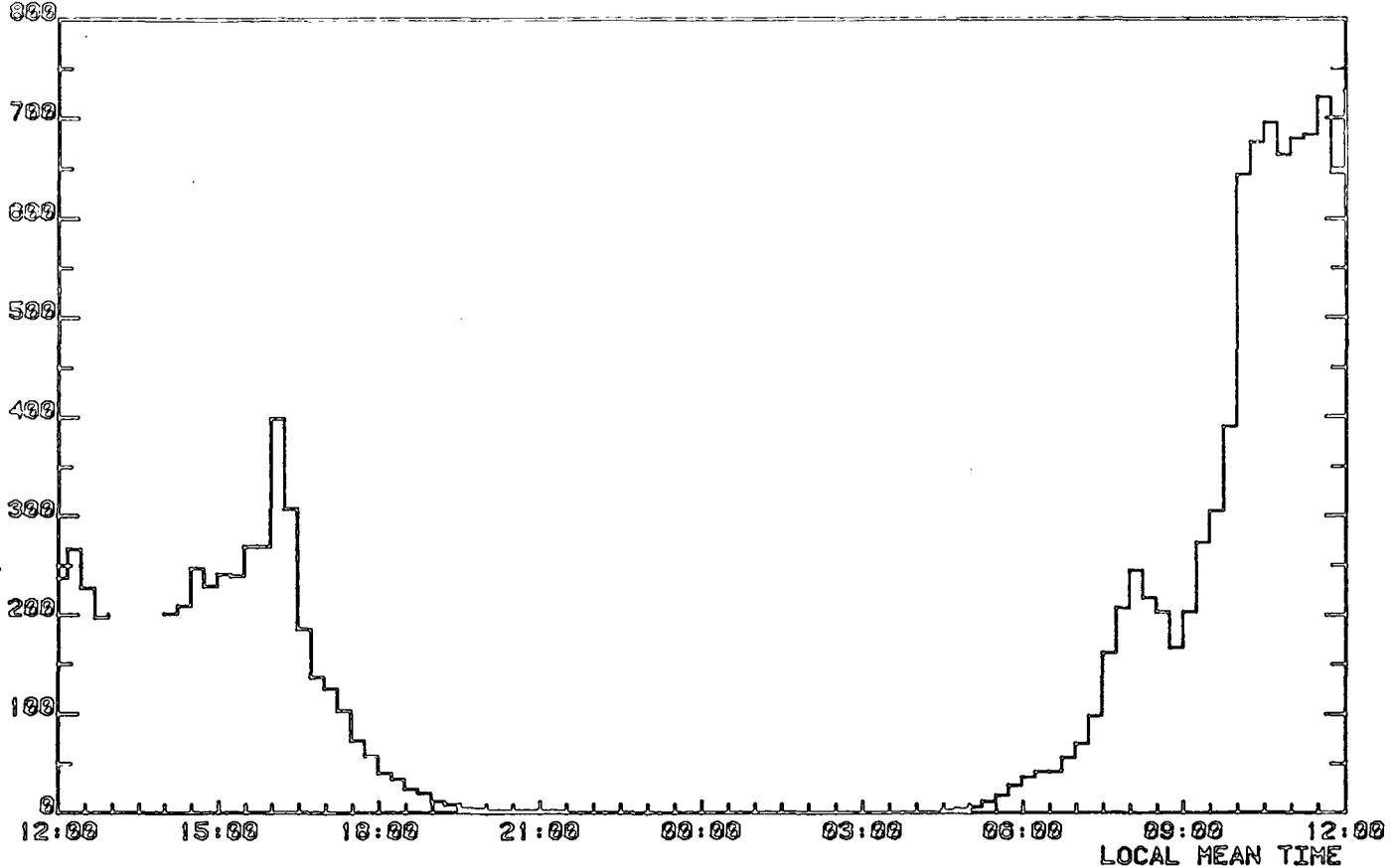
Fig. 6.20   WEATHER DATA RECORDED AT DURHAM OBSERVATORY
                 AV. WINDSPEED FROM 12:00 8-AUG-83 TO 12:00 10-AUG-83.
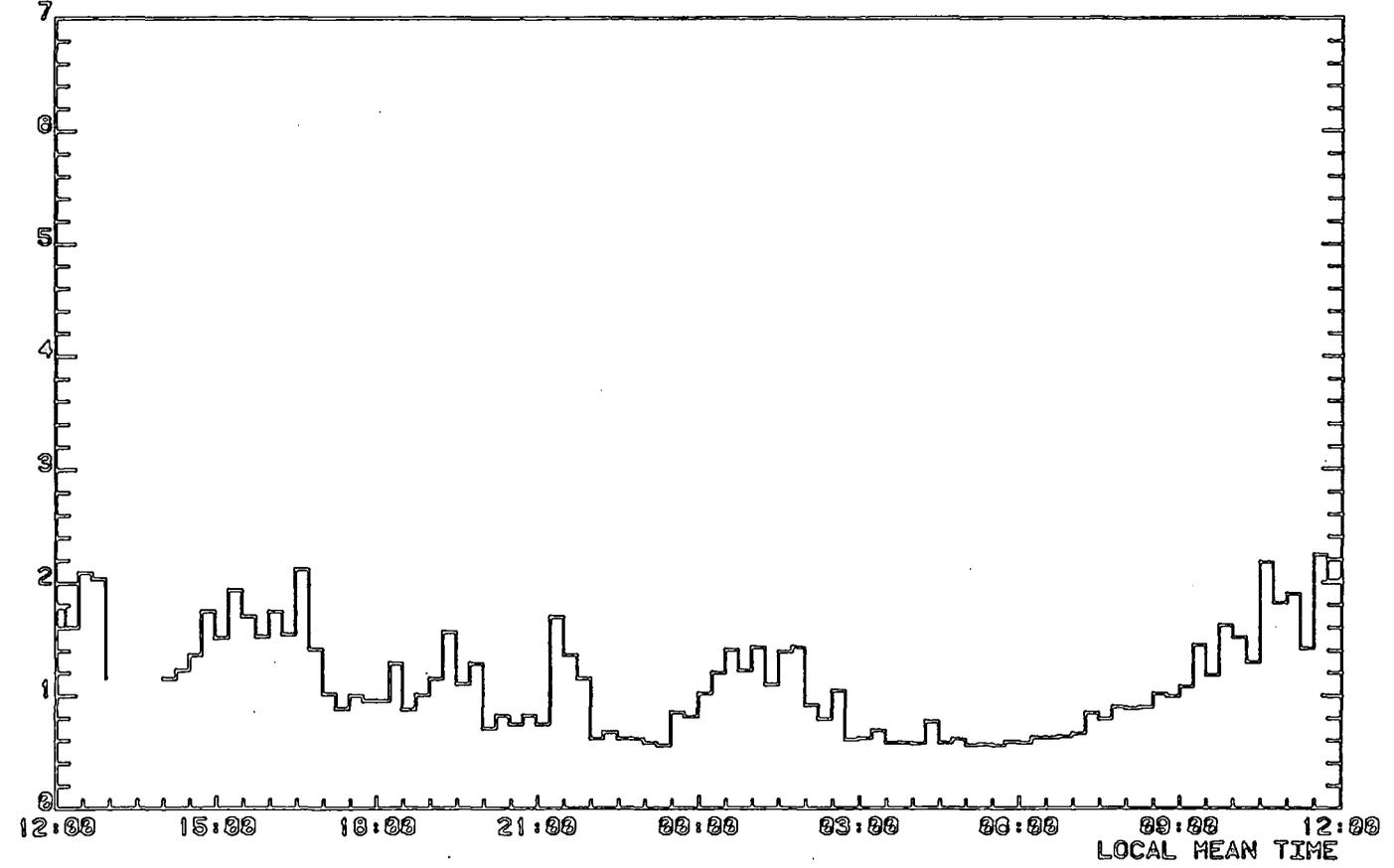
Fig. 6.21   WEATHER DATA RECORDED AT DURHAM OBSERVATORY
AIR TEMPERATURE FROM 12:00 9-AUG-83 TO 12:00 10-AUG-83.
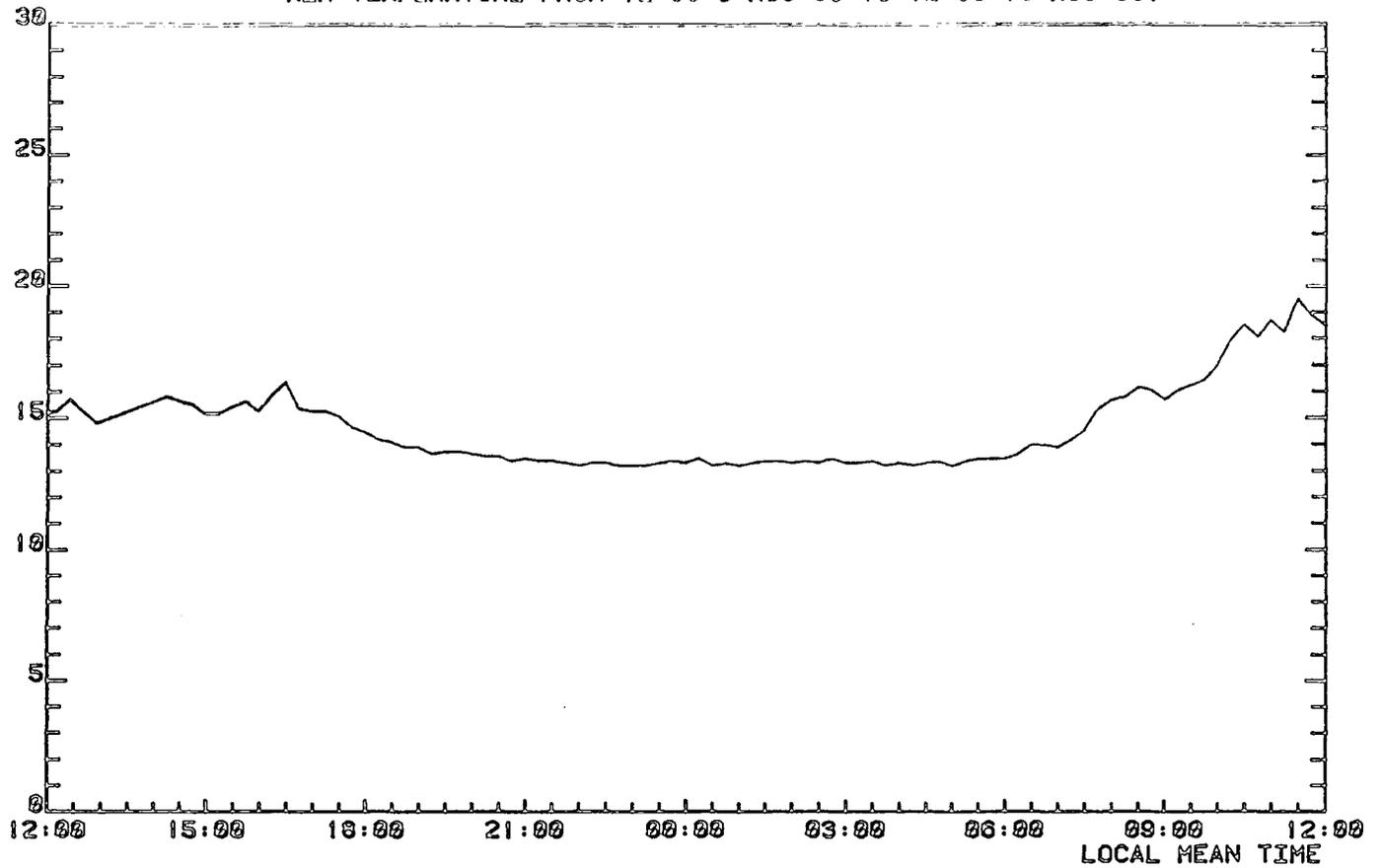
Fig. 6.22   WEATHER DATA RECORDED AT DURHAM OBSERVATORY
WET/DRY BULB DEPRESSION FROM 12:00 9-AUG-83 TO 12:00 10-AUG-83.
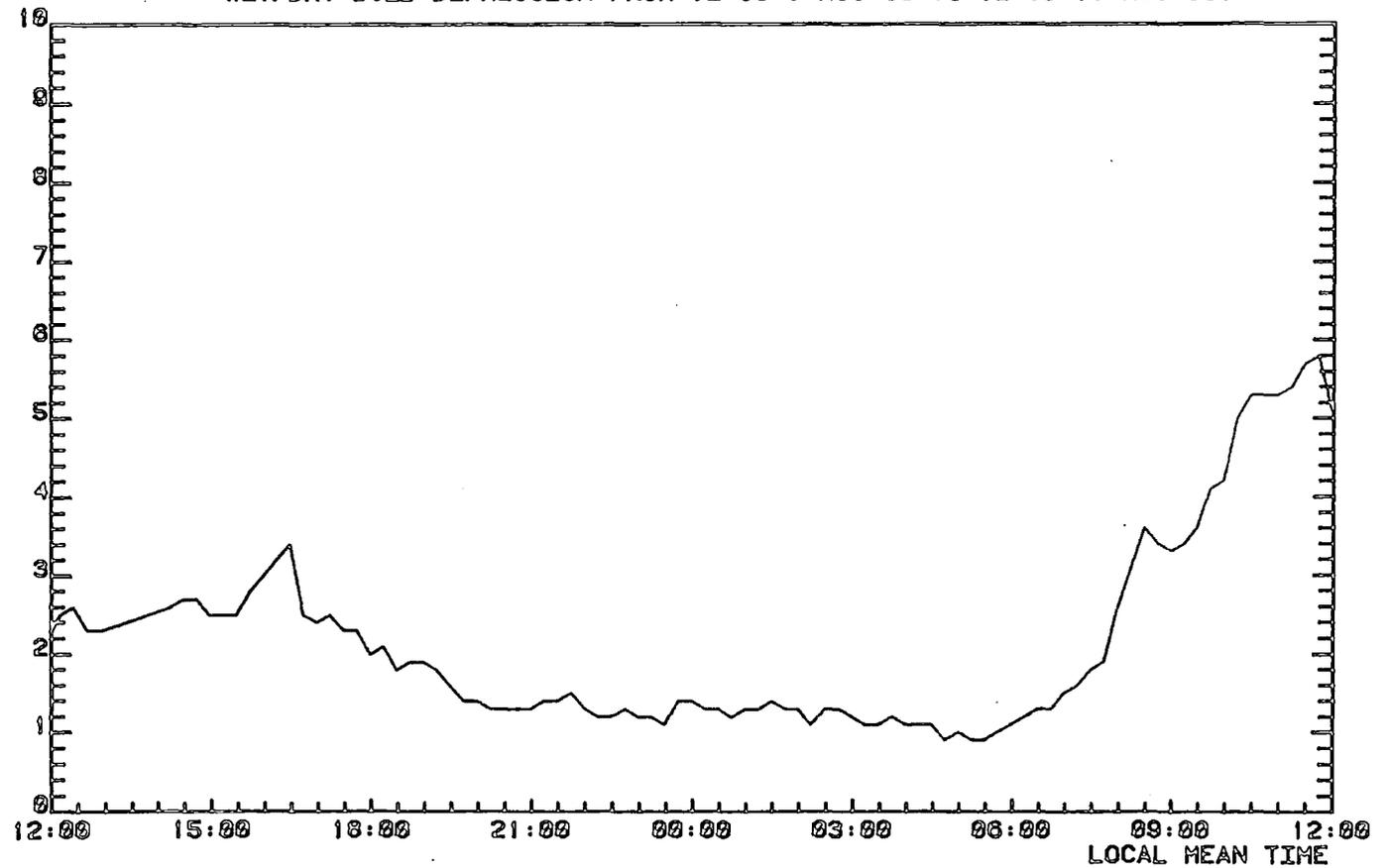
Fig. 6.23   WEATHER DATA RECORDED AT DURHAM OBSERVATORY
             AV. SOLAR RADIATION FROM 12:00 10-AUG-83 TO 12:00 11-AUG-83.
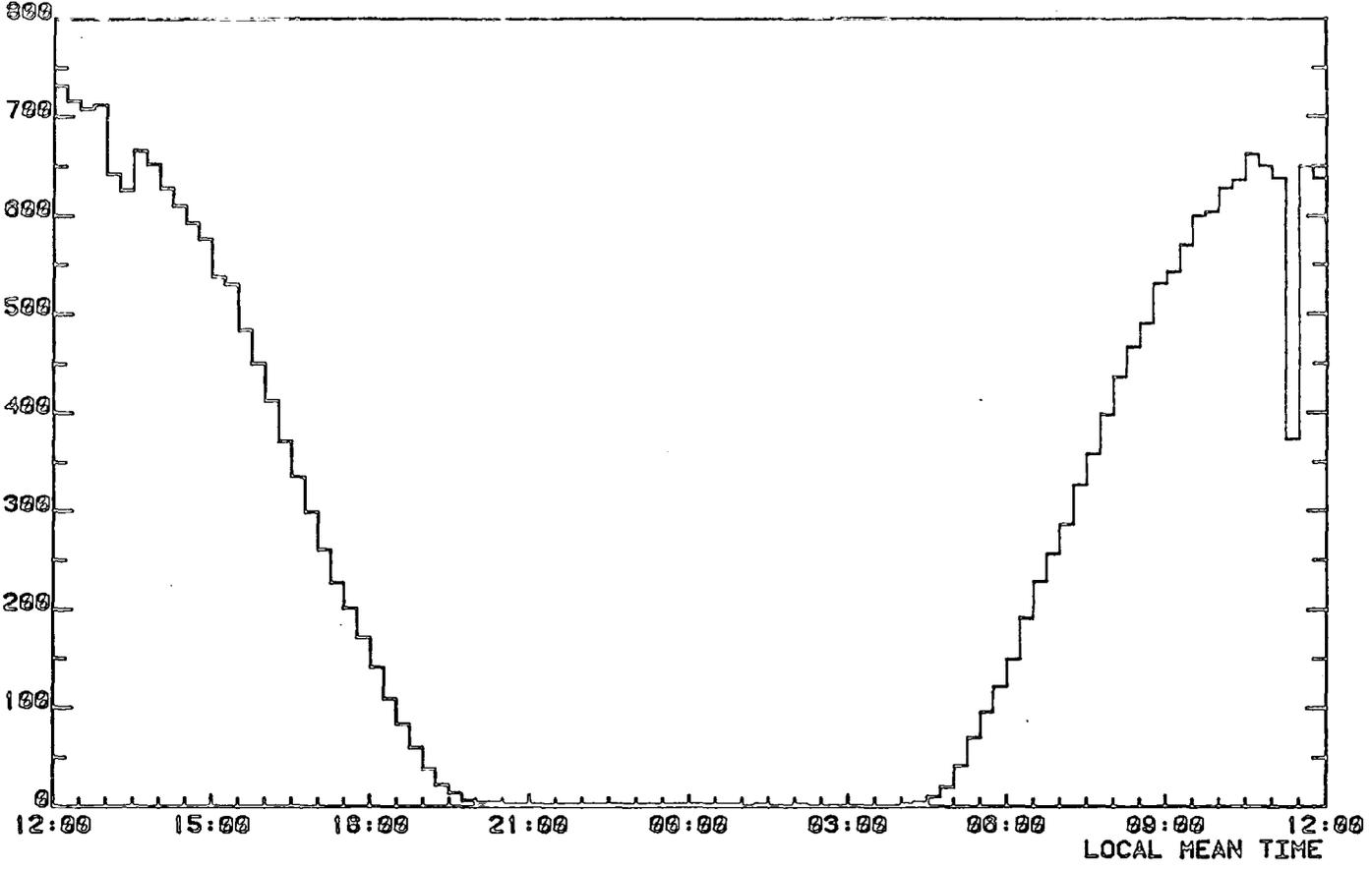
Fig. 6.24   WEATHER DATA RECORDED AT DURHAM OBSERVATORY
             AV. WINDSPEED FROM 12:00 10-AUG-83 TO 12:00 11-AUG-83.
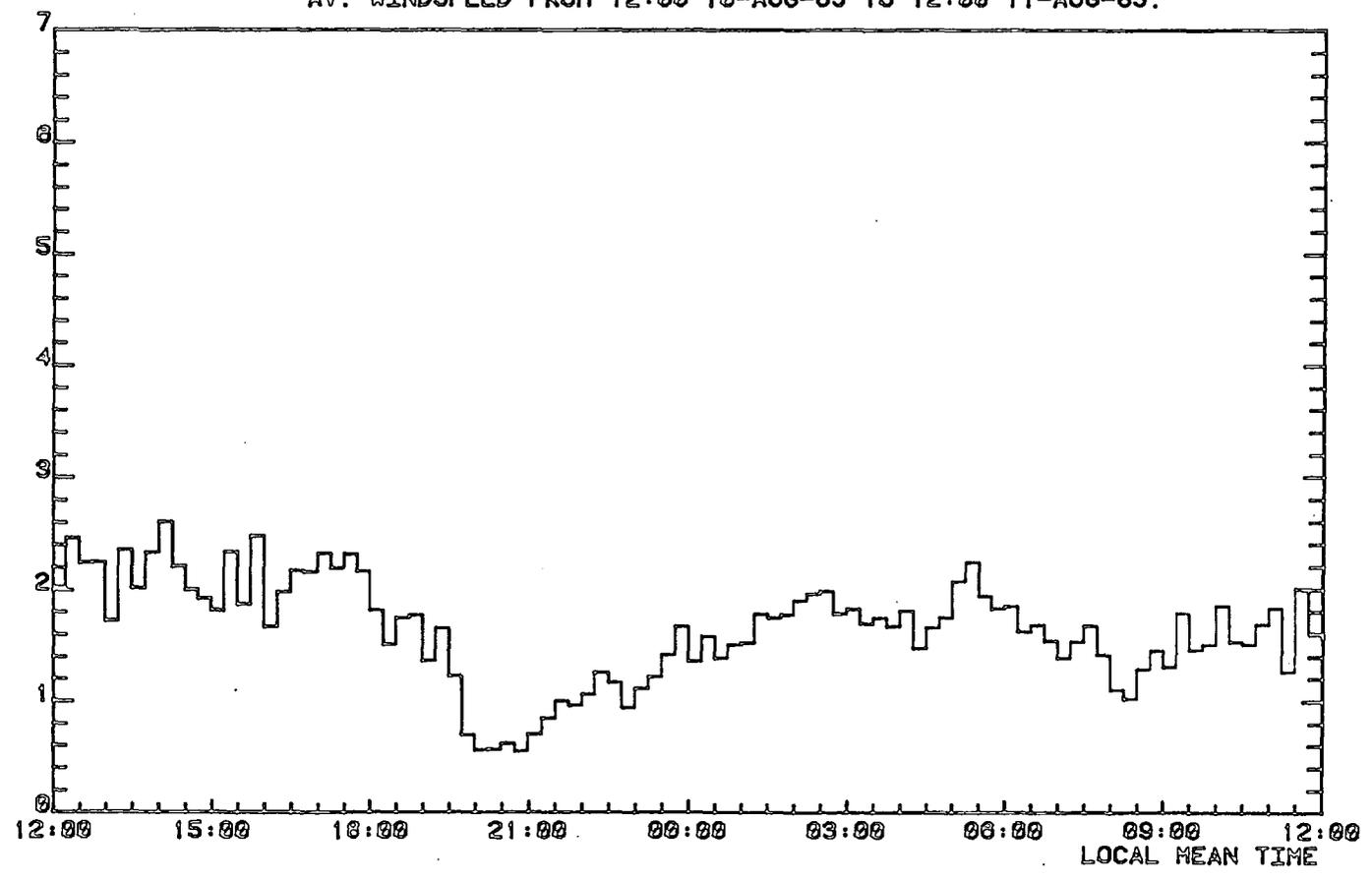
Fig. 6.25   WEATHER DATA RECORDED AT DURHAM OBSERVATORY
AIR TEMPERATURE FROM 12:00 10-AUG-83 TO 12:00 11-AUG-83.
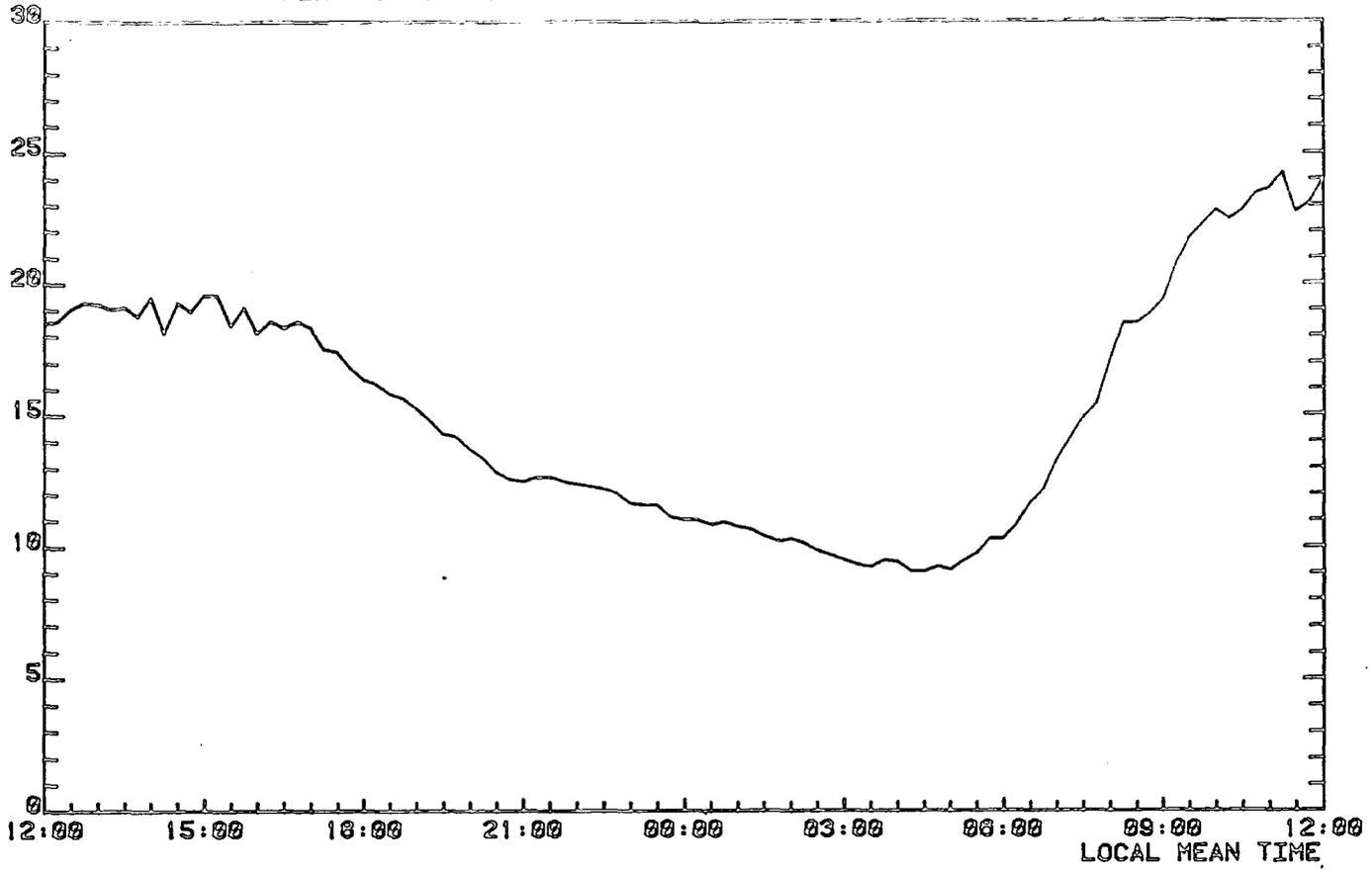
Fig. 6.26   WEATHER DATA RECORDED AT DURHAM OBSERVATORY
WET/DRY BULB DEPRESSION FROM 12:00 10-AUG-83 TO 12:00 11-AUG-83.
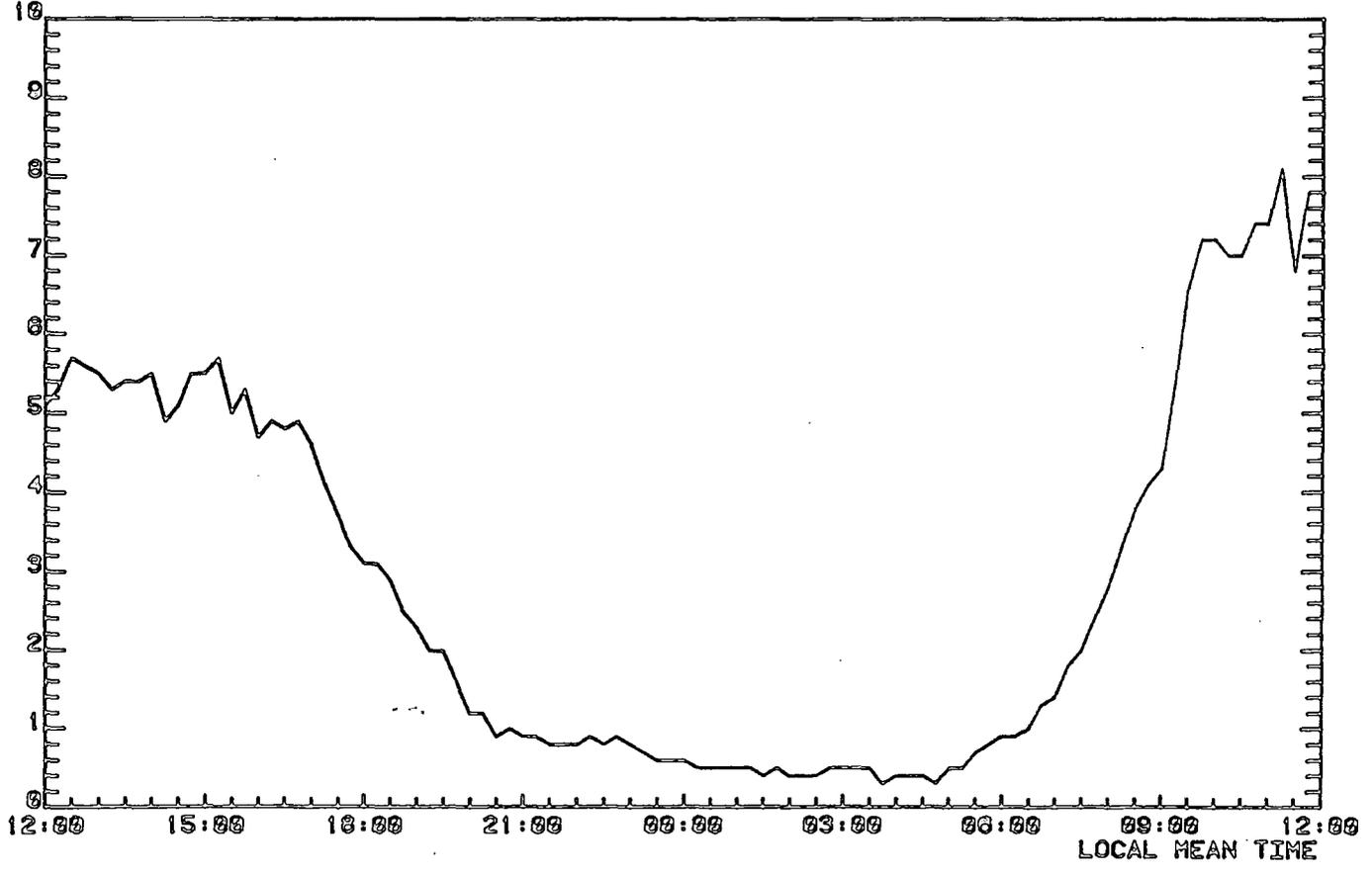
Fig. 6.27   WEATHER DATA RECORDED AT DURHAM OBSERVATORY
              AV. SOLAR RADIATION FROM 12:00 11-AUG-83 TO 12:00 12-AUG-83.
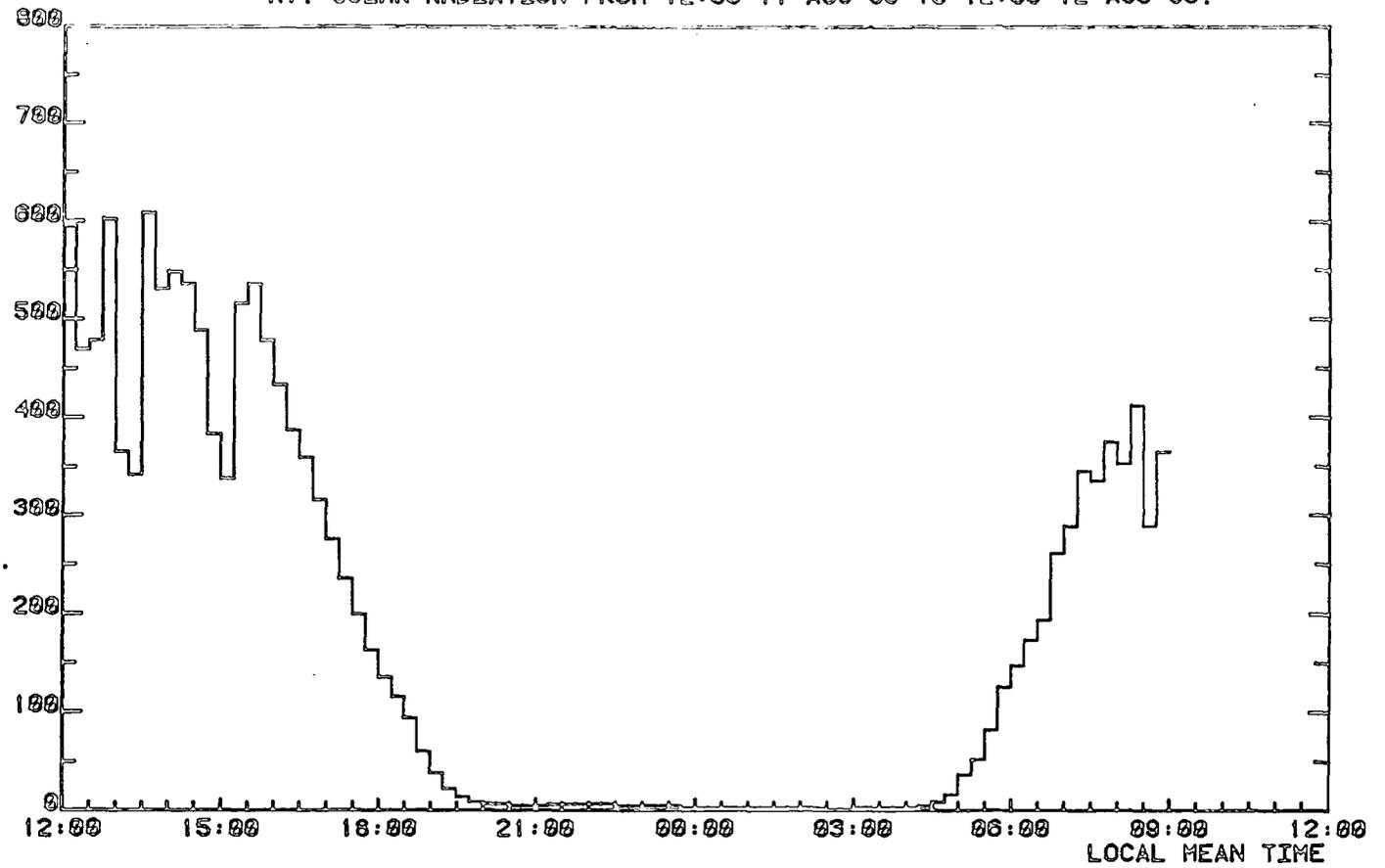
Fig. 6.28   WEATHER DATA RECORDED AT DURHAM OBSERVATORY
                   AV. WINDSPEED FROM 12:00 11-AUG-83 TO 12:00 12-AUG-83.
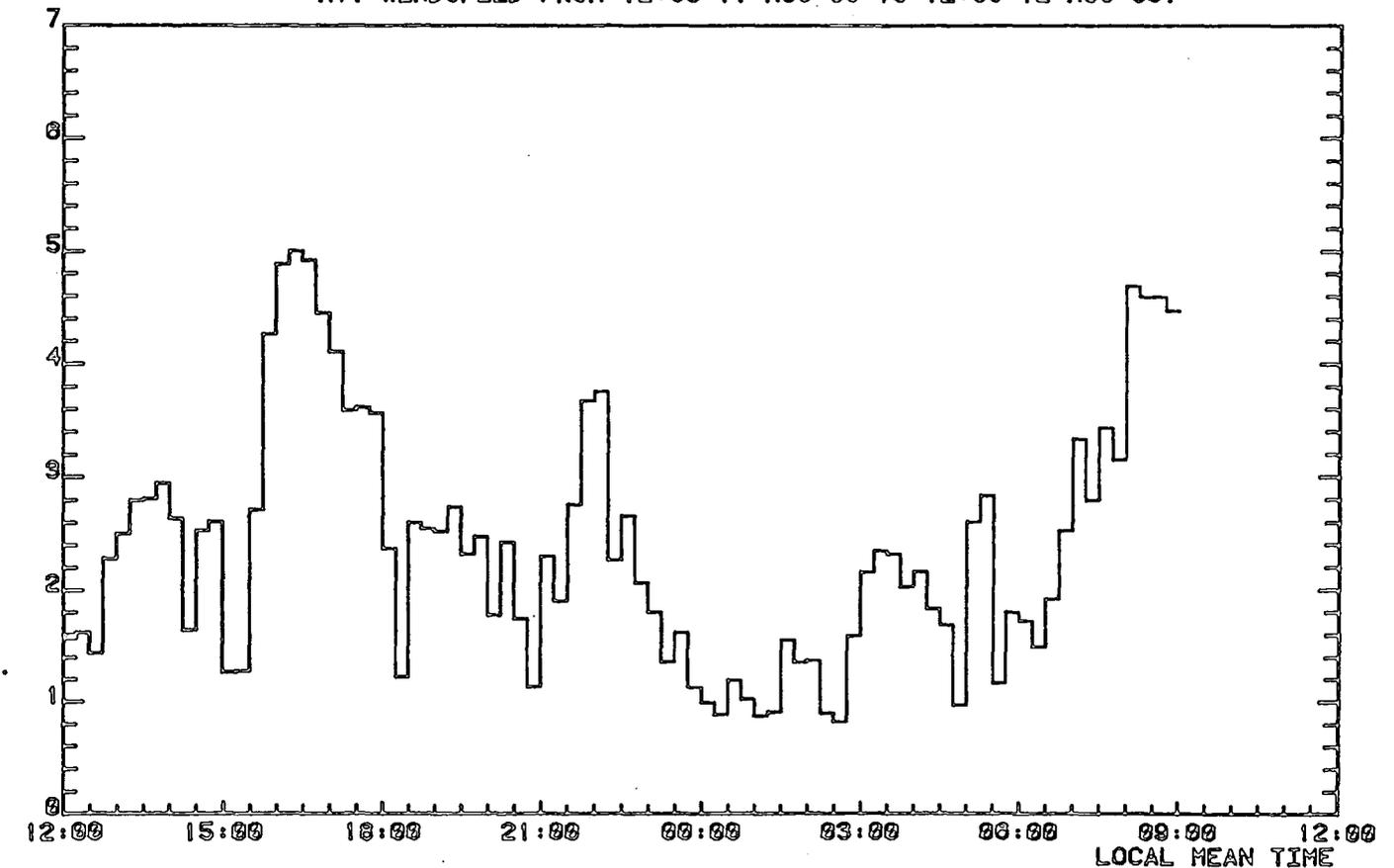
Fig. 6.29 WEATHER DATA RECORDED AT DURHAM OBSERVATORY
AIR TEMPERATURE FROM 12:00 11-AUG-83 TO 12:00 12-AUG-83.
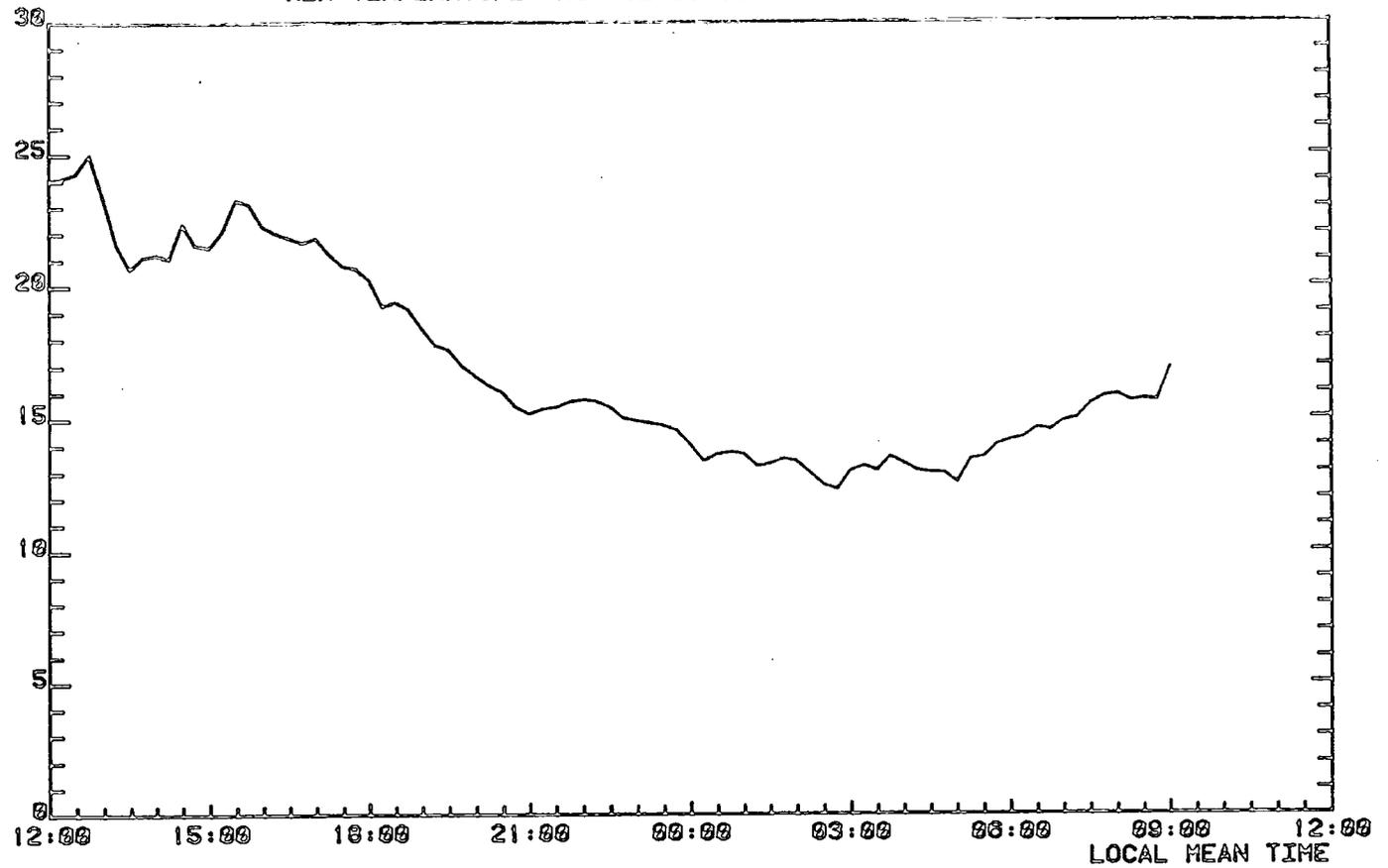
Fig. 6.30 WEATHER DATA RECORDED AT DURHAM OBSERVATORY
WET/DRY BULB DEPRESSION FROM 12:00 11-AUG-83 TO 12:00 12-AUG-83.
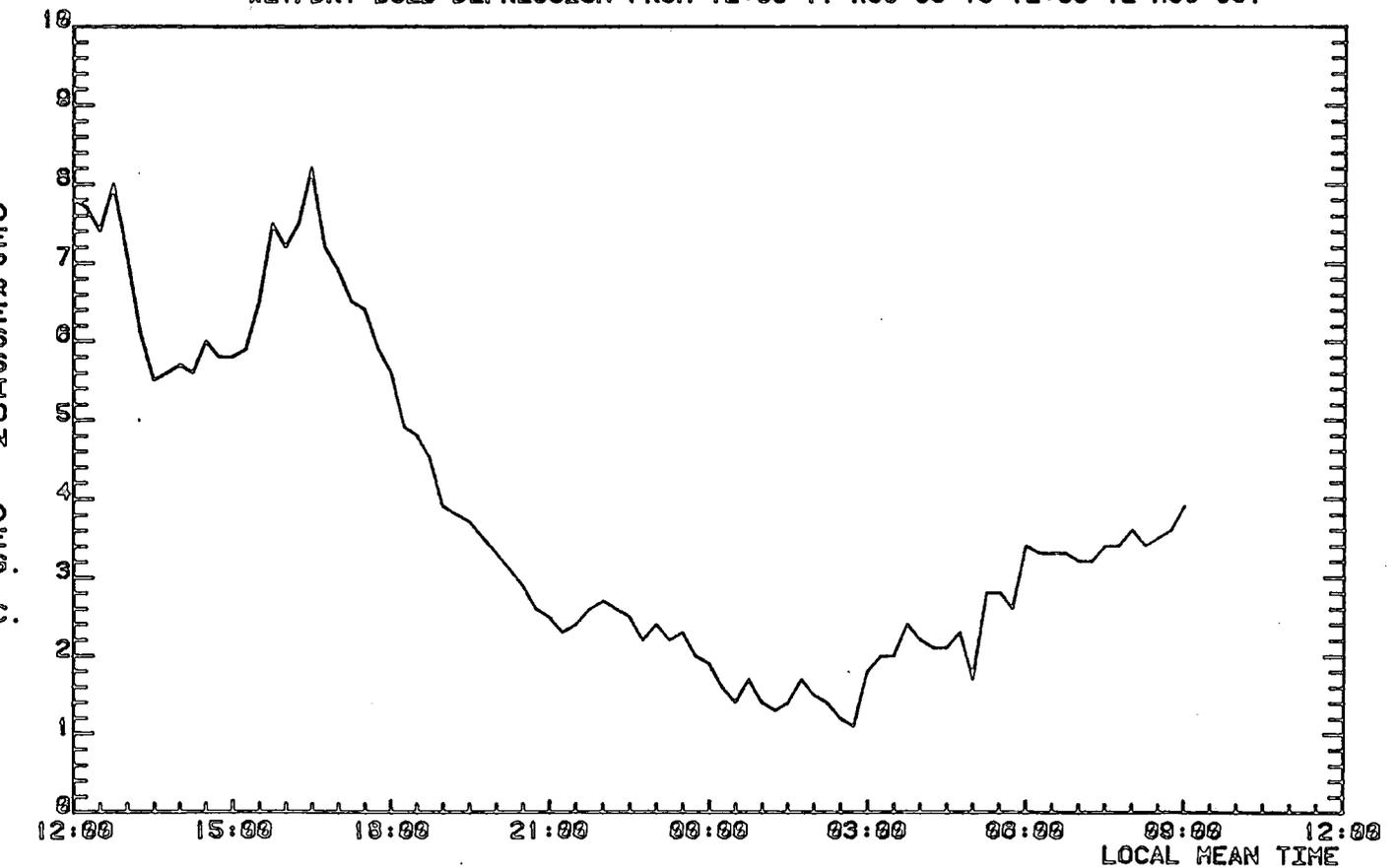
Fig. 6.31   WEATHER DATA RECORDED AT DURHAM OBSERVATORY
AV. SOLAR RADIATION FROM 12:00 12-AUG-83 TO 12:00 13-AUG-83.
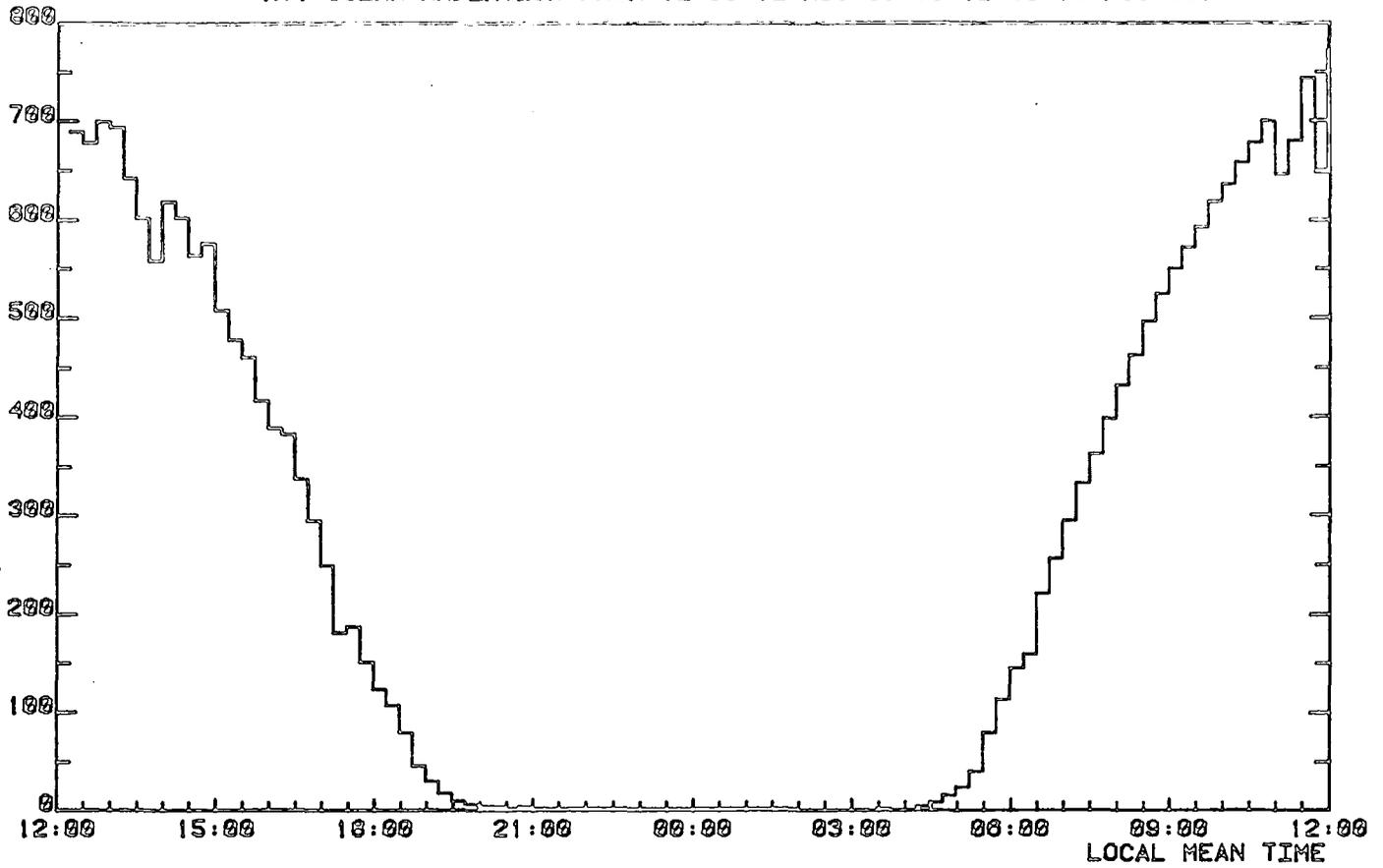
Fig. 6.32   WEATHER DATA RECORDED AT DURHAM OBSERVATORY
AV. WINDSPEED FROM 12:00 12-AUG-83 TO 12:00 13-AUG-83.
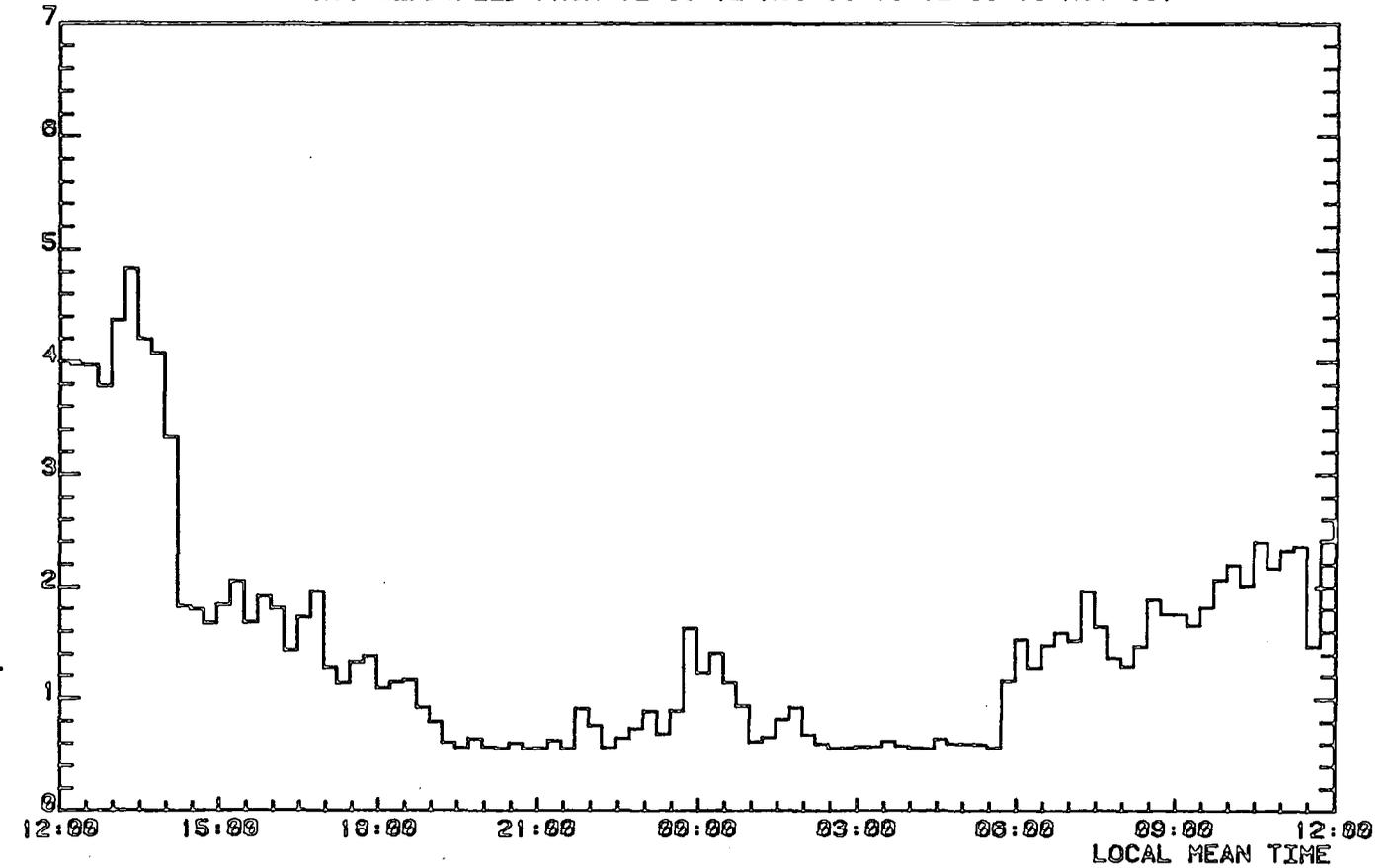
Fig. 6.33   WEATHER DATA RECORDED AT DURHAM OBSERVATORY
AIR TEMPERATURE FROM 12:00 12-AUG-83 TO 12:00 13-AUG-83.
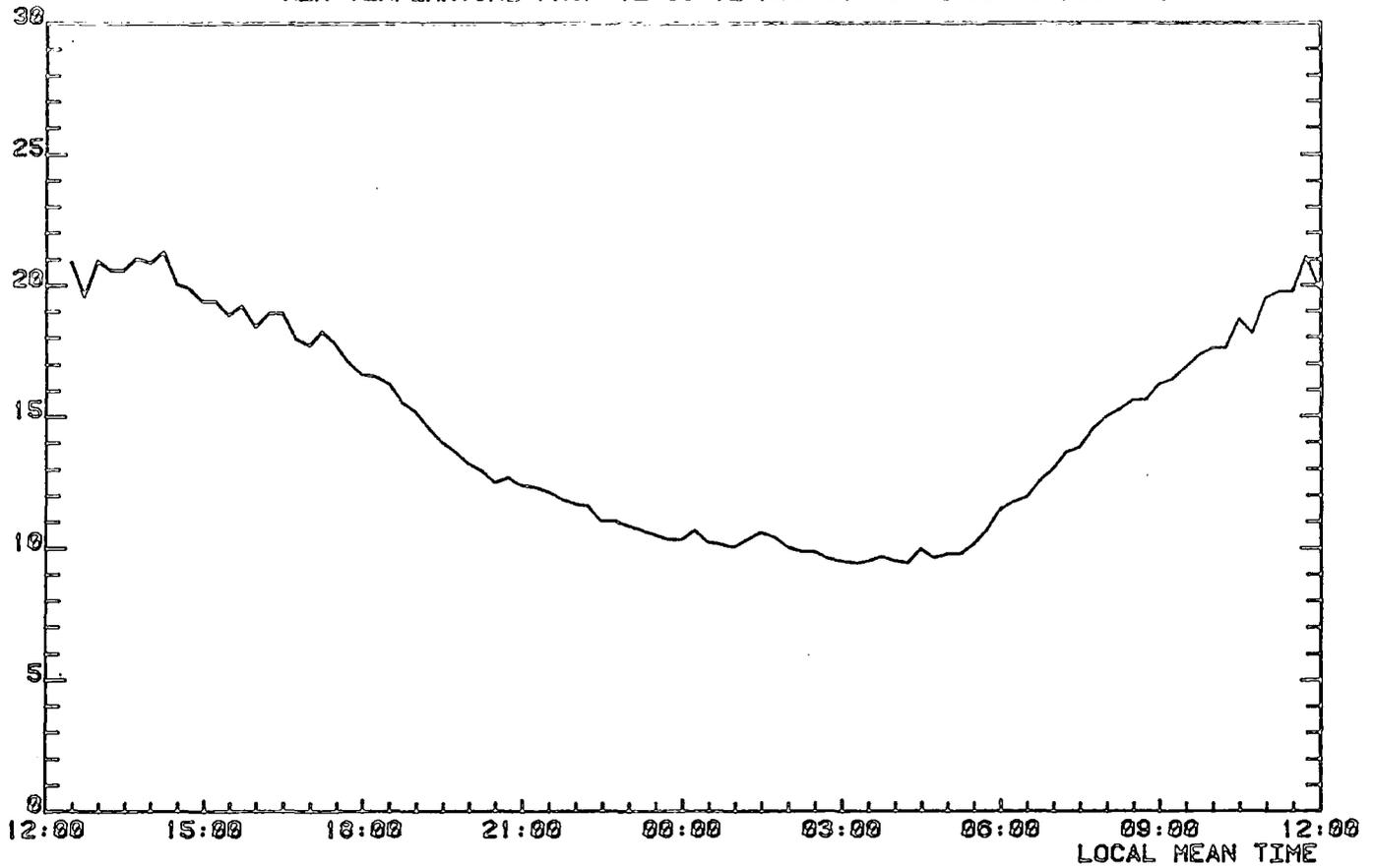
Fig. 6.34   WEATHER DATA RECORDED AT DURHAM OBSERVATORY
WET/DRY BULB DEPRESSION FROM 12:00 12-AUG-83 TO 12:00 13-AUG-83.
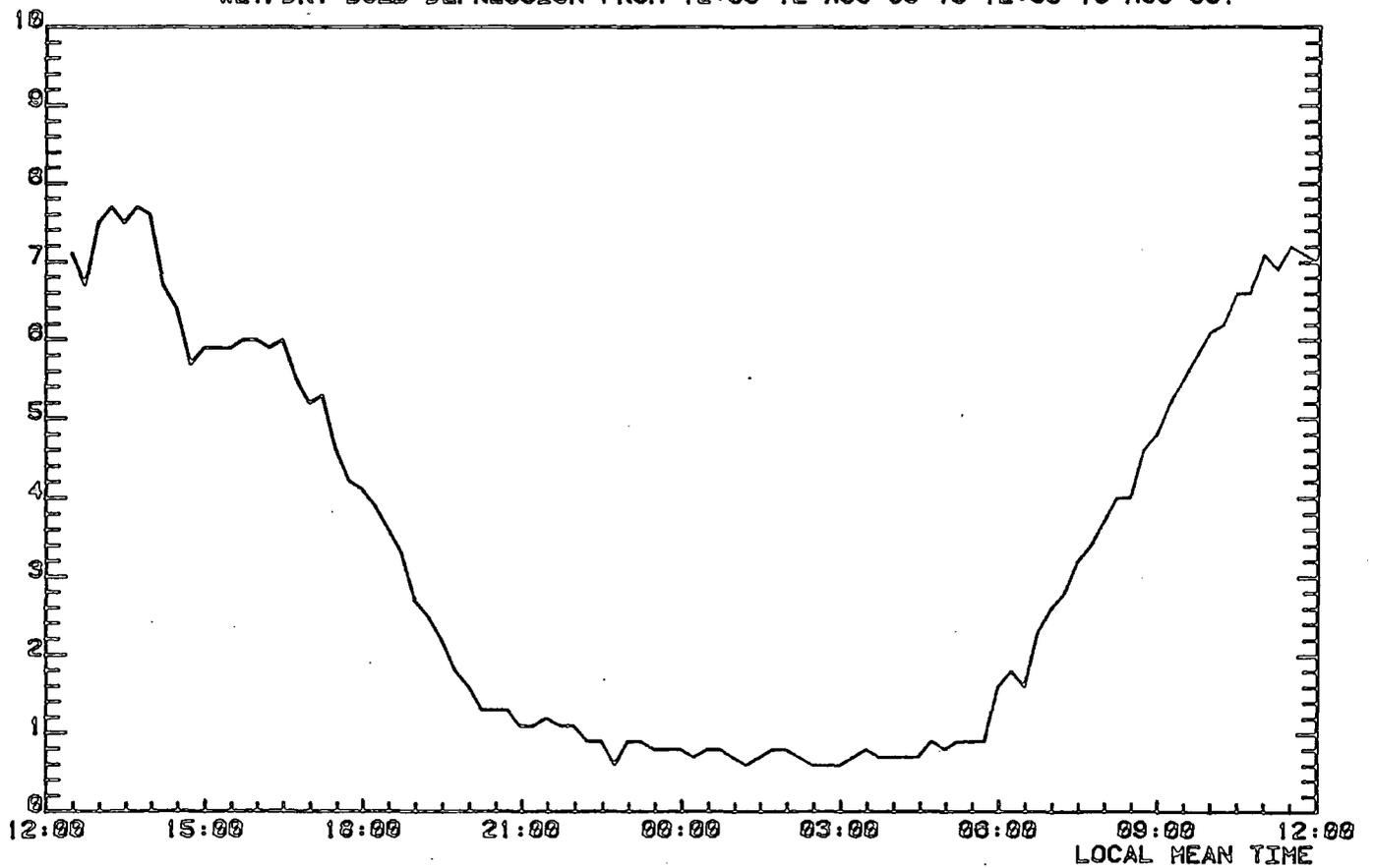
Fig. 6.35

LONG WAVE CLOUD COVER FACTOR FROM 12:00 05-AUG-83 TO 12:00 06-AUG-83.
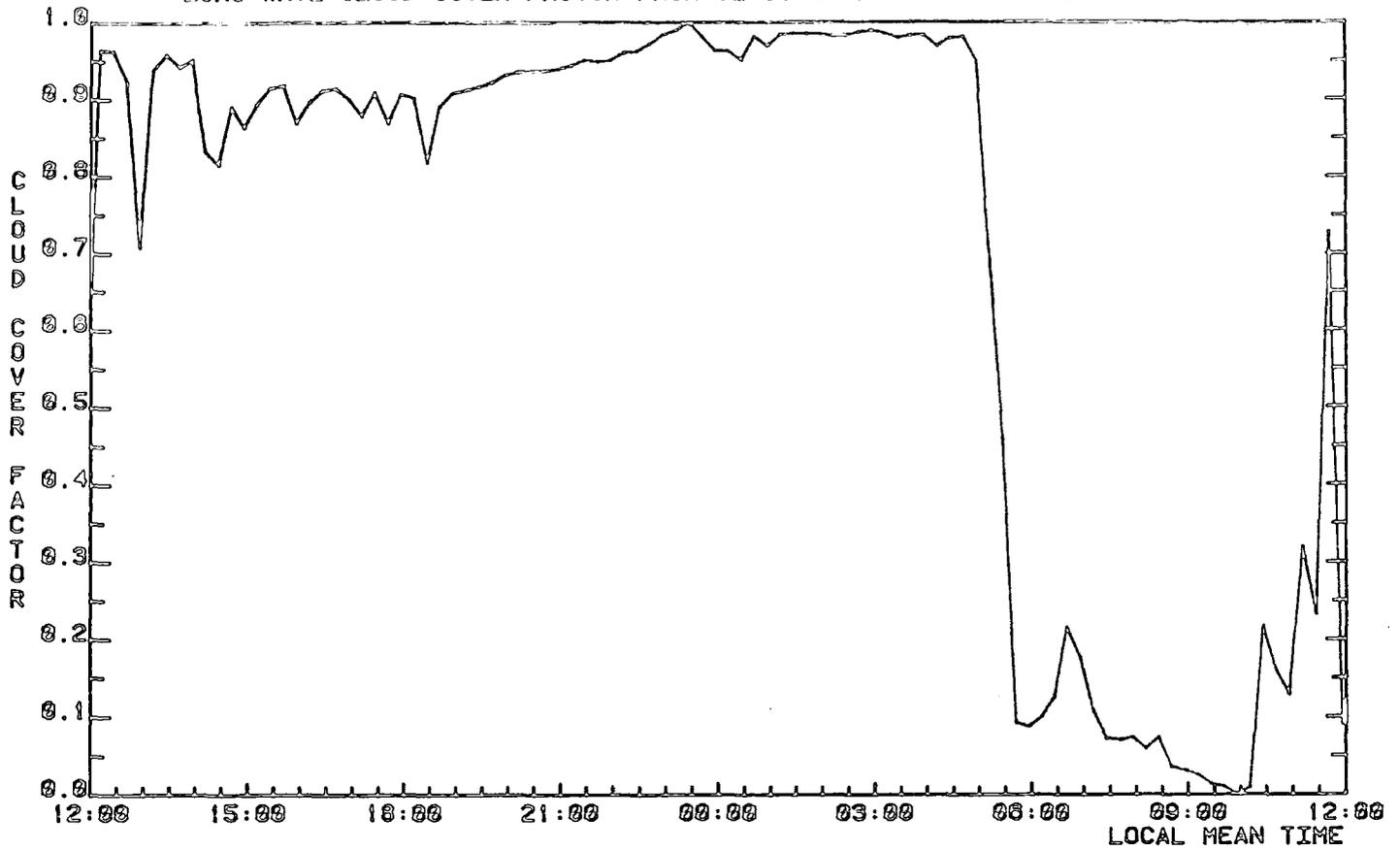
Fig. 6.36

LONG WAVE CLOUD COVER FACTOR FROM 12:00 06-AUG-83 TO 12:00 07-AUG-83.
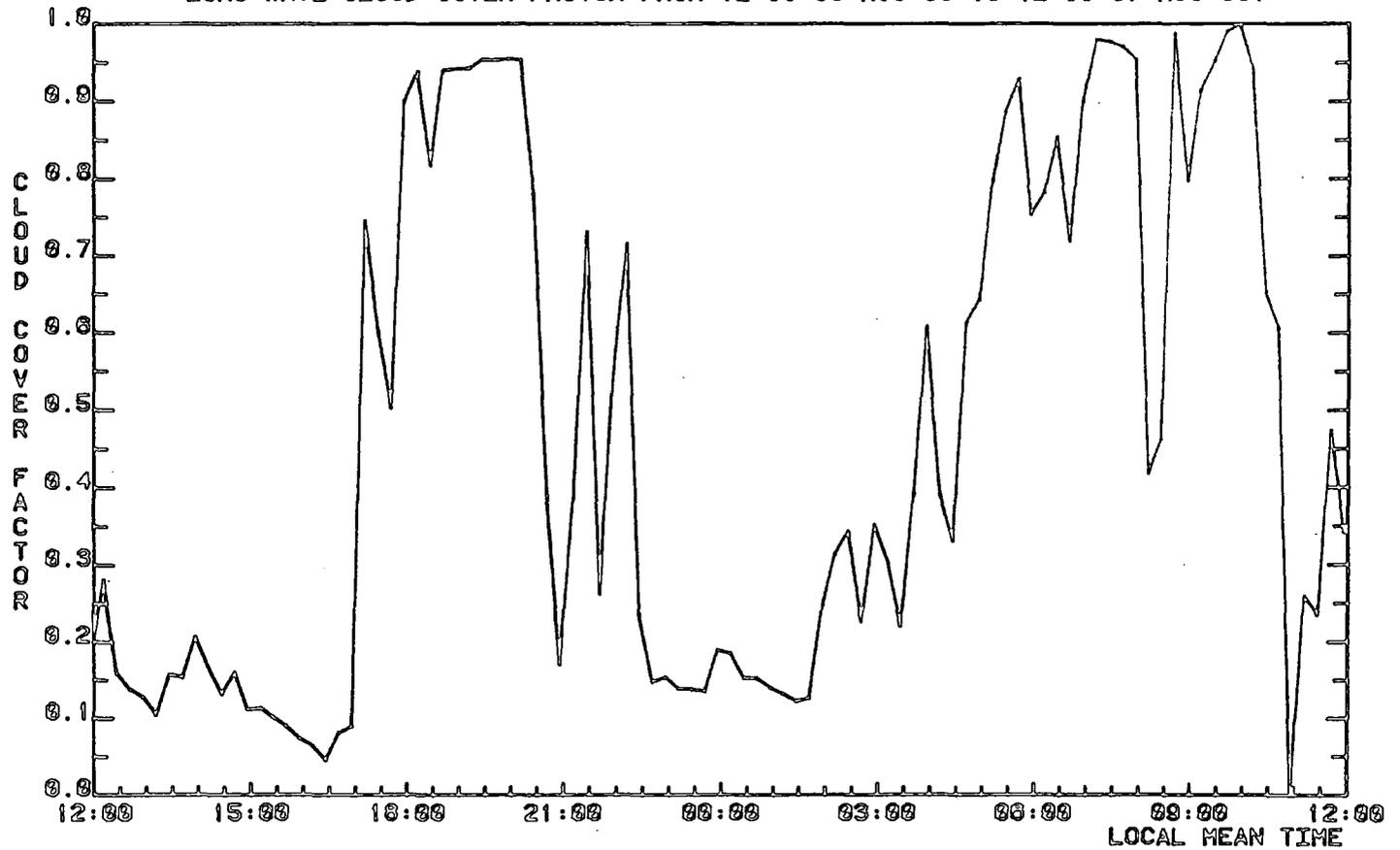
Fig. 6.37

LONG WAVE CLOUD COVER FACTOR FROM 12:00 07-AUG-83 TO 12:00 08-AUG-83.
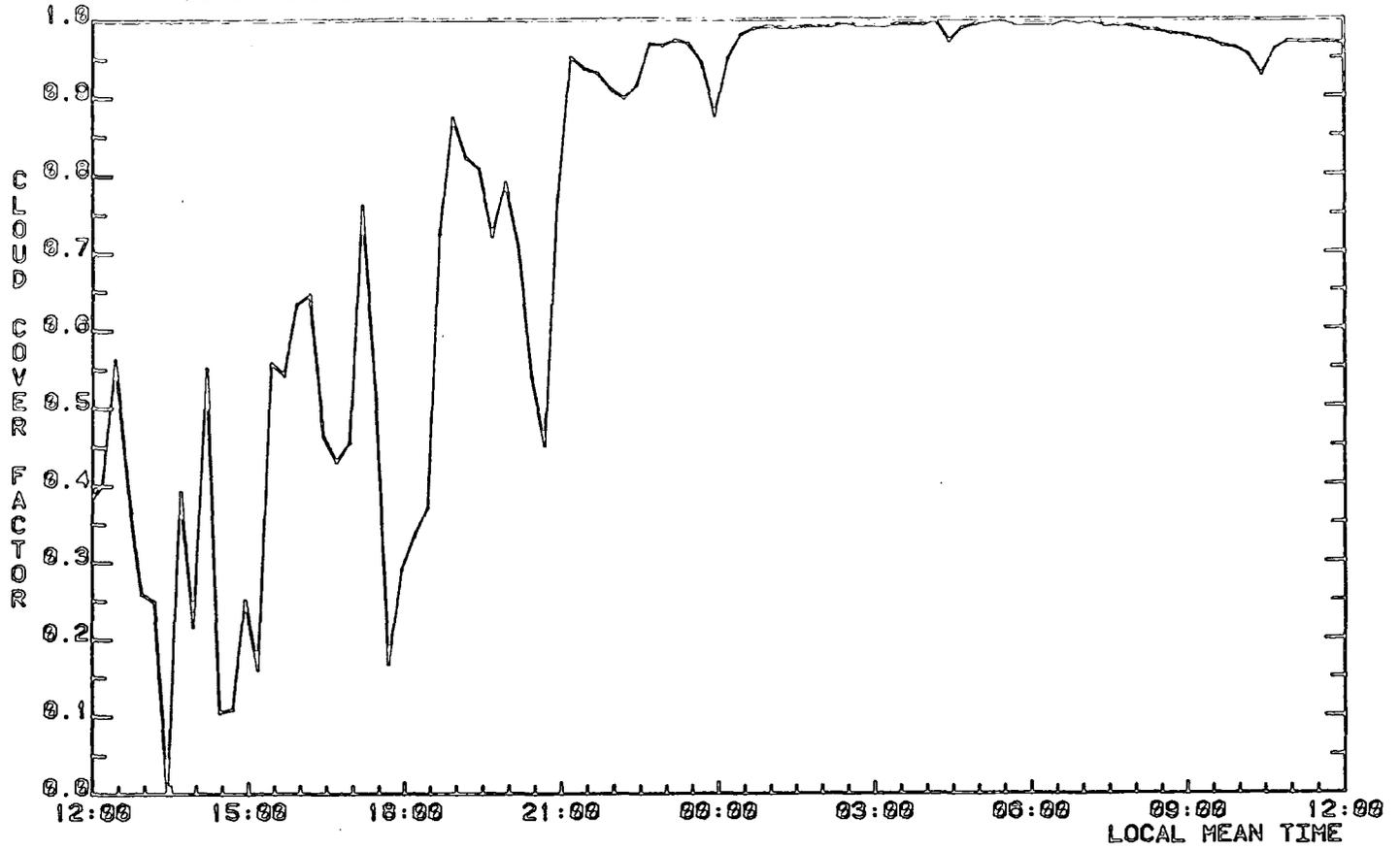
Fig. 6.38

LONG WAVE CLOUD COVER FACTOR FROM 12:00 08-AUG-83 TO 12:00 09-AUG-83.
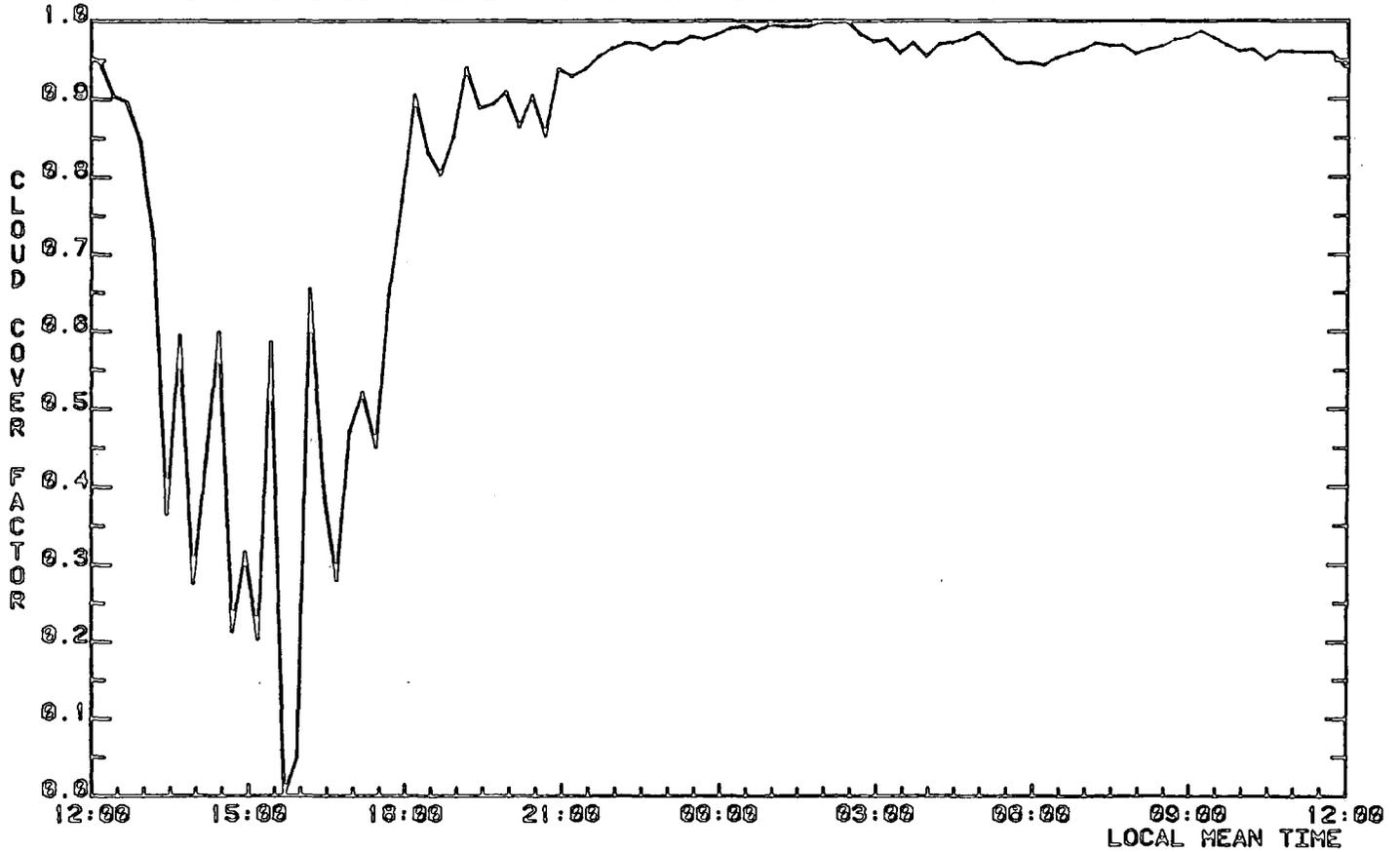
Fig. 6.39

LONG WAVE CLOUD COVER FACTOR FROM 12:00 09-AUG-83 TO 12:00 10-AUG-83.
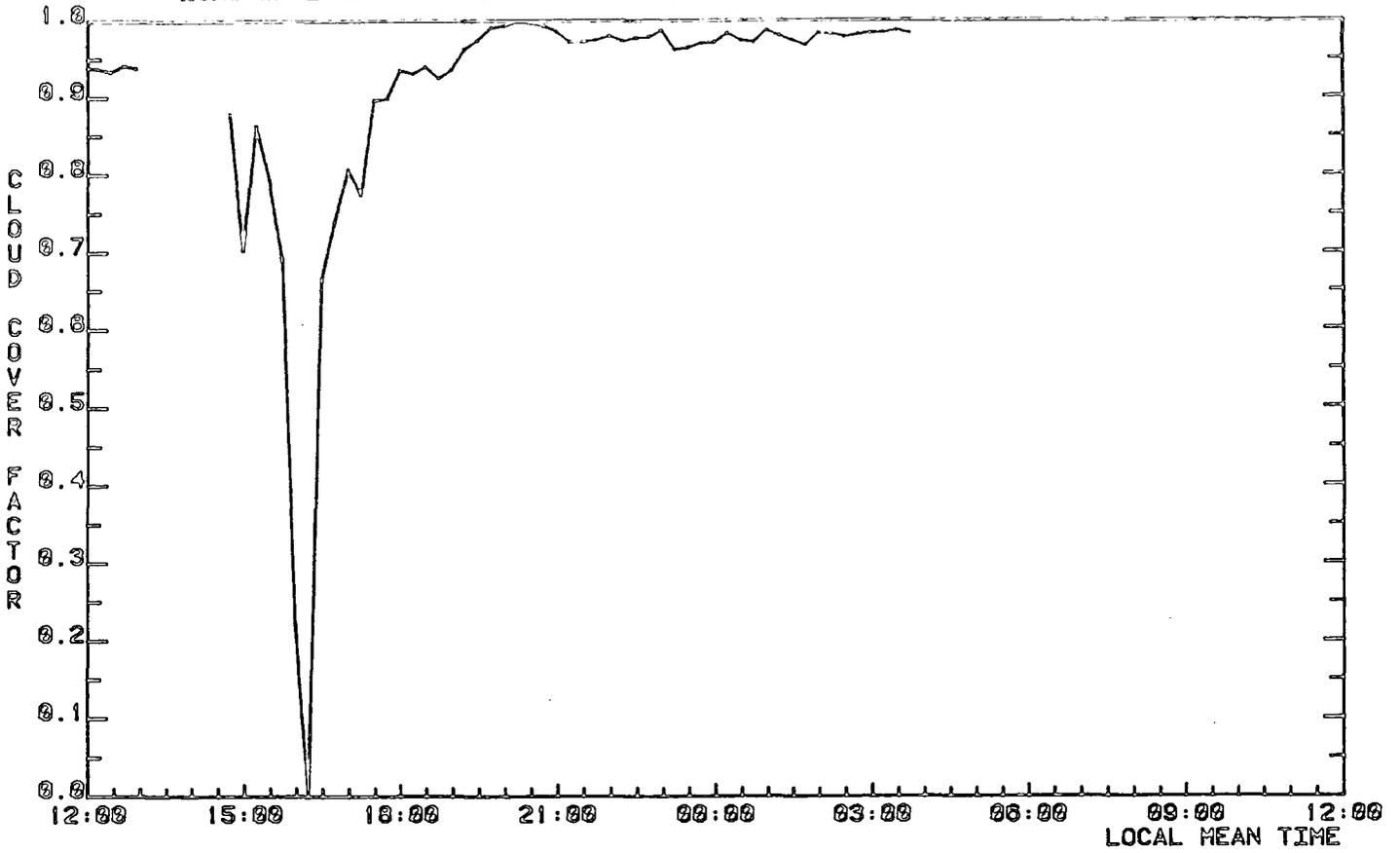
Fig. 6.40

LONG WAVE CLOUD COVER FACTOR FROM 12:00 10-AUG-83 TO 12:00 11-AUG-83.
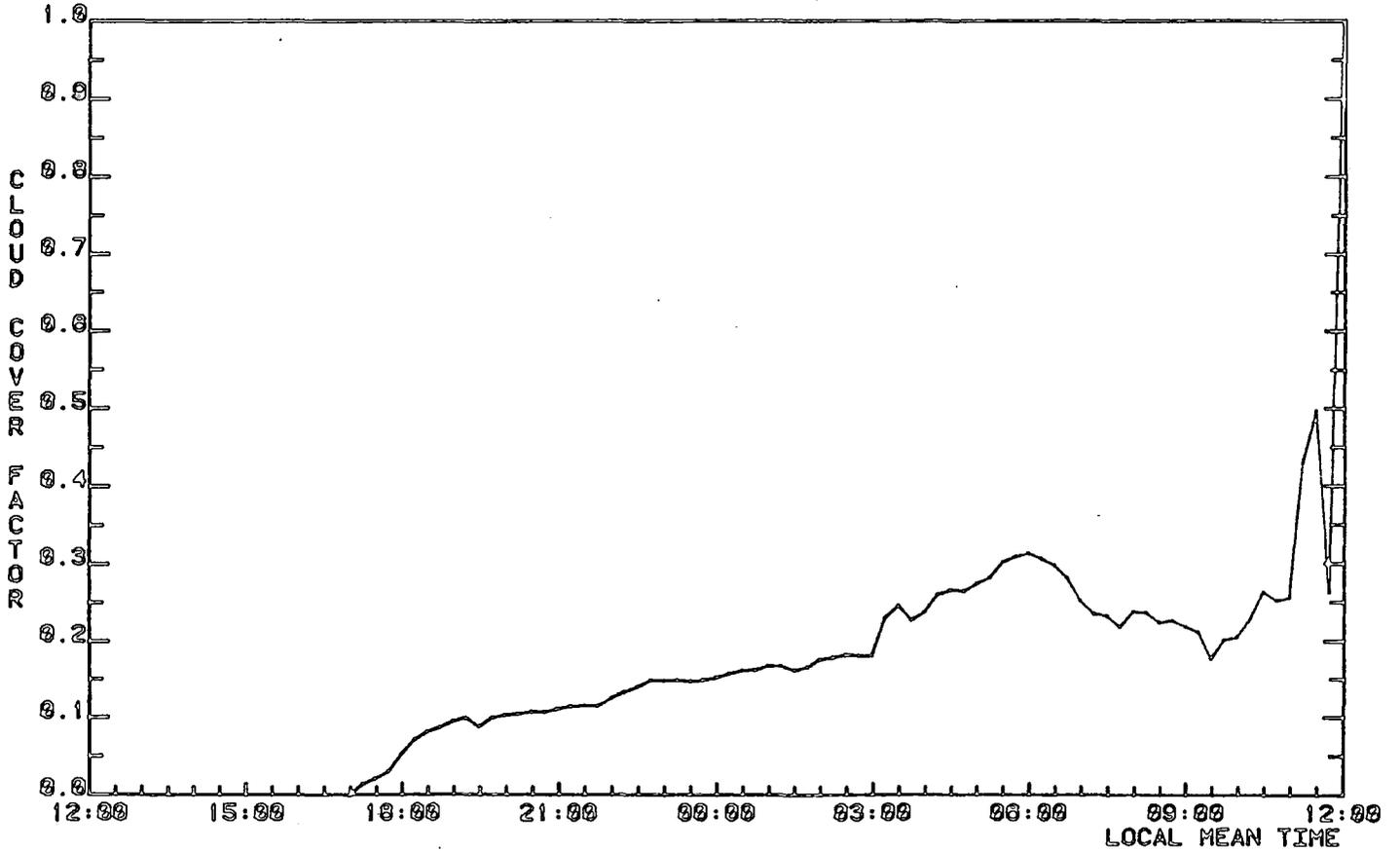
Fig. 6.41

LONG WAVE CLOUD COVER FACTOR FROM 12:00 11-AUG-83 TO 12:00 12-AUG-83.
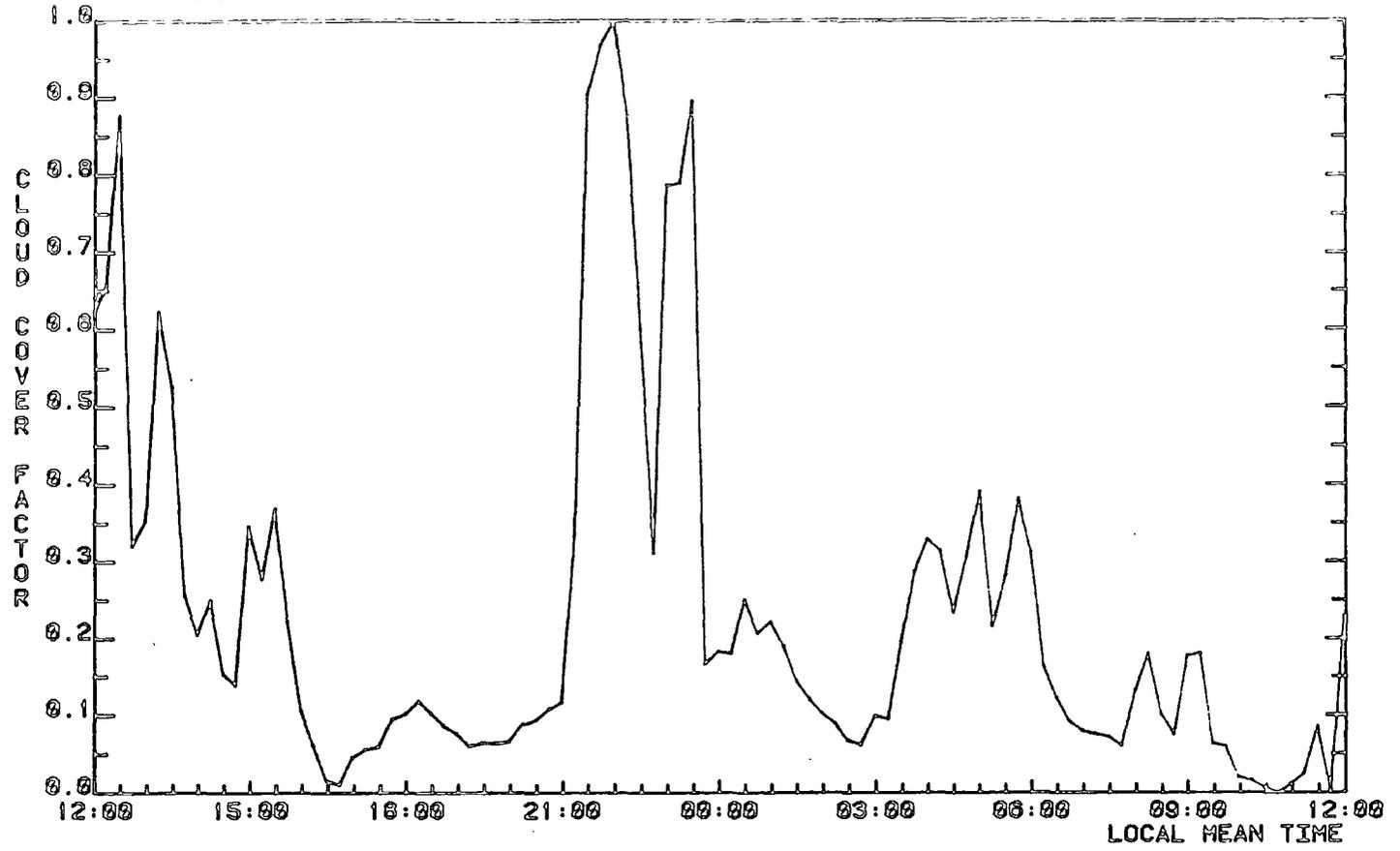
Fig. 6.42

LONG WAVE CLOUD COVER FACTOR FROM 12:00 12-AUG-83 TO 12:00 13-AUG-83.
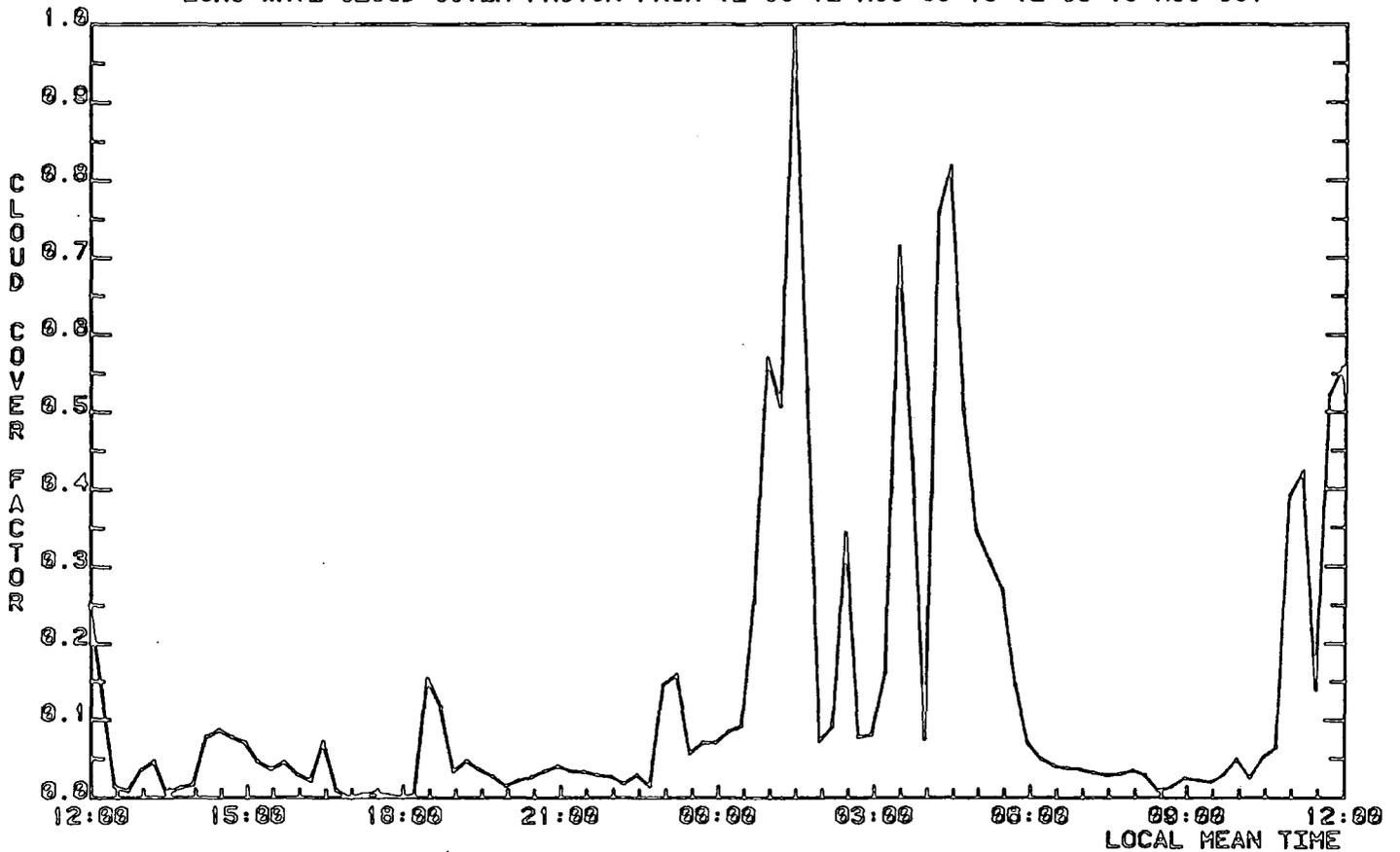
Fig. 6.43   PREDICTED AND MEASURED RADIANT TEMPS. FOR THE SOUTH FACING
              SANDSTONE WALL FROM 12:00 5/8/83 TO 12:00 6/8/83.
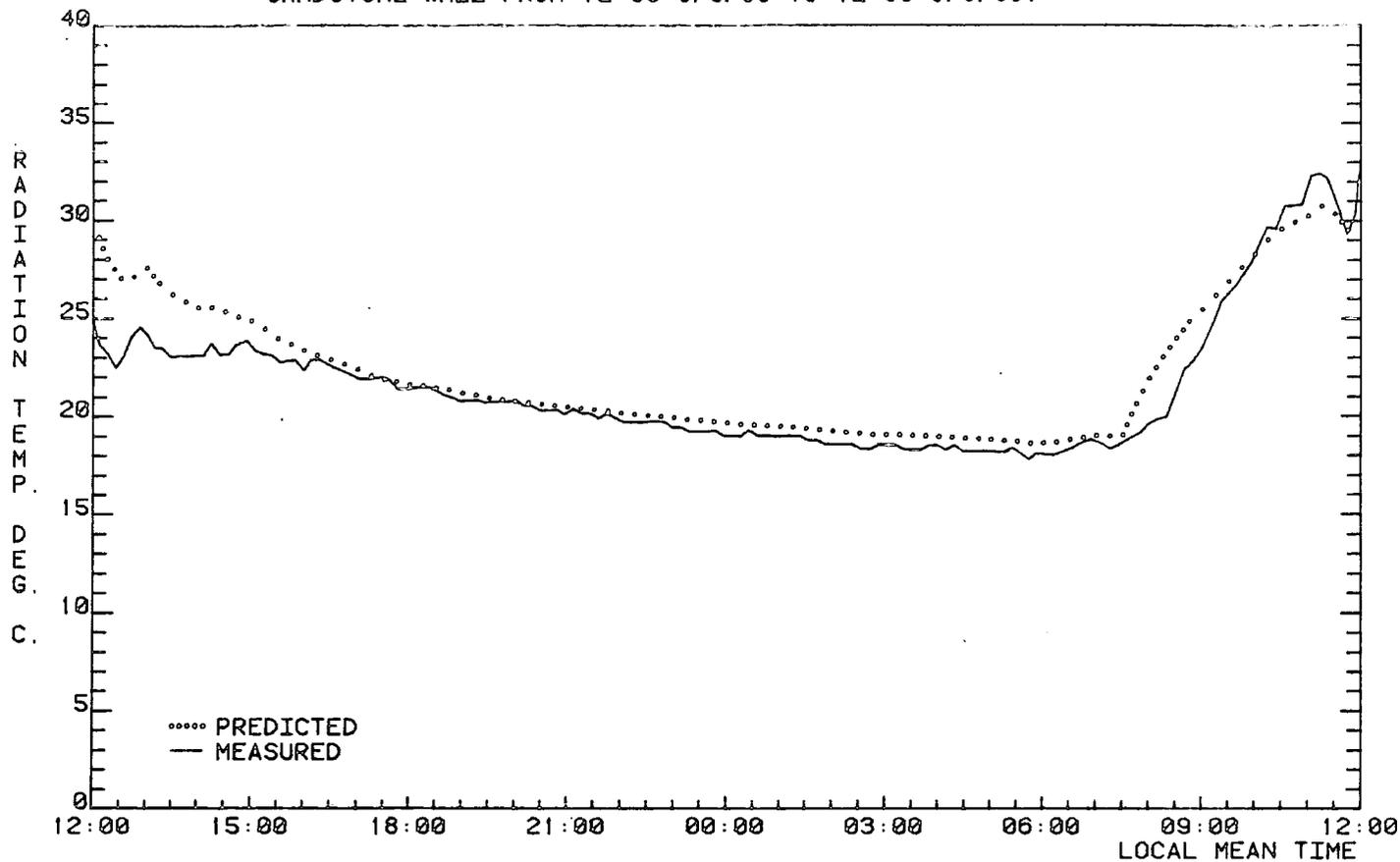
Fig. 6.44   PREDICTED AND MEASURED RADIANT TEMPS. FOR THE SOUTH FACING
              SANDSTONE WALL FROM 12:00 6/8/83 TO 12:00 7/8/83.
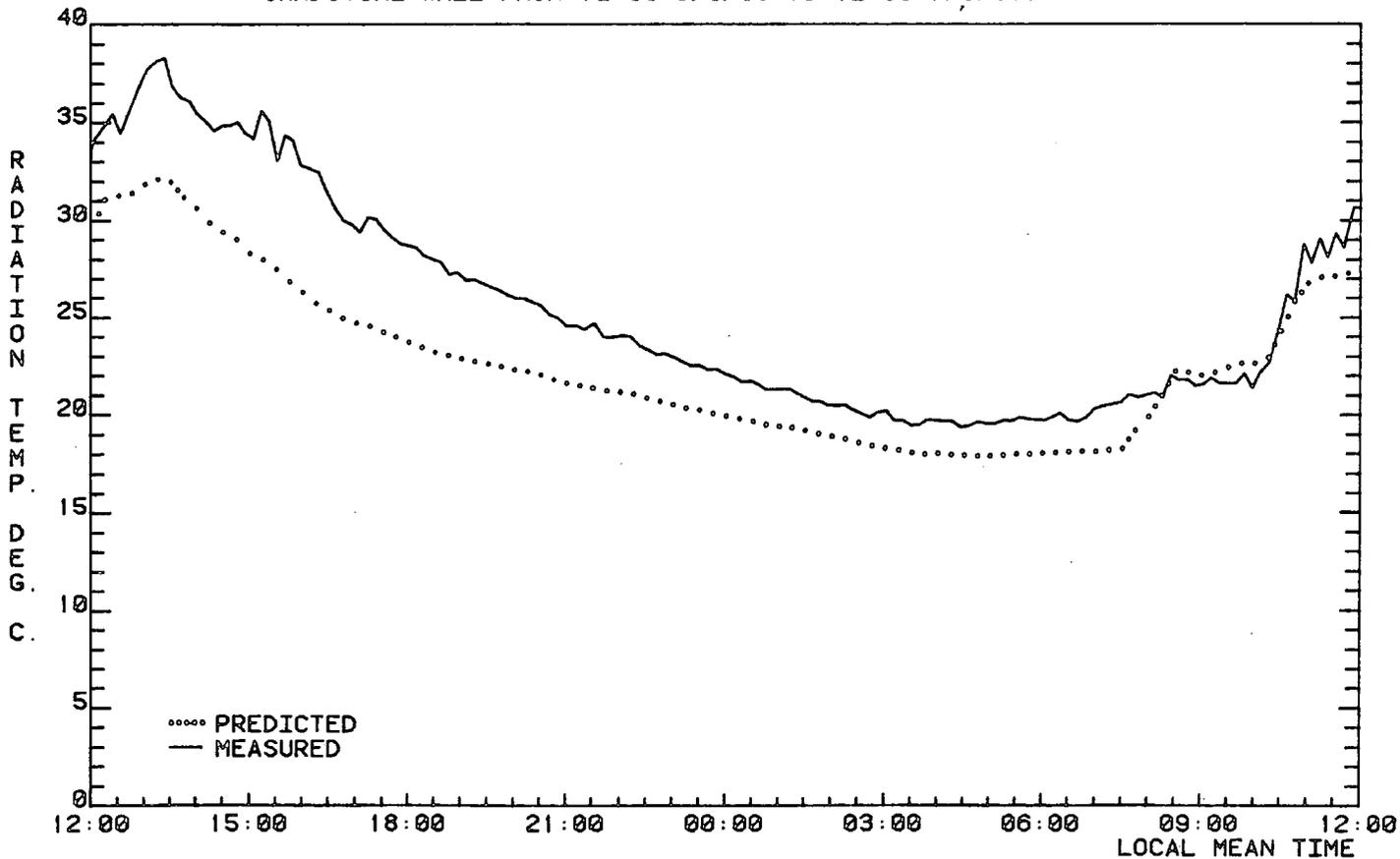
Fig. 6.45   PREDICTED AND MEASURED RADIANT TEMPS. FOR THE SOUTH FACING
             SANDSTONE WALL FROM 12:00 7/8/83 TO 12:00 8/8/83.

RADIATION TEMP. DEG. C.

40
35
30
25
20
15
10
5
0

***** PREDICTED
—— MEASURED

12:00   15:00   18:00   21:00   00:00   03:00   06:00   09:00   12:00
                                                          LOCAL MEAN TIME
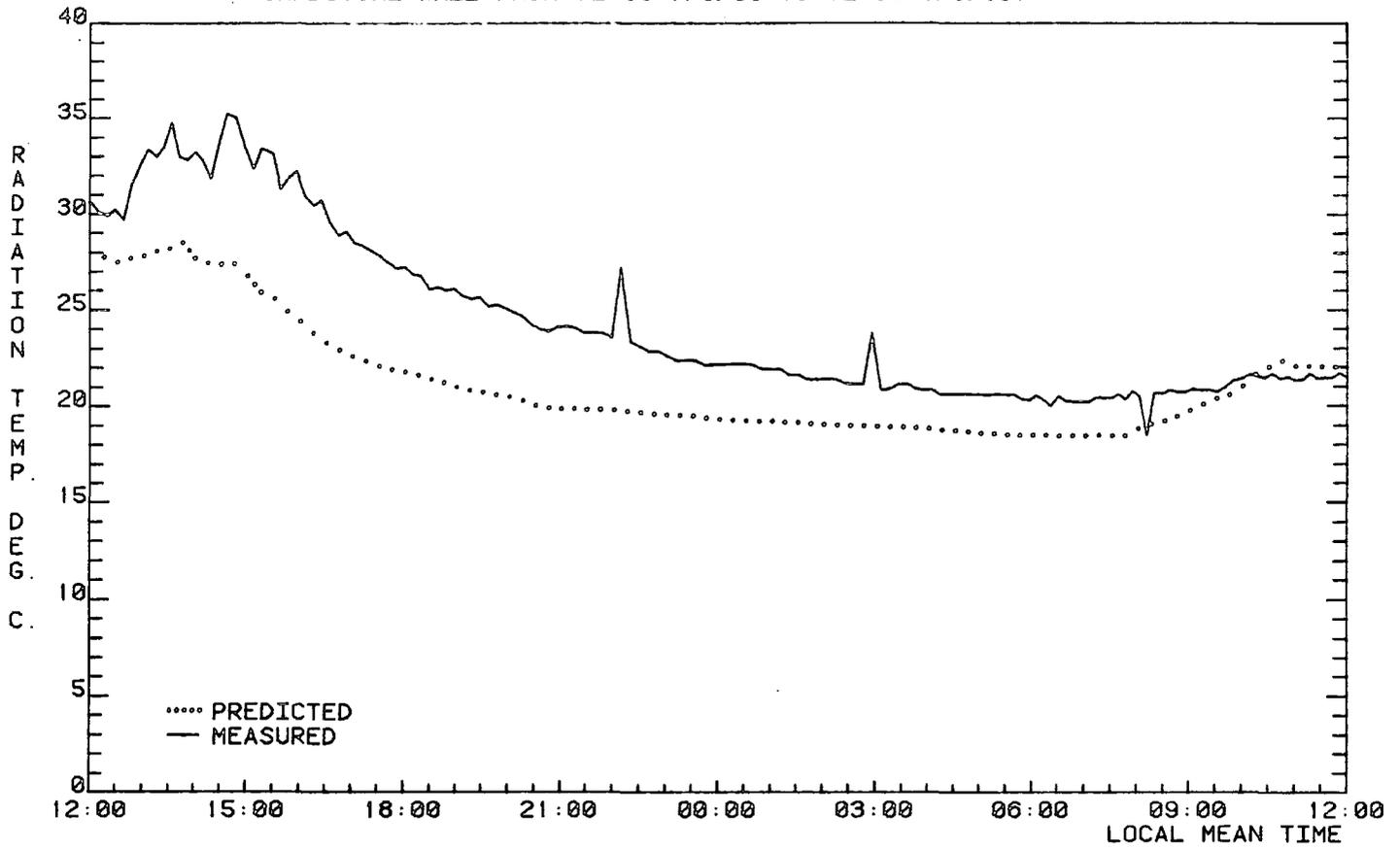
Fig. 6.46   PREDICTED AND MEASURED RADIANT TEMPS. FOR THE SOUTH FACING
             SANDSTONE WALL FROM 12:00 8/8/83 TO 12:00 9/8/83.

RADIATION TEMP. DEG. C.

40
35
30
25
20
15
10
5
0

***** PREDICTED
—— MEASURED

12:00   15:00   18:00   21:00   00:00   03:00   06:00   09:00   12:00
                                                          LOCAL MEAN TIME
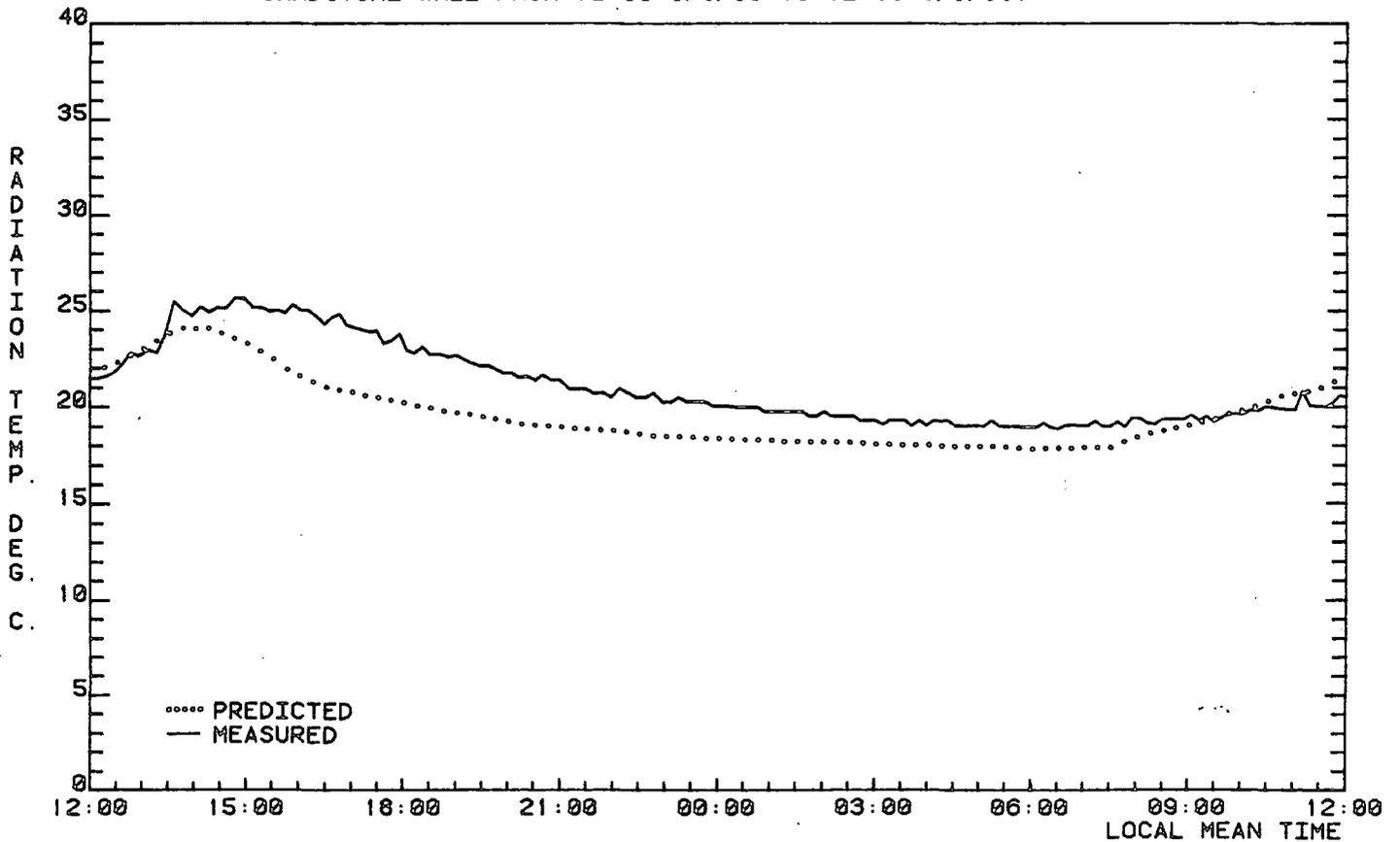
Fig. 6.47   PREDICTED AND MEASURED RADIANT TEMPS. FOR THE SOUTH FACING
            SANDSTONE WALL FROM 12:00 9/8/83 TO 12:00 10/8/83.
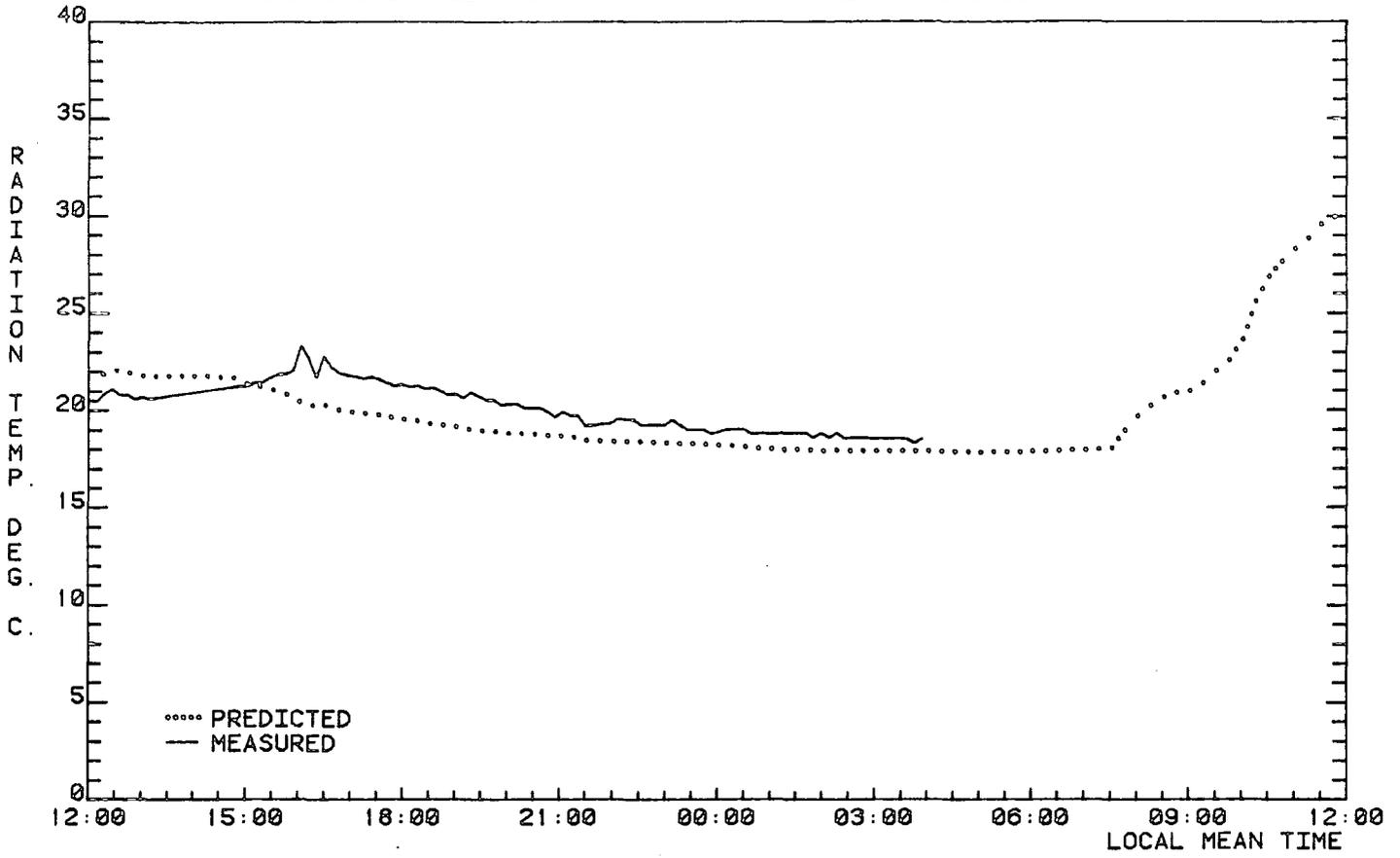
Fig. 6.48   PREDICTED AND MEASURED RADIANT TEMPS. FOR THE SOUTH FACING
            SANDSTONE WALL FROM 12:00 10/8/83 TO 12:00 11/8/83.
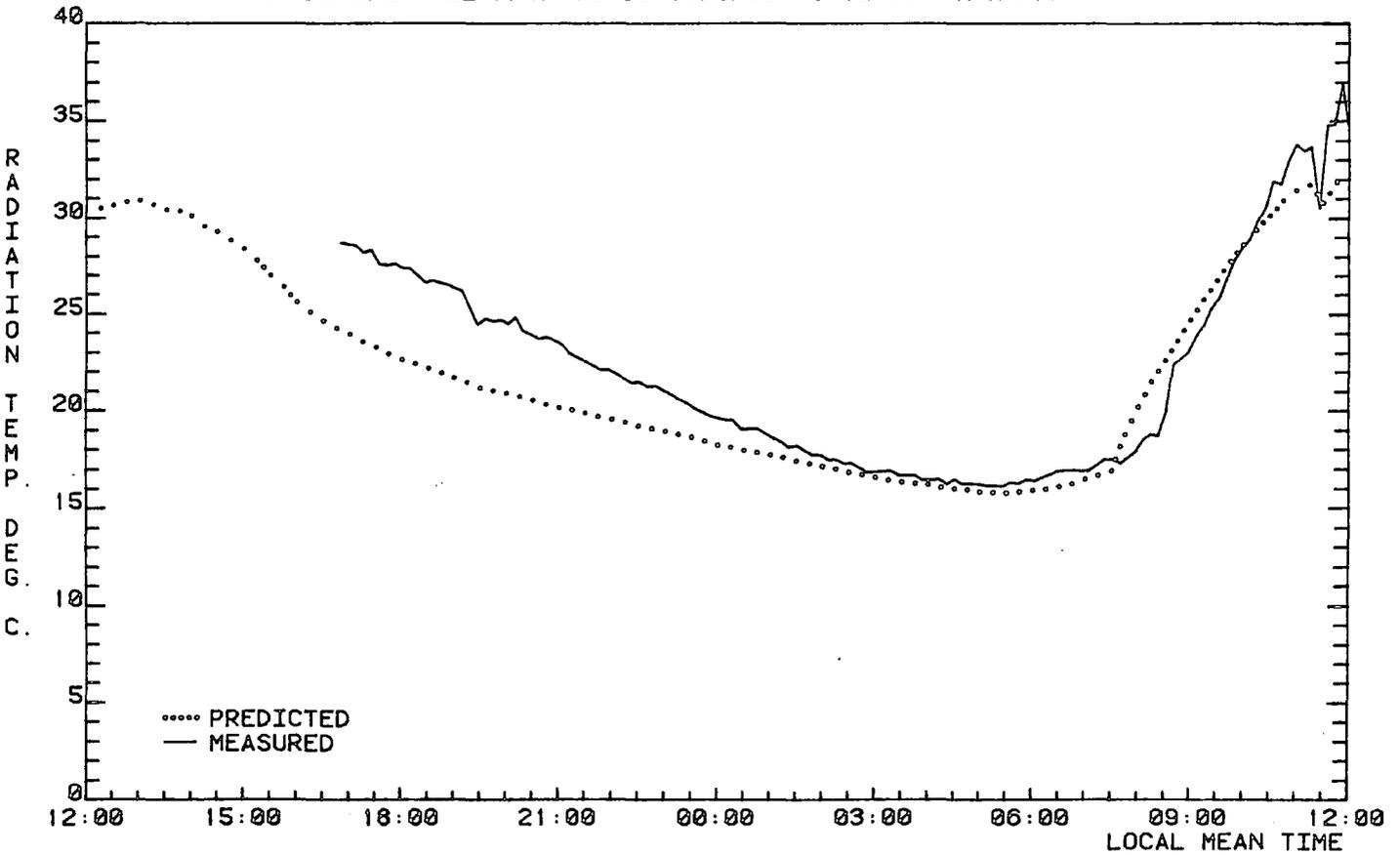
Fig. 6.49   PREDICTED AND MEASURED RADIANT TEMPS. FOR THE SOUTH FACING
SANDSTONE WALL FROM 12:00 11/8/83 TO 12:00 12/8/83.
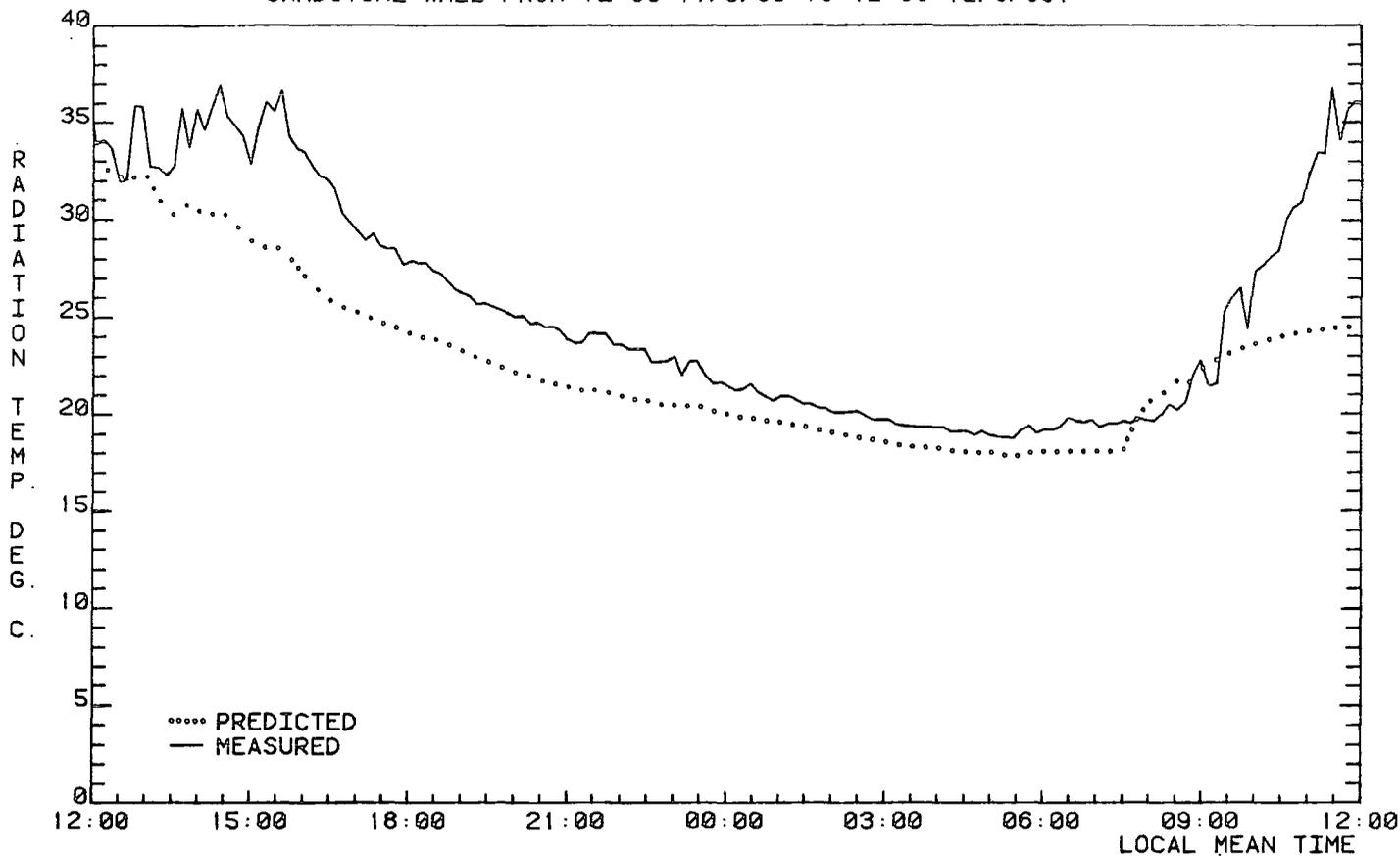
Fig. 6.50   PREDICTED AND MEASURED RADIANT TEMPS. FOR THE SOUTH FACING
SANDSTONE WALL FROM 12:00 12/8/83 TO 12:00 13/8/83.
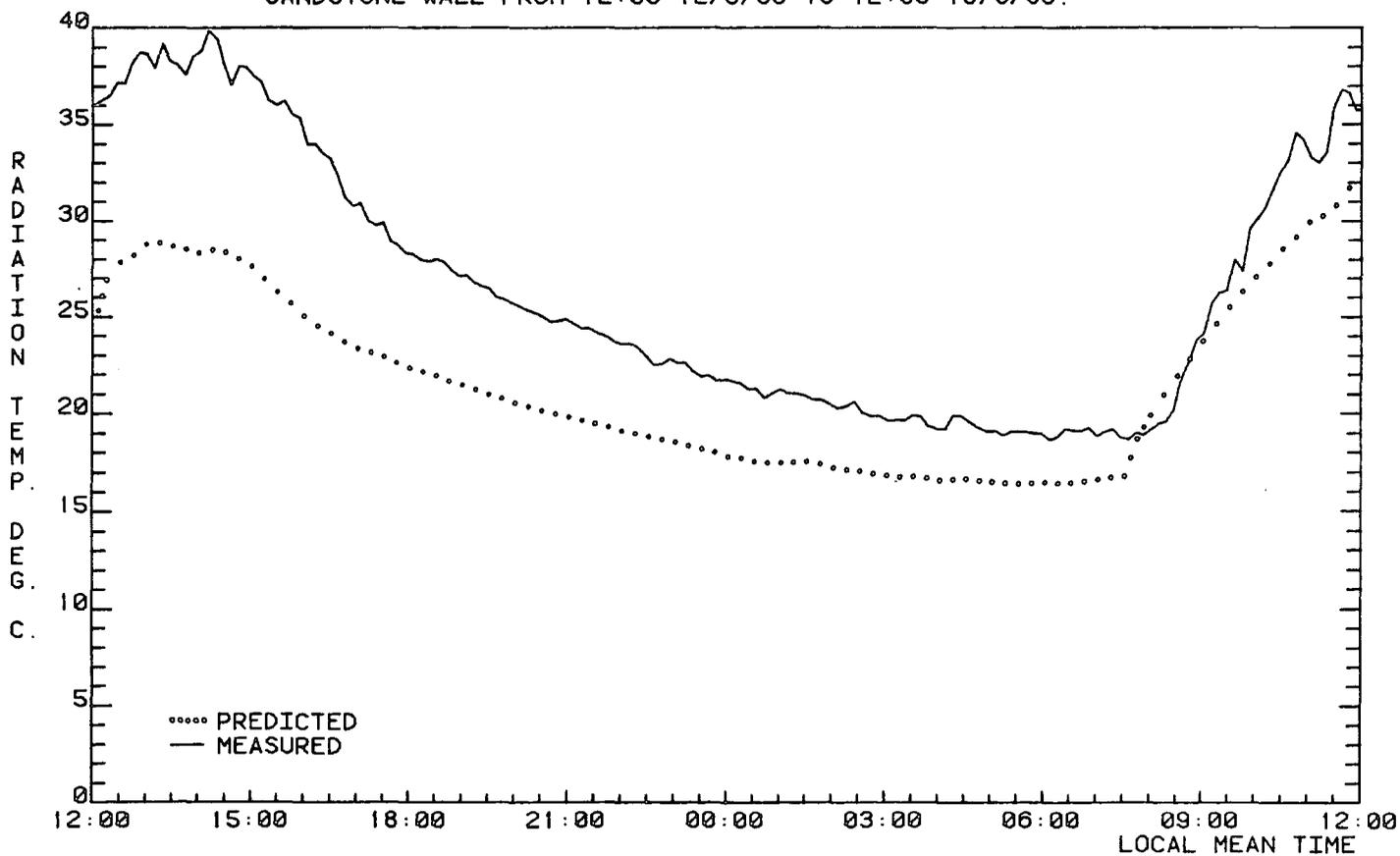
Fig. 6.51   PREDICTED AND MEASURED RADIANT TEMPS. FOR THE SOUTH FACING
             SANDSTONE WALL FROM 12:00 12/8/83 TO 12:00 13/8/83.
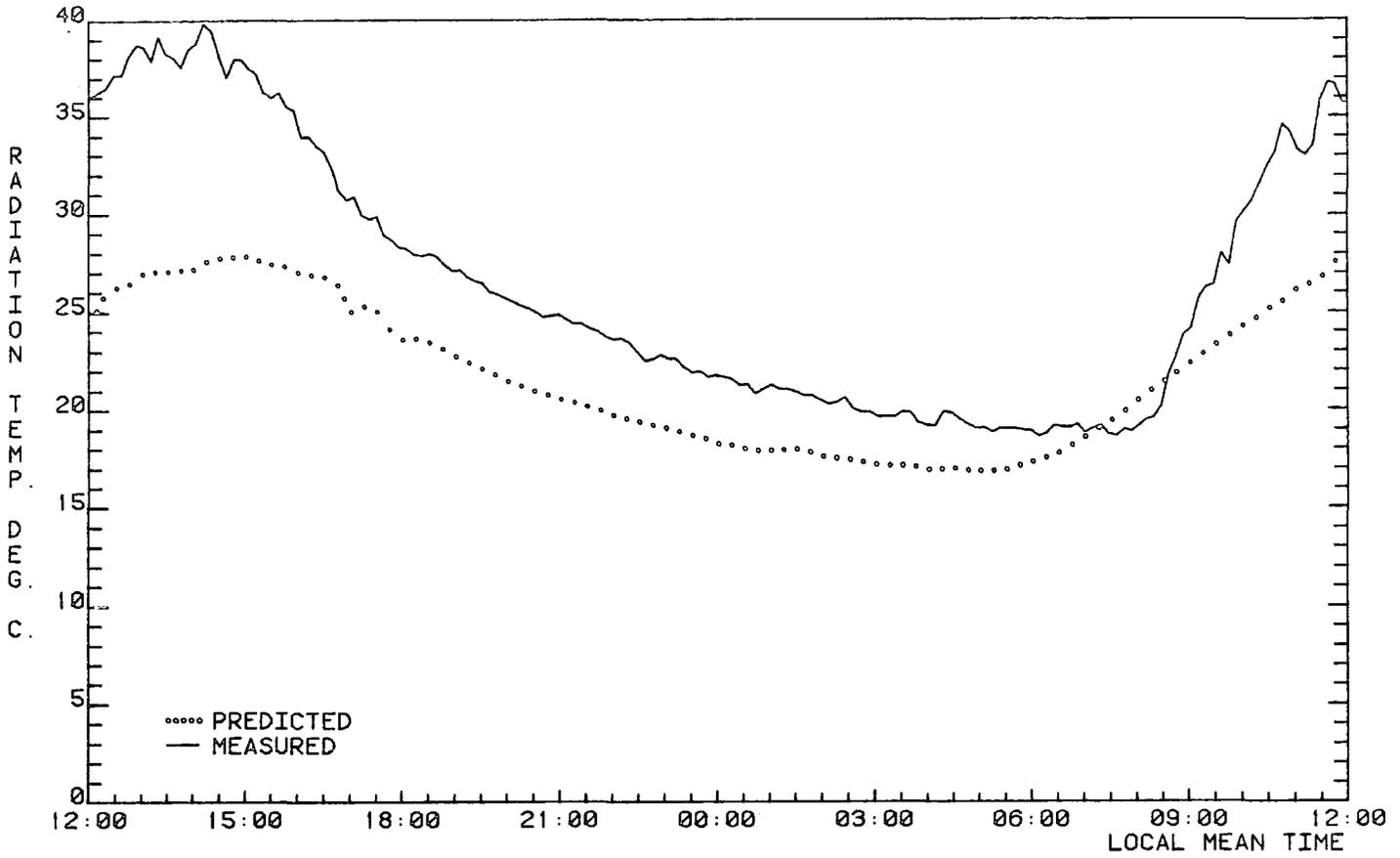
Fig. 6.52   PREDICTED AND MEASURED RADIANT TEMPS. FOR THE SOUTH FACING
             SANDSTONE WALL FROM 12:00 12/8/83 TO 12:00 13/8/83.
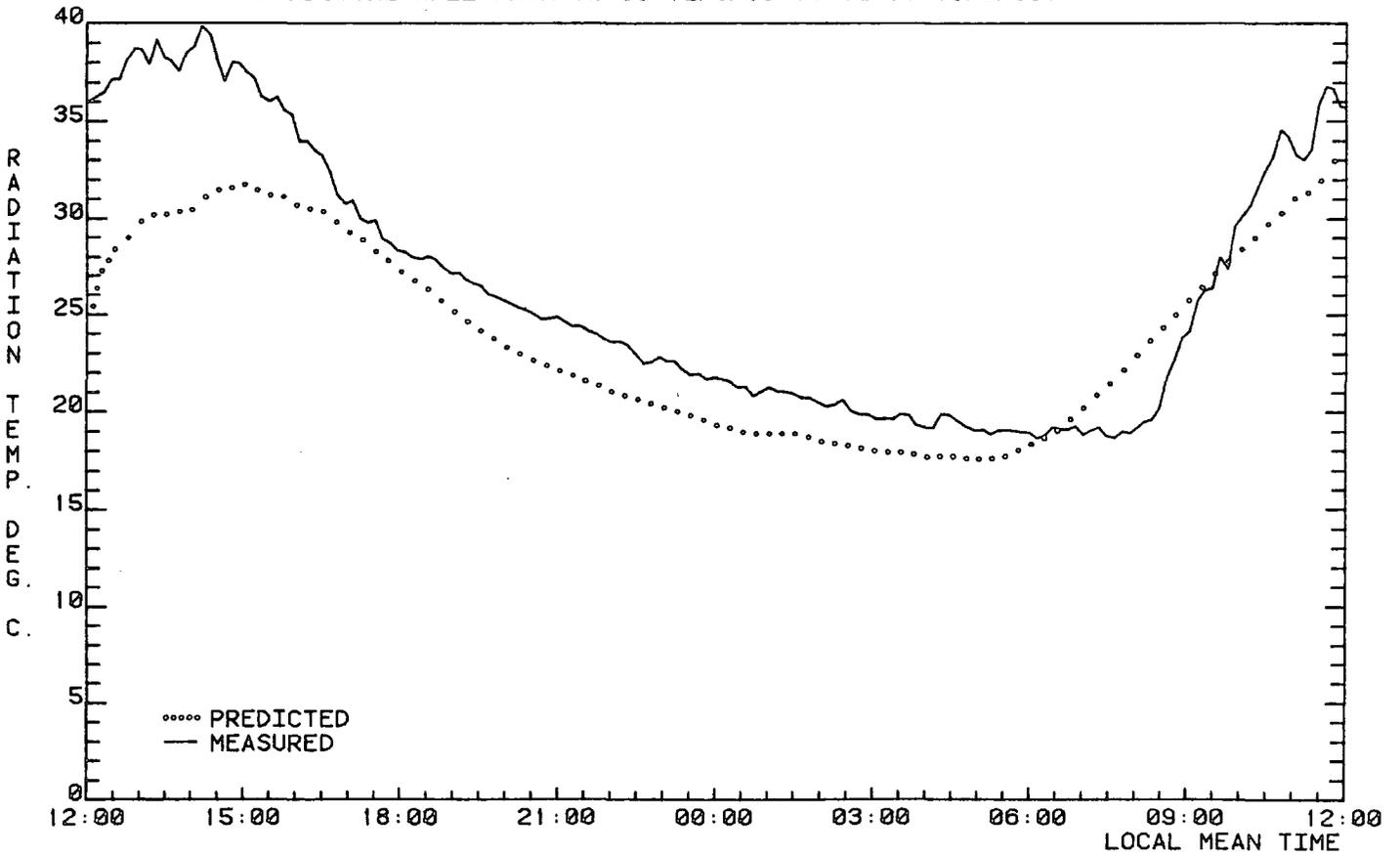
Chapter 7 Conclusion.

7.1 Summary of the previous chapters.

The general purpose model was constructed to simulate the thermal behaviour of simple one-dimensional structures, and the theory behind the model is discussed in Chapter 2. Basically, the model solves the one-dimensional equation of heat conduction for the structure of interest by a numerical method, subject to two boundary conditions. The lower boundary condition is assumed to be represented by a constant temperature at a specified depth within the structure, while the upper boundary condition is derived from the balance of heat fluxes acting at the surface. These fluxes are represented in the model by empirical relationships in terms of commonly measured meteorological and surface parameters.

Initially, a sensitivity analysis was carried out on the general purpose model, and the results are described in Chapter 3. The purpose of this analysis was to gain an understanding of the type and magnitude of effect that variations in the values of the many parameters required as input for the model have on the resulting temperature predictions. This information is useful in two ways. Firstly, to suggest which parameters need to be measured with the greatest care, and secondly, if the temperature predictions of the model were significantly different from expected values, then the results of the analysis may be helpful in deciding if an incorrect value had been used for one of the parameters.

Chapter 4 describes the equipment which was used to collect the data necessary for the validation of the model and the attempt to simulate the thermal behaviour of a sandstone wall. The data were recorded at frequent intervals, and included the values of several meteorological parameters and the radiation temperatures of the sky and terrestrial surfaces of interest. The former were supplied by an automatic weather station, and the latter by a radiometer whose movement was controlled by a Tektronix computer.

The equipment designed to acquire the radiation temperature data has since been redesigned with an emphasis on improved portability and reduced size. The new equipment operates in basically the same way, but is now controlled by a BBC microcomputer. This has the advantage of being much smaller and lighter than the Tektronix computer, while still having the same memory capacity and processing speed. The BBC microcomputer also uses a similar programming language to the Tektronix computer. However, the main advantage of the BBC microcomputer is that it allows the possibility of having several data acquisition systems and a weather station connected together on a computer network. This would allow the operator to run the units independently of each other from a central operation site.

In Chapter 5, the validation of the model under fine weather conditions was described for two multi-layered structures with concrete and asphalt surfaces. The method of validation consisted of a direct comparison between the surface temperatures predicted by the model and those measured by a radiometer. The choice of radiation rather than contact temperatures for the comparison was made for two main reasons. The first was that the measurements made by the radiometer did not cause any disturbance to the surface of interest. Secondly, the results of a comparison between contact and radiation temperature measurements for the same surface, which are given in Section 4.4.3.4, suggested that the radiometer measurements were more sensitive to rapid fluctuations in the surface temperature.

General purpose models similar to the one in use at Durham have been developed by Jacobs, 1976, and Link et al., 1981. In both cases a validation exercise was attempted for a similar type of structure to those with the concrete and asphalt surfaces described in Chapter 5. Jacobs investigated the thermal behaviour of a 20 cm thick layer of asphalt on soil under sunny weather conditions with no cloud. Both materials were assumed to be homogenous, with thermal conductivities and diffusivities independent of position within the structure. The variation of meteorological conditions such

as wind speed, air temperature, and incident short-wave solar flux were measured, and represented by analytical functions in the input data file for the model. The surface temperatures of the asphalt predicted by the model were found to agree with the available measured temperatures to within 0.2 °C over a 24 hour period.

Link et al. used their model to simulate the thermal behaviour of a 10 cm thick concrete pad on soil, and an area of bare soil. Two separate modelling periods of 24 hours were chosen, and meteorological and surface temperature data were recorded every 10 minutes. The weather was fine, and the fraction of cloud cover was assumed to have a constant value of 0.3. Agreement between measurements and predictions was to within 2 °C for the concrete and 3 °C for the bare soil, although it was found that there was an apparent time lag between the behaviour of the measured and predicted temperatures for the soil. This was due to the thermistor being located a short distance below the surface of the soil, and therefore detecting temperature fluctuations at the surface after a delay equal to their propagation time. This effect can also be seen in the investigation of the usefulness of contact temperature sensors in Section 4.4.3. The ability of the model to predict temperature contrasts was also investigated, and the predictions were found to agree with the measurements to within about 4 °C over the modelling period.

In comparison with the results of the two authors discussed above, the work described in Chapter 5 represents a more thorough approach to the validation of the model and provides a greater amount of useful information as to where the model may be applied with confidence. This was a result of two major factors. Firstly, the extensive database of weather and radiometer measurements made at Durham allowed the selection of a validation period of several continuous days with a mixture of sunny and cloudy weather, rather than the single 24 hour periods under ideal weather conditions previously considered. Secondly, the meteorological conditions and radiation temperatures stored in the database were measured at frequent intervals throughout the day

and night, and there were consequently few gaps in the data. It was therefore possible to make accurate allowances for changes in the values of parameters such as the fraction of cloud cover, independent of the time of day.

The results of the validation showed that there was good agreement between the measured and predicted temperatures, and so it is reasonable to assume that the model will produce equally good results for similar types of simple one-dimensional structures under the range of weather conditions which existed while the validation data were acquired. The ability of the model to predict temperature contrasts between two different surfaces was also investigated using the validation data for the concrete and asphalt. The measurement of temperature contrast is less affected by uncertainties in the absolute values of the input data for the model. For example the values of the meteorological parameters can be assumed to be the same for both the concrete and asphalt surfaces as they are reasonably close together. As may be expected, the results of this analysis proved that the model could produce acceptable predictions of the temperature contrast between the types of simple structures considered.

The next stage was to attempt to use the model to simulate the temperature variations of the surface of a south facing sandstone wall. The wall was a far more difficult structure to model than the concrete and asphalt surfaces previously considered, as it was both vertical and shaded for a short period after sunrise. A further difficulty was that the meteorological data used as input for the model were obtained from a weather station located some distance away from the wall, and hence the data were not an accurate representation of the actual conditions at the surface of the wall. The results of the simulation are given in Chapter 5, and it is evident from a comparison between the predictions of the model and measurements made by a radiometer that the model did not simulate the thermal behaviour of the wall particularly well. The possible reasons for this are outlined in Section 5.5, and it is likely that the major source of error is the section of the model

which converts the incident solar radiation measured by the horizontal solarimeter into the direct and diffuse flux components that would be received by the wall. The solution would be to either make direct measurements at the surface of the wall or else to find the angular distribution function for the diffuse flux, although both of these alternatives would be difficult to put into practise.

In summary, it has been shown that the current version of the general purpose model can produce reasonably accurate predictions of the surface temperatures of simple one-dimensional structures, under the meteorological conditions in existence while the validation data were recorded. The model has also been shown to be capable of generating acceptable predictions of the temperature contrast between the surfaces of two different materials.

7.2 Suggestions for future improvements to the general purpose model.

In the course of using the model it has become apparent that there are several areas in which improvements can be made to extend the possible range of applications, and to produce more accurate simulations of thermal behaviour.

Firstly, the results of the attempt to model the thermal behaviour of the sandstone wall suggested that it would be worthwhile to investigate whether any work has been done to determine the angular distribution function of the diffuse solar flux component, which may lead to improved simulations of the thermal behaviour for non-horizontal structures. It may also be possible to find newer, improved parameterisations for the other fluxes used in the equation of energy balance.

Secondly, one of the major problems in using the model is taking the effects of clouds into account. This is particularly important if the solar flux is calculated within the model, and a very simple technique described in Section 2.3.1.1 is currently used to modify the predicted solar flux under the influence of clouds. The model could be improved if a more realistic method of

simulating the effects of clouds could be found, although this would require the characteristic parameters for all the clouds in the sky at a certain time to be specified in more detail. The effects of clouds on the net long-wave flux are taken into account more accurately within the model, as it is possible to make use of the measurements made by the radiometer when pointing at the sky. Even so, this method will only provide a rough estimate of the magnitude of the flux, and could be improved by taking more frequent measurements or by designing a new detector with a suitably wide field of view specifically for the purpose of measuring the flux.

The third area of improvement would be in extending the range of weather conditions under which the model may operate. In particular, it would be useful to take into account the effects of rain, as it was found on examination of the database of measurements made at Durham that the longest period without any recorded rainfall was 10 days at the start of August 1983. It was therefore clear that the effects of rain would need to be included in the model if it was required to be used for periods of several continuous days in the wetter months of the year. Unfortunately, rain has a significant effect on both the surface and material properties of any structure under investigation, and would therefore require modifications to the model in three main areas.

Firstly, a further term must be included in the energy balance equation at the surface to represent the heat flux that the addition of rain causes. This could be achieved with the empirical equation used by Burbidge, 1980, which related the flux due to the rain to more readily measured quantities. The equation is given below;

$$\text{Flux due to rain} = r \times \rho \times s \times (T_1 - T_2) \qquad (7.1)$$

where; r is the rainfall rate (ms^{-1}),

ρ is the density of water,

s is the specific heat capacity of water,

T₁ is the temperature of the surface (K),

and T₂ is the temperature of the rain (K).

The temperature of the rain is calculated from;

$$T_2 = T - (A \times H) + (B \times H) \times \left(1 - \frac{(V_1-V)}{(V_1-V_2)}\right) \times \frac{A}{B} \qquad (7.2)$$

where; T is the air temperature (K),

A is the temperature lapse rate in air (6.5 K.km⁻¹),

B is the temperature lapse rate in cloud (4.2 K.km⁻¹),

V₁ = 8.936 ms⁻¹,

V₂ = 1.218 ms⁻¹,

and V is the raindrop terminal velocity (ms⁻¹).

The raindrop terminal velocity is obtained from reference tables relating the velocity to cloud type and height.

Secondly, the model would have to be able to take into account the changes in the surface and material parameters which occur when materials become wet. The effects of water on surface properties may lead to either an increase or decrease in the surface temperature. When a layer of water forms on a surface, the emissivity will tend to approach unity. If the surface had a low emissivity when dry, then this may result in the radiation temperature of the surface rising as the temperature of the water becomes equal to that of the surface. However, if the layer of water is constantly added to by more rain which is cooler than the surface, then the net effect will be to reduce the surface temperature.

The values of material parameters, such as the thermal conductivity and diffusivity, will be affected as water is absorbed. For example, if a layer of soil is considered, then the presence of water will cause the thermal conductivity to increase as the air in the soil pore spaces is replaced by the more conductive water. The addition of water also increases the specific heat

capacity and the density of the soil. The thermal diffusivity, which is a function of the conductivity, density and specific heat, increases with saturation up to typically 20% and then starts to fall slowly. The modifications to the model which would be needed to take these effects into account would require the specification of additional input data, such as the state of saturation of the surface and the variation of moisture content with depth. However, a simpler method would be to use empirical relationships which determine the material parameters as some function of more readily measured quantities, provided that such equations were available for the particular medium of interest. Alternatively, direct measurements could be made with the appropriate type of sensors.

The third alteration to the model would be to include heat transport by moisture in the equation describing heat conduction through the medium. This would not be easy, although much work has been done on the theory of infiltration.

It is clear that there is much useful work which could be carried out to improve the existing version of the general purpose model. However, the experience gained from using the model in its present form is also useful to suggest directions for the development of future types of model. This is discussed in the next section.

7.3 Suggestions for the future development of new types of models.

There are two ways in which the development of future models may proceed. Firstly, new versions of the general purpose one-dimensional model could be developed to include the capability to predict temperatures for two and three-dimensional structures. This would be achieved with an extended version of the present finite element method used to solve the differential equation of heat transfer. The multi-dimensional models would be capable of predicting temperature profiles within much more complicated media than is possible with the current one-dimensional model, and for example could be

applied to layered structures composed of materials with irregularly shaped boundaries and varying thermal properties.

As an alternative to developing increasingly more complicated models of the same basic type as the current general purpose model, it may be worthwhile to investigate the possibility of creating a simpler model which would predict surface temperatures as a function of only two or three important meteorological parameters. An empirical modelling technique of this type has been suggested by Turver, 1978, who derived a general equation to relate the radiation temperatures of several different surfaces during daylight hours to the ambient air temperature and the incident short-wave solar flux. The equation is written as follows;

$$R(t) = T(t-x) + k.S(t) \qquad\qquad (7.3)$$

where; R(t) is the radiation temperature of the surface at time t,

T(t-x) is the ambient air temperature x hours before time t,

k is a constant,

and S(t) is the short-wave solar flux incident on the surface.

The values of the delay parameter, x, and the constant k, which governs the speed of response to changes in solar flux, are both functions of the thermal capacity of the structure under investigation. Both of these coefficients tend to zero for low thermal capacities. Equation 7.3 was applied to data recorded for a fence, a slate roof, and a brick wall, and the values of k and x were chosen by inspection. It was found that the empirical relationship simulated the observed thermal behaviour of the surfaces to within ± 1 °C.

These results suggest that this technique could be used as the basis for the development of an empirical type of model. However, further work would be required to extend the modelling period to a full 24 hours, and extensive field trails would be needed to determine the types of surfaces and materials to which the empirical equations could be applied.

Appendix.   Software developed for use with the Tektronix 4052 computer.

A.1 Outline of the software library.

An extensive software library written in the BASIC programming language has

been developed for the Tektronix 4052 computer. The programs may be divided

into two main categories; programs which control the operation of the

equipment, and programs used for off-line data analysis.   The first category

covers three programs: the autoguidance and data acquisition program, which is

used for on-line acquisition of temperature data, the program to control the

transfer of weather data from the Microdata logger to the computer, and

thirdly a program which can be used to test if all the equipment connected to

the computer is operating correctly.

The programs in the second category are used for the analysis of the

radiometer, contact temperature sensor, and weather data supplied by the

equipment described in Chapter 4. Basically these programs provide results in

either a graphical form or as a numerical listing. Graphical results can be

displayed on the screen of the computer, or plotted out on paper using the

Tektronix graph plotter. Numerical data can also be displayed on the screen or

listed by the 80-column dot matrix printer, which is connected to the computer

via an interface unit on the GPIB.

The programs are described in more detail in the following two sections.

A.2   Programs for on-line control of equipment.

A.2.1 The autoguidance and data acquisition program.

This program can be used to operate the computer in either of two running

modes.   In the first mode, the positions of the objects for which temperature

data are required are specified by the operator and stored in either a file on

the magnetic tape, or in the memory of the computer. This process is described

in Section 4.6.1 of Chapter 4, and involves using the joystick on the servo

controller to move the pan and tilt head, while observing the field of view of the radiometer marked on the CCTV monitor. After the target sequence has been specified, the other operating mode can be selected. The computer will then point the radiometer at the each of the objects in turn, and record their temperatures on tape. This operation is outlined in Section 4.6.1, and described in greater detail in Section 4.6.2 of Chapter 4.

In the next two parts of this section, the two running modes will be described in more detail, with particular reference to how the program allows the operator to specify the type and amount of data to be recorded.

A.2.1.1 To specify a sequence of objects for subsequent temperature

measurement.

If this running mode is selected, the operator only needs to enter the number of positions to be stored, and then press user definable key number 1 on the computer keyboard when the object is in the field of view of the radiometer. As explained in Section 4.6.2, the computer records the position of an object by two digital values corresponding to the readings from the two potentiometers in the pan and tilt head, which specify the current azimuth and zenith setting for the moveable platform. These readings are stored in the computer as two one-dimensional arrays, each containing the same number of elements as there are objects in the sequence. When the arrays have been filled, the operator can specify a file on a magnetic tape cartridge for the data to be stored on. Provided the file is large enough, the arrays are then written in binary format by the computer. A flowchart showing the operation of this mode is given in Fig. A.1.

A.2.1.2 Acquisition of temperature data.

When this running mode is entered, the computer assumes that the co-ordinates of the objects have already been stored on magnetic tape. The computer therefore prompts the operator to enter the relevant file number, and then

reads in the two arrays. The operator then has to specify whether or not temperature data are to be listed on the printer. There are three options available; data can be printed for every scan of the sequence of objects, for every n^{th} scan, or alternatively all output to the printer may be suppressed. If one of the first two options are selected, the operator may then specify the type of data to be printed from the three choices available. The first option is to print out the readings from all 33 channels in use in the 8-bit ADC units, which corresponds to the 32 contact temperature sensors and the radiometer. Secondly, up to 16 ADC channels for which data are to be printed may be selected by the operator, and thirdly it is possible to specify that only the radiometer reading is to be printed.

The next stage in the program finds a suitable magnetic tape file for the temperature data to be stored in. The operator is therefore instructed to put a tape cartridge in the internal tape drive of the computer, and enters the number of the first file on the tape to be used for data storage. The computer locates the specified file, and examines the tape header. If this shows that it is the last file on the tape, then the program proceeds to the next stage. However, if this is not the case, the computer displays a warning on the screen that recording data on that file will involve erasing previously recorded material, and gives the operator a chance to choose a different file. This precaution is necessary because the computer marks data files as required when in the automatic data acquisition mode, so all files on the tape after the file which has been specified will be over-written.

Lastly, the operator has to check that the real time clock ROM pack in the computer is correctly set to GMT, and to specify how long the system is to remain idle between data acquisition sequences. The servo controller for the pan and tilt head can then be switched to receive control signals from the computer, and routine acquisition of temperature data will begin. The computer will therefore move the pan and tilt head so that it points at each object in the sequence. The times and temperature data from the contact temperature

sensors and radiometer are stored in the memory of the computer, and also listed on the printer if required. The format and types of data stored are specified in the program, and have been discussed in Section 4.7.1. The temperature data are written on tape after the last measurement in the sequence has been made. The computer then moves the pan and tilt head so that it is looking at the first object in the sequence, and the apparatus stays idle for the previously specified time before starting a new data acquisition run. A flowchart showing the operation of the data acquisition system under computer control is given in Fig. 4.35.

A.2.2 Program to transfer weather data from the Microdata logger to the Tektronix computer.

The purpose of this program is to control the transfer of weather data from the Microdata logger to the computer, where the data are stored on a standard magnetic tape cartridge. The transfer takes place between the RS-232C interface on the computer and a compatible interface card inside the logger.

At the start of the program, the data transfer parameters for the interface on the computer have to be set to correspond with the replay interface card inside the data logger. This is achieved by using a "CALL" statement, which transfers control from the standard BASIC operating mode to the relevant routine, which is housed in the RS-232C interface backpack on the computer. In this case, the "RATE" routine is used to set three parameters; the data transfer baud rate, the parity parameter, and the communication error action parameter. The data transfer rate is set to 1200 bits/sec, and the parity parameter is derived from a reference table in the instruction manual for the RS-232C interface. The error action parameter is set so that the number of errors which occur during the data transfer are counted, but do not cause the program to stop when an error is encountered.

The logger now has to be manually set to replay mode at the start of the desired track on the DC300 magnetic tape cartridge, and is connected to the

interface on the computer. The operator then puts a magnetic tape cartridge into the internal tape drive of the computer, and specifies the files on which the weather data transferred from the logger are to be stored. The program then waits until a carriage return is entered from the keyboard before starting the data transfer process.

In the next part of the program, three ASCII character strings are dimensioned to receive the data from the logger, and data transfer is initiated by the computer when it executes the statement "PRINT @40:"Q"", where "Q" is the control character DC1. The primary address of 40 specifies that the data in the BASIC statement are to be sent out from the RS-232C interface. When the logger receives the control character, it begins to send out data in the form of an ASCII string. The computer receives this through the RS-232C interface when it executes the next statement in the program. This is of the form "INPUT @40:A$", where A$ is a string which has been dimensioned to contain the data sent out by the logger. The process of alternately sending out control codes and receiving data from the logger is repeated three times, and the weather data stored in three separate strings.

The three strings are concatenated in the next stage of the program, resulting in a long string containing one or more sets of readings from the the seven different weather recording instruments and the two real time clock cards in the logger. Each set is separated by a fixed time interval, which was 15 minutes for the data recorded at Durham Observatory. In the data string, the relevant channel number precedes each reading, and there are several space characters inserted between the readings. This is next modified to a more compact form suitable for storage on the magnetic tape cartridge in the internal tape drive of the computer. Firstly, it is necessary to find the position in the string of the first reading from the lowest channel number in use on the logger, which in this case is channel zero. The positions of the readings from the other eight channels used on the logger are then located in ascending order. The data recorded for the channels are then removed from the

string, and concatenated to form a more compact representation of the data. This consists of the readings from the nine channels with the channel numbers and space characters removed. The part of the initial long string from which the data was taken is now discarded, and a check made to see if there is another complete set of nine readings left in the remainder of the string. If so, the above reduction process is repeated, and the resulting compact data string is concatenated with the first. However, if there is insufficient data, the remainder of the unreduced string is kept, and more data added to it when the program returns to the section where data are read in through the RS-232C interface. This continues until the compact data string contains the results for 96 scans of the weather recording instruments, when the string is written in a file on the magnetic tape cartridge in the internal tape drive of the computer. This length of data string was chosen so that each file on the tape would contain the results for 24 hours, provided the logger had been set to record data at intervals of 15 minutes.

The above sequence continues until the data for the specified number of days have been read from the logger. The program ends at this point, and the logger can be reset to stop mode either manually or by sending the appropriate control character from the computer.

A.2.3 Test program for the data acquisition system.

This program allows the operator to determine whether the computer and the units connected to the GPIB are functioning correctly. There are five options in all, which are selected with the user definable keys on the computer.

The first three options test units on the GPIB, and the first of these is to read out the current position of the pan and tilt head. When this option is selected, the computer initiates the process to read the voltages from the two potentiometer sensors inside the pan and tilt head. These are then digitized by the 11-bit ADC, and transferred to the computer over the GPIB.

This operation is described in more detail in Section 4.6.2. The readings from the two sensors are then displayed on the screen of the computer as numbers in the range 0 to 2047, corresponding to the reading from the ADC. The manual control joystick on the servo controller can then be used to move pan and tilt head, and if the apparatus is functioning correctly, then a corresponding change in the reading from the ADC should be observed.

The second option allows the operator to examine the readings from the three 8-bit ADC units. The 48 channels available from these units correspond to the 32 contact temperature sensors and the radiometer, with the other 15 channels unused. The data are read from the ADC's via the 11-bit bus controller, and sent to the computer over the GPIB as described in Section 4.3.3. The data are displayed on the screen of the computer as 48 numbers in the range from 0 to 255, corresponding to the output from the 48 ADC channels. The reading from the radiometer can be varied by pointing it at different objects using the pan and tilt head. The contact temperature sensors should display a stable reading, which will increase if they are heated. The other channels are grounded, so give a constant reading of zero.

The third option is used to test for correct operation of the printer and its interface with the computer, on the GPIB. This simply sends a string of 80 characters over the GPIB to the interface, which is then transferred to the printer and listed.

The other two options are concerned with the operation of the computer. The first is to check that the keyboard and display screen are functioning correctly, while the second checks the operation of the internal tape drive. For the latter option, an empty tape cartridge is put in the tape drive, and the computer writes ASCII data in one empty file, and binary data in another. The computer then reads the data from the two files, and verifies that it is the same as the original data.

A.3 Data analysis programs.

There are three types of data for which analysis programs are required; weather data, temperature data from the radiometer, and data from the contact temperature sensors. The programs that have been developed to analyse these data are described in the next three sections.

A.3.1 Analysis programs for radiometer data.

There are three main programs used for the analysis of radiometer data; two of which produce numerical output, while the third displays the temperature data in a graphical form. The programs are described in the following sections.

A.3.1.1 Program to list radiometer data.

There are two versions of this program which apply to the two different types of data storage formats in use; i.e. the format specified in the autoguidance and data acquisition program, and that used for long term storage on 9-track tape. Both versions are constructed in a similar way, with the main difference being in the way that the data string is analysed. The start of the two programs is the same. Firstly, the operator has to specify the range of data files from which the temperatures are required, and the reference number of the particular object in the sequence. For the case of data recorded in the format specified in the autoguidance and data acquisition program, the computer locates the specified starting file on the magnetic tape cartridge, and reads in the first binary string containing the data recorded during the scan of the radiometer over all of the objects in the sequence. The composition of this data string is discussed in more detail in Section 4.7.1. The program then finds the segment of the string containing the time, the temperature data for the specified object, and the reading from the contact temperature sensor attached to the optical unit of the radiometer. The latter two quantities are stored as single ASCII characters in the string, and are firstly converted back to decimal numbers between 0 and 255. The radiation

temperature of the object can then be obtained by using the calibration equation for the radiometer, which is given as Equation 4.1 in Section 4.3.4.

The second version of the program is used for analysis of data which are kept on 9-track tape. This has to be mounted on a tape drive attached to a VAX 750 computer, and data are transferred in an ASCII format to the Tektronix computer through the RS-232C interface. The data format is the same as that described for the transfer process between the Tektronix computer and the VAX computer described in Section 4.7.2. Basically, there are two main differences between the ASCII and the original binary format. Firstly, the readings for the radiometer and the contact temperature sensor are already in decimal form, rather than the ASCII character representation, and secondly the ASCII data are written on the tape such that the information for each target is stored as a separate string. Apart from modifications necessary due to the different data format, this version of the program proceeds in a similar fashion to the previous one. As before, the radiation temperature for the object is calculated using the calibration equation for the radiometer.

The output from the computer consists of the radiation temperature of the object and the time at which it was recorded. This can be listed on the printer or displayed on the screen of the computer.

A.3.1.2 Program to list radiometer data at specified times.

This program was developed to provide radiometer data in a form suitable for use with the modelling programs on NUMAC. The models on NUMAC require the times at which the weather and radiometer data were recorded to be the same. As the weather data were recorded at fixed time intervals of 15 minutes, it is simplest to put these values directly into the NUMAC data files, and then to use an interpolation method with the radiometer data to determine the radiation temperatures at times corresponding with the weather data. There are two versions of this program for use with the binary and ASCII data formats described Section A.3.1.1. The construction of the two versions of the program

is very similar, and in the following description the analysis of the data strings will be dealt with in a general manner applicable to both.

At the start of the program, the operator has to specify the date and initial time for which the interpolated data are required. This information is used to set up an array, T, containing the times from the specified start time to the finishing time, which is normally 24 hours later. The time elements in the array are separated by the specified time interval, which is normally 15 minutes. The operator then has to put a data tape in the internal tape drive of the computer, and specify the first file on which relevant data are stored. The computer finds the file, reads in a data string, and then evaluates the time at which the data for the specified object were recorded. The time is then converted from hours, minutes and seconds to hours and tenths of hours, and from GMT to Local Mean Time (LMT) by subtracting 4 minutes for every degree of longitude that the data recording site was west of the meridian passing through Greenwich. The resulting course of action taken by the program depends on whether the data string was recorded before or after the initial time for which the interpolated data are required.

If the data string was recorded after this time, it is therefore not possible to obtain an interpolated value for the radiation temperature of the object, and so the interpolated temperature is set to an unrealistic number, such as 1000 °C. This can be recognized in the stage of the analysis program when the data are listed, and an appropriate error message generated. This value of the temperature is stored as the first element in the array "Y", which is dimensioned to have the same number of elements as there are times for which interpolated temperatures are required. The program then reads the next element from the array "T", and checks if it is still earlier than the time that the first data string was recorded. If so, the interpolated temperature is set to 1000 °C again, and the next time read in from the array. This process continues until the current time value for which interpolated data are required, T(n), is later the time that the first data string was

recorded, and the program then follows the procedure outlined in the next paragraph.

When the data string was recorded before the start time, T(1), or the first possible time, T(n), for which interpolated data may be calculated if the procedure outlined in the previous paragraph has been followed, the usual criterion for acceptance of the string for subsequent analysis is that it was recorded 15 minutes or less before this time. If the string is not accepted, the next is read in and the above acceptance criterion applied again. When the string is accepted, the radiation temperature is calculated for the specified object by using the calibration equation for the radiometer (Equation 4.1), and is stored along with the time in two arrays as B(1) and A(1) respectively. The next data string is then read in from the file. The time and temperature values are calculated as before and assigned to the variables A1 and B1. However, if this data string was also recorded before the current time for which interpolated data are required, then the time and temperature values from the second data string are stored as array elements A(1) and B(1), overwriting the previous values. The computer then reads in another data string from the data tape, and repeats the process until the following two conditions are satisfied. Firstly, the time that the previous data string was recorded, A(1), is less than 15 minutes before the required time for interpolated data, T(n), and secondly the time that the current data string was recorded, A1, must be before the next required time for interpolated data, T(n+1). These conditions mean that the two data strings are separated in time by less than 30 minutes, ensuring that the result obtained from the interpolation process will be fairly accurate. If these conditions can not be satisfied, the interpolated temperature at time T(n) is set to an unrealistic figure as before, and the next value in the time array, T, is selected. This process is repeated until the current time for which interpolated data are required is just after the time that the current data string was recorded. The time and temperature values from this string, equal to A1 and B1, are then

stored in the A and B arrays as A(1) and B(1). The computer reads in the next data string, and evaluates the new values of A1 and B1. This process continues until the criterion for linear interpolation to proceed is satisfied.

The linear interpolation equation is given below. This is used to give a temperature Y(n) at time T(n), given two data points with time values on either side of T(n).

$$Y(n) = B(I) + \frac{(B1-B(I))}{(A1-A(I))} \times (T(n)-A(1))$$ (A.1)

where;   A(I) = Time of data point recorded before T(n).

B(I) = Temperature measured at time A(I).

A1 = Time of data point recorded after T(n).

B1 = Temperature measured at time A1.

After this equation has been used, the values of A(1) and B(1) are overwritten by A1 and B1, and a new data string read in from the data tape. The program then follows the procedure explained in the previous paragraphs to find the temperature Y(n+1) at time T(n+1). This continues until all the required interpolated temperatures have been found, and the array "Y" is filled.

In the final stage of the program, the temperatures may be listed on the printer or the screen of the computer, along with the corresponding times from the array T. This part of the program also includes a section which detects any temperature readings which are obviously out of the normal operating range of the logger. These may occur intentionaly, for example the 1000 °C readings which are stored in the array when it is not possible to calculate an interpolated temperature at the relevant time, or alternatively may occur due to a fault on the 8-bit ADC or the contact temperature sensor attached to the radiometer. In either case, when the temperature is listed, the computer shows that it is out of range by printing a predefined symbol against it.

The program described above is designed to provide data for only one of

the objects in the sequence scanned by the radiometer. However, another version of the program has been developed to give results for all of the objects. The operation of this program is the same as described previously, except that the arrays which are used have to be dimensioned differently. The interpolated temperature data are stored in a two-dimensional array, which has the same number of rows as there are objects in the sequence, and as before, the same number of columns as there are times in the array T. Also, the arrays A and B are dimensioned to have the same number of elements as objects in the sequence.

The program can also be adapted to evaluate two parameters which are used in the data files set up on NUMAC. These are the representative temperature of the surroundings, TREP, and the long-wave cloud cover factor, CLFAC. In both cases, the values of these parameters are derived from an average of several measurements made by the radiometer. If one of these readings is found to be outside the normal operating range of the radiometer it is not used in the calculation, and an appropriate error message may be generated.

The representative temperature of the surroundings is obtained from the average temperature measured by the radiometer when pointing at objects on the horizon. This parameter is needed when the sky seen by the target to be modelled is partially obscured by distant trees or buildings. The parameter TREP can then be used to estimate the long-wave flux incident on the surface of interest from these objects, provided the fraction of the sky that is obscured is known. However, if the objects obscuring the sky are very close to the surface of interest, then the program to calculate TREP can easily be modified to take account of the temperature of the obscuring objects rather than the horizon temperature.

The long-wave cloud cover factor is obtained from measurements made by the radiometer when pointing at the sky. At Durham Observatory, three measurements were made with the radiometer pointing at about 45° above the horizontal in different directions, and one with the radiometer pointing

vertically upwards. These four measurements were included in the sequence of objects scanned by the radiometer. The temperatures of the sky are firstly calculated in the program from the radiometer data, and the average of these temperatures is stored in an appropriately dimensioned array. When all the data for the 24 hour period of interest have been obtained, the maximum and minimum temperatures in the array are found, and are then assumed to be equivalent to cloud cover factors of zero and one respectively. The other intermediate values of the average sky temperature can then be easily converted to the long-wave cloud cover factor in the range from 0 to 1, as the two quantities are directly proportional to each other.

A.3.1.3 Program to plot radiometer data.

This program is used to plot the variation of the recorded radiation temperature of an object with time, normally over a 24 hour period from 12:00 to 12:00 on the following day. The graph can either be displayed on the screen of the computer, or plotted on paper using the Tektronix 4662 graph plotter.

The first part of the program obtains the temperature data by a method similar to that described in Section A.3.1.1. The operator is able to specify the period over which the graph is to be plotted, although this is usually set to the 24 hour period described above. At the end of the first part of the program the resulting temperature data, and times at which the data were recorded, are stored in two arrays of equal dimension.

In the next stage of the program, the operator firstly has to specify whether the graph is to displayed on the computer screen or plotted on paper. The program uses graphical BASIC commands to specify the region on the screen or plotting surface to be used. If the plotter is specified, the graph will be plotted on an A4 size piece of paper and up to eight different pen colours may be used. The graph plotted on the computer screen is similar, but of different dimensions.

Several variations of this program which have been developed to produce

other graphs. For example, one program is used to plot the variation of the long-wave cloud cover factor with time. The cloud cover factor is derived from the measurements made by the radiometer when it is pointing at the sky, which are normalised to produce a number in the range from 0 to 1 as described in Section A.3.1.2. An example of this type of graph is given in Fig. 4.18. A second version of the program is used to compare the temperatures measured by the radiometer with those predicted by the computer model. The two sets of data may be represented by solid and dotted lines, as for example in Fig. 5.35, or else the multiple colour facility of the graph plotter may be used.

A.3.2 Analysis programs for contact temperature sensor data.

The programs for the analysis of the contact temperature sensor data are similar to those designed for use with the radiometer data, although a program to produce interpolated temperature readings at any desired time, such as that described in Section A.3.1.2, has not been developed. This was because the contact temperature sensor data were not required for use with the mainframe computer models.

A.3.2.1 Program to list contact temperature sensor data.

Initially, the operator specifies the reference number of the sensor from which data is required, and enters the relevant calibration equation. This equation relates the reading from the 8-bit ADC to the contact temperature in degrees Celcius, and was determined for all 32 sensors as described in Section 4.4.1. The operator also has to enter the starting time for which data are required, and the relevant file number on the data tape. The program then proceeds in a similar fashion to that described in Section A.3.2.1, with the main difference being in the use of the data read from the magnetic tape cartridge. Analysis of the data is fairly straightforward, as the readings from all 32 temperature sensors were recorded at the same time as the

radiometer measurement for the first object in the sequence scanned by the radiometer. As before, there are two versions of the program corresponding to the two types of data storage formats in use; i.e. binary data recorded by the standard autoguidance and data acquisition program, and ASCII data normally stored on 9-track magnetic tape. These data storage formats are discussed in more detail in Sections 4.7.1 and 4.7.2 respectively. Both programs convert the data recorded from the specified sensor to a contact temperature. These data, along with the time at which it was recorded, can then be listed on the printer or the screen of the computer.

A.3.2.2 Program to plot contact temperature sensor data.

This program is similar to that described in Section A.3.1.3, but modified to show the variation of output from one of the contact temperature sensors with time. The temperature data are obtained as outlined in the previous section, and at the end of the first part of the program, two arrays are used to store the temperatures and the times at which they were recorded.

The graph may be plotted either on the screen of the computer, or on paper using the Tektronix graph plotter. This program has been used mainly to produce graphs of the type shown in Fig. 4.21 and Fig. 4.27, in which the contact temperature recorded by the sensor is compared with other measurements.

A.3.3 Analysis programs for weather data.

There are two main programs which are used for the analysis of weather data obtained from the automatic weather station. The data are stored on DC300 magnetic tape cartridges as described in Section 4.7.3. The first program lists the data, after using the appropriate calibration equations for the measuring instruments. The second plots the variation of any one of the measured weather parameters over a 24 hour period.

A.3.3.1 Program to list weather data.

This program lists the data produced by all seven instruments connected to the weather station, combined with the date and time at which they were recorded. In the standard version of the program, this information is listed over a 24 hour period from 12:00 to 12:00 the following day, although the program can easily be modified for different times. At the start of the program, the operator specifies the first day for which data are required. This is entered in the form of a number from 0 to 365 or 366, to correspond with the relevant day of the year. The operator then enters the number of the first file on which data are stored, and the computer begins to read in data from the magnetic tape cartridge. As each file contains one long data string, this is initially split up into segments, each consisting of the date, time, and data from each of the seven instruments. The time that the data were recorded corresponds to GMT, so in the next stage of the program, this is converted to LMT by the same process as described in Section A.3.1.2. The program then checks if the resulting time is inside the specified period of interest, in which case the program proceeds to the next section. If not, the next segment is taken from the main data string and the above process repeated.

In the next stage of the program, the segment of the main data string, which contains all the information recorded by the logger at a particular time, is split up into the individual components for analysis. Firstly, a two-dimensional array is set up to contain the data. This is dimensioned to have 9 rows, corresponding to the 9 data items recorded by the logger, and initially 100 columns. The number of columns required depends on the frequency with which data were recorded. This was every 15 minutes in the case of the data from Durham Observatory, so the array requires 96 columns for a graph showing 24 hours of data. The date and time are stored in the first two rows, with the other seven used for the data from the weather sensors. The weather data are firstly converted from the reading recorded by the logger to a value

for the weather parameter in the correct dimensions by using the appropriate calibration equations. These equations were either supplied by the manufacturer of the instrument, or derived from calibration work at Durham. Out of the seven weather sensors in use, the corrected readings from the net radiometer, wet and dry bulb thermometers, anemometer, and raingauge can be easily obtained by using the relevant equation. However, for the wind direction and the average solar radiation, a different approach is taken. For the former, the readings recorded by the logger are in the range from 0 to 1000, corresponding to sixteen possible wind directions. This is represented in the array as a number from 1 to 16, which is used later to print the appropriate compass direction. The reading from the solarimeter as recorded by the logger is stored in the array, and is converted to give the average solar flux in the next stage of the program.

The array is considered to be filled when the current segment of the main data string is found to have been recorded after the end of the period of interest. If necessary, the array is then re-dimensioned so that the empty columns are deleted. The next stage of the program is concerned with the interpretation of the solarimeter data. In theory, this should be simple, as the signal averaging card records a count of 5000 over the interval between readings being taken by the logger when there is no incident flux, and this should increase linearly by 1 count for roughly every 2 Wm^{-2} of incident flux received by the solarimeter. However, it was found when analysing the data that the reading at night was not fixed at 5000, and on many nights was one or two counts below this figure. This was probably due to either radiative and conductive heat exchanges inside the solarimeter, or an error in the real time clock card used in the logger. In the latter case, as the signal average card, which interfaces the solarimeter with the logger, uses a pulse counting technique over a fixed interval measured by the clock, then a small error in the clock could give rise to an incorrect count. It was therefore decided that it would be necessary to find the minimum count recorded by the logger each

night, and use this as a working zero point from which to evaluate the other fluxes. The minimum count recorded is therefore found in the program, and then subtracted from all the other solarimeter readings. The resulting numbers are then converted to a flux in Wm^{-2} using the calibration data supplied by the manufacturer, and stored in the appropriate row of the array.

The final part of the program contains the format statements needed to list the data on the printer or the screen of the computer. The time, and all the weather data except for the wind direction, are listed directly from the two-dimensional array. In the case of the wind direction, the numbers stored in the array are used to take a segment of an ASCII string containing the 16 possible compass directions. The order of these directions is obtained from a calibration graph supplied by the manufacturer. The segment of this string, for example of the form "NNW", is then listed with the numerical data.

A.3.3.2 Program to plot weather data.

The first part of this program is the same as that described in the previous section, and the second part then plots the variation of any one of the seven weather parameters over the 24 hour period of interest. The graph may be plotted either on the screen of the computer, or on paper using the Tektronix graph plotter, and typical examples are shown in Fig. 5.5 to Fig. 5.8 for four different weather parameters.
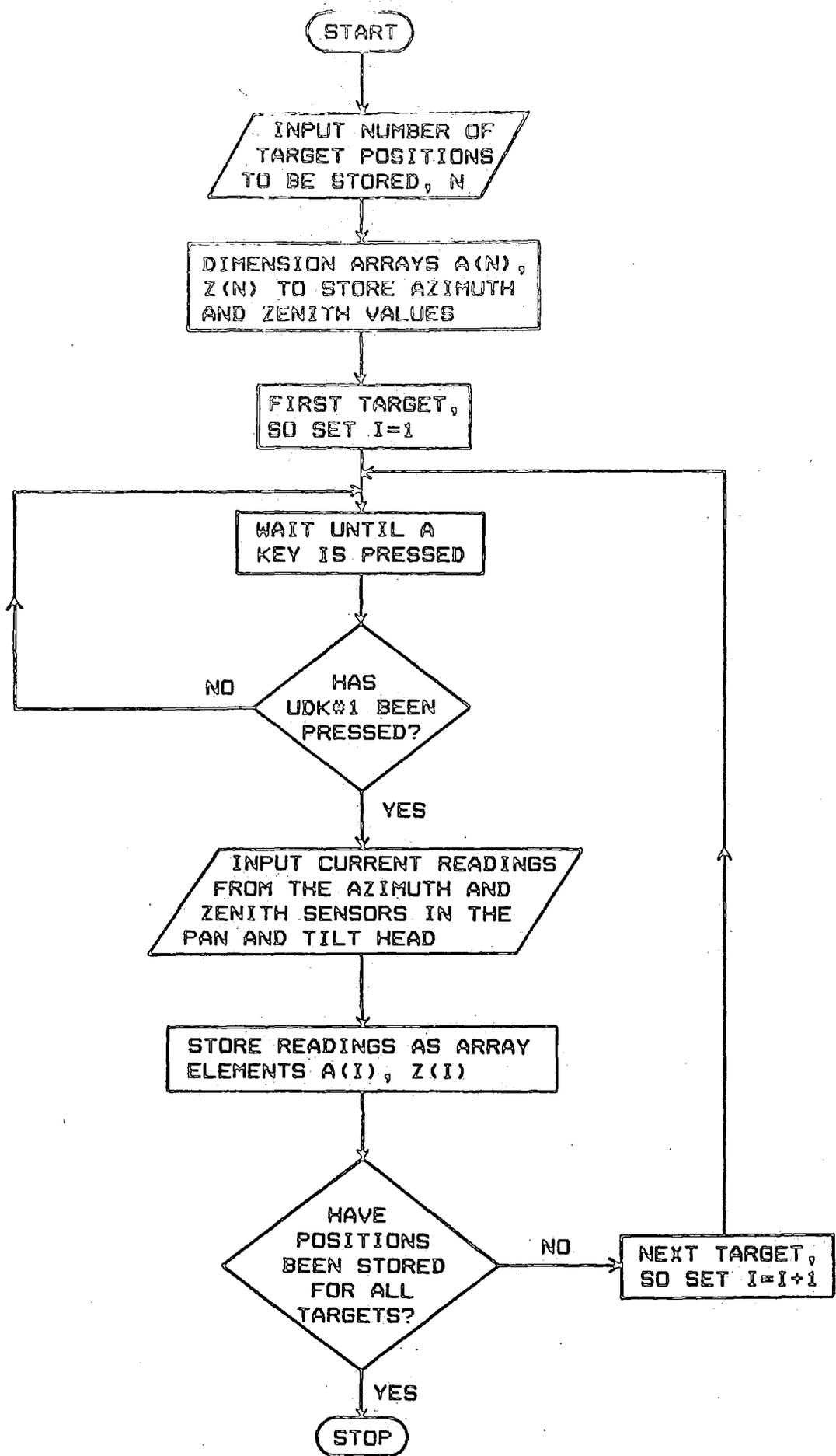
Fig. A.1   Flowchart for the Target Acquisition Process.

References.

L.K. Balick, L.E. Link, R.K. Scoggins, and J.L. Solomon, "Thermal modelling of terrain surface elements", U.S. Army Engineer Waterways Experiment Station, Technical Report EL-81-2, 1981.

R. Burbidge, "Study of modelling and assessment techniques for future ATGW - weather related systems performance modelling", Final Report on MOD PE Contract No. K/MGW11b/897, British Aerospace Dynamics Group, Bristol, Sept. 1980.

G. Hübner and C.C. Gladen, "Tirex 81: Comparative evaluation of temperature measurement techniques", Sept.1981.

S.B. Idso, "A set of equations for full spectrum and 8 to 14 micron and 10.5 to 12.5 micron thermal radiation from cloudless skies", Water Resources Research, 17,2 (1981) 295-304.

P.A.M. Jacobs, "Simulation model to calculate the surface temperature of an asphalt layer", Report PHL 1976-32, National Defence Research Organization TNO, The Hague, Netherlands (1976).

A.B. Kahle, "A simple thermal model of the Earth's surface for geologic mapping by remote sensing", J. Geophysics. Res. 82 (1977) 1673-1680.

B.A. Kimball, S.B. Idso and J.K. Aase, "A model of thermal radiation from partly cloudy and overcast skies", Water Resources Research, 18,4 (1982) 931-936.

K.Ya Kondratyev, "Radiation in the atmosphere", Academic Press, New York, 1969.

A.A. Lacis and J.E. Hansen, "A parameterisation for the absorption of solar radiation in the earth's atmosphere", J. Atmos. Sci. 31 (1974) 118-133.

Meteorological Office, "Measurement of solar and terrestrial radiation", Handbook of Meteorological Instruments (Second Edition), Vol. 6, HMSO, London, 1982.

Meteorological Office, "Observer's handbook", Fourth Edition, HMSO, London, 1982.

T.R. Oke, "Boundary layer climates", Methuen, 1978.

M.N. Ozisik, "Radiative transfer", J. Wiley and Sons, New York, 1973.

G.W. Paltridge and C.M.R. Platt, "Radiative processes in meteorology and climatology", Elsevier scientific publishing company, Amsterdam, 1974.

W.D. Sellers, "Physical climatology", University of Chicago Press, Chicago (1965).

K.E. Turver, "Measurements of target and background signatures in the far infrared spectral region", S.C.R.D.E. Internal Report, Colchester, June 1978.

K. Watson, "Geologic applications of thermal infrared images," Proceedings of the IEEE, pp. 128-137, January 1975.

Acknowledgments.

I would firstly like to thank Professor B. H. Bransden for the provision of facilities in the Department of Physics at the University of Durham. I am also grateful to my supervisor, Dr. K. E. Turver, for his advice and encouragement.

Dr. A. B. Rimmer is thanked for his assistance and many helpful discussions regarding the computer models. I would also like to thank my father, Mr. T. E. Hughes, for drawing many of the diagrams in Chapter 4.

Finally, the Science and Engineering Research Council, and the Stores and Clothing Research and Development Establishment, Colchester, are gratefully thanked for the award of a CASE studentship.